A STUDY OF REWETTING PHENOMENA

by

Andrew K.H. Kim

A thesis
presented to the University of Ottawa
in partial fulfillment of the
requirements for the degree of
Doctor of Philosophy
in
Mechanical Engineering Department

OTTAWA, Ontario, 1983

ABSTRACT

The objective of the present thesis was to study the mechanisms involved in the rewetting phenomena which have a particular importance during the reflooding phase of emergency core cooling conditions in a reactor. This thesis is composed of two major parts: experimental study and analytical study.

In the experimental study, extensive experimental works on rewetting of hot channels with various channel geometries and different flooding modes were carried out to study the various parametric trends on the propagation of the rewetting front. The major parameters studied which affect the rewetting process were coolant flow rates, coolant inlet subcooling, initial wall temperature, wall thickness, wall material, power generation rates, and axial location along the channel as well as the flow channel geometry.

Some of the channel geometries considered here include single tube rewetting on the inside surface as well as outside surface, annular flow channel and "L"-shaped test section. The flooding modes studied are bottom flooding, top flooding and horizontal flooding. In the case of "L"-shaped test sections, THF(Top-followed-by-Horizontal-Flooding) and HBF(Horizontal-followed-by-Bottom-Flooding) were studied.

The effect of each parameter on rewetting velocity and the process of the rewetting phenomena for various channel geometries and flooding modes are discussed in detail based on the experimental results.

In the analytical study, an analysis to calculate more accurate heat transfer coefficient in the Inverted Annular Flow Region was developed.

From the result of the experimental study as well as from the authors previous numerical analysis[1], it was observed that the precursory cooling just ahead of the rewetting front and the rewetting temperature are two of the most important parameters affecting the rewetting velocity. Since rewetting temperature, Tq, was already studied in the authors previous work[1], naturally the precursory cooling just ahead of the rewetting front is studied in the present analysis.

The present analytical study is confined to a model which will calculate the heat transfer coefficient of the inverted annular flow film boiling in the downstream region of the rewetting front in a bottom flooding mode. This analysis was based on the concept of assuming the Inverted Annular Flow Region as a concentric annulus with a core tube moving at a certain speed.

The result shows that the heat transfer coefficient calculated using this analysis is very close to the value of the experimental heat transfer coefficient. The analysis was also incorporated into the author's previous computer simulation model[1] which predicts the rewetting velocity of the single tube bottom flooding mode, and significant improvement over previous results was observed.

Also to obtain physical insight into the problems associated with the reflooding phenomena, a visual study of the rewetting process for various flooding modes and channel geometries was carried out using high speed still photography. Some of the photographs as well as indepth description of the rewetting process of various channel geometries and flooding modes observed by visual study are presented.

ACKNOWLEDGEMENTS

The author wishes to express his deep sense of gratitude to Dr. Y. Lee who initiated and supervised the present work. His valuable help, guidance and painstaking discussions which were extremely helpful in getting the end results of this project, are deeply appreciated.

Appreciation is also expressed to the staff members of the Department of Mechanical Engineering, for their interest and encouragement throughout the course of the study.

The financial support for the present study provided by the Atomic Energy Control Board of Canada through the Department of Supply and Services is gratefully acknowledged.

The author wishes to thank those who are especially important to him - his family; his parents and his wife, Anne. The author remembers their sacrifices and encouragement.

TABLE OF CONTENTS

Contents | page

Contents

page

Contents page

LIST OF FIGURES

Figure		Page
4.12	Top Flooding in "L"-shaped Test section	193
5.1	Vapour Velocity Profile in the Vapour Gap	196
5.2	Heat Flux Distribution in the Annulus Gap	197
5.3	Flow Chart	198
6.1(a)	Reproducibility of Test Results ..	199
6.1(b)	Effect of Initial Wall Temperature and Wall Thickness	200
6.1(c)	Effects of Coolant Flow Rate and Inlet Subcooling	201
6.1(d)	Effect of Power Generation	202
6.2	Circumferential Temperature Distributions in Horizontal Flooding	203
6.3 - 6.8	Results of Partial Blockage Test ..	204
6.9 - 6.15	Results of Top Flooding	210
6.16	Pressure Transient	217
6.17 - 6.21	Comparison of Flooding Modes	218
6.22 - 6.23	Effect of Tube Diameter	223
6.24 - 6.25	Rewetting Velocity in Annular Test section	225

Figure		Page

NOMENCLATURE

B	Biot number
C_p	Specific heat
d	Wall thickness
D	Diameter
de	Effective diameter
g	Gravitational constant
G	Mass flow rate
h	Heat transfer coefficient
h_{fg}	Specific heat of evaporation
k	Thermal conductivity
K	Constant in Reichardt equation
L	Distance from the rewetting front
P	Peclet number
P_r	Prandtle number
q	Heat flux
$\dot{q}$	Heat generation rate in the test section
Q	Heat transfer rate in the element
r	Radial distance
R	Radius
R_e	Reynolds number
t	Time
T	Temperature
u	Velocity
U	Rewetting velocity
V	Velocity

x	Axial distance
y	Y-axis, axis through the thickness of the test section
z	Z-axis, axis along the test section
Z_q	Distance from the rewetting front
α	Thermal diffusivity
γ	Void fraction
δ	Wall thickness
ε	Eddy diffusivity
θ_w	Non-dimensionalized temperature, $\frac{T_w - T_s}{T_q - T_s}$
μ	Dynamic viscosity
ν	Kinematic viscosity
π	3.14159
ρ	Mass density
τ	Shear stress

Superscripts

+	Nondimensionalized
*	Actual radius

Subscripts

AX	Axial heat conduction
b	Bulk
e	Effective
EL	Heat generation in the element
H	Heat

HF	Convective heat transfer
i	Inside
ℓ	Liquid
LOSS	Heat loss to the surrounding
m	Maximum velocity
M	Momentum
o	Outside
q	Rewetting
RAD	Radiation heat transfer
s	Saturation
v	Vapour
w	Wall

Chapter I

INTRODUCTION

Rewetting refers to the phenomenon of estabishment of liquid coolant contact with very hot solid surfaces. The rewetting phenomenon is of particular importance during the reflooding phase of emergency core cooling conditions in a reactor.

Since the introduction of nuclear reactor as energy sources, a serious and prolonged public debate has been made on the hazards, real or imaginary, that these systems may present to the environment and the public. Thus, the safety aspects of nuclear reactor design have been continuously subjected to more detailed and exact studies than the usual engineering practice demands.

To avoid or minimize nuclear fuel cladding failure, coolant-cladding contact must be re-established during the reflooding phase of emergency core cooling following a "Loss-of-Coolant Accident" (LOCA) in a water-cooled power reactor. This process is generally referred to as rewetting or quenching.

For the BWR- and PWR-type reactors with vertical fuel rods clustered in a reactor vessel, rewetting is accomplished in emergency cooling by either top spray or bottom reflooding. In the top spray cooling with and without confinement, a liquid film attaches to the upper part of the rods and rewetting takes places at the edge of this film as it slowly moves downwards. In the bottom flooding case, the rewetting front moves at approximately constant velocity as a two-phase mixture rises around the fuel rod, and depending on the coolant flow rate it might be well below the apparent level of liquid or froth. Once the rewetting occurs, the surface heat is removed consecutively by various modes of heat transfer such as, for example, transition boiling, nucleate boiling and convective heat transfer to the liquid. The dry side of the rod experiences in turn forced convective cooling by steam vapour, dispersed-flow film boiling and continuous-film boiling.

A considerable number of works on the rewetting phenomena have been published to date. However, recent reviews on both theoretical and experimental studies show that these studies are all concerned with vertical flows. The rewetting mechanism in the CANDU PWR should differ significantly from that of the light water reactor(LWR) because the structure of the reactor core and the primary heat transport system of the CANDU PWR is quite different from that of the LWR of a pressure vessel type. The coolant flow channels of the CANDU PWR are horizontal, and it is obvious that the two-phase fluid flow and heat transfer are affected by the orientation of the flow channel with respect to the gravitational force field.

In the present study, extensive experiments were performed in various flow channel geometries including horizontal flooding. Also, to observe the mechanisms involved in the rewetting phenomena, a visual study was carried out with eight different types of flooding modes. The objective of this thesis is to obtain a better understanding of the mechanisms involved in all rewetting phenomena by carrying out extensive experimental work including visual studies, together with detailed numerical analysis to identify the dominant parameters affecting the rewetting process. The author's previous analysis[1] together with experimental data in different flooding modes, flow geometries and shapes of the test section show that the two most important parameters which affect the rewetting process in confined flow spaces are the precursory cooling just ahead of the rewetting front, and the rewetting temperature, Tq. Therefore, a theoretical analysis is carried out to obtain more accurate heat transfer coefficients in the inverted annular flow region during the rewetting process. In the analysis, the vapour flow in the inverted annular flow region is considered as a flow between a concentric annulus with the inner boundary moving at the liquid velocity.

Chapter II
LITERATURE SURVEY

The systems used for Emergency-Core-Cooling(ECC) depend on the reactor designs. While the bottom flooding with water is employed in the pressurized water cooled reactors (PWR), the bottom flooding is supplemented with top spraying in the boiling water reactors (BWR).

In Canadian pressurized heavy water reactors (CANDU PWR), ECC water is injected into individual horizontal pressure tubes through the headers by feeder pipes.

The surface temperature of a given location in the core fuel bundles during the reflooding/rewetting transient may go through a maximum as illustrated in Fig.2.1, because it cannot decrease until the heat removal exceeds the heat generation. The maximum is generally known as the turn-around temperature and the corresponding time the turn-around time. The rate of the subsequent temperature decrease after the turn-around depends on the flooding modes employed and reaching a certain point, a sudden drop in temperature in the order of hundreds of degrees in a very short period can be observed, if the temperature is greater than the rewetting temperature.

The physical mechanisms of this sudden temperature drop, which is known as the rewetting process (also referred to as apparent rewetting, quenching, calefaction or sputtering) are still not clear. However, the corresponding temperature is not the Leidenfrost temperature. The rewetting temperature in this thesis is defined as the temperature which was obtained by intersecting the tangent just before the rewetting process to the tangent at the steepest point of the wall temperature versus time traces as shown in Fig.2.1.

The lack of understanding of how the phenomenon is initiated made it necessary to use various analytical models to provide functional relationships among the many governing variables as well as many experimental investigations to obtain some quantitative data.

A considerable number of studies on the subject have been published in recent years and several extensive review papers on both analytical and experimental studies are available in both open and some limited-circulation literature[2-5]. This review will summarize what has been achieved and will provide the most recent developments in the field of rewetting phenomena.

2.1 EXPERIMENTAL STUDIES

The experimental data for top spray cooling and bottom reflooding show a complicated dependence of the rewetting front velocity on various system variables such as wall temperature, coolant flow rate and subcooling, pressure, wall material and surface condition. Duffey and Porthouse[6] compared their experimental data of both top spray cooling and bottom flooding and found that for the same rod material and dimensions, mass flow rate and rod temperature, the rewetting rates are similar for both a falling film in an unconfined flow space and bottom flooding. They concluded that the physical processes involved in the rewetting of high temperature surfaces are identical for both falling water films and bottom flooding. However, the results of the present study, as will be seen, indicate that there is a significant difference in the rewetting velocities between the unconfined top flooding (falling water film) and bottom flooding. This is understandable because the rewetting processes involved in the unconfined top flooding and bottom flooding are quite different. In bottom flooding, precursory cooling ahead of the rewetting front plays a major role while in the unconfined top flooding, there is very little precursory cooling.

A brief review on the experimental studies is categorized by flooding mode as top flooding, bottom flooding and horizontal flooding.

2.1.1 Top Flooding

With top-spray cooling of a single rod with no flow confinement, very poor heat transfer may exist downstream of the quench front and in this case axial conduction will clearly dominate. However, when the rods are confined in a flow channel and cooled by a spray entering from the top of the bundle, a counter current flow of rising steam and falling droplets and liquid film is created. If the rising steam velocity exceeds a certain critical velocity, the progression of the liquid film is halted and the droplets may be prevented from falling downwards. In this case the progression of the quench front will also be hydrodynamically controlled. This situation was examined by Chan and Grolmes[7].

Duffey and Porthouse[8] carried out a visual study of the top spray cooling without confinement using high-speed photography. Their study shows that there is a narrow region of vigorous nucleate boiling immediately behind the rewetting front. In this nucleate boiling region, an aerosol of droplets of diameter of 0.5 mm and less is produced, caused by the nucleate boiling. Duffey and Porthouse[8] also observed that at low liquid flows the liquid running down the surface did so as a rivulet rather than as a continuous film. This was also observed by Yu et al.[9]. Duffey and Porthouse[8] attributed this to variations in surface conditions and vertical alignment.

Duffey and Porthouse[8] and Bennett et al.[10] studied the effect of wall temperature on quench front velocity and found that increasing the initial wall temperature decreases the rewetting velocity. Bennett et al.[10] plotted the inverse rewetting velocity against the tube wall temperature and found that the inverse of the rewetting velocity increased linearly with the tube wall temperature for temperature above a certain critical value. However, Duffey and Porthouse[8] found a slight tendency for the slope to increase with temperature when the data were plotted in this way. For temperatures below the critical value, the rewetting velocity appears not to depend on wall temperature. This critical temperature was defined by Bennett et al.[10] as the sputtering temperature.

In the high pressure and steam environment test, the study of flow rate effects by Elliott and Rose[11] in which tests were conducted at four different flow rates showed that there was no flow rate effect on rewetting velocity. Thompson[12] also found that the rewetting rate is independent of cooling water flow rate when the environment is steam and the pressure greater than atmospheric. A very comprehensive investigation of liquid flow effects at low pressure and air environment was that of Duffey and Porthouse[8] and their results show that the rewetting velocity increases as the liquid flow rate increases. Yu et al.[9] claim that the main reason for this difference is that in the atmospheric tests the water at the quench front is subcooled, whereas, in steam environment test the water is saturated at the quench front.

Yoshioka and Hasegawa[13] conducted low pressure tests in an air environment in which they changed the subcooling of injected liquid and observed a significant increase in rewetting velocity with increasing subcooling. This was also observed by Yu et al.[9]. It was suggested by Piggot and Porthouse[14] that the observed effect results from an increase in heat transfer coefficient with subcooling behind the quench front. Thompson[12], however, argued that the effect is due to an increase in the rewetting temperature with water subcooling at the quench front.

The systematic investigation of system pressure have usually been confined to small subcoolings for the injected liquid. The test of Bennett et al.[10] and Elliott and Rose[11] show that the rewetting velocity increases with increasing pressure. Thompson[12] also confirms this fact, but he argues that the increase in rewetting rate with pressure is due to an increase in sputtering temperature, not due to an increase in heat flux in the vicinity of the interface. The top spray experiment by Naitoh[15] agrees with this. Naitoh[15] observed no system pressure effect on the heat transfer coefficients.

Piggott and Duffey[16] observed from their experimental data that their Zircalloy tube rewetted faster than the empty stainless steel tube by a factor of about 2 at the highest flows and 2.8 at the lowest flows. This is in agreement with theoretical investigations[12,17,18,19,20] which show that rewetting velocity is inversely proportional to the cladding volumetric specific heat.

Elliott and Rose[11] also did a systematic investigation of different materials, in which other variables were kept constant. They repeated the experiments with Inconel, stainless steel and Zircaloy. Initially, they found no significant difference between the inconel and stainless steel tests. However, they conducted further tests with another stainless steel tube and found a significant increase in rewetting velocity. They concluded that these differences are likely due to changes in surface conditions with time. The rewetting velocities obtained with the Zircaloy tube were found to be higher than those for the other tubes. Piggott and Porthouse[14] and Yu et al.[9] also observed a tendency for the rewetting rate to increase with successive tests and have attributed this increase to the build up of deposits on the surface. However, Bennett et al.[10] observed the opposite effect. They found a substantial reduction in the rewetting rate with a heavily oxidised surface. Therefore, it is possible that surface deposits can affect the rewetting process in two ways which result in opposite effects. The increased roughness for an oxidised surface could increase the wet-side coefficient and therefore improve the heat transfer. On the other hand the deposit inserts an extra thermal resistance which could more than offset the improvement in the coefficients.

The effect of surface finish was studied by Piggott and Porthouse[14]. They artificially changed the nature of the surface by shot blasting and by silver plating. The shot blasting caused the rewetting velocity to increase by a factor of three while silver plating halved the velocity. Piggott and Duffey[16] also did the falling film experiments with three different surface finishes, original, silver-plated and shot-blasted. They obtained results similar to those of Piggott and Porthouse[14]. As explanation for these observations given by Dua and Tien[21] is that the surface roughness increases the wet-front velocity by manifesting its effect in the increased rewetting temperature and the enhanced cooling effectiveness in the sputtering region.

Dua and Tien[21] did an experimental study of rewetting of a copper tube by a falling film of liquid nitrogen. They compared their data of smooth-surface and rough-surface experiments, and found that the rewetting temperature and the heat flux for a smooth surface is lower than that for a rough surface. The increase of the rewetting temperature with surface roughness implies that it is easier to rewet a rough surface than it is to rewet a smooth surface. A plausible physical explanation for this effect comes from the fact that a rough surface tends to break or destroy the vapor film and thus facilitate the direct contact between the liquid film and the hot surface.

Yu et al.[9] carried out falling film experiment with saturated water in a steam environment and observed that leaving the electrical power on or turning it off during a run did not affect the result. This confirms the finding of Bennett et al.[10]. The argument is that the heat fluxes around the quench front are very much higher than the fluxes due to the electrical input. Although low electrical fluxes do not affect the heat transfer processes in the region of the quench front, they do affect the heat transfer remote from the quench front where the fluxes due to stored heat in the rod are much lower. When the experiment was performed with subcooled water in an atmospheric environment, the rewetting velocity was observed to be decreasing with increasing power input during the experiment. Thus, Yu et al.[9] found it necessary to include the heat input from the rod power in the calculation of subcooling at the quench front. However, from our study, it is found that this correction of the coolant subcooling due to power generation in the rod is almost negligible. Rather, the power input during the transient is expected to affect the wall temperature ahead of the rewetting front.

Simopoulos et al.[22] used a low-pressure Freon-113 loop to simulate two-phase high-pressure water flow phenomena. Their experimental results show the same trends as the other results using water in a steam environment and confirm the feasibility of simulating rewetting phenomena in water by the use of Freon. They observed that the inverse rewetting rate increases almost linearly with the initial wall temperature and the rewetting rate increases with the system pressure, which behaviour is similar to that of water. They found no evidence of a significant liquid flow rate effect on rewetting velocity. This is in agreement with other results on water in steam environment.

2.1.2 Bottom Flooding

Visual studies of bottom flooding were performed by Duffey and Porthouse[6], Case et al.[23], and Kaminaga and Uchida[24]. All three papers describe observations made in an annulus with a hot central tube. They all describe a region of nucleate boiling behind the quench front but there are differences in the description of the behaviour ahead of the quench front. Duffey and Porthouse's description is, "the excess fluid passing the quench front formed a dispersed flow region of liquid and vapour coupled with film boiling". Case et al.[23], however, described an extensive "film boiling" region ahead of the quench front which breaks down to give a "mist flow" region at a distance of the order of 10 to 200 mm ahead of the quench front (the distance grows as the quench front moves up the channel). Kaminaga and Uchida[24] also described extensive film boiling. They observed that immediately after the coolant reached a heated section, boiling occurred and vapour bubbles were generated over the flow area, and since the liquid level advanced at a higher speed than the quench front did, the boiling region was lengthened with time. They also found that nucleate boiling did not occur uniformly in the radial direction of the rod, but a wavy distribution on the heated rod existed to connect circumferential incipient boiling points. They proposed that the change in heat transfer regimes at a given location of the heated rod during bottom flooding follows the sequence of vapour cooling, film boiling, nucleate boiling and liquid forced convection.

Andreoni and Courtaud[25] also conducted visual studies of bottom flooding and noted that it was possible for permanent wetting to occur ahead of the quench front where there was a heat sink. It occurred at the busbar at the top of the test section or where there were support grids for the centre rod. This gave rise to quenching with a falling film as is the case with top flooding. Thus a quench front travelling up the channel would meet a quench front travelling down the channel. This was also observed by Yu et al.[9]. In their case, they found the presence of a falling film rewetting front initiated on the cold tubing near the top current clamp. In some cases this film extended well down the test section.

Duffey and Porthouse[6,18] and Case et al.[23] observed that the quench front proceeded at a uniform velocity along the channel. This finding was confirmed by some of the tests of Andreoni and Courtaud[25] but in other tests the velocity fell as the front proceeded along the channel. They attributed this reduction in velocity to the raising in temperature of the liquid which reached the quench front. This velocity reduction has also been observed by Campanile and Pozzi[26] and Martini and Premoli[27]. This change in velocity appears to depend on the liquid input flow rate and temperature, and on the initial wall temperature. Andreoni and Courtaud[25] and Martini and Premoli[27] found that the quench front velocity becomes more uniform as the flow rate is increased, as the inlet liquid subcooling is increased or as the initial wall temperature is increased.

To study the effect of channel geometry, Duffey and Porthouse[18] conducted experiments in an annulus with a hot centre tube in which they changed the flow area by changing the outer tube diameter. Their results indicate that, for the same inlet liquid velocity, there is a small decrease in quench time with increasing flow area and that this decrease in quench time is more marked at high initial wall temperatures. The results of Case et al.[23] also show a decrease in quench time with a larger flow area when comparisons are made at the same inlet velocity.

Increase in rewetting time with increasing initial wall temperature have been observed by many experimenters[14,18,23-29]. However, the degree of dependency of rewetting time on the wall temperature is different among workers. Thompson[28] observed a very sharp increase in rewetting time with initial wall temperature in tests on a simulated CANDU reactor bundle. On the other hand, Reidle and Winkler[29], working with a simulated PWR bundle, observed only a small effect of rewetting time on initial wall temperature. This difference is probably due partially to the difference in channel geometry which affects the cooling effect ahead of the quenching front.

All experimenters observed that the rewetting velocity increased with increasing flooding flow rate. Duffey and Porthouse[18] suggested that this flow rate effect results from increasing the wet side heat transfer coefficient with higher inlet flows. This improves the rate of axial heat conduction and hence leads to a faster rewetting rate. Thompson[12] on the other hand, suggested that the inlet flow rate affects precooling on the dry side rather than the heat transfer in the wet side.

Nearly all experimenters have found that the quench front velocity is less than the coolant supply velocity. However, Duffey and Porthouse[18] observed that sometimes rewetting velocities are higher than supply velocities. Possibly, due to the inlet quality, there are sometimes vapour voids behind the rewetting front, and these vapour voids are giving effectively a higher supply velocity.

All experimenters except Martini and Premoli[27] have observed a decrease in quench time with increasing inlet subcooling. Yu et al.[9] found that the use of subcooled water in bottom flooding had a much greater effect than had been the case with the falling film. This is possibly due to vapour condensation at the quench front by the bulk liquid. However, Martini and Premoli[27] observed a definite decrease in quench time with subcooling at atmospheric pressure but at pressures from 5 to 20 bar there was very little effect of subcooling. They did not provide any explanation for this difference in behaviour at different pressure. It must be that the dependence of subcooling at the high pressure (hence high saturation temperature) is too small to be noticed in the scatter of the experimental data.

Piggott and Porthouse[14,30] conducted a series of tests at atmospheric pressure with a range of inlet subcoolings from 14 to 78 C. They found the results for different flow rates and subcoolings came together when plotted in the form of inverse rewetting velocity against flow rate multiplied by subcooling.

Test have been conducted with claddings of stainless steel, inconel, Zircaloy, silica and copper to study the effect of cladding materials. Case et al.[23] repeated similar tests with copper and stainless steel cladding in an annular test section and they found that the rewetting velocity is higher with the copper tube. Cadek et al.[31] repeated experimental tests with both Zircaloy and stainless steel cladding in a simulated PWR test section. They found the quench times for Zircaloy cladding to be shorter than for stainless steel. They attributed this to the lower heat capacity of the Zircaloy. However, Piggott and Duffey[16] observed that the effects of changing the cladding or filler material were smaller than those noted in the falling film experiments. Our present study with both the stainless and inconel test-sections for all three modes of flooding showed that the rewetting velocities of inconel test-sections were faster than those of stainless steel test-sections. The higher rewetting velocity of the inconel test-section is mainly due to its higher thermal conductivity, k, and lower volumetric heat capacity, Cp ρ. It seems that the values of Biot numbers for practical purposes are rather small. Therefore, the qualitative effect of thermal conductivity and volumetric heat capacity of the test-section can be deduced from a simple one-dimensional analysis such as proposed by Yamanouchi[37]. That is:

$$P = B^{0.5} \left(\frac{T_w - T_q}{T_q - T_s} \right)$$

It must be also pointed out that the rewetting temperature is also affected by Cp ρ and k which, in turn, affect the rewetting process.

To study the effect of surface finish, Piggott and Duffey[16] did the bottom flooding experiment with three different surface finishes: original, silver-plated and shot blasted. They found that surface finish does not affect bottom flooding quench rate significantly.

Piggott and Duffey[16] did water temperature measurements during the bottom flooding experiments. The water temperatures were measured as the quench front passed the mid-point of the measuring section. Their measurements show that ~~at~~ low flow rates the water at the quench front is saturated and at higher flows the subcooling at the quench front is approximately proportional to the flow rate.

Lauer and Hufschmidt[32] did an experimental investigation of the heat transfer in the vicinity of the quench front and the rewetting temperature in bottom flooding with a thick-walled stainless steel cylindrical rod. They made the flooding area very large to minimize the precooling effects due to evaporation. The heat flux density was obtained from the gradient of the transient temperature at the rod surface. They observed that the flooding rate and system pressure did not affect significantly the transient boiling heat transfer and the rewetting temperature in their range of parameters. However, they observed a strong influence of local fluid subcooling on the transient film boiling heat transfer and rewetting temperature. Higher values of heat flux density and rewetting temperature were achieved with increasing fluid subcooling. This can be explained with a thinned vapour film due to the strong increase of heat transfer at the vapour-liquid boundary.

A large number of atmospheric-pressure data obtained from an internally-cooled tubular test section undergoing bottom reflooding were examined by Yu and Yadigaroglu[33] in order to determine the dependence of the heat transfer coefficient in the region immediately downstream of the quench front. They observed from their data an exponential decay of the heat transfer coefficient with distance from the quench front. Based on this finding, they adopted

$$h = h_q \cdot \exp(-a \cdot d \cdot z_q)$$

as the form of empirical correlation of the heat transfer coefficient immediately downstream of the quench front during bottom reflooding. The coefficients h_q and "a" depend on conditions at the quench front only.. The variation of the coefficients h_q and "a" was each correlated in terms of physically controlling parameters. The best-fit correlation was as a function of parameters combining the reflooding velocity, the velocity of the quench front, the equilibrium quality rise due to release of the energy stored in the wall by the passage of the quench front, and the local equilibrium quality just upstream of the quench front. Yu and Yadigaroglu[33] observed that heat transfer downstream of the quench front increases both with subcooling in the subcooled region and with quality in the positive-quality region. The effect of subcooling was also observed by Lauer and Hufschmidt[32]. The increase of heat transfer with quality in the positive-quality range is probably due to the increase of the steam velocity with quality. Their experimental data and proposed correlation show no explicit dependence on wall temperature.

Yadigaroglu[34] observed that increasing the flooding rate reduces the quench time and enhances heat transfer throughout the transient. This influence is due to the introduction of larger quantities of liquid into the channel and to the increase in liquid entrainment. They found that the effect of flooding rate is important at low flooding rates but becomes less pronounced as the flooding velocity increases. They also observed that an increase in power increases the quench time at low flooding rates, but the effect is much less pronounced at high flooding rates.

Kaminaga and Uchida[24] measured coolant temperature and inner surface temperature of the outer quartz tube in their annular geometry bottom flooding experiment. Their results show that before the liquid level reaches a certain point, the fluid in the channel is superheated steam (about 300 C), and between the liquid level and the quench front (in the film boiling region), the coolant temperature is nearly constant (94-95 C) and almost uniform over the flow area even if the inlet coolant temperature was as low as 20 C. The coolant temperature below the quench front (in the liquid forced convection region) is slightly higher than the inlet value. This indicates that a large amount of heat was transferred to the coolant around the quench front and the boiling caused the coolant to be mixed due to a small flow area. They also measured the rewetting temperature and they observed that the rewetting temperature decreases with an increasing elevation, although measured values have a large amount of scatter, and it decreases with an increasing inlet coolant temperature.

2.1.3 Horizontal Flooding

The most important difference in the characteristic of the horizontal flooding is the stratified nature of the coolant flow. Obviously, this is due to the effect of the channel orientation to the gravitational field. For horizontal flooding, due to flow stratification, the channel is quenched in the sequence of bottom, midside and top at a given location. Also, due to the gravitational effect there are three distinctive regions near the rewetting front: the totally rewetted, the partially rewetted and a skewed invert annular region.

To the author's knowledge, the present research project initiated early in 1976 was the first to study the effect of channel orientation. In 1980, Chan and Banerjee[35] presented their results of a horizontal flooding experiment. They performed an experimental study on the rewetting of a hot horizontal tube using 2-meter long Zircaloy-2 tube as the test section because of its relatively low thermal expansion coefficient. They observed from their experiment that the rewetting front is highly stratified and the top of the channel at different locations always rewet later than the bottom. This re-confirms the finding of our experimental study. The bottom region of the channel is precooled significantly before quenching because of stable film boiling. From the experimental results obtained, Chan and Banerjee[35] defined three rewetting velocities with respect to the quenching of the top, mid-side and bottom of the channel. They found that the three rewetting velocities in general are not equal and deviate more from each other at high inlet flow rates. Our study[1] also shows that the rewetting velocities at the top and bottom of the channel are different in horizontal flooding. However, contrary to the findings of Chan and Banerjee[35], our result shows that the difference in rewetting velocity decreases with increasing coolant inlet flow rate.

Chan and Banerjee[35] found that the rewetting velocity decreases as the initial dry wall temperature increases which is in agreement with all existing investigations for vertical channel flooding. They obtained a linear relationship when the inverse rewetting velocity is plotted against the initial dry wall temperature.

For the effect of inlet flow rate on rewetting velocity, they found that the rewetting velocity increases as inlet flow rate increases. This is also in agreement with other vertical experiments. Their explanation for this effect is that an increase in inlet flow rate increases the amount of water entrained in the "liquid tongue" and hence increases the film boiling heat transfer in the dry region.

Chan and Banerjee[35] observed an interesting phenomenon in their experimental result. Under certain conditions the rewetting velocity can be higher than the inlet flow velocity. They observed this when both inlet flow rate and initial wall temperature are low. Their explanation for this phenomenon is that at the start of the transients, water is directed into the heated section with a constant flow rate, and since the channel is dry, the flow is stratified and the leading edge can acquire a velocity considerably higher than the inlet flow velocity; this high leading edge velocity, together with low wall temperature, can result in a rewetting velocity higher than the inlet flow velocity.

They observed that the effect of inlet water subcooling changes depending on the initial wall temperature. For high wall temperatures, the rewetting velocities are lower for lower inlet water subcooling. The opposite is true for lower wall temperatures. They gave no clear reason for this effect.

2.2 REVIEW OF ANALYTICAL WORK

The analysis of the rewetting phenomenon involves the solution of the coupled equations of heat diffusion within the surface and of fluid flow and coolant boiling heat transfer. All analytical models of the rewetting process have a common basis. They solved the Fourier equation for heat conduction in the rod by assuming simplified boundary conditions which represent the heat transfer process at the solid surface. Various procedures have been proposed for the solution of the Fourier conduction equation for a wall undergoing rewetting. Published models of the rewetting process include simple one-dimensional solutions in two axial regions, one-dimensional solutions in three axial regions with or without precursory cooling, one, two and three dimensional numerical-difference techniques using temperature dependent heat transfer coefficient, and analytical two-dimensional solutions.

All these models cannot be directly compared to experimental data because numerical values must be assigned to the rewetting temperature, Tq, and the effective heat transfer coefficient, h, in the solutions. Therefore, in order to apply any of the listed models to a practical case, the values of the rewetting temperature and the heat transfer coefficient must be assumed or usually deduced from the steady-state pool boiling curves. These values are very difficult to estimate in most cases. The uncertainties involved in the estimation can easily override the accuracy obtained by a given model.

The following assumptions are usually made to make the problem easier to solve.

1. The wall is a homogeneous lamina of infinite height and uniform thickness, d, having constant physical and thermal properties.
2. The rewetting front velocity, U, is constant and the temperature distribution is invariant with respect to the advancing quench front.
3. The dry side of the wall is insulated while the wet side is cooled.
4. There is no heat generation in the wall.
5. The reference coolant temperature is constant and equal to the saturation temperature T_S.

The second assumption is justified in most cases since it has been shown that for a surface at a uniform initial temperature the quenching front reaches an asymptotic constant velocity very rapidly[36]. This allows the removal of the time variable which is combined with the axial coordinates Z in a new independent variable. Assumptions 3 to 5 are not general assumptions and not used in some cases. With the above assumptions the governing equation reduces to :

$$\frac{\partial^2 T}{\partial y^2} + \frac{\partial^2 T}{\partial z^2} + \frac{\rho C_p \cdot u}{k} \cdot \frac{\partial T}{\partial z} = 0 \quad \ldots\ldots\ldots\ldots (2.1)$$

The boundary conditions are :

$T = Ts$ at $Z = -\text{infinity}$ ....(2.2a)

$T = Tw$ at $Z = +\text{infinity}$ ....(2.2b)

$\frac{\partial T}{\partial y} = 0$ at $y = 0$ ....(2.2c)

$-k\left(\frac{\partial T}{\partial y}\right) = h(T - T_s)$ at $y = d$ ....(2.2d)

The rewetting temperature enters in the solution of the problem as the temperature at which a discontinuity in the variation of h occurs.

Equation (2.1) and four boundary conditions(2.2a-2.2d) determine the complete two-dimensional problem. One-dimensional solutions are obtained by ignoring any transverse temperature gradients in the wall and assuming that the temperature is uniform throughout its thickness. This assumption holds only for thin walls (B < 1) and low values of the heat transfer coefficient, h, and of the quench velocity.(i.e. for small Peclet and Biot numbers)

2.2.1 One-dimensional Solutions

One-dimensional solutions of the quenching problem consist of dividing the wall axially into a number of regions, and the heat transfer coefficient being specified in each region. The only differences among the various available solutions stem from the assumed variation of the heat transfer coefficient with temperature and the number of regions used.

One-dimensional solutions were proposed first by Semeria and Martinet[17] and by Yamanouchi[37]. The wall was divided axially into a wet and a dry region. The heat transfer coefficient was considered to be constant in the wet region and zero on the dry surface ahead of the quench-front. In this case the rewetting velocity can be analytically determined as :

$$u^{-1} = \frac{\rho C_p}{2}\sqrt{\frac{d}{hk}}\sqrt{\left[\frac{2(T_w - T_g)}{T_g - T_s} + 1\right]^2 - 1} \quad \ldots\ldots\ldots\ldots (2.3)$$

In an attempt to account for the high value of the heat transfer coefficient near the quench front, Sun et al.[38] developed a solution for three distinct regions. A dry and adiabatic region ahead of the rewetting front, a sputtering region immediately behind the rewetting front and a continuous liquid film region further upstream.

Another one-dimensional solution was recently presented by Sun et al.[39] to account for cooling by droplets and vapor in the region immediately ahead of the wetting front. The effect of this precursory cooling is characterized by a heat transfer coefficient decaying exponentially with distance from the rewetting front. An implicit solution was obtained for the dimensionless rewetting front velocity by introducing two parameters, N and a, to define the shape of the heat transfer coefficient, downstream of the rewetting front,

$$h_3 = \frac{h_2}{N} \cdot e^{-az} \qquad (2.4)$$

As N approaches infinity the solution approaches the values predicted by Yamanouchi[37]. Sun et al.[39] used this model to correlate high flow rate data obtained by Duffey and Porthouse[8] by adjusting the value of N according to the flow rate. An empirical correlation is suggested for N as a function of mass flow rate:

$$N = 800 \cdot G^{-1.4} \qquad (2.5)$$

where G in g/cm.s is the spray flow rate per unit perimeter. However, the effect of precursory cooling in low quench rate experiments that can be predicted by a one-dimensional model might be usually negligible.

Chun and Chon[40] proposed a three-region model which consists of one wetted region characterized by a high constant heat transfer coefficient, a dispersed-flow film boiling region precooled by a lower heat transfer coefficient and a superheated-vapor region which is assigned a negligibly small heat transfer coefficient. The temperature profile in the wet region is obtained by solving the governing equation, while a linear temperature profile is assumed in the dispersed-flow region, and a constant temperature in the superheated region. The continuity equation for the coolant is used with a simple heat balance to calculate the amount of water in the dispersed-flow region and the degree of superheat in the vapour region. The rewetting front velocity is calculated by a total heat balance over the test section. The results are sensitive to the values of the parameters used.

Piggott and Porthouse[30] showed in their thermal conduction analysis of rewetting, that the heat transfer coefficient associated with rewetting may be taken as an arbitrary function of surface temperature, rather than a constant, without changing the dependency of rewetting velocity on the other variables. Therefore, they suggest that the constant heat transfer coefficient value used in previous expressions for the rewetting velocity should be replaced by an effective heat transfer coefficient which is proportional to the product of mass flow rate and inlet subcooling.

Duncan and Leonard[41] extended the one-dimensional solution of Yamanouchi[37] to a more general case by the inclusion of a uniform heat generation term. The following expression was obtained for the inverse rewetting velocity:

$$u^{-1} = \rho \cdot C_p \cdot \sqrt{\frac{d}{hk}} \cdot \frac{(T_w - T_q)}{(T_q - T_s - \dot{q}/h)} \qquad (2.6)$$

This result implies that the liquid film will not advance(ie. U=0) if the surface heat flux is such that the surface temperature is maintained above the rewetting temperature, which is a physically expected result. In practice, heat is generated only in the core of the fuel rod and a two-dimensional analysis is needed to investigate the effects of heat generation on the rewetting velocity.

Thompson[12] argues, based on his analysis, that only a certain wall thickness takes part in the rewetting process, and this critical thickness depends on thermal conductivity, dry region surface temperature, and ambient pressure. However, for practical purposes he suggests that the critical thickness can be considered to be about 0.5 mm for rewetting in a steam environment. He also argues that thermal conductivity is important only if the wall thickness is less than the critical thickness.

To eliminate to some extent the basic assumption of uniform temperature throughout the wall thickness and still maintain the mathematical simplicity of a one-dimensional solution, Ishii[42] used the penetration depth, δ, as an effective wall thickness in the sputtering region. The results of this model depend on the accuracy of estimating the penetration depth δ.

In general, heat transfer analysis by one-dimensional models results in overestimation of the rewetting temperature and of the wet-region heat transfer coefficient when used to correlate experimental data obtained at high Peclet and Biot numbers.

2.2.2 Two-dimensional Solutions

Semeria and Martinet[17] formulated the two-dimensional problem even before the first solutions became available. The mathematical complications involved in an exact two-dimensional solution have forced most of the investigators[19,20,43] to deal with no more than two axial heat transfer regions. However, recently Dua and Tien[44] included the effect of precursory cooling in the two dimensional problem.

A general solution to the two-dimensional conduction equation may be obtained by separation of variables. This approach was used by Duffey and Porthouse[6,18], who solved Eq.(2.1) for $h = 0$ in the hot region and $h =$ constant in the wetted region. The temperature distribution is given by:

$$T(y,z) = K + \sum^{N} (A_n \cdot \sin\beta_n \cdot y + B_n \cdot \cos\beta_n \cdot y) \cdot \left\{ C_n \cdot \exp\left[z \cdot \left(-p^* + \sqrt{p^{*2} + \beta_n^2}\right)\right] + D_n \cdot \exp\left[z \cdot \left(-p^* - \sqrt{p^{*2} + \beta_n^2}\right)\right] \right\} \quad \cdots\cdots (2.7)$$

where $p^* = \frac{\rho C_p \cdot u}{2k} = \frac{P}{2d}$

k = thermal conductivity , P = Peclet number

An,Bn,Cn,Dn, and K are constants and β_n is the separation constant. The rewetting velocity was obtained by neglecting all terms but the first in the series. This approximation was shown later to lead to inaccuracies by Blair[26]. For small Biot numbers, the first-order solution reduces to the one-dimensional solution of Yamanouchi[37]. For large Biot numbers (B >> 1):

$$u^{-1} = \frac{\pi \rho C_p \cdot \theta_w}{2h} \quad \cdots\cdots\cdots\cdots\cdots\cdots\cdots\cdots (2.8)$$

which is independent of the thickness of the cladding and of thermal conductivity. Duffey and Porthouse[6] also considered the transition between these two extremes.

A more accurate solution by separation of variables is presented by Coney[19]. The constants of the series expansion were calculated by matching the temperature and axial heat flux distributions in the wet and dry regions at a large number (up to 150) of discrete interface points. Coney's results can be approximated by

$$\frac{B}{P} = 1.6 \left(\frac{T_w - T_s}{T_g - T_s} \right) \cdot \left(\frac{T_w - T_s}{T_g - T_s} - 1 \right) \quad \cdots\cdots\cdots\cdots (2.9)$$

provided (B/P)<1. The formula remains approximately valid at higher values of (B/P).

The two-dimensional solution for a cylindrical rod is given by Blair[43]. As in the planar case the method of separation of variables is used to construct two infinite series expansions for the temperature in the wet and dry regions of the rod. The coefficients of the series are found again by matching the temperature and their axial derivatives at the quench front interface. All the terms are retained by deriving an accurate asymptotic formula for the terms which are then summed analytically. The resulting asymptotic solution for P>1 and (B/P)<1 is:

$$\frac{T_w - T_s}{T_g - T_s} \approx 1 + \frac{B}{\pi P}\left(2 + \frac{\pi}{2P} + \frac{2}{P^2}\right) + \frac{B^2}{2\pi^2 P^2}\left(\frac{8}{3} - \pi^2 - \frac{13\pi}{6P}\right) \qquad (2.10)$$

For P>>1 the first order approximation of Eq.(2.10) yields:

$$u^{-1} = \frac{\pi \rho C_p}{2h}\left(\frac{T_w - T_g}{T_g - T_s}\right) \qquad (2.11)$$

which is different from the solution of Duffey and Porthouse[6,18]. The discrepancy is attributed to the fact that Duffey and Porthouse used only the first term of the expansion.

Explicit solutions for the limiting cases of large and small Peclet numbers were obtained by Tien and Yao[20] who utilized the Wiener-Hopf technique and the kernel-substitution method. Functional relationships among the three dimensionless parameters are presented for the two-region model with no precursory cooling. The solution for small Peclet numbers reduces to :

$$\frac{A}{P} = \frac{\theta_o}{1-\theta_o} \qquad \cdots\cdots\cdots\cdots\cdots\cdots\cdots\cdots\cdots (2.12)$$

where $\theta_o = \dfrac{T_w - T_g}{T_w - T_s}$ and $A = \dfrac{3B}{3+B}$

while for large Peclet numbers,

$$\frac{B}{P} = 1.707\left(\frac{\theta_o}{1-\theta_o}\right) + 1.457\left(\frac{\theta_o}{1-\theta_o}\right)^2 \cdots\cdots\cdots (2.13)$$

Yao[45] developed an expression taking the heat generation and heat convection in the dry and wet region into consideration. His expression involves five parameters. In his analysis, Yao[45] assumes that the dry region is surrounded by steam which is superheated to the initial wall temperature. Therefore, heat is convected from the steam to the surface in the dry region instead of from the surface to the steam. Consequently, this model predicts that the rewetting rate decreases as the dry side heat transfer coefficient increases. If heat generation in both the wet and dry region, and heat convection in the dry region is neglected(ie. $Q \approx 0$, $h_d \approx 0$), then his expression reduces to the two-dimensional conduction model of Tien and Yao[20] for small Peclet numbers.

Dua and Tien[46], following the earlier work of Andersen and Hansen[47] found approximate relationships between a modified Biot number and the Peclet number. The modified Biot number $\bar{B}$ is defined as

$$\bar{B} = B \cdot \frac{(1-\theta_o)^2}{\theta_o} \quad \text{where} \quad \theta_o = \frac{T_w - T_g}{T_w - T_s} \quad \cdots\cdots\cdots (2.14)$$

Using these relationships they have fitted the theoretical results of Tien and Yao[20] by an expression valid over the entire range of Biot numbers,

$$P = [\, \bar{B}\,(1 + 0.40 \cdot \bar{B}\,)^{1/2} \quad \cdots\cdots\cdots\cdots\cdots\cdots\cdots (2.15)$$

This formula agrees with the theoretical results at the limits B >> 1 and B << 1, provides an approximate interpolation for intermediate values of B, and could be useful for practical applications.

Solutions of the two-region, two-dimensional problem were also proposed by Yoshioka and Hasegawa[48]. However, in their solution, the radial temperature distribution at the location of the quench front was assumed instead of being calculated.

Edwards and Mather[49] considered exponential variation of the heat fluxes both upstream and downstream of the rewetting front. This assumption completely decouples the heat transfer inside the wall from heat transfer to the coolant but permits an exact solution. Their study demonstrates an increase in the rewetting front velocity due to heat losses immediately ahead of the quench front. The exponential coefficient for the upstream (hot) region has been taken as inversely proportional to the Peclet number. Dua and Tien[44] accounted for the effect of precursory cooling by assuming a constant heat transfer coefficient in the wet region, while precursory cooling was characterized by an exponentially decaying heat flux.

Sawan et al.[50] developed an expression using two wet regions plus a dry region with zero heat transfer coefficient, and two reference temperatures (the incipient boiling temperature and the sputtering temperature). Heat generation and inlet subcooling are also taken into account. They obtained a parametric expression involving 8 parameters.

Bonakdar and McAssey[51] presented a method for the solution of the two-dimensional rewetting conduction problem with an arbitrary heat transfer coefficient profile. They assumed that the coolant fluid temperature is constant and the heat transfer coefficient is a function of axial position. Their analysis divides the general heat transfer coefficient profile into several uniform heat transfer regions. The two-dimensional conduction equation is solved using the method of separation of variables into a series expansion solution for each uniform heat transfer coefficient region. The complete solution is then determined by matching the temperature and the temperature gradient at the interfaces between regions. They also obtained numerical results for a three region model involving a dry, wet and sputtering region. From these numerical results, they proposed the following conclusions : (1) A very short sputtering region will control the rewetting process. (2) For the case examined, a linear relationship exists between the heat transfer coefficient in the sputtering region and the rewetting temperature. (3) Two dimensional effects exist upstream of the rewetting front for approximately two to three slab thicknesses. (4) For a fixed rewetting temperature, the rewetting velocity increases with Biot number.

The analytical models of the quenching phenomenon show, in general, an implicit relationship between three nondimensional parameters, the Peclet numbers, the Biot number and a dimensionless temperature. In order to apply any of the described models to a practical calculation of rewetting velocity, heat transfer coefficients and rewetting temperatures have to be supplied. These values are very difficult to estimate in many cases. The uncertainties involved in their estimation can override the accuracy obtained by the model. Explicit solutions for the rewetting velocity can be obtained analytically only for the limiting cases of either large or small Biot and Peclet numbers. Even in these limiting cases experimental data are still required for correlating the rewetting temperature and the wet-region Biot number.

2.2.3 Numerical Solutions

Thompson[52] presented one-dimensional numerical solutions of the conduction problem for the case where the heat transfer coefficient in the wet region varies with the third power of the wall superheat. He solved the energy equations numerically by a quasi-linearization technique combined with the finite-difference method. The experimental data of Bennett et al.[10] were analyzed with this model to compute the heat transfer coefficient on the wet side.

Thompson[53] also presented two-dimensional numerical solution of the conduction problem in cylindrical co-ordinates for the case where the heat transfer coefficient in the wet region varies with the third power of the wall superheat. Such a dependence of heat transfer coefficient on wall temperature exists in the case of nucleate boiling. The wall temperature at the interface of the wet and dry area is assumed to be equal to the rewetting temperature, and it is assumed that the wall is wetted and nucleate boiling occurs up to this temperature. At higher wall temperatures, film boiling is assumed to occur and the heat transfer coefficient is several orders of magnitude smaller. From his analysis, he concluded that beyond a certain sheath thickness, which depends on thermal conductivity, downstream temperature, and ambient pressure, neither the wall thickness nor type of heating affects the rewetting rate. He also conclude that the rewetting rate is nearly independent of heat flux and thermal conductivity, but increases with pressure and decreases with volumetric heat capacity.

Elias and Yadigaroglu[54] developed a computer-oriented one-dimensional axial conduction model which accounts for the large variations of the heat transfer coefficient near the quench front and for the temperature dependence of the thermal and physical properties of the wall. Heat generation in the wall was included in their model. In their analysis, they assumed that the rewetting process has reached an asymptotic state such that the pellet, cladding and coolant temperature distributions move together at a constant rewetting velocity U. Thus, an observer moving at this velocity sees an apparant steady state. The one-dimensional heat-conduction equation was solved by dividing the quenching zone into small segments of arbitrary temperature increment and constant properties and heat transfer coefficient. The velocity of the rewetting front, the length of the quenching zone and the temperature profile were obtained by a trial-and-error method. In order to understand the combined effects of this temperature and of the initial wall temperature on the predected rewetting velocity, calculations were carried out for various values of the ratio

$\theta_w = (Tw - Ts)/(Tq - Ts)$, and they observed a strong variation of the rewetting velocity with rewetting temperature. The rewetting velocity is more sensitive to the value of the parameter θ_w for low initial wall temperatures and for high rewetting temperatures. Elias and Yadigaroglu[54] compared their model with experimental data of other workers, and found that experimental results taken at low coolant flow rates correlates very well with the model using available correlations for the heat transfer coefficient, and rewetting temperature of 260 C. However, for useful application of the present model, a better definition of the temperatures at the point of critical heat flux and the rewetting temperature in the rewetting front, as well as accurate correlations for the heat transfer coefficient is necessary.

Yu et al.[9] solved the two dimensional (radial and axial) heat conduction equation numerically. They assume only two regions, one wet (constant heat transfer coefficient) and one dry (zero heat transfer coefficient). Their results are in the form of tables or graphs and can be used for any input conditions. The solution of Yu et al.[9] is considered the most exact as it involves a summation of 151 terms of two infinite series expansions. They also proposed correlations giving the quenching heat transfer coefficient and rewetting temperature as a result of their analysis. They suggest that these correlations may be combined with the previously reported conduction analysis to predict rewetting rates under a wide range of conditions.

Martini and Premoli[55] developed a computational model, called TRE, which predicts single fuel rod thermal transient, starting from the time at which coolant, with a known flow rate, reaches fuel element bottom, and terminating when the fuel element is completely quenched. They introduced some hypotheses to simplify their model, such as, heat transfer in the radial direction being described by a two-cell model while axial conduction is neglected. The fuel rod is subdivided in several axial nodes. The thermal transient of each node is computed by a balance between the heat generated and the heat transferred to the coolant. Wall temperature, when reaching a value Tq(quenching temperature) prefixed in the input, is assumed to drop instantaneously to the saturation temperature. The value of the quenching temperature is to be derived by experiments. In their model, a satisfactory evaluation of the film boiling heat transfer coefficient and the quenching temperature is required, since they strongly affect the quenching front progression velocity. The validity of their model reduces as axial heat conduction becomes important.

The analyses to determine rewetting velocity in horizontal channels are very limited. Salcudean et al.[56] solved the quasi-steady-state three-dimensional heat conduction equation by a finite difference method and obtained numerical solutions for the rewetting processes in horizontal channels. They assumed three distinct regions in their physical model; wetted region, transition region and the dry region. In the wetted region, they assumed the circumferential variation of the heat transfer coefficient to be a cosine function, while in the dry region, they assumed that no precursory cooling takes place.

As stated before, all analytical models cannot be directly compared to experimental data because numerical values must be assigned to the rewetting temperature, Tq, and the effective heat transfer coefficient, h, in the solutions.

To provide a physical basis for understanding the observed rewetting phenomena and to show that the effect of the rewetting temperature in the rewetting analysis is one of the most important parameters, the author[1,67] presented an analytical model based on six heat transfer regions to predict the temperature-time trace curves at various axial locations of vertical circular channels during the bottom flooding transient. Appropriate heat transfer coefficients for each region are calculated and the rewetting temperature is obtained by empirical correlation of experimental data using dimensional analysis[79]. A substantial agreement was obtained between the analytical and experimental results and this demonstrates the dominant role played by the rewetting temperature in the analysis of rewetting phenomena. The study also showed that the effect of the two-phase flow heat transfer behind the rewetting front is, contrary to what has been assumed, minor and that the axial conduction plays a minor role also in the confined flooding modes.

Chapter III

EXPERIMENT

3.1 MAIN EXPERIMENTAL APPARATUS

The main experimental loop consisted of two sections, one fixed on the laboratory floor and the other on a pivotable mounting which allowed experiments to be carried out with test sections at any angle between horizontal and vertical. The general layout of the major components is shown schematically in Fig. 3.1(a).

The fixed section consisted of a water demineralizer, capable of treating 0.4 m^3 per hour, a preheater of 0.2 m^3 capacity, a main supply boiler operating at water temperatures up to 200 C and at pressure up to 2100 KPa, and two flow rate transducers mounted in parallel. Each transducer had a two-way valve mounted in series with it, so that either transducer could be selected depending on the flow rate to be measured. One transducer covered the lower end of the flow rate(6 to 60 g/s), and the other the higher end(35 to 350 g/s). In the later period of the study, one of the transducer (higher range one) was replaced with turbine type flow meter. The flow meter had a range up to 630 g/s. The movable section consists of a by-pass circuit, the test section, a pair of quick acting valves to divert the coolant flow to or away from the test section, an exhaust condenser system for retaining and condensing the steam which was produced in the test section, and a reverse tank for the coolant. All these components were supported on a mounting, consisting of a pair of vertical members with a frame pivotally mounted between them. The pivoting frame clamps onto the condenser and the reverse tank. Lengths of flexible hose (heavy duty Aeroquip rubber hose) were used to connect the water leads to the movable unit. All pipings and fittings for the entire apparatus were made of stainless steel to avoid unwanted contamination. The main experimental apparatus was first designed by Gamblin and further details regarding main experimental apparatus can be obtained from Gamblin's report[80]. A picture of the main experimental apparatus is shown in Fig.3.1(b).

Each test-section (total of 20 test-sections) was instrumented with many chromel-alumel thermocouples, spot-welded onto the outside and/or inside wall surface at 10 to 12 different axial positions, and two to four were around the circumference at a given axial location. The test-sections were heated by an a.c. power source capable of 30 KW at up to 1500 amps. The terminal clamps, made of copper, were attached to both ends of the test-section, and Fiberfrax was used for the insulation. Pressure transducers were connected to the test-sections for inlet and outlet pressure measurements. The test-sections were washed with distilled water followed by acetone rinses before they were installed in the apparatus.

Two additional separate apparatuses were designed and constructed to study unconfined top flooding rewetting along the outside surface of circular flow tubes and also for the visual study of the rewetting phenomena in various flooding modes. The details of these experimental apparatus are discussed later in the appropriate sections.

3.2 EXPERIMENTAL PROCEDURE

Using either the preheater or the main supply boiler, the water têmperature was set at a given degree of subcooling. The power to the test-section was turned on and the wall temperature was brought up to the desired value by increasing the power stepwise. Experiments were performed by diverting the water of a given flow rate, flowing at steady-state conditions in the bypass circuit, to the test section while the power was either maintained or switched off depending on the selection of the test parameters.

The signals from the thermocouples, from the transducers for flow rate and pressures were monitered continually on Hewlett Packard digital high-speed data acquisition system (H.P. 5050B digital recorder, 2901A input scanner and 2401C intergrating digital voltmeter) together with multi-channel recorders (Watanabe Type WA611-1 and Hewlett Packard 7100BM strip chart recorder). The variation of the water flow rate during the course of the experiment was usually very small. The temperature-time trace curves for several axial locations were produced by the multi-channel recorders which were connected to certain thermocouples. The rewetting velocities and the rewetting temperatures were obtained from the temperature-time traces as shown in Fig. 3.2. The rewetting velocity is calculated as

$$u_{ij} = \frac{\Delta z_{ij}}{\Delta t_{ij}}$$

where u_{ij} is the rate of the rewetting front propagation between two particular thermocouples of interest, Δz_{ij} is the axial distance between the thermocouples, and Δt_{ij} is the time interval taken between these two rewetting fronts. Therefore, it is necessary to establish the point when the actual rewetting front passes the particular thermocouple. However, this is extremely difficult, if not impossible. But, for the calculation of rewetting velocities, it suffices to determine only a reference point for a given temperature-time trace. This is done by taking the intersection of the gradients of the trace before the point where there is a rapid fall in temperature and at the steepest portion of the fall. This technique is also generally used by other workers[14,37,56].

The physical characteristics of the test-section channel geometries are given in Table 1.

Since the thermocouples were welded onto the outside tube wall, it is required to have the solution of the "inverse" heat transfer problem, to obtain the wall temperature transient on the inside surface where the actual rewetting phenomenon takes place. There are many solutions to the problem, including lengthy graphical and integral methods, but an exact analytical solution as a rapidly convergent series developed by Burggraf[68], and applied to a hollow cylindrical body insulated at the outside wall with a measured temperature variation with time, by Plummer et al.[69], was used here. This is because the method requires only To(t) to determine Ti(t).

The surface heat flux to the coolant may be extracted from the data by using the energy balance for the length Z of the test section.

$$\Delta z \cdot \frac{\pi}{4}(D_o^2 - D_i^2)(\rho C_p)_w \cdot \frac{dT_w}{dt} = Q_{EL} - Q_{HF} - Q_{AX} - Q_{RAD} - Q_{Loss} \quad \cdots (3.1)$$

Q_{HF}=heat transfer to the coolant

Q_{EL}=heat generation in the element

Q_{AX}=axial heat conduction

Q_{RAD}=radiation heat transfer

Q_{Loss}=heat loss to the surrounding

It is assumed here that the axial conduction heat flux may be approximated by a one-dimensional conduction model. Based on this assumption, Q_{AX} may then be approximated to be

$$\frac{\pi}{4}(D_o^2 - D_i^2)\frac{k}{U^2} \cdot \frac{d^2T_w}{dt^2} \cdot \Delta Z \quad \cdots\cdots\cdots\cdots (3.2)$$

using the relationship

$$\frac{dT_w}{dz} = \frac{1}{u}\frac{dT_w}{dt}$$

Q_{RAD} is significant at high wall superheats but is very small near the rewetting front. Therefore, it is neglected in the present study.

$Q_{LOSS} = q_{LOSS}(T_w) \cdot \pi \cdot D_o \cdot \Delta z$ was obtained from calibration tests.

After substitution with appropriate values with above assumptions, Eqn.(3.1) becomes,

$$q_{HF} = \frac{D_o^2 - D_i^2}{4 D_i} \left[\dot{q} - (\rho C_p)_w \frac{dT_w}{dt} - \frac{k}{u^2}\frac{d^2T_w}{dt^2} \right]$$
$$- q_{LOSS}(T_w) \cdot \frac{D_o}{D_i} \quad \cdots\cdots\cdots\cdots (3.3)$$

The above equation can be evaluated using the measured values of dTw/dt. Finally, the inside heat-transfer coefficient can be evaluated from $h = q_{HF}/(T_w - T_s)$.

3.3 TEST CONDITIONS

3.3.1 Single Bottom and Horizontal Flooding

Test sections No. 1-4 are straight tubes of stainless steel or Inconel X-750. The length of test sections are approximately 3.5 meters and diameter is 15.9 mm or 19.1 mm. Tube wall thickness varies between 0.89 mm and 1.65 mm.

These test sections were used to study the rewetting phenomena in bottom and horizontal flooding mode.

3.3.2 Flow Blockage Tests

The four test-sections(No. 5-8) used in these experiments were made of Inconel X-750. The overall length of the test sections were 3.5 meters, and the outside diameter and the wall thickness were 15.9 mm and 1.2 mm respectively.

The test-sections with 25% and 50% flow area reduction were made of eight sections, six of which are 0.5 meters in length to simulate closely CANDU fuel bundles, and two 0.3 meters. Seven flow blockage plates were welded together with these 8 pieces as shown in Fig. 3.3.

A total of 50 chromel-alumel thermocouples were spotwelded on the outside wall surface. The locations of thermocouples are shown also in Fig. 3.3 where they are identified by letters and numbers. Letter N indicates that four thermocouples were placed at 90° intervals around the circumference and M for two which were placed such that when the test section is horizontal, one will be at the top and the other at the bottom side of the tube. L indicates that only one thermocouple is attached at the top of the tube when the test-section is horizontal. Numbers are used to identify their relative position from the entrance.

3.3.3 Unconfined Top Flooding

To study unconfined top flooding rewetting along the outside surface of circular tubes, a separate new experimental apparatus, in addition to the loop used for above, was designed and constructed in such a way that the related thermal-hydraulic phenomena could be investigated visually as well. A schematic diagram of the new apparatus is shown in Fig. 3.4.

The apparatus consists of a water supply at different temperatures, a rotameter, a by-pass loop, a specially designed coolant injection nozzle assembly, power supply, test-sections with removable transparent outer jackets, thermocouples to measure the surface temperature of the test-sections and coolant.

To avoid or minimize bowing of the test-sections, due to thermal expansion and contraction during the test, a tension of about 450 Newton was applied at the end of the test-section.

The inlet nozzle assembly which was successful in providing a uniform film of water for the unconfined top-flooding experiment is shown in Fig. 3.5.

3.3.4 Confined Top Flooding

Test sections No. 11-12 are 3 meters long tubes of S.S.304. To study the effect of flow area in the confined top flooding, two different diameter tubes were selected. Test sections No. 11 and 12 have outside diameters of 1.59 m and 2.46 m respectively. Tube wall thickness are same for both test sections. The flow loop in the main experimental apparatus was slightly modified to accommodate these test sections in the top flooding mode.

3.3.5 Annular Test Sections

Test sections No. 14-16 are annular test sections. To investigate the effects of various parameters on rewetting in a concentric annular geometry, an effort has been made to design various components of annular test-sections which will be subjected to very high temperatures. The specially designed connector assemblies for the inlet and outlet, and for the mid-section of the annular test-section are shown in Figs. 3.6 and 3.7.

A technique to install thermocouples by spot-welding inside of small core tubes has been perfected and has been used for test-sections Nos. 14 to 16 which had 13 thermocouples on the inside surface. Another 16 thermocouples were also installed onto the outside wall surface of the outer-tube of the test-section No. 16.

Test-sections No.14-15 had glass outer tubes, and were used in the bottom flooding mode, while test-section No.16 had a stainless steel outer tube, and was used for bottom and horizontal flooding modes with both walls heated.

The major difficulty for test-section No.16 was to design a core support mechanism which must not only isolate both the core and outer tubes electrically but also be able to sustain the severe deformation of the core tube during the horizontal rewetting process. The problem was overcome by having specially developed Fired Alumina ceramic supports (Fig.3.8) placed every 500 mm along the axial direction, in conjunction with four 200 kg springs installed at the end of the core tube. The support occupied 25% of the flow passage area.

Both the outer and core tubes are directly heated electrically and the power levels to both tubes can be adjusted separately to provide different wall temperatures.

Thirteen chromel-alumel thermocouples were spot-welded onto the inner surface of the core-tube using a specially designed spot-welder and sixteen chromel-alumel thermocouples on the outside wall of the outer tube. Fig. 3.9 show the position of the thermocouples, as well as the physical dimension of the annular test-section.

3.3.6 L-shaped Test Sections

Test-sections No. 17-18 are L-shaped test-sections, made of 25.4 mm O.D. and 1.65 mm wall thickness S.S.304. The other physical dimensions, and the location of 25 chromel-alumel thermocouples are shown in Fig. 3.10. The reason for this study is that the CANDU reactor has horizontal fuel channels and vertical feeder tubes, while BWR reactor has vertical fuel channels with horizontal feeder tubes, and these "L"-shaped test sections simulate the rewetting behavior in the reactor more closely than simple straight tubes.

For the L-shaped test-sections, both the top-followed-by-horizontal flooding (THF) and the horizontal-followed-by-bottom flooding (HBF) modes were accommodated in the main experimental apparatus with minor modifications. One of the two L-shaped test-sections has an elbow made of 25.4 mm I.D. Swagelok elbow connector, while the second had an elbow made of the same tube with a radius of 0.127 m. All the thermocouples were spot-welded onto the outside surfaces of the test-sections. Since the test-sections were directly heated electrically, the temperature of the elbow section made of Swagelok was lower than the other section of the test-section.

Chapter IV

VISUAL STUDY

To obtain physical insight into the problems associated with reflooding phenomena, visual studies on various flooding modes of single circular tubes and on bottom and horizontal flooding of an annular test-section were made using high-speed still photography.

The apparatus for the visual study of unconfined top flooding consists of a water supply at different temperatures, a rotameters, a by-pass loop, coolant injection nozzle assembly, power supply, test-sections of S.S.304 and Inconel X-750, and thermocouples to measure the surface temperature of the test-section and coolant. A schematic diagram of the apparatus is shown in Fig.3.4.

For the concentric annular bottom flooding study, Test-section #14 which had a stainless steel core tube and glass outer tube, was used. To measure the core tube wall temperature, thermocouples were spot-welded on the inside surface of the core tube, and drawn out through one end of the core tube. Because of high core tube wall temperatures and possible contact between thermocouple wires and the core tube, a special high temperature resistant thermocouple wires (K type, HG/HG) were used.

The test-sections of simple circular, L-shaped and concentric annular channels are all made of quartz tubing wound with nicrome-wire for heating. Concentric annular test-sections, for use in the visual study of bottom and horizontal flooding with both walls heated, are made of quartz tubings with nicrome-wire wound on the inside surface of the core tube and on the outside surface of the outer tube. The test loop consists of a water supply with a temperature control, a rotameter, a by-pass loop, an injection assembly, power supply, specially designed connectors for the test-sections, and thermocouples to measure the approximate surface temperature of the test-sections, coolant and other peripheries. Quartz glass tubes used for all visual studies except annular tests are 15 mm O.D. and 1.2 mm wall thickness. Annular test sections used 15 mm O.D. quartz tubing as core tube and 30 mm O.D. quartz tubing with 1.8 mm wall thickness as outer tube.

4.1 UNCONFINED TOP-FLOODING

The photograph in Fig.4.1 shows that there is an extremely narrow region of the order of less than 1/2 mm of vigorous boiling just behind the well-defined rewetting front. It is very difficult to say whether boiling is nucleate, transition or film. If the tube is not heated, then the water would just flow down along the surface as a film. However, when tube is heated, water flow establishes a rewetting front, and water flows as a film along the cooled surface of the rod down to the rewetting front. Since the propagation rate of this rewetting front is much slower than the water flow rate, the excess water is ejected at the rewetting front forming a truncated cone shape. This truncated cone is made of the ejected droplets, ranging in diameter from about 2-3 mm to very small sizes. Near the top, the cone, at times, seems to be formed by a sheet of water, which then breaks up into irregular droplets as it falls off.

With the coolant temperature below about 60 C, it was often difficult to maintain a uniform continuous film of coolant flowing down the circular convex surface. Frequently, the flow was rivulent as reported by Duffey et al.[42] and once the flow became unstable, instability accelerates at such a rate that the test-section became severely bowed due to the severe temperature gradient set around the periphery.

It was also seen from the photographs that the unwetted region below the rewetting front remains completely dry and that the precursory cooling seems to be confined by radiation only.

This is clearly seen from Fig.4.2 also, in which the surface heat flux distributions obtained from Test-sections #3 and #10 using Eqn.(3.3) near the rewetting fronts of both the confined and unconfined top-flooding experiments are compared. One can see that for the confined top-flooding, the precursory cooling is significant.

Therefore, one can conclude that any analytical model for the rewetting process in a confined space must not ignore the contribution of precursory cooling, especially if the inside diameter of the flow channel is less than about 25 mm.

The presence of unheated transparent outer jackets (Di=30 and 50 mm) seemed to have very little effect on the precursory cooling, and hence on the rewetting velocity. However, this cannot be true if the temperature of the outer jacket is higher than rewetting temperature.

4.2 ANNULAR BOTTOM FLOODING WITH AN UNHEATED OUTER JACKET

The typical bottom flooding phenomena in a concentric annulus with an unheated outer jacket are shown in Fig.4.3. Figure 4.3(a) is taken at Z=0.25 m, while Fig.4.3(b) is at Z=0.45 m, where Z is the distance from the inlet of the coolant. As can be seen in the photographs, the length of the bubble region grows as the rewetting front moves up the flow channel. A similar observation was reported by Case et al.[40] who stated that there was an extensive "film boiling" region ahead of the quench front which broke down to give a "mist flow" region at a distance of order 10 to 200 mm ahead of the quench front. From our photographs, similar to those of Fig.4.3, it is very difficult to define precisely whether the flow ahead of the rewetting front was the film boiling region.

The thermocouple signal seemed to indicate that the wall temperature at a given location along the test-section tube reached its "apparent" rewetting temperature when the bottom of this "film boiling" region reached that particular position.

It was also noted that when the front is near the upper end of the test-section, a new rewetting region occurs ahead of the primary rewetting front. In such a case, a rewetting front travelling up the flow channel would meet the secondary rewetting front travelling down the channel.

Since the circumferential rewetting for the bottom flooding in the annulus was almost uniform, the severe bowing of the core tube due to non-uniform rewetting often observed in unconfined top-flooding, did not occur.

4.3 TOP-FLOODING, VERTICAL SINGLE TUBE

In top flooding, when the tube is not heated up to a very high temperature, coolant water flows down along the inside surface of the tube as a continuous film. This phenomenon was observed in both low and high flow rates.

Top flooding of a very hot test tube shows slightly different rewetting phenomena depending on the flow rates. When the coolant flow rate is very low ($G < 100\ kg/m^2.s$), the coolant water flows down the cooled inside surface of the tube to the rewetting front and, since the rewetting front velocity is much slower than the coolant injection flow rate, excess water is ejected at the rewetting front splashing down through the middle of the tube forming a thin continuous sheet of water (as illustrated in Fig.4.4(b)). The rewetting front is not uniform along the circumference and the front is very unsteady. If the test tube is heated continuously during the experiment with very low coolant flow rates, then dry spots appear in the water film at the upstream of the rewetting front, and this dry spot enlarges to a certain size before being rewetted again by another local rewetting front. This phenomenon appears in several locations in random order but continuously.

When coolant flow rate is large ($G > 100\ kg/m^2.s$), the rewetting phenomenon starts in the same fashion as in a low flow rate case, however, soon after, the upstream of the rewetting front is filled with a mixture of water and vapour bubbles instead of a continuous water film, and the coolant ahead of the propagating rewetting front forms a continuous rod-like formation as shown in Fig.4.4(a). In both cases, the inside wall temperature was approximately between 350 and 400 C. Fig.4.4(c) through 4.4(f) show the details of the two-phase flow ahead of the moving rewetting front. The shutter speed was 1/2000 sec.

Fig.4.4(c) and 4.4(d) indicate that, when the coolant injection rate in terms of superficial mass velocity is above 100 mm/s, the region ahead of the rewetting front in confined top-flooding through a vertical single tube can be modelled as inverse annular film boiling.

As the injection flow rate decreases, the diameter of the fluid flow "rod" becomes thinner and for flow rate less than 100 mm/s, as stated above, the coolant immediately ahead of the front forms a thin sheet as seen in Fig.4.4(e).

4.4 BOTTOM FLOODING, VERTICAL SINGLE TUBE

The coolant flow structure ahead of the moving rewetting front for the bottom-flooding in a vertical single tube shown in Figs. 4.5(a) to 4.5(c) is very similar to that observed in confined top-flooding (Figs. 4.4(a) and 4.4(c)), except the rewetting front region is a homogeneous mixture of water and numerous vapour bubbles produced by boiling. Again, since the rewetting velocity is slower than the coolant flow rate, the excess water is pushed upward forming a irregular rod shape through the middle of the tube surrounded by vapour. This rod shape formation is not continuous and becomes thinner until it eventually breaks up into large globules.

The effect of the coolant injection rate on the flow structure in the bottom-flooding was relatively minor compared to that in the confined top-flooding.

The present visualization clearly showed that the fluid-structure, ahead of the propagating rewetting front, in both top and bottom flooding in circular ducts are very similar and that the flow in the region can be modelled as an inverse annular film boiling (followed by dispersed flow for lower flow rates). The flow at higher flow rate was not steady as previously mentioned in the case of the top-flooding of a vertical channel.

Although the flow structure ahead of the rewetting front for confined top-flooding and bottom-flooding in vertical tubes, as seen in Figs. 4.4(a) through 4.5(d), are similar to a certain extent, the flow modelling must take into consideration the differences in the flow regimes involved in principle.

4.5 HORIZONTAL FLOODING, SINGLE TUBE

Fig.4.6(a) shows the stratified flow when the channel wall temperature is at about the same temperature as the coolant fluid, and the coolant injection flow rate is less than 100 mm/s. The velocity of the stratified water flow front is much faster than the preset coolant injection flow rate because the cross-sectional area of the stratified flow is less than that of the tube area. For rewetting with this low flow rate, there is a short region of vigorous boiling beyond which the fluid breaks up into globules moving down along the channel as they become smaller, as seen in Figs. 4.6(b) and 4.6(c). The front tip of the stratified flow shows numerous bubbles forming, produced by vigorous boiling, and this seems to be a rewetting front.

Fig.4.6(f) shows a typical adiabatic flow along the horizontal channel with flow rates above 100 mm/s. Since the channel has to be filled, there is an initial region of stratified flow followed by completely filled flow. Because of the particular nature of the filling of the channel, the rewetting for these flow rates has three distinct flow regimes in the vicinity of the rewetting front; continuous stratified flow behind the rewetting front, a short region of vigorous boiling and continuous stratified inverse annular film boiling flow, as seen in Fig.4.6(g). Eventually, the stratified inverse and skewed annular film boiling flow breaks up into large globules gliding downstream as shown in Fig.4.6(h).

4.6 BOTTOM FLOODING, INCLINED SINGLE TUBE

When the hot tube is inclined, because of the effect of the gravitational field, the coolant flow just ahead of the rewetting front becomes asymmetric and the column breaks into globules which slide upstream, as shown in Fig.4.7. This flooding mode shows some characteristics of both bottom and horizontal flooding. At the rewetting front, there are numerous bubbles formed due to boiling and at the upstream of this front, a continuous stratified water column, sometimes broken up as a large water globules, flows upstream at a very fast speed.

4.7 ANNULAR FLOODING WITH BOTH WALLS HEATED

Fig.4.8(a) shows the annular test-section with both walls heated. The central core tube, 15 mm O.D. and 12.6 mm I.D., was heated by a wound nichrome-wire inserted inside the core, whereas the outside tube, 30 mm O.D. and 26.4 mm I.D., was heated by a nichrome-wire wound outside the tube. Quartz tubing was used for both the outer and core tubes to minimize the bowing of the channel during the rewetting transient. The test-section, about 800 mm in length, was mounted on the main reflooding loop to study flooding in both vertical and horizontal orientations.

Figs. 4.8(b) and 4.8(c) show the rewetting phenomena in a horizontal annular test-section where both boundaries are heated to about 350-400 C. The coolant injection flow rates were about 50 mm/s and 100 mm/s, respectively. In both cases, the flow behind the rewetting front becomes stratified and the coolant flow ahead of the front forms a tongue-shaped structure in the lower passage of the annular space. The rewetting front itself is a bubbly region in which water is boiling, even though it is not clear whether this is nucleate boiling or transition boiling. The rewetting front exists in two places, one on the bottom part of the outer tube and the other on the bottom part of the core tube, and the bottom rewetting front (rewetting of outer tube) is always ahead of the top rewetting front (rewetting of core tube), probably due to gravitational effect. For higher flow rates, the tongue-like formation in the region ahead of the front remains the same but in a less distinguishable form and the level of the stratified flow increases with time as in a single horizontal tube(Fig.4.8(d)). In this case, further upstream, as in a horizontal single tube, the entire annular section is filled with coolant, as illustrated in Fig.4.8(e).

In the bottom flooding of an annular test section with both walls heated, when water is first introduced to the bottom of the test section, water starts to boil and it forms a bubbly region, the same as the case observed in the section 4.2 (Fig.4.3(a)). However, the top of the bubbly region (interface between the bubbly water and air) is very rough and some of the water is broken off from the rough interface and forms large water globules which is flowing upward as in the case of single tube bottom flooding. These large water globules decrease in size as it flows upward in the test section due to evaporation. As shown in Fig.4.9, the length of the bubbly region increases with time. With higher inlet coolant flow rates, the phenomenon is the same except there are fewer water globules flowing upward ahead of the bubbly region. An explanation for this change is that as the flow rate increases, the rewetting velocity increases and also the bubbly region interface moves upward at a much faster speed. Therefore, the bubbly region interface catches up to some of the water globules flowing upward ahead of the bubbly region.

4.8 THF, L-SHAPED CIRCULAR TUBE

To simulate a vertical feeder with a horizontal fuel channel in CANDU type reactors, the rewetting phenomena in a single L-shaped circular duct were investigated visually as well as quantitatively.

The fluid flow during the rewetting transient in an L-shaped duct can be divided into three regions, as schematically illustrated in Fig.4.10.

As illustrated, three rewetting fronts are established in an L-shaped channel with Top-followed-by-Horizontal-Flooding modes; two fronts in the vertical section (Region 1 and Region 2) and one in the horizontal part of the test-section (Region 3).

The fluid flow structure observed during the rewetting transient of L-shaped test section in Region 1 is somewhat different from that of vertical top-flooding. When coolant water is first introduced to the top of the test-section, the coolant water flows down along the inside surface of the tube as a film and the front end of the film has vigorous boiling with excess water splashing down through middle of the tube just like in the case of confined top flooding. However, soon after, bubbly water accumulates in the tube a few centimeters upstream of the rewetting front as shown in Fig.4.11. A probable explanation for this phenomenon is that all the excess water is not splashed down from the rewetting front, and some of the excess water is accumulating in the upstream of the rewetting front. There is a certain pressure exerted into the bubbly water column caused by vapour flowing upward, so the bubbly water column does not reach to the rewetting front and establishes a few centimeters above the rewetting front with a water film in between. Initially, the length of the bubbly water column is very short (30-40 mm), but it increases with time. As the rewetting front flows down, the length of the water film above the rewetting front also increases as well as the length of the bubbly water column. Meanwhile the vapour pressure in the vertical tube builds up continuously until the vapour pressure is higher than the weight of the bubbly water column in the top. Then the vapour pushes the water column out of the top of the test section and escapes from the tube. The rewetting front is disturbed by this process. However, it quickly establishes itself again at almost the same position, and also the bubbly water column establishes again in the upstream of the rewetting front. The length of the water column increases with time until again it is pushed out of the test-section. The reason for the rewetting front establishing itself again at the same position seems to be obvious. The rewetting front in Region 1 would occur at the lowest position where the wall temperature is not above the rewetting temperature, and since the wall temperature distribution in the vertical section is not changed by above process, the rewetting front would occur at the same position. This process of vapour escaping the test-section is executed at a very short time, so when this occurs, it looks like a small explosion in the tube. This cycles until the vertical section is completely quenched.

The flow structure in Region 2 is somewhat similar to bottom-flooding of a circular vertical tube, but with a much reduced flow rate. In this region, the main heat transfer seems to be due to precursory cooling, radiation to vapour and fluid droplets and axial conduction along the duct wall, starting from the elbow where the coolant was partially accumulated.

The flow regimes in Region 3 are very similar to those observed in flooding of a horizontal simple channel. As shown in Figs. 4.12(d) and 4.12(e), there is a short length of vigorous boiling followed by broken-up fluid globules moving along the channel as they become smaller due to evaporation. This was observed in Figs. 4.6(b) to 4.6(d).

The complete progress of rewetting process of THF (Top-followed- by-Horizontal-Flooding) in "L"-shaped test section is visually shown in Figures 4.12(a) to 4.12(e).

Chapter V
ANALYSIS

The objective of the present analysis is to predict the local heat transfer parameters at the downstream of the rewetting front, inside a hot vertical tube with upward flow of a liquid coolant.

The experimental results and the author's previous numerical analysis[1] of rewetting phenomena show that the rewetting temperature and the precursory cooling just ahead of rewetting front are most important parameters affecting the rewetting velocity. Therefore, having an accurate heat transfer coefficient in the downstream of the rewetting front is very important for the analysis. Since rewetting temperature, T_q, was intensively studied before[1], it is a natural extension that the method to obtain a more accurate heat transfer coefficient in the inverted annular flow region during the reflooding is pursued here.

Several attempts were made to correlate Inverted Annular Film Boiling data with ~~pool~~ film-boiling correlations, namely the classical Bromley correlation[58]. The work of Bromley, and subsequent similar formulations including the effects of convection and subcooling of the liquid, do not account, however, for the fact that in the case of Inverted Annular Film Boiling, heat transfer takes place in a channel in the presence of two-phase flow. Thus these formulations do not account correctly for the strong effect of mass flux. Other workers[70-72] obtained the inverted annular flow heat transfer coefficient based on steady state case with constant heat flux. In the case of rewetting of hot channel, the inverted annular flow is not steady state flow in the usual sense, and the heat flux changes depending on many parameters. The present study is confined to a model which will calculate the convective heat transfer coefficient of the inverted annular flow film boiling in the downstream region of the rewetting front in a bottom flooding mode. In the analysis, the inverted annular flow is taken as a concentric annulus with core tube moving axially at a certain speed. The vapour flow in the annular gap is considered as turbulent flow. The model takes into account the variation of the annular gap and the core tube speed due to the unsteady nature of the inverted annular flow film boiling in rewetting phenomena.

5.1 GENERAL APPROACH

Knowing the liquid mass flux and void fraction, the average liquid velocity is calculated (detail shown in Appendix 1). For vapour velocity, it is assumed that the velocity profile in the vapour gap of the inverse annular flow is the same as that of a concentric annulus in the region from the outer wall to some point in the inner region where the velocity equals the liquid core velocity. That is, if we extrapolate the vapour velocity profile of the inverse annular flow into the inside liquid core at a certain point as shown in Fig.5.1, the velocity will be zero, and we can call the distance from the center line to this imaginary plane as R_i. This is because the core is moving at a certain velocity. We can assume that the vapour velocity profile is the same as the velocity profile of a concentric annulus with the inner radius, R_i and the outer radius, R_o.

The governing energy equation is obtained for the element in the fluid flow, and with a known heat flux ratio distribution, the heat flux at the tube wall is calculated. The turbulent Prandtl number is assumed to be unity and the eddy diffusivity is calculated from the velocity profiles.

The general approach of the analysis is established as follows:

(i) Liquid core velocity is calculated.

(ii) Using vapour velocity profiles, the imaginary radius and shear stress distributions are obtained.

(iii) From the energy equation, the local heat fluxes are calculated.

(iv) From the steps (i) to (iii) above, the vapour mass flux gradient is now obtained.

(v) For the new element, the new vapour mass flux, vapour quality and void fraction are calculated.

(vi) With new vapour void fraction, new liquid core radius is obtained.

(vii) For the new element, the steps (i) to (vi) above are repeated.

5.2 VAPOUR VELOCITY PROFILE

Fig. 5.1 shows the schematic diagram of the vapour velocity with the appropriate nomenclature. Here, R_i is an unknown value. However it can be calculated knowing that $V=V_\ell$ at $r=Ri^*$.

The maximum velocity radius R_m is given by Leung et al.[59] as

$$R_m = R_i \cdot \left\{ \frac{1 + (\alpha_1)^{1-n}}{1 + \left(\frac{1}{\alpha_1}\right)^n} \right\} \qquad \cdots\cdots (5.1)$$

where, $\alpha_1 = \frac{R_o}{R_i} < 10$ [60] and $n=0.343$

It was shown by Park[60] that Eqn.(5.1) by Leung fits his extensive experimental data very well.

For the velocity profile in a concentric annulus, Levy[61] assumed that the plane of zero shear is located at the maximum velocity point and postulated that Reichardt's expression[62] for the eddy diffusivity of momentum applies to the flow region on both sides of the plane of zero shear. Therefore, Reichardt's expression can be written as,

$$\frac{\varepsilon_M}{\nu} = \frac{K}{6}|(R-R_m)| \cdot \frac{\sqrt{\tau_R/\rho}}{\nu} \cdot \left[1-\left(\frac{r-R_m}{R-R_m}\right)^2\right] \cdot \left[1+2\left(\frac{r-R_m}{R-R_m}\right)^2\right] \quad \text{.........(5.2)}$$

Above Eqn.(5.2) is valid on both sides of the plane of zero shear. For the region next to the outer tube wall ($Rm < r < Ro$), the eddy diffusivity for momentum is obtained by having K, τ_R and R as Ko, τ_{R_o} and Ro. Similarly, the diffusivity near the core tube wall is derived by substituting Ki, τ_{R_i} and Ri into the equation.

Equating the eddy diffusivity at the plane of zero shear gives,

$$\frac{K_o}{K_i} = \frac{R_m - R_i}{R_o - R_m} \cdot \sqrt{\frac{\tau_{R_i}}{\tau_{R_o}}} \quad \text{.........(5.3)}$$

Also from a force balance, we obtain

$$\frac{\tau_{R_i}}{\tau_{R_o}} = \frac{R_o}{R_i} \cdot \frac{R_m^2 - R_i^2}{R_o^2 - R_m^2} \quad \text{.........(5.4)}$$

The shear-stress distribution on both sides of the zero shear plane can be described from a force balance by

$$\tau_r = \tau_R \cdot \frac{R}{r} \cdot \frac{r^2 - R_m^2}{R^2 - R_m^2} \quad \text{.........(5.5)}$$

From the Reynolds equation with the concept of eddy diffusivity for momentum, ε_M, the application of momentum theorem, gives an expression for shear stress τ_r.

$$\tau_r = \rho(\nu + \varepsilon_M) \cdot \frac{du}{dy} \quad \text{.........(5.6)}$$

where $y = |r - R|$

Combining above two shear stress equations, Eqns.(5.5) and (5.6), with non-dimensionalization and integration gives

$$u^+ = \frac{1}{K} \ln\left[1.5\, y^+ \frac{1+\eta}{1+2\eta^2}\right] + \frac{2S(1-S)}{K(1+S)(2S-1)} \cdot \ln\left(\frac{1+\eta}{2}\right)$$
$$+ \frac{1}{2}\, \frac{S(1-S)(1-3S)}{K(1+S)[S^2+\frac{1}{2}(1-S)^2]} \cdot \ln\left(\frac{1+2\eta^2}{3}\right)$$
$$+ \frac{6}{K(1+S)} \cdot \frac{\ln[\eta(1-S)+S]}{[(\frac{1-S}{S})^2-1][2(\frac{S}{1-S})^2+1]}$$
$$+ \frac{\sqrt{2}}{K} \cdot \frac{(1-S)S}{1+S} \cdot \frac{\tan^{-1}\sqrt{2} - \tan^{-1}\eta\sqrt{2}}{S^2+\frac{1}{2}(1-S)^2} + C_2 \quad \cdots\cdots (5.7)$$

where $u^+ = \dfrac{u}{\sqrt{\tau_R/\rho}}$, $y^+ = \dfrac{y\sqrt{\tau_R/\rho}}{\nu} = \dfrac{|(r-R)|\sqrt{\tau_R/\rho}}{\nu}$

$\eta = \dfrac{r-R_m}{R-R_m}$, $S = \dfrac{R_m}{R}$

The above expression derived by Levy[61] would make the computation unnecessarily complex.

Roberts[63] derived a very simple velocity profile based on the assumption that the shear stress is constant across the flow section, which is too coarse an assumption.

Park[60] used a linear shear stress distribution in his study for the derivation of a reasonably simple velocity profile in the developing boundary layer. His argument was that as long as the choice of the shear stress distribution is consistent with one that agrees well with experimental results for the pipe flow case, a function of shear stress distribution which would lead to a much simpler and more convenient velocity profile than those given by Levy[61] would seem to be more practical. According to Deissler's[64] study, the variation across the flow boundary layers of the shear stress have a negligible effect on the velocity distributions.

Using linear shear stress distribution, the velocity profile is given as:

$$u_j^+ = -\frac{3}{\psi} \left| R_m^+ - R_j^+ \right| \cdot \ln \cdot \left| \frac{K_j \cdot \delta_j^+ - 4 K_j \cdot \delta_j^+ \cdot \eta_j^2 - \psi}{K_j \cdot \delta_j^+ - 4 K_j \cdot \delta_j^+ \cdot \eta_j^2 + \psi} \right| + C_j \qquad (5.8)$$

where
$$\delta_j^+ = \left| R_m^+ - R_j^+ \right|$$
$$\eta_j = \frac{\delta_j^+ - y_j^+}{\delta_j^+}$$
$$\psi_j = (9 K_j^2 \cdot \delta_j^{+2} + 48 K_j \cdot \delta_j^+)^{1/2}$$

superscript + indicates non-dimensionalized, and subscript j either inner or outer region; i or o.

Constant C_j is obtained by forcing the velocity profile to pass through point $u_j^+ = 12.8$ and $y_j^+ = 26$. A value of 0.4 for K_o was used in the analysis because it has been shown[61,65] that the mechanism of the flow outside of the radius of maximum velocity is very similar to that occurring in pipe flow.

Park[60] used Deissler's[64] expression for the eddy diffusivity for regions close to each wall (i.e. sub-layer) with the assumption of constant shear stress in the sub-layer which is

$$u^+ = \int_0^{y^+} \frac{dy^+}{1 + n^2 \cdot u^+ \cdot y^+ \cdot [1 - \exp(-n^2 u^+ \cdot y^+)]} \quad \cdots\cdots (5.9)$$

for $y^+ \leq 26$

where $n^2 = 0.0154$

However, the above expression for u^+ is too complicated to be used in our analysis, because the only way to use above expression is by numerical integration with several iterations (of trial and error).

Another good expression which represent the sub-layer velocity profile reasonably well is the Von Karman equation[73]. The expression is

$$\text{for} \quad 0 \leq y^+ \leq 5 \qquad u^+ = y^+$$

$$5 \leq y^+ \leq 30 \qquad u^+ = 5 \ln y^+ - 3.05 \quad \cdots\cdots (5.10a)$$

In the present study, we forced the core region velocity profile u^+ to pass through a point which is $y^+=26$, $u^+=12.8$ according to Park's experimental results. Therefore, the sub-layer velocity profile also has to pass through the point $u^+=12.8$, $y^+=26$. The Von Karman sub-layer velocity profile was modified so that it would pass through the point ($u^+=12.8$, $y^+=26$). The modified Von Karman sub-layer velocity profile is;

$$0 \leq y^+ \leq 5 \qquad u^+ = y^+$$
$$5 \leq y^+ \leq 26 \qquad u^+ = 4.73 \ln y^+ - 2.61 \quad \cdots\cdots (5.10b)$$

The Reynolds number of vapour in the annular gap is defined as;

$$Re = \frac{U_b \cdot de}{\nu} = \frac{U_b \cdot 2(R_o - R_i^*)}{\nu} \quad \cdots\cdots\cdots (5.11)$$

where U_b=average vapour velocity

The average vapour velocity, U_b, can be obtained from either the given vapour mass flow rate, G_v, or the vapour velocity profile.

The vapour mass flow rate G_v is

$$G_v = U_b \cdot \pi \cdot (R_o^2 - R_i^{*2}) \rho_v$$

Therefore Reynolds number is

$$Re = \frac{U_b \cdot 2(R_o - R_i^*)}{\nu} = \frac{2 \cdot G_v}{\pi \cdot \mu_v \cdot (R_o + R_i^*)} \quad \cdots\cdots (5.12)$$

Reynolds number can also be obtained from the known velocity profile. The average vapour velocity, U_b, is

$$U_b = \frac{\int_{R_m}^{R_o} 2Ur\,dr + \int_{R_i^*}^{R_m} 2Ur\,dr}{(R_o^2 - R_i^{*2})}$$

Therefore Reynolds number is;

$$Re = \frac{4}{b+1}\left[\frac{1}{R_i^{*+}}\cdot\int_{y_i^{*+}}^{y_{mi}^{+}} u_i^{+}\cdot(y_i^{+}+R_i^{+})\,dy_i^{+}\right.$$

$$\left.+\frac{b}{R_o^{+}}\cdot\int_{0}^{y_{mo}^{+}} u_o^{+}\,(R_o^{+}-y_o^{+})\cdot dy_o^{+}\right] \quad\text{........}(5.13)$$

where $b = \frac{R_o}{R_i^{*}}$

superscript + means non-dimensionalized

$y_i^{*}=Ri^{*}-Ri$, $y_{mi}=Rm-Ri$

$y_i=r-Ri$, $y_{mo}=R_o-R_m$, $y_o=R_o-r$

u_i=velocity profile in the inner region, and

u_o=velocity profile in the outer region

Now, with the above information, one can obtain inner radius Ri and shear stress, τ, as well as the vapour profile in the annulus gap, by iteration. The steps are as follows:

(1) Assume value for Ri.

(2) Get value of τ_{R_i}(shear stress at Ri) which satisfies the boundary condition (at $r^{+}=Ri^{*+}$, $u^{+}=V_\ell^{+}$).
Once τ_{R_i} is obtained, τ_{R_o} can be calculated from force balance given by Eq.(5.4).

(3) Calculate Reynolds number between Ri^{*} to Ro (using Eqn. 5.13) and check this Reynolds number against given Reynolds number (Eqn.5.12).
If the two Reynolds numbers are not same, then iterate again with the new value of Ri until the two Reynolds numbers are same. The new Ri value is selected based on the Reynolds number difference and previously selected Ri value (ie. if calculated Reynold number is too small, then increase Ri value)

Once the Ri value is known, the wall shear stress and the vapour velocity profile can be easily obtained.

5.3 ENERGY EQUATION

It can be shown that the energy equation in the element is given as

$$-\frac{q}{\rho C_p} = (\alpha + \varepsilon_H)\frac{\partial T}{\partial y} \quad \cdots\cdots (5.14)$$

For constant heat flux q, intergration of the above gives

$$-\frac{\rho C_p}{q}\sqrt{\frac{\tau_w \cdot g_c}{\rho}} \cdot \int_{T_w}^{T_j} dT = \int_0^{y_j^+} \frac{P_r}{1 + P_r \frac{\varepsilon_H}{\nu}} \cdot dy^+ \quad \cdots\cdots (5.15)$$

However, in this study, heat flux in the annular gap can not be assumed to be constant. Therefore, let $q/q_o = f(r)$, where q_o is the heat flux at the test section as shown in Fig.5.2. Intergration of Eqn.(5.14) with the above condition gives,

(a) in the outer region

$$\frac{\rho C_p \cdot (T_w - T_j)}{q_o}\sqrt{\frac{\tau_{wo}}{\rho}} = P_r \cdot \int_0^{y_j^+} \frac{f(r)\, dy^+}{1 + P_r \cdot \frac{\varepsilon_H}{\nu}} \quad \cdots\cdots (5.16)$$

(b) in the inner region

$$\frac{\rho C_p \cdot (T_j - T_s)}{q_o} \cdot \sqrt{\frac{\tau_{wi}}{\rho}} = P_r \cdot \int_{y_i^+}^{y_j^+} \frac{f(r) \cdot dy^+}{1 + P_r \frac{\varepsilon_H}{\nu}} \quad \cdots\cdots (5.17)$$

where for the eddy diffusivity for heat, ε_H, the Reichardt expression is used with an assumption that the turbulent Prandtl number is unity.

Now, the heat flux distribution is obtained by energy balance. An energy balance made on annular fluid elements (as shown in Fig.5.2) between r and (r+dr) gives

$$-2\pi r\, dx\, q + 2\pi (r+dr)\, dx \left(q + \frac{\partial q}{\partial r} \cdot dr\right) = 2\pi r\, dr\, \rho u C_p \cdot \frac{\partial T}{\partial x} \cdot dx \quad \cdots\cdots (5.18)$$

Rearranging, we have

$$\frac{\partial}{\partial r}(r \cdot q) = r \rho u C_p \cdot \frac{\partial T}{\partial x} \quad \cdots\cdots (5.19)$$

Integrating above Eqn.(5.19) from Ro to r,

$$\int_{R_o q_o}^{r \cdot q} d(r \cdot q) = \int_{R_o}^{r} r \rho u C_p \cdot \frac{\partial T}{\partial x}\, dr \quad \cdots\cdots (5.20)$$

$$\therefore \quad rq - R_o \cdot q_o = \int_{R_o}^{r} r \rho u C_p \cdot \frac{\partial T}{\partial x}\, dr \quad \cdots\cdots (5.21)$$

The overall energy balance gives

$$2\pi R_o \cdot dx \cdot q_o - 2\pi R_i^* \, dx\, q_i = \rho U_b \cdot C_p \cdot (\pi R_o^2 - \pi R_i^{*2}) \frac{dT_b}{dx} \cdot dx \quad \cdots\cdots (5.22)$$

Rearranging,

$$2(R_o \cdot q_o - R_i^* \cdot q_i) = \rho U_b \cdot C_p \cdot (R_o^2 - R_i^{*2}) \frac{dT_b}{dx} \quad \cdots (5.23)$$

where U_b is the average vapour velocity and

T_b is the bulk vapour temperature.

As a first trial, we assume $\frac{dT_b}{dx} = \frac{dT}{dx} = \frac{\partial T}{\partial x}$ which is true for constant heat flux.

Velocity u can be replaced by u_b, because it has been shown by Barrow[66] that for established flow the choice of function for velocity profile to obtain the heat flux distribution across the annular space for the case of asymmetric heating has a minor effect on the final heat transfer calculation. Therefore the assumption of $u = u_b$ has little effect on heat transfer calculation.

Combining Eqn. (5.21) and (5.23) and rearranging

$$\frac{q}{q_o} = \frac{1}{r}\,\frac{(R_o - R_i^{*}\cdot q_i/q_o)}{(R_o^2 - R_i^{*2})}\cdot(r^2 - R_o^2) + \frac{R_o}{r} \quad \cdots\cdots (5.24)$$

Let $q_i/q_o = A$, in which case

$$\frac{q}{q_o} = f(r) = \frac{1}{r}\,\frac{(R_o - R_i^{*}\cdot A)}{(R_o^2 - R_i^{*2})}\,(r^2 - R_o^2) + \frac{R_o}{r}$$

$$= \frac{(R_o - R_i^{*}A)}{(R_o^2 - R_i^{*2})}\,r + \frac{R_i^{*}\cdot A\cdot R_o^2 - R_i^{*2}\cdot R_o}{(R_o^2 - R_i^{*2})}\cdot\frac{1}{r} \quad \cdots (5.25)$$

Substituting this f(r) into Eqn. (5.16) and (5.17) for outer region and inner region heat flux calculation, we get

$$\frac{\rho_v C_{p_v}\cdot(T_w - T_s)}{q_o}\,u_{\tau_{w_o}} = \frac{P_r\cdot(R_o^{+} - R_i^{*++}\cdot A)}{(R_o^{+2} - R_i^{*++2})}\int_0^{y_{mo}^{+}}\frac{(R_o^{+} - y^{+})\,dy^{+}}{1 + P_r\cdot\frac{\varepsilon_H}{\nu}}$$

$$+ \frac{P_r\cdot(R_i^{*++}A\cdot R_o^{+2} - R_i^{*++2}\cdot R_o^{+})}{(R_o^{+2} - R_i^{*++2})}\cdot\int_0^{y_{mo}^{+}}\frac{dy^{+}}{(1 + P_r\frac{\varepsilon_H}{\nu})(R_o^{+} - y^{+})}$$

$$+ \frac{u_{\tau_{wo}}}{u_{\tau_{wi}}}\cdot\frac{P_r\cdot(R_o^{++} - R_i^{*+}\cdot A)}{(R_o^{++2} - R_i^{*+2})}\cdot\int_{y_i^{+}}^{y_{mi}^{+}}\frac{(R_i^{+} + y^{+})\,dy^{+}}{1 + P_r\cdot\frac{\varepsilon_H}{\nu}}$$

$$+ \frac{u_{\tau_{wo}}}{u_{\tau_{wi}}}\,\frac{P_r\cdot(R_i^{*+}\cdot A\cdot R_o^{++2} - R_i^{*+2}\cdot R_o^{++})}{(R_o^{++2} - R_i^{*+2})}\cdot$$

$$\cdot\int_{y_i^{+}}^{y_{mi}^{+}}\frac{dy^{+}}{(1 + P_r\cdot\frac{\varepsilon_H}{\nu})(R_i^{+} + y^{+})} \quad \cdots\cdots\cdots\cdots (5.26)$$

where $u_{\tau_{wo}}$ and $u_{\tau_{wi}}$ are shear velocities.

Ro^{++} means Ro non-dimensionalized using inner shear velocity $u_{\tau_{wi}}$ for parameter conformity, and

Ri^{*++} means Ri^{*} non-dimensionalized using outer shear velocity $u_{\tau_{wo}}$ for parameter conformity.

The heat transfer coefficient, h, is defined as;

$$h = \frac{q_o}{(T_w - T_s)} \qquad \cdots\cdots(5.27)$$

Here, heat flux q_o is heat lost in the tube wall per unit area and heat flux q_i is heat going into liquid core per unit area. Therefore, q_i is the heat flux which will heat the liquid temperature when the liquid temperature is below the saturation temperature.

In the liquid core, the heat flux at $r = R_i^*$ is

$$q_i = -\rho_\ell \cdot C_{p\ell} \cdot (\varepsilon_H + \alpha) \cdot \left.\frac{\partial T}{\partial r}\right|_{r=R_i^*} \qquad \cdots\cdots(5.28)$$

Using Eqns. (5.19) and (5.28) in the liquid core gives

$$\frac{1}{r}\frac{\partial}{\partial r}\left[r \cdot \rho \cdot C_p \cdot (\varepsilon_H + \alpha)\frac{\partial T}{\partial r}\right] = u_\ell \cdot \rho \cdot C_p \cdot \frac{\partial T}{\partial x} \qquad \cdots\cdots(5.29)$$

Now, since ρ and Cp can generally be assumed constant in the element

$$\frac{1}{r}\frac{\partial}{\partial r}\left[r \cdot (\varepsilon_H + \alpha)\frac{\partial T}{\partial r}\right] = u_\ell \cdot \frac{\partial T}{\partial x} \qquad \cdots\cdots(5.30)$$

by rearranging and integrating,

$$\int_0^{R_i^*} \frac{\partial}{\partial r}\left[r(\varepsilon_H+\alpha)\frac{\partial T}{\partial r}\right]dr = r\cdot(\varepsilon_H+\alpha)\frac{\partial T}{\partial r}\bigg|_0^{R_i^*}$$

$$= \int_0^{R_i^*} r\cdot u_\ell\cdot\left(\frac{\partial T}{\partial x}\right)dr \quad \cdots\cdots\cdots\cdots (5.31)$$

Now, the increase of liquid bulk temperature is defined as

$$\rho u_\ell \cdot C_p\cdot\pi\cdot R_i^{*2}\cdot\frac{dT_{b\ell}}{dx} = \int_0^{R_i^*}\rho u C_p\cdot 2\pi r\cdot dr\cdot\frac{\partial T}{\partial x} \quad \cdots\cdots (5.32)$$

Therefore, combining Eqns. (5.31) and (5.32),

$$\frac{\partial T}{\partial r}\bigg|_{R_i^*} = \frac{u_\ell}{2}\cdot\frac{R_i^*}{(\varepsilon_H+\alpha)}\cdot\frac{dT_{b\ell}}{dx} \quad \cdots\cdots\cdots\cdots (5.33)$$

The heat flux going into liquid core is

$$q_i = -\rho_\ell\cdot C_{p\ell}\cdot(\varepsilon_H+\alpha)\frac{\partial T}{\partial r}\bigg|_{r=R_i^*} = h_\ell\cdot(T_s-T_{b,\ell}) \cdots (5.34)$$

$$\therefore\ h_\ell = \frac{-\rho_\ell\cdot C_{p\ell}\cdot(\varepsilon_H+\alpha)\frac{\partial T}{\partial r}\Big|_{r=R_i^*}}{T_s-T_{b.\ell}}$$

$$= \frac{-\rho_\ell\cdot C_{p\ell}\cdot\frac{u_\ell}{2}\cdot R_i^*\cdot\frac{dT_b}{dx}}{T_s-T_{b.\ell}} \quad \cdots\cdots\cdots\cdots (5.35)$$

Substituting for $(T_S-T_{b,\ell})$ in Eqn.(5.35), the expression for h_ℓ is (detail given in Appendix 2)

$$h_\ell = \frac{\frac{1}{2}\rho_\ell\cdot C_{p\ell}}{0.584\ R_i^*\int_0^{R_i^*}\frac{\cos\left(\frac{r}{R_i^*}\cdot\frac{\pi}{2}\right)-1}{r(\varepsilon_H+\alpha)}dr + 0.9173\int_0^{R_i^*}\frac{\sin\left(\frac{r}{R_i^*}\cdot\frac{\pi}{2}\right)dr}{(\varepsilon_H+\alpha)}}$$

$$\cdots\cdots\cdots\cdots (5.36)$$

and $q_i = h_\ell\,(T_S-T_{b,\ell})$ $\cdots\cdots\cdots\cdots$ (5.37)

where T_b =liquid bulk temperature.

Now that q_i is known from Eqns. (5.34) and (5.36), we can calculate q_o through iterations using Eqns. (5.25) and (5.26), and hence h defined by Eqn.(5.27).

5.4 VAPOUR MASS FLUX CALCULATION

From the energy balance on the vapour control volume, we obtain,

$$2R_o \cdot q_o - 2R_i^* q_i = R_o^2 \cdot \frac{dE_v}{dx} - R_o^2 \cdot h_f \cdot \frac{d\dot{G}_v}{dx} \quad \cdots\cdots(5.38)$$

where Ev=energy flux= $\frac{1}{\pi R_o^2} \cdot \int_{R_i^*}^{R_o} 2\pi \rho_v \cdot u_v \cdot h_g \cdot r \cdot dr \quad \cdots\cdots(5.39)$

h_f=enthalpy of water at saturation temperature

$\dot{G}_v$=vapour mass flux= $\frac{G_v}{\pi R_o^2}$

Now, $E_v = h_g \dot{G}_v$

where h_g=vapour enthalpy at temperature T.

Therefore,

$$2R_o \cdot q_o - 2R_i^* q_i = R_o^2 (h_g - h_f) \frac{d\dot{G}_v}{dx} + R_o^2 \cdot \dot{G}_v \frac{dh_g}{dx} \quad \cdots\cdots(5.40)$$

In the author's previous study[1], the vapour superheat in the inverted annular film boiling was neglected. However, in the present study, some vapour superheat in the annulus vapour gap was considered. We let 10% of the total heat from the tube wall was used for the vapour superheat. *

Therefore

$$\pi R_o^2 \cdot \dot{G}_v \frac{dh_g}{dx} = 0.1\,(2\pi R_o \cdot q_o) \quad \cdots\cdots(5.41)$$

---

* The difference in calculated rewetting velocity using this assumption is about 3% compared to the case of no vapour superheat.

Substituting Eqn.(5.41) into Eqn.(5.40), we can obtain the increase in vapour mass flux along X-direction, $(\frac{d\dot{G}_v}{dx})$.

5.5 COMPUTATION

The convective heat transfer coefficient h in the inverted annular flow region was calculated for various experimental conditions using the present analysis. In the computation, several subroutines were used to calculate the imaginary radius Ri and the wall shear stress by iteration.

Many thermodynamic properties used in the computation such as density, viscosity and thermal conductivity of water and vapour, specific energy of vapour and emissivity of tube and vapour, are function of temperatures. In the computation, these values are all calculated for each temperature variance using subroutines.

The author's previous analysis[1] shows that the two most important parameters which affect the rewetting velocity is the rewetting temperature and the heat transfer rate in the region ahead of the rewetting front. As will be discussed in chapter 6, the present analysis gives a heat transfer coefficient in the inverted annular flow region which is much closer to the experimental heat transfer coefficient than the previously used Bromley-type equation[1]. Therefore, the heat transfer coefficient of the inverted annular flow region obtained in the present analysis is tried in the author's previous computer simulation model[1] to show the improvement of the prediction of the rewetting velocity.

The computer simulation model predicts the temperature-time trace curve at various axial locations of the vertical circular channel under the bottom flooding conditions, thus predicting the rewetting rate of a hot vertical channel.

In the simulation model the rewetting process was divided into six heat transfer regions namely, SINGLE PHASE STEAM, DISPERSED FLOW, INVERTED ANNULAR FLOW, TRANSITION BOILING, NUCLEATE BOILING and SINGLE PHASE LIQUID REGION.

In the computation, small elements were considered and in each element, coolant water is heated and its temperature and vapour quality as well as the wall temperature are calculated using appropriate heat transfer equations according to the flow region.

Rewetting velocity is obtained from two temperature-time trace curves at different locations of the test tube by knowing the "rewetting time" and the location of the temperature-time trace curve, because rewetting velocity Uq is the propagation rate of the rewetting front along the test section in the direction of the coolant water flow.

The initial reference wall temperature distribution of the computational model was chosen to be as close to the experimental initial reference wall temperature distribution as possible. The experimental initial wall temperature distribution is not uniform, but is different along the axial distance. To obtain the same reference wall temperature profile for the computational model as the experimental temperature profile, four axial locations along the test tube were chosen. Two of these locations were chosen near each end and the other two were around the middle about 1 m apart. At those four locations, the initial wall temperature Tw and the experimental rewetting temperature Tq were obtained. The initial reference wall temperature distribution of the computational model is calculated by interpolating along the channel between the four experimental wall temperatures at the specific axial locations.

The experimental rewetting temperature distribution along the axial distance is also calculated using the same method (interpolation between the four rewetting temperatures).

For reference, the program flow chart for this computation is shown in Fig.5.3 and the FORTRAN IV computer program can be found in Ref.[1].

Chapter VI

RESULTS AND DISCUSSIONS

This thesis include two major parts, experimental study and analytical study. In the experimental study, a total of 23 different test sections were used in the experiment to study the various parametric trends on the propagation of the rewetting front. The major parameters which affect the rewetting process are coolant flow rates, coolant inlet subcooling, initial wall temperature, wall thickness, wall material, power generation rates, and axial location along the channel as well as the flow channel geometry and orientation. These parameters as well as others are discussed in detail for various flooding modes.

From the result of the experimental study as well as from the authors previous numerical analysis[1], it was observed that the precursory cooling just ahead of the rewetting front and the rewetting temperature are two of the most important parameters affecting the rewetting velocity. Since rewetting temperature, Tq, was already studied in the author's previous work[79], naturally one aspect of the precursory cooling just ahead of the rewetting front is studied in the present analysis. The present analytical study is confined to a model which will calculate the heat transfer coefficient of the inverted annular flow film boiling in the downstream region of the rewetting front in a bottom flooding mode. The results of the analysis are discussed in detail and also compared with experimental results in this chapter.

6.1 EXPERIMENT

6.1.1 Bottom and Horizontal Flooding

Piggott and Porthouse[14], and Yu et al.[9] reported that during their early test runs, rewetting velocities showed progressive improvement with time, but then subsequently remained consistent. These investigators concluded that the effect was due to initial surface oxidation.

Contrary to this, the present test runs indicated, as shown in Fig.6.1(a), that the rewetting rate progressively deteriorated during the first few days of the experiment after a new test-section was installed. Subsequently, the rewetting rate remained practically constant.

The effect must be due to a "deposit" on the surface of the test-sections. The deposit affects the rewetting results in two ways: firstly, it alters the thermal properties of the test-section surface, and secondly, the number and characteristics of active nucleation sites on the surface. Since the effects of these two are difficult to predict, it is not possible to predict how they would affect the rewetting rate itself. All pipings and fitting were made of stainless steel in the present apparatus so that little contamination was expected from these sources. This was confirmed visually for a few test sections.

All the experimental results reported here are those obtained after about 7 days of preliminary test operation for each test-section.

(a) Effect of Initial Wall Temperature

A decrease in rewetting velocity was always observed with increasing initial wall temperature as shown in Fig.6.1(b), in all test-sections used. This is in agreement with other experimenters[14,18,23-29] who also observed decreasing rewetting velocity with increasing initial wall temperature. The general trend is also qualitatively in agreement with the analytical prediction[37,43,44]. Since the cooling ahead of the rewetting front affects the rewetting velocity with increasing coolant flow rates, it can be expected that the effect of the initial wall temperature is much more pronounced with higher coolant flow rates. Our experimental results confirm this trend, which implies that the rewetting rate is affected by the wall temperature just ahead of the rewetting front, Tq, which is defined as the "rewetting temperature" in the present study.

(b) Effect of Coolant Flow Rate and Subcooling

Most of the theoretical analyses[2,3] on the rewetting process do not recognize explicitly the effect of coolant flow rate. This is because the analyses require prescribed values of the heat transfer coefficient and the rewetting temperature which are usually thought to have certain constant values[37,44].

On the other hand, it has been known from experimental work that the rewetting velocity increases with increasing coolant flow rate[2,3]. Our results, as shown in Fig.6.1(c), all indicate that an increase in the coolant flow rate always resulted in a higher rewetting velocity at a given condition. This is partially due to improved precursory cooling and also due to an increase in rewetting temperature which increases the rewetting velocity; this is, as will be seen in section 6.2, shown also by our analysis.

The rewetting velocity increased with increasing inlet sub-cooling of coolant flow when all other conditions were kept constant during test run as shown in Fig.6.1(c). This finding was also observed by other workers[9,12,18].

(c) Effect of Wall Thickness and Material

Experiments were conducted in which the wall thickness of test-sections was changed while keeping other variables as constant as possible. Even at wall thicknesses between 0.89 mm and 1.65 mm (which are greater than the critical wall thickness proposed by Thompson[12] by a factor of 2 to 3) the rewetting velocity inversely varied approximately to the 2/3 power of the wall thickness.

When all other variables were kept constant, the rewetting velocity of the Inconel test-section was greater than that of the stainless steel test-section.

The higher rewetting velocity of the inconel test-section is mainly due to its higher thermal conductivity, k, and lower volumetric heat capacity, $C_p \rho$.

Thompson[53] concluded in his two-dimensional numerical analysis, that the effect of thermal conductivity of the wall material on the rewetting velocity was rather complex due to the existence of a critical wall thickness of about 0.5 mm. For very large values of Biot numbers, this could be true, but the values of Biot numbers for practical purposes are rather small, being generally less than one. Therefore, the effect of thermal conductivity and volumetric heat capacity of the test section generally follows the trend predicted by such simple one-dimensional analysis as proposed by Yamanouchi[37]. That is, the rewetting velocity is inversely proportional to the volumetric heat capacity and proportional to the square root of the thermal conductivity of the wall material.

(d) Effect of Power Generation

Some test runs were made with electrical power to the test-section kept on and off, to see the effect of power generation during the rewetting transient.

The results show(Fig.6.1(d)) that the effect of power input during the rewetting transient is to decrease the rewetting velocity. The trend has been predicted by Duncan and Leonard[41] who extended the one-dimensional solution of Yamanouchi[37] to a more general case by the inclusion of a uniform heat generation term. The numerical solution of the two-dimensional model by Thompson[53] also confirmed the effect.

(e) Effect of Channel Orientation

Case et al.[23] described in their paper the observations of rewetting phenomena in bottom flooding in a vertical annulus with a hot central core tube. They reported that the rewetting front was clearly defined, and was almost uniform around the circumference of the wetting surface. This implies that nearly uniform distributions of coolant phase and rewetting velocity were maintained.

However, when the coolant water is injected into a horizontal channel, a non-uniform phase distribution may arise under the influence of the gravitational force. The temperature distributions obtained with Test Section No.4 (Table 1) are shown in Fig. 6.2. From this figure it may be deduced that the fluid flow ahead of the quenching front would experience a stratified flow with skewed inverted fluid flow boiling along the lower part, and dispersed fluid flow along the upper part of the horizontal channel. Along the upper part, the heat transfer from the wall surface to the vapor may be relatively small. Therefore the rewetting velocity on the bottom of the horizontal tube should be much faster than the rewetting velocity on the top part.

The average rewetting velocity is obtained by the algebraic average of top and bottom rewetting velocities. The average rewetting velocity of the horizontal tube could also be defined by the propogation rate of the quenching front at the mid-side of the horizontal tube. In this report, the first method was used to get the average rewetting velocity of the horizontal channel.

The average rewetting velocity of a horizontal channel is about 20-30% lower than that of a vertical channel, all other experimental conditions being kept constant as shown in Fig.6.1(c). However, the difference decreases with an increase in the coolant flow rate. This relatively low rewetting velocity is thought to be due to the coolant flow stratification which results in a lower average heat transfer coefficient in the vicinity of the rewetting front. The flow stratification also seems to affect the rewetting temperature which also appeared to influence the propagation rate of the front.

6.1.2 Effect of Partial Flow Blockage

It can be easily postulated that some coolant flow subchannels could be partially or totally blocked during a loss-of-coolant accident due to ballooned fuel rods, because of the high temperature and large difference between the internal fission gas pressure and coolant pressure during the accident. The end plates and fuel rod bearing pads, especially in CANDU reactors, also disturb the ECC fluid flow.

A large number of experiments related to rewetting phenomena have been mostly concerned with undisturbed simple flow configurations and rod bundle geometry, except for a few such as those of Cermak et al.[74] and Davis[57].

Cermak et al.[74] studied the effects of flow blockage on bottom flooding under the PWR-FLECHT program. Blockages of 50 and 75% of the flow area of a 5x5 array in the center of a 7x7 rod bundle were investigated with 3.66 meter long heated rods with an axial cosine heat generation distribution. Their results showed that at a flooding rate of 0.152 m/s, the maximum temperature rise in heater rod was the same for 0, 50 and 75% flow blockage, but at lower flooding rates of 0.051 and 0.102 m/s, a higher temperature rise in the heater rod for the 0% blockage case than for the 75% flow blockage case was observed. They concluded that bottom flooding heat transfer effectiveness is not impaired with the flow blockage configurations tested.

Davis[57] also studied the effect of flow restrictions under emergency core cooling conditions as a part of PWR-FLECHT program. He conducted tests with six different blockage configurations and concluded that severe flow blockage of the small fuel pin array did not result in significant reduction in the effectiveness of cooling the array by emergency cooling flooding.

The experimental studies cited above not only dealt with flow restriction in the vertical channel orientation, but also were confined to rod bundle geometries. Although experimental results obtained from rod bundle geometries are more realistic and should yield practical information, the details of the physical mechanisms involved are more or less lost due to the complex experimental conditions. For these reasons, the effect of partial flow blockage on the rewetting phenomena in both vertical and horizontal channels are first studied employing a simple circular geometry.

In the present series of experiments, flow area reductions of 25% and 50% were obtained by placing orifice and venturi type blockages along the channels.

(a) Propagation of Rewetting Fronts

For both vertical and horizontal flow channel orientations, it has been shown that, under most conditions the rewetting front propagates at an almost constant rate when there is no flow restriction in the flow channel. However, with a partial flow blockage by orifice plate type flow obstructors, the present experiment seems to suggest that two completely different modes of the rewetting process are involved.

Figure 6.3 shows the temperature histories recorded for the region near No.4 blockage orifice plate (located at z = 1.80 m) when the coolant flow area is reduced by 25% with the test conditions indicated. About 16 seconds from the moment the reflooding started to take place at the entrance of the test section, No.4 blockage orifice plate (at z = 1.80 m), has already been wet, as seen from its temperature trace. However, at this same moment, the main quenching front propagating along the channel is still at about z = 0.50 meters (this quenching front is called "primary" in this study) and proceeds at an almost constant rate of about 75 mm/s. At t = 22 seconds, the point at z = 1.825 meters is already wetted and the point z = 1.775 meters is wet at t = 25 seconds, whereas at t = 23 seconds the primary quenching front is still located at about z = 1.05 meters.

This peculiar phenomenon is much more clearly illustrated in Fig. 6.4. The early quenching of the orifice plates must result from the vapor liquid mixture produced at the upstream region moving quickly along the channel. When secondary quenching fronts are formed at the locations of orifice plates, it can be seen from Fig. 6.4 that they proceed in both directions at an almost constant velocity, and for the case of Fig. 6.4 at about 4 mm/s, (compared to 75 mm/s for the primary quenching velocity). The secondary quenching fronts propagate at their own velocity until they are met by the primary front which propagates at its own specific velocity. Since the velocity of the primary quenching front is more than 15 times faster than that of the secondary quenching front, the two quenching fronts meet near the blockages. The location where these two fronts come together, varies depending on the experimental conditions. Therefore, in order to compare the rewetting velocities in partially blocked and 0% blocked channels, the primary rewetting velocity must be used.

Figure 6.4 also implies that different rewetting mechanisms are involved in these two quenching fronts. While the propagation of our so-called "secondary" quenching front is mainly controlled by the axial heat conduction, that of the primary quenching front is achieved by hydrodynamic cooling.

(b) Effect of Channel Orientation

The same characteristics of rewetting were also observed when the channel was horizontal. However, the effect of partial flow blockage coupled with that of channel orientation is rather complex. For the same experimental conditions with 0% blocked flow channel geometry, the rewetting velocity of horizontal channels is about 10 to 30% lower than that of vertical channels. This difference is attributed to the gravitational force which makes the coolant flow stratified. It was assumed that vapor fluid flow is dominant along the upper part of the channel with skewed inverse annular fluid flow dominant along the bottom. Since the heat transfer process of the latter is more efficient than that of the former, rewetting takes place first at the lower part. However, with orifice plates in place, the sequence of rewetting around the circumference, in general, is not as consistent as it was in the case of 0% flow blockage. This implies that the presence of a partial flow blockage impedes the formation of flow stratification. This is especially pronounced with decreasing flow rates and increasing blockage factor as shown in Fig. 6.5.

(c) Effectiveness of Flow Blockage

Davis[57], reported that the effectiveness of emergency core cooling was enhanced even if flow blockages were introduced into the subchannel flow areas. The test results shown in Fig. 6.5 are in agreement with his observation. It can be seen that in vertical channels, the effect of the presence of flow blockage on the rewetting velocity is relatively small for $G < 200$. However, $G > 200$, the difference of rewetting velocities increases markedly. As much as a

25% increase in rewetting velocity was observed at G = 400 for the test-section with 25% flow blockages. This increase is reduced to about 10% when the flow area was reduced by 50%.

As mentioned earlier, the rewetting velocity in the horizontal unblocked channel was about 10 to 30% slower than that in the vertical unblocked channel for the same test condition. The difference in rewetting velocity, due to its orientation, becomes less significant with increasing blockage factor and decreasing coolant flow rate as seen in Fig. 6.5. This may be due to the fact that the presence of orifice plate type blockages impedes the formation of flow stratification and this, in turn, introduces in a horizontal channel a nearly uniform phase distribution of the coolant similar to that can be found in a vertical channel.

Figure 6.5 also indicates that the rewetting velocity increases with increasing coolant flow rate in all cases. The effect of coolant inlet subcooling was to increase the rewetting velocity, but it became less significant with decreasing coolant flow rates.

(d) Effect of Initial Wall Temperature

The effect of initial wall temperature in partially blocked channels was similar to that of unblocked channels; a decrease of the rewetting velocity with increasing initial wall temperature as shown in Fig. 6.6. The effect of partial flow blockage on the rewetting velocity is more pronounced with decreasing initial wall temperature. The same trends were also observed in horizontal channels. When the power is left on during the reflooding transient, the wall temperature continues to rise until the heat removal exceeds the heat generation rate. It was observed, in the present study, that the turn-around temperature in horizontal channels was higher than that of vertical channels for the same experimental conditions. This is obvious as the rewetting velocity in the horizontal channel was always slower than that of the vertical channel for the same test condition. As it was with the difference in the rewetting velocity due to the channel orientation, the difference in the turn-around temperature becomes less significant with increasing flow blockage factor.

(e) Effect of Heat Generation Rate

The effect of heat generation (almost constant) during the reflooding transient coupled with the presence of partial flow blockages is shown in Fig. 6.7. Its effect is very similar to those of initial wall temperature.

Figs. 6.5, 6.6 and 6.7 all indicate that flow area reductions by orifice plate blockages, up to 50%, enhance the effectiveness of rewetting for all test conditions studied and that the highest rewetting velocity seems to occur at the flow blockage of about 30 - 35%.

(f) Effect of Blockage Type

With Test-Section No.7, which had verturi type flow blockages, the "primary" as well as the "secondary" quenching fronts observed with Test-Sections Nos.5 and 6 were again observed as shown in Fig. 6.8. However, the role of the "secondary front" with Test-Section No.7, seems to be less significant. This is expected due to the less abrupt change of flow channel geometry in the axial direction. However, the propagation rates of the "primary quenching front" were about 10 to 50% higher than those of Test-Section No.5, which had a 25% flow reduction blockage of the orifice type. This was unexpected and no physical explanation was presented. To confirm these unusual and unexpected results, Test-Section No.8 was manufactured which has 3 orifice and 3 venturi-type blockages of 25% flow reduction. Tests were done with both venturi ahead of orifice-type blockage and orifice ahead of venturi-type blockage and the result confirms the finding of experiment No.5-7. The rewetting velocity in the channel with venturi-type blockage is faster than that of the orifice-type blockage. One possible explanation could be that while orifice-type blockage disturbs and retards the coolant flow, the venturi-type blockage enhances the coolant flow velocity, thus having the effect of increased coolant flow rate.

6.1.3 Unconfined Top Flooding

(a) Effect of Coolant Flow Rate

In the top flooding, Bennett et al.[10] reported that they could not observe the effect of coolant flow rate on the rewetting velocity, while Duffey and Porthouse[18] reported that the effect was significant.

Bennett et al. used an annular test-section with one 0.3 meter long heated inner tube, whereas Duffey and Porthouse used four circular tube test-sections ranging from 0.1 to 0.25 meters in length. Our test-sections were 1.23 to 1.42 meters in length. The results shown in Figs. 6.9 to 6.11 indicate clearly that although the effect of coolant flow rate is less significant compared to that of the confined top-flooding mode, the coolant flow rates do affect the rewetting velocity. This is obvious since, even though the rewetting front for unconfined top-flooding is limited to an extremely narrow region, it is still hydrodynamically affected.

(b) Effect of Precursory Cooling

In Figs. 6.9 to 6.11, the results of the unconfined top-flooding are compared to those of the confined top-flooding tests, and it can be clearly seen that precursory cooling due to the heated confinement has a significant effect on the rewetting phenomena. The rewetting velocity of the confined top-flooding is faster than that of the unconfined top-flooding, by a factor ranging from 2 to 4, for Di=15 mm.

(c) Effect of Initial Wall Temperature

The previous results with bottom flooding experiments and flooding of horizontal channels have shown that a decrease in rewetting velocity was always observed with increasing initial wall temperature.

Fig. 6.12 again indicates the same trend, that an increase in rewetting velocity is obtained with decreasing initial wall temperature. The effect of precursory cooling due to the confinement of flow space is also clearly illustrated in the figure.

(d) Effect of Inlet Subcooling

Also, the trend of increasing rewetting velocity with increasing coolant inlet subcooling in the bottom flooding and flooding of horizontal channels is again seen with the present case of unconfined top flooding tests as shown in Fig. 6.13. Since the effects of precursory cooling due to the confinement of flow space are seen in Fig. 6.12, the comparison with that of the confined top-flooding is not made in Fig. 6.13.

(e) Effect of Heat Generation Rate

It is shown in Fig. 6.14 that the effect of heat generation rate during the transient on the rewetting velocity is not insignificant for all bottom, horizontal and confined top flooding cases.

The results from our unconfined top flooding tests also indicate (Fig. 6.15) that the rewetting time was lengthened with increasing heat generation rate, but its effect on the rewetting velocity seems to be less, compared to that of confined cases.

(f) Effect of Presence of Unheated Flow Boundary

The presence of unheated transparent outer jackets (Di=30 and 50 mm.) seemed to have very little effect on the precursory cooling, hence on the rewetting velocity. However, this cannot be true if the temperature of the outer jacket is higher than the rewetting temperature.

6.1.4 Confined Top Flooding

One of the experimental constraints in the present study is that the pressure drop across the test-section must be kept constant during the test period.

With the present apparatus, the typical variation of inlet and outlet pressure obtained during a given test condition is shown in Fig. 6.16. Although there is a time variation of pressure up to +/- 2 psi at about 3-6 hz for the conditions of Fig. 6.16, the time averaged pressure drop across the test section seemed to remain almost constant during the test period. Similar phenomena were observed in all confined top flooding experiments. The variation of coolant flow rate was generally small and usually under +/- 5% of the designated flow rate.

Most of the theoretical analyses on the rewetting process, be they analytical or numerical, do not explicitly recognize the effect of coolant flow rate. This is because the analysis requires prescribed values of heat transfer coefficients in the region of interest.

In top-flooding experiments, Bennett et al. [10] reported that the effect of coolant flow rate on the rewetting velocity is negligible, while the results of Duffey and Porthouse [18] on top-flooding show that the effect is significant.

The results of this study on the effect of coolant flow rate, shown in Figs. 6.17 and 6.18, indicate that an increase in the coolant flow rate resulted in a higher rewetting velocity for a given condition.

As seen in the previous section, the mechanism of rewetting in top-flooding is quite different, depending upon whether the falling coolant film has confined space or not. The experiment of Bennett et al.[10], was carried out on the outside of the heated tube of an annulus, while the results of the present study, which show the significant effect of the coolant flow rate, was carried out inside a heated channel. The difference due to the confinement of space will be further discussed in the next section.

(a) Effect of Flow Area

Since the precursory cooling ahead of the rewetting front has a significant effect on the rewetting phenomena in confined top-flooding modes, the effect of the flow area ahead of the propagating rewetting front was studied using two test-sections differing only in their inside diameters. The results, shown in Figs. 6.17 and 6.19, clearly show that the effect of the inside tube diameter on the propagation rate of the rewetting front is significant for the range of parameters studied. It must be pointed out that in Fig. 6.17, coolant flow rate is expressed in $\bar{G}$(g/mm.s), while in Fig. 6.19, in G(kg/m^2.s).

The figures illustrate that an increase in the channel flow area in the confined top-flooding mode results in a lower rewetting velocity at a given test condition. The effects of parameters such as coolant inlet subcooling initial wall temperature etc., were similar to those of bottom flooding.

However, the results of the present study also suggest that the effect of the inside tube diameter on the rewetting velocity becomes less significant with increasing values of the inside tube diameter. This is deduced from the fact that the results from test-section No. 12 (Di=22.1 mm) are comparable to those of the unconfined top-flooding experiment with test-section No. 9, which are shown in Fig.6.17.

(b) Effect of Inlet Geometry

With large inside diameter test-sections, the study also showed that the size of coolant inlet diameter to the test-section has a very important effect. When the coolant inlet diameter was relatively small compared to that of the test-section (say 1 to 3), it seemed that the coolant water shot off through the middle of the test-section tube, instead of rewetting the tube from the inlet, especially when the flow rate was large ($G > 200$). On such occasions, there formed two rewetting fronts propagating at their own specific rates. Therefore, the overall rewetting time will be shorter. The results shown in Figs. 6.17 and 6.19 are those of the primary fronts only.

(c) Comparison of Various Flooding Modes

The confined top-flooding results are compared in Fig. 6.18 with previous results of bottom flooding of vertical channels, and those of flooding of horizontal channels. The comparison indicates that the confined top-flooding results lie in about the middle of two cases. This suggests that there is a difference in the hydrodynamic aspects of rewetting processes involved, between top and bottom flooding. As can be deduced from Fig. 6.20, the post-CHF flow regimes involved in the two flooding systems are quite different.

In Fig. 6.21, the results of the initial wall temperature on the rewetting velocity for three different test sections are compared. The figure shows a decrease in the rewetting velocity with increasing initial wall temperature. Again, the results of confined top flooding seem to lie between those of bottom flooding of vertical and horizontal channels, similar to the case of changing the coolant flow rate. Fig. 6.21 also shows the effect of variation in the coolant flow rate.

(d) Effect of Heat Generation Rate

Even though Bennett et al.[10] reported that there was no significant difference in the results, after conducting top-flooding tests with the power both on and off during the course of the rewetting experiment, our previous test results of bottom flooding and rewetting of horizontal channels show that the rewetting time was lengthened with an increase in power input for the range of flow rates(100 to 400 mm/s) studied. Although the heat generation rate could not affect the hydrodynamic heat transfer processes in the region of the rewetting front, it should affect the wall surface temperature, and increase the heat flux due to the increased heat content.

The results from our top-flooding tests, as shown in Fig. 6.14, indicate that the rewetting velocity decreased with increasing power input during the tests. Fig. 6.14 again illustrates that the results gained from the top-flooding rewetting process generally lie between those of bottom flooding and of rewetting of horizontal channels.

The velocity of the rewetting front in confined top-flooding seemed to remain constant as the front proceeded down the test-section, as it did for bottom and horizontal flooding of hot channels.

6.1.5 Effect of Tube Diameter Test

It was seen in Fig. 6.17 that the effect of tube diameter on the rewetting velocity in the confined top-flooding mode was significant. This is mainly due to the precursory cooling ahead of the rewetting front.

To see if this is also true for both the bottom and horizontal modes in a single tube, two identical tubes having different inside diameters, test-section Nos. 4 and 13, were used in the experiment.

Some typical results from the bottom flooding experiment are shown in Fig. 6.22 which indicates that for high initial wall temperature, the rewetting velocity is faster for the larger diameter tube, whereas for low initial wall temperature, it seems to suggest the opposite is true.

For horizontal flooding, it can be seen in Fig. 6.23 that the effect of the tube inside diameter seems to have almost no effect on the rewetting velocity when the coolant flow rate is expressed in $G(kg/m^2.s)$.

The difference in the effects of the tube inside diameter for different modes of flooding in a simple tube must be due to the different fluid flow regimes associated with that particular mode of flooding. However, how it affects the final result is not yet clear and more study will be needed.

6.1.6 Annular Bottom Flooding

The geometry of the coolant flow channel must have an important role on the rewetting phenomena. This is expected as the flow regime in the vicinity of the rewetting front must be strongly affected by the geometry of the flow channel.

Two annular test-sections with the hot core tubes, Nos.14 and 15, were used in the experiment. The flow area variation by a factor of 1.4 was obtained by changing the core tube diameter.

(a) Effect of Geometry

Duffey and Porthouse[18] who used two annular test-sections with a hot center tube in which they changed the flow area by a factor of about two by changing the outer tube diameter report that for the same flow (i.e. $\dot{G}$ in g/s by our definition) through the channel, the rewetting time increased by about 20% in the larger channel for low initial wall temperatures, but at high initial wall temperatures, the rewetting times for both channels were about the same.

Our results, shown in Fig. 6.24, indicate that for low flow rates ($\dot{G}$ in g/s less than 60) the effects of flow area seem to be negligible, but for high flow rates for the same flow through the annuli, the rewetting velocity increased in the larger annulus (No.14) for the ranges of the variables studied. This is quite contrary to the trend reported above by Duffey and Porthouse[18]. Since the effect of the increasing flow area in the case of annular test-sections with a hot center core has the effect of increasing the degree of inlet sub-cooling of the coolant, the trend observed in Fig. 6.24 must be correct.

(b) Effect of Coolant Flow Rate

Duffey and Porthouse's results also indicate that, for the same inlet liquid velocity (i.e. G in $kg/m^2.s$ by our definition), there is a small decrease in rewetting time (e.g. increasing rewetting velocity) with increasing flow area and that this increase is more marked at high initial wall temperatures.

This is similar to our results shown in Fig. 6.25 where the rewetting velocity is plotted against the flow velocity, G. Again for low flow velocity, the effect of flow area seems to be insignificant. With low flow rates, either in G or $\dot{G}$, the effect of "equivalent" inlet subcooling must be very small and this may explain the negligible effect on the rewetting velocity.

Increasing the flow rate seems to bring about increased effect of coolant flow rates as seen in Figs. 6.24 and 6.25 and this may be that the increased flow area acts as increased coolant sub-cooling at the rewetting front.

(c) Effect of Initial Wall Temperature

A decrease in rewetting velocity was always observed with increasing initial wall temperature in both annular test-sections as illustrated in Fig. 6.26. This is qualitatively in agreement, not only with the analytical prediction for the bottom flooding in a simple tube, but also with the experimental results made on all the modes of flooding studied (illustrated in Figs. 6.12, 6.21 and 6.26).

Since the cooling ahead of the rewetting front affects the rewetting phenomenon with increasing coolant flow rates, it can be expected that the effect of the initial wall temperature should be much more pronounced with higher coolant flow rates. This is again confirmed by our results as shown in Fig. 6.26 for both single tubular and annular test-sections. This implies that the rewetting rate is strongly affected by the wall temperature just ahead of the rewetting front,* Tq, which was defined as the "rewetting temperature" in the present study.

(d) Effect of Heat Generation Rate

As was for the experiment with a single tube, some tests were made with electrical power to the test-sections kept on to see the effect of the heat generation rate during the rewetting transient. As was expected, the effect of the heat generation is, to moderate degree, to reduce the slope of the temperature-time transient and hence the velocity, just as for all bottom, horizontal and confined top flooding cases of single tubes. This is shown in Fig. 6.27.

(e) Comparison of Single and Annular Test-section with only Core Tube Heated

In Fig. 6.28, the results of the annular test-section are compared with those obtained in a single tube for the effects of initial wall temperature and of coolant flow rate. The general trends are similar for both test-sections, but quantitatively differ greatly as the effect of geometry is an additional effect which is difficult to isolate. The difference seen in Fig. 6.28 can be analogous to the trend seen in Figs. 6.24 and 6.25, because the flow area of the annular test-section is about 8 times larger than that of the single tube. It can be expected, therefore, that the effect of coolant sub-cooling must be more significant with the annular test-section, especially for larger flow rates.

Annular horizontal flooding was tried with test-sections No. 14 and No. 15. However, it was not possible to obtain any experimental results because the outer glass tubes cracked as soon as the coolant was injected. This was due to the severe bowing of the core tubes in spite of about 400 pounds tension applied, to prevent the core tube from bowing. Further experimental work on annular horizontal flooding with both walls heated is discussed in section 6.1.7.

6.1.7 Annular Bottom and Horizontal Flooding

In their review paper, Butterworth and Owen[3] stated that there was no experimental evidence to show that there was any effect of channel geometry on the quench front (rewetting) velocity. At the same time, they also concluded that there was insufficient data to prove that there was no effect.

Aside from the fact that how much liquid is being supplied to a certain rod in rod bundles and as to how well distributed the coolant liquid is on that rod, the present author has shown that the fluid flow near the region of propagating rewetting front has a significant effect on the rewetting velocity. Since the fluid flow in a channel is affected by the channel geometry, it is quite possible that the channel geometry may affect the rewetting velocity, even with the same mode of flooding.

Another effect which has been neglected is the effect of heating boundary. In an annular channel, the result from the channel where only one wall is heated, must be different from that of the channel where both walls are heated.

To clarify these points, concentric annular test-section (test section No.16), whose walls can be heated seperately were used for bottom and horizontal flooding modes.

6.1.7.1 Annular Bottom Flooding (ABF mode)

The effects of the initial wall temperature, coolant flow rate and coolant inlet sub-cooling on the rewetting velocity in a concentric annular test-section with both walls heated are shown in Figs. 6.29 and 6.30.

When the temperature of the both walls are the same, the effects of these parameters are very similar to those observed in the bottom flooding of a simple vertical tube. This implies that if the coolant flow rate is given in mass per unit area and unit time (e.g. $kg/m^2.s$ or $lb/ft^2.hr$), and the flow area is the same, the effects of initial wall temperature, coolant flow rate and coolant inlet subcooling on the rewetting velocity seem to be little affected by the channel geometry, provided that the channel cross-section does not have sharp corners. However, when the walls of the annular test-section were not equally heated, the effect can sometimes be significant as can be seen in Figs. 6.29(a), 6.29(b) and 6.30(a). It is observed in Fig. 6.30(a) that when only one wall is heated, the average rewetting velocity is faster than that of the case where the both walls are heated, with all other parameters being maintained equal. This is obvious as the heat capacity of the former is less than that of the latter, and consequently the amount of heat to be removed by the same coolant mass flow rate is less, resulting in faster rewetting velocity for the former.

When the walls are not maintained at the same temperature at the beginning of the flooding, the picture is a little more complex as can be seen in Figs. 6.29(a) and 6.29(b).

When the inner wall temperature was kept at the different temperature from that of the outerwall, its effect on the rewetting velocity is very small as illustrated in Fig. 6.29(a). On the other hand, when the outer wall temperature was kept at the different temperature, its effect is significant as seen in Fig. 6.29(b). That is, when $T_{wi} \neq T_{wo}$, u_q is strongly affected by T_{wo}. This is mainly due to the greater heat capacity of the outer wall. If we define non-dimensional parameters δ^* and T_{δ}^* as

$$\delta^* = \frac{\delta_i \cdot D_i}{\delta_o \cdot D_o} \qquad (6.1)$$

and

$$T_{\delta^*} = \delta^* \cdot \frac{T_{wi}}{T_{wo}} \qquad (6.2)$$

respectively, we can conclude the following:

(i) for $T_{\delta}^*=1$, neither wall has any dominant effect on,

(ii) for $T_{\delta}^* \ll 1$, the effect of the outer wall is dominant, and

(iii) for $T_{\delta}^* \gg 1$, the effect of the inner wall is dominant.

6.1.7.2 Annular Horizontal Flooding (AHF mode)

For horizontal flooding of a channel having a central core (the simplest simulation of rod-bundle channels) with both walls heated, the definition of quenching (rewetting) velocity must be reviewed.

The rewetting velocity is generally defined as:

$$u_{ij} = \frac{\Delta z_{ij}}{\Delta t_{ij}} \qquad (6.3)$$

where u_{ij} is the rate of the rewetting front propagation between two particular points of interest, Δz_{ij}, and Δt_{ij} is the time interval taken between the two rewetting fronts. The rewetting velocity defined by Eq.(6.3) is here called "Apparent" rewetting velocity to differentiate it from "Effective" rewetting velocity which is defined as

$$u_e = \frac{z_{total}}{t_{q,total}} \quad \cdots\cdots\cdots\cdots\cdots\cdots (6.4)$$

where z_{total} is the entire length of the heated channel or rod of interest and $t_{q,total}$ is the time when every point in the channel or rod is completely rewetted.

The second definition by Eq.(6.4) is necessary as the apparent rewetting velocity conventionally defined by Eq.(6.3) become meaningless when it is applied to a certain section of the horizontal channel during the reflooding. As seen in Figs. 4.6 and 4.8 of the visual study, the top sections of both single and annular test-sections are never rewetted in the usual sense. This phenomenon in a concentric annular test-section with both walls heated is more pronounced at the lower coolant flow rate.

In bottom and top flooding in a vertical tube or annulus, it was seen that the rewetting front was clearly defined and was almost uniform around the circumference of the channel. This indicates that uniform distributions of coolant phase and rewetting front were maintained during the reflooding transient.

However, when the coolant water is injected into horizontal heated channels, a non-uniform phase distribution arises under the influence of the gravitational force.

(a) Wall Temperature Distribution during Transient

The axial temperature distributions of the concentric annular test-section with the both walls heated are shown in Figs. 6.31 and 6.32. From these figures with the visualization of Figs. 4.8a to 4.8e, we see that the coolant flow ahead of the quenching front is a stratified flow with skewed inverted fluid flow boiling along the lower part of the annulus, and dispersed fluid flow along the upper part of the annular test-section. Along the upper part, small water droplets may collide with the walls of both the core and outer tubes and the heat transfer from the wall surfaces to the dispersed flow may be relatively small compared to that of the lower part.

In Figs. 6.31 and 6.32, we can see that the lower parts of both the core and outer tubes, and the upper part of the core tube go through the usual rewetting transient characterized by the steep axial temperature gradients in a very short period of time. The upper parts of the outer tube, however, does not exhibit the usual characteristics of any rewetting process. It is evident from the broken lines of Fig. 6.32, the heat transfer from the upper part of the outer tube is that of convective nature, and circumferential conduction within the wall. As a result, the upper parts of both the outer and core wall decrease at a slower rate than those at the lower parts of the annulus with the both wall heated.

(b) Effect of Flow Rate and Inlet Subcooling

Coolant flow rates affect the stratification of the fluid flow in a horizontal channel and therefore affect the rewetting process as shown in Fig. 6.33. For G=200 $kg/m^2.s$, the entire annulus goes through the usual rewetting transient, though the upper parts of both the core and outer tubes rewet slower than the lower part. However, as the coolant flow rate becomes less than 100 $kg/m^2.s$, the upper part of the annulus is not cooled by "rewetting" process, but by the convection by vapour which may have entrained water droplets.

If we are to apply Eq.(6.3) to calculate the rewetting velocity, we would obtain such as shown in Fig. 6.34. For G=200 $kg/m^2.s$, we see that the rewetting velocity is almost independent of the circumferential location. However, for G $<$ 100 $kg/m^2.s$ the "apparent" rewetting velocity approaches infinite values at the uppermost part of the outer wall. This is due to the definition given by Eq.(6.3).

The effects of coolant flow rate, coolant inlet temperature (inlet sub-cooling) and initial wall temperature on the apparent rewetting temperature in an annulus are shown in Fig. 6.35. The effects of these parameters are, in general, similar to those observed in the bottom flooding of a simple vertical tube or annulus, though the actual magnitudes depend on the circumferential position. As the figure illustrates, the "apparent" rewetting velocity at the upper part of the outer tube approaches to infinity with decreasing coolant flow rate, decreasing coolant inlet sub-cooling and increasing initial wall temperature. This does not imply that the rewetting is better for the upper part of the outer tube. The higher apparent rewetting velocity is the result of the defect in the definition of Eq.(6.3).

An interesting observation can be made in Fig. 6.35. For $G < 100\ kg/m^2.s$, the entire annulus except the upper-most part of the outer tube is rewetted uniformly. However, this does not mean that the rewetting front is uniform at a given axial position during the transient. Since the fluid is stratified at the beginning of the injection even with $G > 100\ kg/m^2.s$, the rewetting front is bound to be inclined toward the up-stream. Therefore, even though appears to be the same, the quenching time at a given axial position of the channel is circumferentially dependent.

To avoid a rewetting velocity of an infinity as seen in Fig. 6.35, the definition of an effective rewetting velocity defined by Eq.(6.4) is used for the same data which were reduced to give Fig. 6.35 and the results are given in Fig. 6.36. One can see in the figure that the effective rewetting velocity is circumferentially dependent.

It must be pointed out here that the new rewetting velocity is only a definition and that it can be useful for the interpretation of the data obtained. However, the effects of coolant flow rate, initial coolant sub-cooling and initial wall temperature on the rewetting seem to be similar to those observed previously in bottom flooding.

In Fig. 6.37, the rewetting process in a horizontal annulus with both walls heated are shown for two different coolant flow rate.

With G=200 $kg/m^2.s$, it is clearly seen that the rewetting front propagates towards the downstream and from the bottom to the top with an inclined rewetting front within a given cross-section of the annulus.

However, with low coolant flow rate of 50 $kg/m^2.s$, the inclined rewetting front is more pronounced with much decreased velocity. Only the lower half of the annulus goes through the rewetting process in the usual sense, and the upper part remains void for a long period of time.

These quenching processes can also be observed from the surface heat flux distributions along the axial position which were calculated from the time history of the wall temperature. It can be seen in Fig. 6.38 that for G=200 $kg/m^2.s$ (as well as for high inlet sub-cooling and low initial wall temperature), the rewetting proceeds toward downstream and from the bottom to the top of the annulus. The maximum heat flux is comparable to that of CHF for the range of parameters involved.

However, with low coolant flow rate of 50 $kg/m^2.s$ (as well as for low inlet sub-cooling and high initial wall temperature), the heat flux distributions shown in Fig. 6.39 exhibits a very interesting phenomenon.

While the rewetting proceeds downstream and from the bottom to the top, the top of the inner core tube does not experience the usual rewetting process. It seems that as soon as the lower part of the core tube is rewetted, the top part of the core is rapidly cooled by circumferential heat conduction before the coolant can reach there (the coolant is stratified). The same cannot be said for the outer tube as the circumferential distance between the bottom and top of the outer tube is much longer than that of the core.

6.1.8 "L"-shaped Test Section

Test-sections No.17-18 are L-shaped test sections used for two different flooding modes: horizontal flooding followed by bottom flooding or top flooding followed by horizontal flooding. The CANDU reactor has horizontal fuel channels and vertical feeder tubes while the BWR reactor has vertical fuel channels with horizontal feeder tubes, and these L-shaped test-sections would simulate the rewetting behavior in the reactor more closely than simple straight tubes.

6.1.8.1 Top-followed-by-Horizontal Flooding: THF

(a) Wall Temperature Distribution during Transient

Typical axial wall temperature distributions, as a function of time during a rewetting process in the L-shaped test-section with Swagelok elbow by THF mode are shown in Fig. 6.40.

At the beginning of the transient, a reasonably uniform temperature distribution at the central portion of both the vertical and horizontal sections was obtained. However, due to the greater wall thickness of the elbow section made of Swagelok fitting, its temperature was always much lower than the expected rewetting temperature.

Fig. 6.40 implies that the effect of the elbow at lower temperature on the overall rewetting transient in an L-shaped test-section should be significant. Since the end and elbow effects are due to unavoidable practical consideration in experiments, the results from only the middle portions of the vertical and horizontal sections of the L-shaped test-section, where a reasonably uniform temperature remained from the beginning of a test, are reported.

Since the cooling ahead of the rewetting front increases in the direction of flow, the wall temperature ahead of the front must decrease in the dry region where the temperature was initially uniform and constant. This is clearly illustrated in Fig. 6.40.

(b) Propagation of Rewetting Fronts

Unlike a simple tube test-section where a single rewetting front propagates axially, the present study showed that there exists three separate rewetting regions during the transient as seen visually. This peculiar rewetting phenomenon of the THF mode in an L-shaped channel can be clearly seen in Fig. 6.40, and is due to the presence of the elbow section which remained at lower temperature than other part of the test-section at the beginning of a test. When the coolant is first introduced into the channel, the major portion falls through the center core of the channel of the vertical section without touching the walls, due to the higher wall temperature than the rewetting temperature, and hits the elbow section. Since the temperature of the elbow section is about 100-200 C lower than other parts of the channel, the elbow section is wetted the moment the water hits it.

The water then flows through the horizontal section of the channel, thus creating the third rewetting front, in addition to the two fronts established in the vertical section; one top-flooding and the other pseudo-bottom-flooding starting at the elbow section. Therefore, the rewetting phenomena of THF mode in an L-shaped channel will be discussed by dividing the test-section into three regions as illustrated in Fig. 6.41. Fig. 6.40 also shows rewetting of the top and bottom of the horizontal section of the channel. The rewetting front is very much inclined, and the bottom of the channel usually rewets faster than the top. The visualization showed that the rewetting fronts in the vertical section seemed to be unsteady.

(c) Effect of Coolant Flow Rate

For a given experimental condition, it can be seen in Fig. 6.42 that the rewetting velocities in all three regions increase as the coolant flow rate increases. This is in agreement with the results of other works in both the confined and unconfined flooding modes. This increased rewetting velocity results from the increased precursory cooling on the dry side as well as the increased "apparent" rewetting temperature.

An interesting phenomenon can be ~~seen~~ in Fig. 6.42 where the present results are quantitatively compared against the results obtained from a simple vertical and horizontal channel.

As far as the effect of the coolant flow rate is concerned, the agreement is very good in Regions 1 and 3 of Fig. 6.41. This is more or less expected as there is no particular reason that the rewetting mechanics involved should differ. However, this is not true in Region 2, which is equivalent to bottom flooding with a reduced flow rate. The flow rate, G, is the injected coolant mass flow rate at the entrance of the L-shaped channel, but in Region 2, only a part of the incoming coolant is accumulating above the elbow section and this, in turn, affects the rewetting front which creeps up the vertical section in the opposite direction of the coolant flow. Therefore, the agreement between the present results in Region 2 cannot be expected to agree with those of the bottom-flooding in a simple vertical channel. This is indeed the case as shown in Fig. 6.42(b).

As was observed before in a horizontal channel, the rewetting velocities of the top and bottom of the horizontal section of the channel, though not exactly equal, are close to each other. This is illustrated in Fig. 6.42(c).

(d) Effect of Inlet Subcooling

The rewetting velocity is increased with increasing subcooling, (Ts-Tc), of coolant flow at the inlet of the test channel in Region 1 and 2. However, in Region 3, the effect seems to be negligible as seen in Fig. 6.43. One possible explanation for ~~this~~ is that the coolant which arrives at the entrance of Region 3 has already gone through the vertical section and therefore has lost whatever degree of inlet sub-cooling it originally had.

The increased rewetting velocity with increased inlet coolant sub-cooling must result from an increase in the effective heat transfer coefficient with subcooling in the region just ahead of the rewetting front as well as an increase in the apparent rewetting temperature.

(e) Effect of Heat Generation Rate

Previous test results of various flooding modes showed that the rewetting time was lengthened with an increase in power input for the range of test-parameters studied. Since more heat has to be removed, a lower rewetting velocity is expected and the trend can be easily predicted analytically.

The present results as shown in Fig. 6.44, indicate that this is indeed correct. That is, the rewetting velocity decreased with increasing power input during the tests.

6.1.8.2 Horizontal-followed-by-Bottom Flooding: HBF

(a) Wall Temperature Distribution during Transient

Typical axial wall temperature distribution for a representative test run is shown in Fig. 6.45. This is similar to that of THF mode shown in Fig. 6.40. Since the end and elbow sections are at lower temperature than other parts of the test-section at the beginning of a given test run, three distinctive rewetting regions are again observed in HBF mode. However, instead of the two separate rewetting fronts being in the vertical section in THF mode, these two fronts appear in the horizontal section in HBF mode. Again, this is due to the elbow section which remained at lower temperature than the other part of the test-section at the beginning of a test run.

The rewetting of the bottom and top of the horizontal section again displayed the characteristics of horizontal flooding, that is the rewetting front is very much inclined and that the bottom of the channel rewets ahead of the top of the channel. Wetting of an "L"-shaped channel by HBF mode involves three rewetting fronts, as in THF mode, therefore the effect of various parameters on the rewetting phenomena will be discussed by again dividing the test-section into three regions as illustrated in Fig. 6.41. However, unlike region 2 of THF mode, Region II of HBF mode has characteristics very similar to the presence of a flow blockage in a single straight tube. Also, the effect of hydrodynamics in that region seems to be less than that in Regions I and III.

(b) Effect of Coolant Flow Rate

As was in THF mode, for a given experimental condition, increasing coolant flow rate increased the rewetting velocities in Regions I and III as seen in Fig. 6.46. In the figure, also compared were the results of THF mode against those from the present HBF mode.

(c) Comparison of HBF and THF

The data from Region I of HBF is compared against those from Region 3 of THF in Fig. 6.46 as they are comparable to each other in the rewetting mode, horizontal flooding. Difference seen in the figure between the two modes must be due mainly to the fact that with HBF mode the effect of coolant inlet subcooling still influences the rewetting phenomena.

In Fig. 6.46, the results from Region 2 of THF mode shown in Fig. 6.42(b) were also compared with those from Region III of HBF mode. As discussed before, the flooding in Region 2 of the THF is not exactly equivalent to bottom flooding in a vertical channel. However, the flooding in Region III of HBF is in no way different from that of a bottom flooding mode in a simple vertical channel. The comparison shown in Fig. 6.46 demonstrates that the rewetting mechanism involved in the vertical section of an L-shaped channel is very much affected by the mode of flooding.

(d) Effect of Inlet Subcooling

It was seen before that the effect of inlet sub-cooling was negligible in Region 3 of THF mode. However, the effect of coolant sub-cooling at the inlet of the test-channel in

Region I of HBF mode is not negligible as seen in Fig. 6.47. This is because the coolant arriving at Region I of HBF did not lose its sub-cooling while the coolant reaching at Region 3 of THF already lost most of its sub-cooling, hence no significant role could be played.

(e) Effect of Heat Generation Rate

The results of both THF and HBF modes as shown in Fig. 6.48, indicate that the rewetting velocity decreased with increasing power input during the tests.

Since more heat must be removed with increased heat generation, which could not have affected the hydrodynamics involved significantly, a lower rewetting velocity can be expected in both modes of THF and HBF. This is clearly demonstrated in Fig. 6.48.

6.1.8.3 Quenching Time in L-shaped Channel

Quenching of the L-shaped channel by both the THF and HBF modes for typical test runs was illustrated in Figs. 6.40 and 6.45, respectively. It can be observed in Figs. 6.40 and 6.45 that since the quenching of an L-shaped channel by either mode of flooding always involved three different rewetting regions, the maximum quenching time for an L-shaped channel under a given test condition is dependent on the axial location. This is illustrated in Figs. 6.49 and 6.50

for THF and BHF modes, respectively. The dependency on the axial location is much more pronounced in THF mode. The maximum time to completely quench the channel did not correspond to the time required to reach the exit of the channel, rather it occurred in the vertical section of the channel as shown in Fig. 6.49. To illustrate that the maximum quenching time for a given test run is a function of test conditions, Tq,max was plotted as functions of coolant flow rate and initial wall temperature in Fig. 6.51 for THF mode. The trend is somewhat similar to those observed in Figs. 6.42 and 6.46.

For HBF mode, the phenomena shown in Fig. 6.50 are very similar to those observed in a rewetting transient in a single straight channel with orifice-type blockages equally spaced along the axial direction.

6.2 RESULT OF ANALYSIS

In the analysis, heat transfer coefficients in the inverse annular flow region of a single tube in the bottom flooding mode was calculated. Comparison of the results of analysis with experimental results are discussed in this section.

Figure 6.52 shows heat transfer coefficient vs. wall temperature in the inverse annular flow region. The inverse annular flow region is defined as the region downstream of the rewetting front where the wall temperature is higher than the rewetting temperature and the thermodynamic vapour quality is less than 3%[75]. The region where the vapour quality is larger than 3% is considered as dispersed flow region. Experimental convective heat transfer coefficient was obtained from the experimental temperature-time trace curve (using Eqn.3.3). By knowing the slope of the temperature drop with time, we can calculate the total heat transfer rate at a given moment of time from the law of energy conservation.

From the experimental heat transfer coefficient as well as the rewetting velocity of the test section, we can calculate the thermodynamic vapour quality and subsequently the void fraction using Martinelli-Nelson correlation[76] at a particular location of the test section for various times during the rewetting test. In certain location of the test section, by knowing void fraction and wall temperature at a particular time, a heat transfer coefficient in the inverted annular flow region is calculated using the present analysis presented in sections 5.1 to 5.4.

The experimental heat transfer coefficient is also compared with Bromley-type heat transfer coefficient[77]. In the author's previous model[1] for the bottom flooding, a Bromley-type equation was used to calculate the heat transfer coefficient in the inverted annular flow region. The Bromley-type equation is given as:

$$Q = 0.943 \left[\frac{K_v^3 \cdot \rho_v \cdot (\rho_\ell - \rho_v) \cdot g \cdot \lambda'}{\mu_v \cdot (T_w - T_\ell) \cdot L} \right]^{1/4} \cdot (T_w - T_\ell) \qquad \ldots\ldots\ldots (6.5)$$

where $\lambda' = h_{fg} \cdot \left[1 + \frac{0.4 \, \Delta T \cdot C_{pv}}{h_{fg}} \right]$

Figure 6.52 shows a comparison of these three heat transfer coefficients. Compared to the Bromley-type heat transfer coefficient which was used in author's previous model[1], the heat transfer coefficient obtained using the present analysis is much closer to the experimental heat transfer coefficient. This indicates that the present analysis of calculating heat transfer coefficient in the inverted annular flow region is a significant improvement over the Bromley-type equation or other pool boiling based equations, even though the present analysis requires local void fraction and takes much longer computational time.

Figures 6.53 to 6.55 are illustrations of the distribution of the three heat transfer coefficients over the wall temperatures for different experimental conditions. In general, all three confirm that the heat transfer coefficient obtained by the present analysis is much closer to the experimental coefficient than the coefficient obtained by the Bromley-type equation.

The effects of inlet subcooling and coolant flow rate on the heat transfer coefficient in the inverted annular flow region are shown in Figs. 6.56 and 6.57. Figures show that both experimental and analytical heat transfer coefficient in inverted annular flow region increase with increasing inlet subcooling and coolant flow rate. This agrees with the finding of Chan and Yadigaroglu[78] qualitatively whose experimental and analytical study also show the increasing heat transfer with increasing coolant flow rate and subcooling.

As stated in section 5.5, temperature-time trace curves of the bottom flooding rewetting process is obtained by substitution of the present analysis which calculates inverted annular flow region heat transfer coefficients into previous computer simulation model[1]. These temperature-time trace curves for various experimental conditions are compared with the experimental temperature-time trace curves as well as the old curves that was obtained by computer model using a Bromley-type equation.

Figure 6.58 shows the comparison of experimental T-T plot with present calculated T-T plot and previously calculated T-T plot. The calculated T-T plots using the present analysis are much closer to that of the experimental T-T plot than the calculated T-T plot using Bromley-type equation.

Also the rewetting time predicted by the present analysis are quite comparable to the experimental rewetting time(as shown in Fig.6.58), whereas the rewetting times predicted by the previous analysis are somewhat off from the experimental ones.

Figures 6.59 and 6.60 show the T-T plots obtained by three different methods for different experimental conditions. Both graphs confirm the findings mentioned before.

Since the rewetting velocity Uq is obtained from two temperature-time trace curves at different locations of the test tube by knowing the "rewetting time" and the location of the temperature-time trace curve, the present analysis should predict rewetting velocity Uq which is closer to the experimental value than the previous analysis.

Figures 6.61, 6.62 and 6.63 show the general pattern of the rewetting velocity over various parameters. Fig. 6.61 shows the effect of coolant flow rate on the rewetting velocity. Fig. 6.62 shows the effect of inlet subcooling and the effect of initial wall temperature on the rewetting velocity is shown in Fig. 6.63. Both the analytical and experimental rewetting velocities, as discussed earlier in section 6.1, show the same pattern of increasing in value with increasing coolant flow rate and inlet subcooling and also with decreasing initial wall temperature. In all three figures, it is shown that using the present analysis will give more accurate prediction of rewetting velocity Uq of bottom flooding rewetting process. This would confirm the finding of previous study[1] which states that one of the two main parameters which affect the rewetting process is the heat transfer rate immediately downstream of the rewetting front.

This is clearly shown in Fig.6.64 which shows the accuracy of the computed rewetting velocities compared to the experimental rewetting velocities. The circles are the rewetting velocities calculated with the present analysis whereas triangles are the previously calculated rewetting velocities using a Bromley-type equation for the inverted annular flow region. The figure shows that less than 50% of the previously calculated rewetting velocities fall within +/- 10% line while others have about 20% difference from the experimental rewetting velocities. Rewetting velocities computed using the present analysis are much closer to the experimental rewetting velocities. All of them have values within +/- 10% of the experimental rewetting velocities.

The main objective of the present analysis was to obtain a method of calculating accurate heat transfer coefficient in the inverted annular flow region and to re-confirm the findings of the previous study[1]. As has been presented, the both objectives are achieved in this analysis.

Since the numerical simulation of the bottom flooding rewetting process used in this study is same as the one used in the author's previous study[1] except the heat transfer coefficient used in the inverted annular flow region, the details of the simulation model and other results are not presented in this thesis.

Chapter VII

CONCLUSION

The objective of the present study was to have better insight and also to identify the mechanisms involved in the rewetting phenomena which have particular importance during the ECC of nuclear reactors.

Extensive experimental work on rewetting of hot channels including visual studies were carried out with various channel geometries and different flooding modes. The effect of each parameter on rewetting velocity and the process of the rewetting phenomena for different channel geometries and flooding modes are discussed in detail in the present thesis. The heat transfer coefficient in the downstream of the rewetting front was re-identified as one of the most important parameters by the present study as was first identified by our previous analysis[1]. Therefore, an analysis to calculate the heat transfer coefficient in the inverted annular flow region was developed in the present thesis. This analysis was based on the concept of assuming the inverted annular flow region as a concentric annulus with moving core tube.

Some of the main findings of the present study are:

1. From the visual study of the rewetting process, the general six heat transfer regimes in various modes of flooding were identified.
2. Results of the analysis re-confirmed the findings of a previous study[1] which identified that having more accurate heat transfer coefficients in the immediate downstream of the rewetting front improves the computation of rewetting velocities substantially.
3. From the experimental study, it was found that the general pattern of the rewetting velocity for various flooding modes is that the rewetting velocity increases with increasing coolant flow rate, decreasing initial wall temperature, increasing inlet coolant subcooling and decreasing power generation rate during the test.
4. For the bottom flooding of a concentric annulus with both walls heated, the thermal capacity of each wall had a significant effect on the resulting rewetting velocity.
5. For the horizontal flooding of a concentric annulus, using the conventional definition of rewetting velocity ("apparant" rewetting velocity) gave misleading results; therefore a new definition of "effective" rewetting velocity is proposed.
6. The results of experimental studies of "L"-shaped test channel showed that unlike a simple straight

channel, there exist at least three distinctive rewetting regions and the maximum time to quench the whole channel does not necessarily correspond to the time required to quench the exit part of the channel.

Recommendation for Further Study

The major problems in all analytical models of the rewetting process are the poor understanding of the local heat transfer coefficient distribution along the flow channel during the transient, and the rewetting temperature. These are obviously related to the fluid flow distribution. A major effort must, therefore, be made to the determination of;

1. the flow distribution in the channel during the transient, especially in multi-rod fuel bundle channels
2. the local heat transfer coefficient distribution along the fuel channel in the horizontal flooding, and
3. the rewetting temperature, either analytically or empirically as a function of system parameters.

Most of the parametric effects on the rewetting phenomena have been identified in the present study. However, there are still a few system parameters whose effects on the rewetting process are not identified or confirmed. They are;

1. power distribution,
2. inlet coolant vapour quality,

3. effect of surface aging (or degradation due to long period of radiation and scale formation), and
4. flow oscillation.

Finally, the scaling rationale must be clarified.

REFERENCES

1 Kim, A., An Analysis of Rewetting Phenomena in Vertical Channels M.A.Sc. Thesis, 1980, University of Ottawa

2 Sawan, M.E., and Carbon, M.W., A Review of Spray-cooling and Bottom-flooding Work for LWR Cores Nuclear Eng. and Design, Vol. 32, pp. 191-207. 1975

3 Butterworth, D., and Owen, R.G., The Quenching of Hot Surfaces by Top and Bottom Flooding - A Review European Two-Phase Flow Group Meeting, Haifa, June 1975 (AERE - R7992)

4 Elias, E., and Yadigaroglu, G., The Reflooding Phase of the LOCA in PWRs. Part 2: Rewetting and Liquid Entrainment Nuclear Safety, Vol. 19, No.2, pp. 160-175, 1978

5 Carbajo, J.J., and Siegel, A.D., Review and Comparison among the Different Models for Rewetting in LWR's Nuclear Eng. and Design, Vol. 58, pp.33-44, 1980

6 Duffey, R.B. and Porthouse, D.T.C., The Rewetting of Hot Surfaces by Falling Films and Bottom Flooding Central Electricity Generating Board, Report No. RD/B/N2530, 1973

7 Chan, S.H., and Grolmes, M.A., Hydrodynamically Controlled Rewetting ASME Paper 75-HT-70, 1975

8 Duffey, R.B., and Porthouse, D.T.C., Experiments on the Cooling of High Temperature Surface by Water Jets and Drops Proceedings of the CREST Specialist Meeting on Emergency Core Cooling for Light Water Reactors, Munchen, October, 1972

9 Yu, S.K.W., Farmer, P.R., and Coney, M.W.E. Methods and Correlations for the Prediction of Quenching Rates on Hot Surfaces Int. J. Multiphase Flow, Vol. 3, pp. 415-443, 1977

10 Bennett, A.W., Hewitt, G.F., Kearsey, H.A., and Keeys, R., The Wetting of Hot Surfaces by Water in a Steam Environment at High Pressure U.K.A.E.A. Report No. AERE-R5146, 1966

11 Elliott, D.F., and Rose, P.W., The Quenching of a Heated Surface by a Film of Water in a Steam Environment at Pressures up to 53 bar U.K.A.E.A. Report No. AEEW-M976, 1970

12 Thompson, T.S., Rewetting of a Hot Surface Proc. 5th Int. Heat Transfer Conf., Tokyo, Vol. 4, pp. 139-144, 1974

13 Yoshioka, K., and Hasegawa, S., A Correlation in Displacement Velocity of Liquid Film Boundary formed on a Heated Vertical Surface in Emergency Cooling J. of Nuclear Science and Technol., Vol. 7, No. 8, pp.418-425, 1970

14 Piggott, B.D.G., and Porthouse, D.T.C., Water Reactor Emergency Core Cooling: The Effect of Pressure, Subcooling and Surface Condition on the Rewetting of Hot Surfaces Central Electricity Generating Board, Report No. RD/B/N2692, 1973

15 Naitoh, M. Heat Removal by Top Spray Emergency Core Cooling Multi-Phase Flow and Heat Transfer SYMP.-workshop, Miami beach, Fla, Apr. 16-18, 1979, pp. 419-421

16 Piggott, B.D.G., and Duffey, R.B., The Quenching of Irradiated Fuel Pins Nuclear Eng. and Design, Vol.32, pp. 182-190, 1975

17 Semeria, R., and Martinet, B., Calefaction Spots on a Heating Wall: Temperature Distribution and Resorption Proc. Inst. Mech. Engrs., Vol. 180, pp. 192-205, 1966

18 Duffey, R.B., and Porthouse D.T.C., The Physics of Rewetting in Water Reactor Emergency Core Cooling Nuclear Eng. and DEsign, Vol. 25, pp.379-394, 1973

19 Coney, M.W.E., Calculations on the Rewetting of Hot Surfaces Nuclear Eng. and Design, Vol. 31, pp. 246-259, 1974

20 Tien, C.L., and Yao, L.S., Analysis of Conduction Controlled Rewetting of a Vertical Surface J. of Heat Transfer, Trans. ASME, pp. 161-165, 1975

21 Dua, S.S., and Tien, C.L., An Experimental Investigation of Falling-Film Rewetting Int. J. Heat Mass Transfer, Vol.21, pp. 955-965, 1978

22 Simopoulos, S.E., El-Shirbini, A.A., and Murgatroyd, W., Experimental Investigation of the Rewetting Process in a Freon-113 Vapour Environment. Nuclear Eng. and Design, Vol.55, pp. 17-24, 1979

23 Case, P., Hein, D., Riedle, K., and Schneider, E., The Rewetting Process of Hot Surfaces by Bottom Flooding European Two-Phase Flow Group Meeting, Bruxelles, June 4-7, 1973

24 Kaminaga, F., and Uchida, H., Reflooding Phenomena in a Single Heated Rod (Part 1, Experimental Study) Bulletin of the JSME, Vol.22, No. 169, pp. 960-966, 1979

25 Andreoni, D., and Courtaud, M., A Study of Heat Transfer during the Reflooding of a Single Rod Test Section Proceedings of the CREST Specialist Meeting on Emergency Core Cooling for Light Water Reactors, Munchen, October 18-20, 1972

26 Campanile, A., and Pozzi, G.P., Low Rate Emergency Reflooding Heat Transfer Tests in Rod Bundle Proceedings of the CREST Specialist Meeting on Emergency Core Cooling for Light Water Reactors, Munchen, October 18-20, 1972

27 Martini, R., and Premoli, A., Bottom Flooding Experiments with Simple Geometries under Different E.C.C. Conditions Proceedings of the CREST Specialist Meeting on Emergency Core Cooling for Light Water Reactors, Munchen, October 18-20, 1972

28 Thompson, T.S., Simulated Bottom-Flooding Emergency Cooling of a Closed-spaced Rod Bundle European Two-Phase Flow Group Meeting, C.S.N. Cassaccia, June 6-8, 1972

29 Riedle, K., and Winkler, F., ECC - Reflooding Experiments with a 340-Rod Bundle Proceedings of the CREST Specialist Meeting on Emergency Core Cooling for Light Water Reactors, Munchen, October 18-20, 1972

30 Pigott, B.D.G., and Porthouse, D.T.C., A Correlation of Rewetting Data Nuclear Eng. and Design, Vol. 32, pp. 171-181, 1975

31 Cadek, F.F., Dominicis, D.P., and Leyse, R.H., PWR - FLECHT (Full Length Emergency Cooling Heat Transfer): Final Report Westinghouse Electric Corporation, Report No. WCAP-7665, 1971

32 Lauer, H., and Hufschmidt, W., Heat Transfer and Surface Rewet during Quenching European Two-Phase Flow Group Meeting, Erlangen, May 31-June 4, 1976

33 Yu, K.P., and Yadigaroglu, G., Heat Transfer Immediately Downstream of the Quench Front during Reflooding ASME Paper, 79-HT-48, 1979

34 Yadigaroglu, G., The Reflooding Phase of the LOCA in PWRs. Part 1: Core Heat Transfer and Fluid Flow Nuclear Safety, Vol.19, No.1, 1978 pp. 20-36

35 Chan, A.M.C., and Banerjee, S., Refilling and Rewetting of Hot Horizontal Systems Basic Mech. in Two-Phase Flow and Heat Transfer, Winter Annual Meeting of ASME, Chicago, Ill., pp. 103-121, Nov. 16-21, 1980

36 Bukur, D.B., and Isbin, H.S., Numerical Solution of the Yamanouchi Model for Core Spray Cooling Nuclear Eng. and Design, Vol. 23, pp. 195- , 1972

37 Yamanouchi, A., Effect of Core Spray Cooling in Transient State After Loss-of-Coolant Accident J. Nuclear Science and Technol., Vol. 5, pp. 547-558, 1968

38 Sun, K.H., Dix, G.E., and Tien, C.L., Cooling of a Very Hot Vertical Surface by a Falling Liquid Film J. of Heat Transfer, Trans. ASME, Vol. 96, pp. 126-131, 1974

39 Sun, K.H., Dix, G.E., and Tien, C.L., Effect of Precursory Cooling on Falling-Film Rewetting J. of Heat Transfer, Trans. ASME, pp. 360-365, 1975

40 Chun, M.H., and Chon, W.Y., Analysis of Rewetting in Water Reactor Emergency Core Cooling Inclusive of Heat Transfer in the Unwetted Region ASME paper 75-WA/HT-32, 1975

41 Duncan, J.D., and Leonard, J.E., BWR Standby Cooling Heat Transfer Performance Under Simulated Loss-of-Coolant Conditions between 15 and 300 psia GEAP-13190, May 1971

42 Ishii, M., Study on Emergency Core Cooling J. Br. Nucl. Energy Soc., Vol. 3, pp. 237-242, 1975

43 Blair, J.M., An Analytical Solution to a Two-Dimensional Model of the Rewetting of a Hot Dry Rod Nuclear Eng. and Design, Vol. 32, pp. 159-170, 1975

44 Dua, S.S., and Tien, C.L., Two-Dimensional Analysis of Conduction Controlled Rewetting with Precursory Cooling J. of Heat Transfer, Trans. ASME, Vol. 98, pp. 407-413, 1976

45 Yao, L.S. Rewetting of a vertical surface with Internal Heat Generation Solar and Nuclear Heat Transfer, AIChE symposium 73(164) (1976) 46-50

46 Dua, S.S., and Tien, C.L., A Generalized Two-Parameter Relation for Conduction Controlled Rewetting of a Hot Vertical Surface Int. J. of Heat and Mass Transfer, Vol. 20, pp. 174-176, 1977

47 Andersen, J.G.M., and Hansen, P., Two Dimensional Heat Conduction in Rewetting Phenomenon Danish Atomic Energy Commission Research Establishment, Riso, Denmark, Report No. NORHAV-D-6, June 1974

48 Yoshioka, K., and Hasegawa, S., An Analytical Model for Displacement Velocity of Liquid Film on a Hot Vertical Surface Nuclear Science and Tech., Vol. 12, pp. 735-741, 1975

49 Edwards, A.R., and Mather, D.J., Some U.K. Studies Related to the Loss of Coolant Accident Paper presented at the Water Reactor Safety Meeting, Salt Lake City, March 26-28, 1973

50 Sawan, M.E., Zaki, G.M., and Temraz, H.M., Trans. ANS 30(1978) 387-388

51 Bonakdar, H., and McAssey, Jr., E.V., A Method for Determining Rewetting Velocity under Generalized Boiling Conditions ASME Paper 80-WA/HT-40, 1980

52 Thompson, T.S., An Analysis of the Wet Side Heat Transfer Coefficient During Rewetting of a Hot Dry Patch Nuclear Eng. and Design, Vol. 22, pp. 212-224, 1972

53 Thompson, T.S., On the Process of Rewetting a Hot Surface by a falling Liquid Film Nuclear Eng. and Design, Vol. 31, pp. 234-245, 1974

54 Elias, E., and Yadigaroglu, G., A General One-Dimensional Model for Conduction-Controlled Rewetting of a Surface Nuclar Eng. and Design, Vol. 42, pp. 185-194, 1977

55 Martini, R., and Premoli, A., A Simple Model for Predicting E.C.C. Transients in Bottom Flooding Conditions Paper presented at CREST Specialist Meeting on Emergency Core Cooling for Light Water Reactors, Munich, October 18-20, 1972.

56 Salcudean, M., Bui, T.M., and Lee, Y., A Three Dimensional Analysis for the Rewetting Process of Hot Channels ASME Paper 78-HT-27, 1978

57 Davis, P.R., Experimental Studies of the Effect of Flow Restrictions in a Small Rod Bundle Under Emergency Core Coolant Injection Conditions Nuch. Tech., Vol.11, pp.551-556, 1971

58 Bromley, L.A., Heat Transfer in Stable Film Boiling Chem. Eng. Progr., Vol.46, pp.221-227, 1950

59 Leung, E.Y., Kays, W.M., and Reynolds, W.C. Heat Transfer with Turbulent Flow in Concentric and Eccentric Annuli with Constant and Variable Heat Flux Report AHT4, Sanford Univ. (1962)

60 Park, S.D., Developing Turbulent Flow and Heat Transfer in Concentric Annuli An Analytical and Experimental Study PhD thesis, Univ. of Ottawa (1971)

61 Levy, S., Turbulent Flow in an Annulus J. of Heat Transfer, ASME, Vol.89, pp.25-31, 1967

62 Reichardt, H., Complete Representation of Turbulent Velocity Distribution in Smooth Pipe Zeitschrift fur angewandte Mathematik und Mechanik, Vol.31, pp.208-219, 1951

63 Roberts, A., A Comment on the Turbulent Flow Velocity Profile in a Concentric Annulus Int. J. of Heat and Mass Transfer, Vol.10, pp.709-712, 1967

64 Deissler, R.G., Turbulent Heat Transfer and Friction in the Entrance Regions of Smooth Passages Trans. ASME, Vol.88, pp.1221-1223, 1955

65 Park, S.D., and Lee, Y., Diabatic Turbulent Flow in the Entrance Region of Concentric Annuli Paper No.70-CSME-9, 84th Annual Meeting, Eng. Inst. of Canada, 1970

66 Barrow, H. Semi-Theoretical Solution of Asymmetric Heat Transfer in Annular Flow Journal Mech. Eng. Sci., Vol.2, pp.331-336, 1960

67 Kim, A., and Lee, Y. A Numerical and Experimental Study of the Rewetting Process in Bottom Flooding Proc. 7th Int. Heat Transfer Conf. 4, pp.181-187, Munchen, 1982

68 Burggraf, O.R. An Exact Solution of the Inverse Problem in Heat Conduction Theory and Applications J. of Heat Transfer, Trans. ASME, Series C, 86, pp.373-382, 1964

69 Plummer, D., Iloeje, O., Griffith, P., and Rohsenhow, W. A Study of Post Critical Flux Heat Transfer in a Forced Convection System M.I.T. Tech. Report No. 73645-80, 1973

70 Rankin, S., Forced Convection Film Boiling Inside of Vertical Pipes Ph.D. Thesis, Chemical Engineering, University of Delaware, 1961

71 Dougall, R., and Rohsenow, W., Film Boiling on the Inside of Vertical Tubes with Upward Flow of the Fluid at Low Qualities M.I.T. Tech. Report No. 9079-26, 1963

72 Kalinin, E., Balashov, G., Berlin, I., and Liventsov, V., A Mathematical Model of Heat Transfer for Forced-Convective Film Boiling J. of Engineering Physics, Vol.33, 1977

73 Schlichting, H., Boundary Layer Theory McGraw Hill Book Co. Inc., 6th Edition, 1968

74 Cermak, J.O., Leyse, R.H., and Dominics, D.P., Effect of Flow Blockage on Bottom Flooding Heat transfer Effectiveness (FLECHT) Nucl. Tech., Vol.11, pp.557-561, 1971

75 Groeneveld, D.G., and Gardiner, S.R.M., Post-CHF Heat Transfer Under Forced Convective Conditions Symposium on the Thermal and Hydraulic Aspects of Nuclear Reactor Safety, Vol.1, AECL-5883

76 Martinelli, R.C., and Nelson, D.B., Prediction of Pressure Drop during Forced Circulation Boiling of Water Trans. ASME, Vol.70, pp.695, 1948

77 Clement, P., Deruaz, R., Raymond, P., Regnier, P., and Reocreux, M., Development of Reflood Codes FLIRA and PSCHIT. Physical Modeling and Interpretation of Ersec Experiments. 5th Annual Water Reactor Safety Research Information Meeting, Washington, 1977

78 Chan, K.C., and Yadigaroglu, G., Calculation of Film Boiling Heat Transfer above the Quench Front during Reflooding. EXP. and ANAL. MODEL of LWR SAF. EXP., Presented at the Natl. Heat Transfer Conf. 19th, Orlando, Fla., July 27-30, 1980

79 Kim, A., and Lee, Y., A Correlation of Rewetting Temperature. Letters in Heat and Mass Transfer, Vol.6, No.2, pp.117-123, 1979

80 Gamblin, W., and Lee, Y., The Design of an Experimental Apparatus to Measure Transient Post Dryout Heat Transfer. Dept. of Mech. Eng., Univ. of Ottawa, 1976

Appendix I

LIQUID CORE VELOCITY CALCULATION

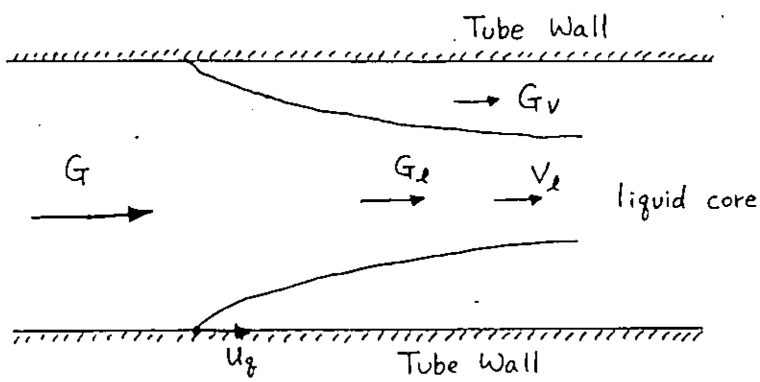

G = total mass flow rate of water at the inlet(g/s)

G_ℓ = water mass flow rate

G_v = vapour mass flow rate

At any point, $G = G_\ell + G_v$

In fixed frame, $G_\ell = V_\ell \cdot A_\ell \cdot \rho_\ell$

where, V_ℓ = average water velocity of liquid core

A_ℓ = cross-sectional area of the liquid core

ρ_ℓ = mass density of water

Therefore, liquid core velocity in fixed frame is

$$V_\ell = \frac{G_\ell}{A_\ell \cdot \rho_\ell} = \frac{G - G_v}{\rho_\ell \cdot A \cdot (1-\gamma)}$$

where, A = total cross-sectional area of the tube

γ = void fraction

Appendix 2

LIQUID CORE HEAT TRANSFER COEFFICIENT

Let $$\frac{\partial T}{\partial x} = f(r)\,\frac{dT_b}{dx} \qquad \cdots\cdots (1)$$

function f(r) should satisfy the boundary conditions,

$$\left.\frac{\partial T}{\partial x}\right|_{r=R_i^*} = 0$$

$$\left.\frac{\partial T}{\partial x}\right|_{r=0} = \text{finite}$$

function f(r) selected that satifies the above boundary condition is

$$f(r) = C\cdot\cos\left(\frac{r}{R_i^*}\cdot\frac{\pi}{2}\right)$$

Substituting for $\frac{\partial T}{\partial x}$ in Eqn.(5.32)

$$\int_0^{R_i^*} r\left(\frac{\partial T}{\partial x}\right)dr = \int_0^{R_i^*} r\cdot\left(C\cdot\cos\left(\frac{r}{R_i^*}\cdot\frac{\pi}{2}\right)\frac{dT_b}{dx}\right)dr$$

$$= C\cdot\frac{dT_b}{dx}\cdot\int_0^{R_i^*} r\cdot\cos\left(\frac{r}{R_i^*}\cdot\frac{\pi}{2}\right)dr = \frac{R_i^{*2}}{2}\cdot\frac{dT_b}{dx} \qquad \cdots\cdots (2)$$

Solving Eqn.(2), we obtain C=2.1614

$$\therefore\ \frac{\partial T}{\partial x} = 2.1614\cdot\cos\left(\frac{r}{R_i^*}\cdot\frac{\pi}{2}\right)\frac{dT_b}{dx}$$

Therefore, Eqn.(5.30) can be written as

$$\frac{1}{r}\cdot\frac{\partial}{\partial r}\left(r\cdot(\varepsilon_H+\alpha)\frac{\partial T}{\partial r}\right) = U_\ell\cdot\frac{\partial T}{\partial x} = 2.1614\cdot U_\ell\cdot\cos\left(\frac{r}{R_i^*}\cdot\frac{\pi}{2}\right)\frac{dT_b}{dx}$$

$$\cdots\cdots (3)$$

Integrating Eqn.(3),

$$r(\varepsilon_H+\alpha)\frac{\partial T}{\partial r} = U_\ell \cdot \frac{dT_b}{dx}\Big[0.876\, R_i^{*2}\cdot \cos\Big(\frac{r}{R_i^*}\cdot\frac{\pi}{2}\Big)$$

$$+ 1.376\, R_i^*\cdot r\cdot \sin\Big(\frac{r}{R_i^*}\cdot\frac{\pi}{2}\Big)\Big] + C_1 \quad \cdots\cdots\cdots (4)$$

Applying boundary condition ($\frac{\partial T}{\partial r}=0$ at r=0)

$$C = -0.876 \cdot R_i^{*2}\cdot U_\ell \cdot \frac{dT_b}{dx}$$

Substituting C_1 into Eqn.(4) and rearranging,

$$\frac{\partial T}{\partial r} = U_\ell \cdot \frac{dT_b}{dx}\cdot 0.876 \cdot R_i^{*2}\cdot \frac{1}{r(\varepsilon_H+\alpha)}\Big(\cos\Big(\frac{r}{R_i^*}\cdot\frac{\pi}{2}\Big)-1\Big)$$

$$+ U_\ell\, \frac{dT_b}{dx}\cdot 1.376 \cdot R_i^{*2}\cdot \frac{1}{(\varepsilon_H+\alpha)}\, \sin\Big(\frac{r}{R_i^*}\cdot\frac{\pi}{2}\Big) \quad \cdots\cdots\cdots (5)$$

Integrating and rearranging Eqn.(5),

$$T = U_\ell \cdot \frac{dT_b}{dx}\, 0.876\, R_i^{*2}\cdot \int_{R_i^*}^{r} \frac{\cos\Big(\frac{r}{R_i^*}\cdot\frac{\pi}{2}\Big)-1}{r(\varepsilon_H+\alpha)}\, dr$$

$$+ U_\ell\, \frac{dT_b}{dx}\, 1.376\, R_i^*\cdot \int_{R_i^*}^{r} \frac{\sin\Big(\frac{r}{R_i^*}\cdot\frac{\pi}{2}\Big)}{(\varepsilon_H+\alpha)}\, dr + C_2 \quad \cdots\cdots\cdots (6)$$

Applying 2nd boundary condition($T=T_s$ at $r=R_i^*$), $C_2 = T_s$

Therefore Eqn.(6) becomes,

$$T - T_s = 0.876\cdot R_i^{*2}\cdot U_\ell \cdot \frac{dT_b}{dx}\int_{R_i^*}^{r} \frac{\cos\Big(\frac{r}{R_i^*}\cdot\frac{\pi}{2}\Big)-1}{r(\varepsilon_H+\alpha)}\, dr$$

$$+ 1.376 \cdot R_i^* \cdot U_\ell \cdot \frac{dT_b}{dx} \cdot \int_{R_i^*}^{r} \frac{\sin\left(\frac{r}{R_i^*} \cdot \frac{\pi}{2}\right)}{(\varepsilon_H + \alpha)} \, dr \cdots\cdots\cdots\cdots (7)$$

For the case of parabolic temperature profile,

$$T_s - T_b = (T_s - T_{r=0}) \cdot \frac{2}{3}$$

Therefore,

$$T_s - T_b = 0.876 \cdot R_i^{*2} \cdot U_\ell \cdot \frac{dT_b}{dx} \cdot \frac{2}{3} \cdot \int_0^{R_i^*} \frac{\cos\left(\frac{r}{R_i^*} \cdot \frac{\pi}{2}\right) - 1}{r(\varepsilon_H + \alpha)} \, dr$$

$$+ 1.376 \; R_i^* \, U_\ell \cdot \frac{dT_b}{dx} \cdot \frac{2}{3} \cdot \int_0^{R_i^*} \frac{\sin\left(\frac{r}{R_i^*} \cdot \frac{\pi}{2}\right)}{(\varepsilon_H + \alpha)} \, dr$$

TABLE 1. Test Sections

Test-Section No.	1	2	3	4	5	6
Tube Material	S.S. 304	S.S. 304	Inconel X-750	S.S. 304	Inconel X-750	Inconel X-750
Tube O.D. mm	19.1	19.1	15.9	15.9	15.9	15.9
Tube Wall Thickness mm	1.65	0.89	1.2	1.2	1.2	1.2
Tube I.D. mm	15.8	17.32	13.86	13.86	13.86	13.86
Flow Blockage %					25	50
Blockage Type					orifice	orifice
Tube Length, m	4	3.5	3.5	3.5	3.5	3.5
Flow Area, mm^2	196.1	235.6	143.1	143.1	143.1	143.1
Flooding Mode	Bottom Horizontal	Bottom Horizontal	Bottom Horizontal	Bottom Horizontal	Bottom Horizontal	Bottom Horizontal

TABLE 1. Test Sections

Test-Section No.	7	8	9A	9B*	10	11A
Tube Material	Inconel X-750	Inconel X-750	S.S. 304	S.S. 304	Inconel X-750	Inconel X-750
Tube O.D. mm	15.9	15.9	15.9	15.9	15.9	15.9
Tube Wall Thickness mm	1.2	1.2	1.2	1.2	1.2	1.2
Tube I.D. mm	13.86	13.86	13.5	13.5	13.5	13.5
Flow Blockage %	25	25				
Blockage Type	venturi	venturi orifice				
Tube Length, m	3.5	3.5	1.4	1.4	1.3	3.0
Flow Area, mm^2	143.1	143.1				143.1
Flooding Mode	Bottom Horizontal	Bottom Horizontal	Unconfined Top flooding	Unconfined Top fldg	Unconfined Top fldg	Confined Top fldg

* 9B is same as 9A except test section is covered by 2 inch diameter glass tube

TABLE 1. Test Sections

Test-Section No.	11B	12	13	14	15	16
Core tube Material	S.S. 304	S.S. 304	S.S. 304	S.S. 304	S.S. 304	S.S. 304
Core tube O.D. mm	15.9	24.6	24.6	15.9	25.4	15.9
Core tube Wall thickness, mm	1.2	1.2	1.2	1.2	1.2	1.2
Outer tube Material				glass	glass	S.S. 304
Outer tube O.D. mm				44.4	44.4	38.1
Outer tube Wall thickness, mm				1.7	1.7	1.65
Tube Length, m	3.0	3.0	3.0	1.8	1.8	2.4
Flow Area, mm^2	143.1	387	387	1122	814	808
Flooding Mode	Confined Top fldg	Confined Top fldg	Bottom Horizontal	Bottom	Bottom	Bottom Horizontal

Test-Section No.	17	18				
Test-Section Geometry	"L"-shaped	"L"-shaped				
Tube Material	S.S. 304	S.S. 304				
Tube O.D. mm	25.4	25.4				
Tube Wall thickness mm	1.65	1.65				
Corner	Swagelok	5"-curve				
Vertical Length mm	2.4	2.4				
Horizontal Length mm	2.55	2.55				
Flow Area mm^2	384	384				
Flooding Mode	THF HBF	THF HBF				

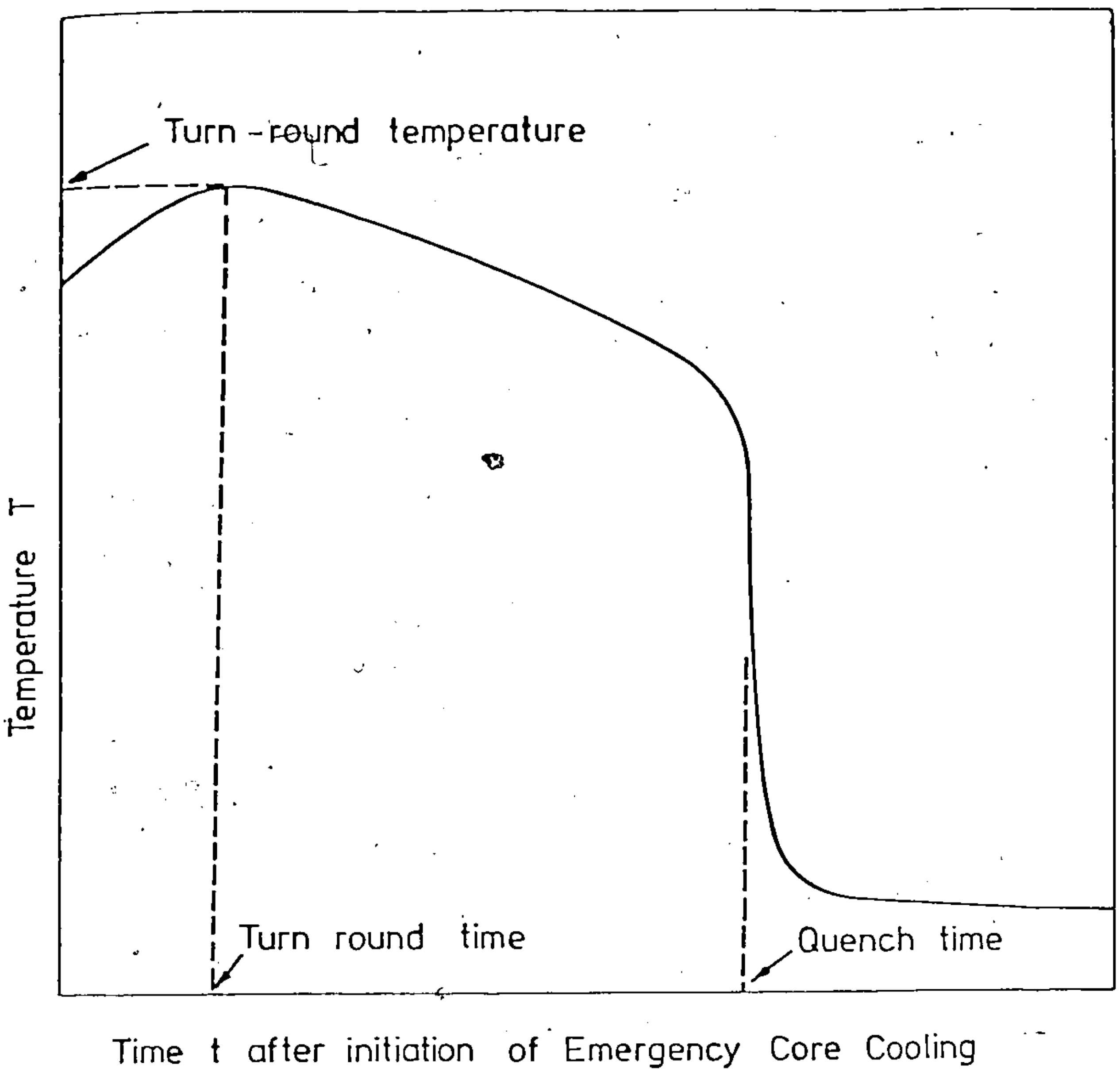

Fig. 2.1 Temperature History of a Point on a Test Section during Reflooding Transient.

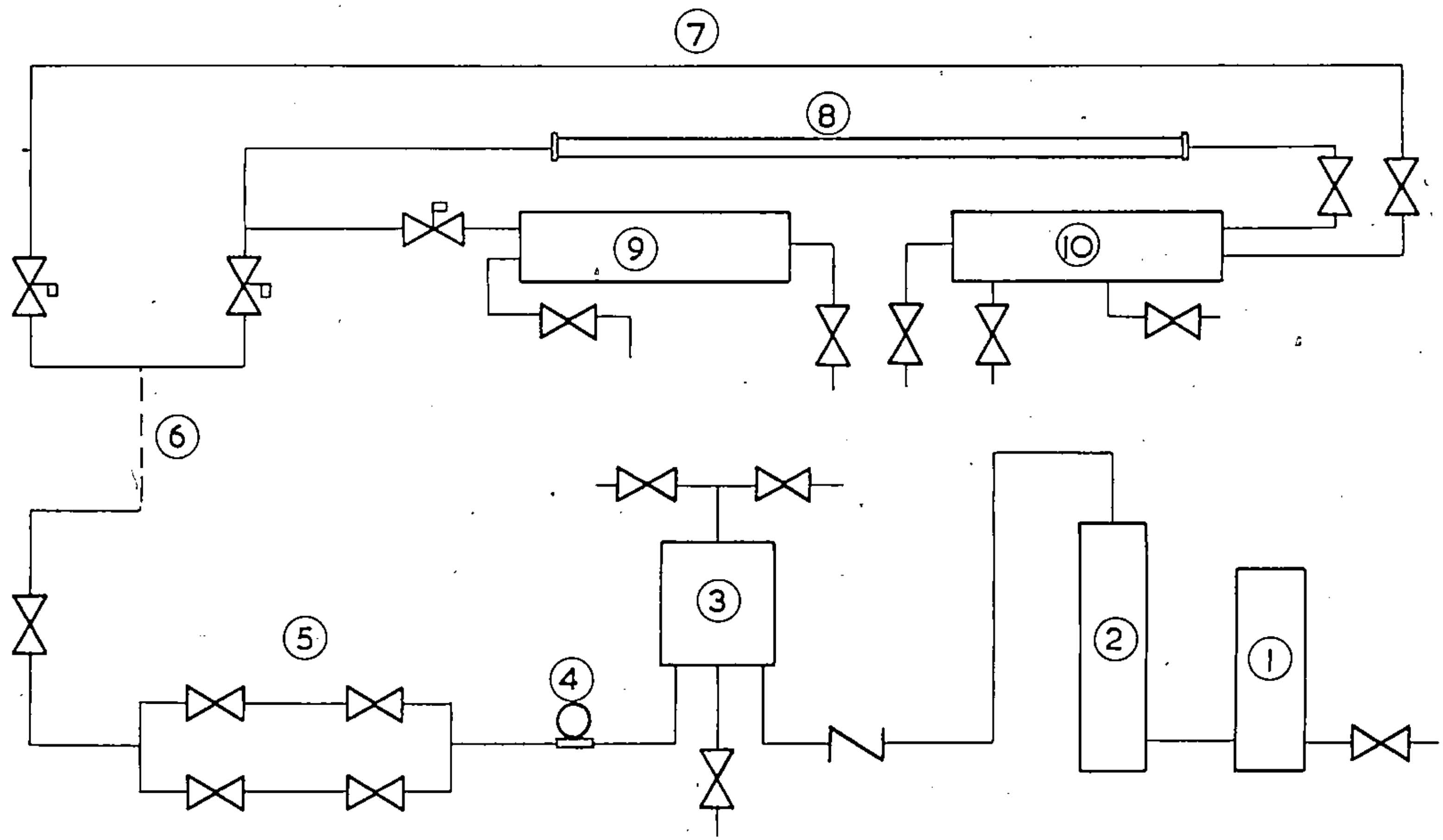

1. Water Demineralizer
2. Preheater
3. Main Supply Boiler
4. Flow Circurator
5. Flow Measurement
6. Flexible Connection
7. By-pass
8. Test-Section
9. Reverse Tank
10. Condensing Tank

Fig. 3.1(a) Test Apparatus

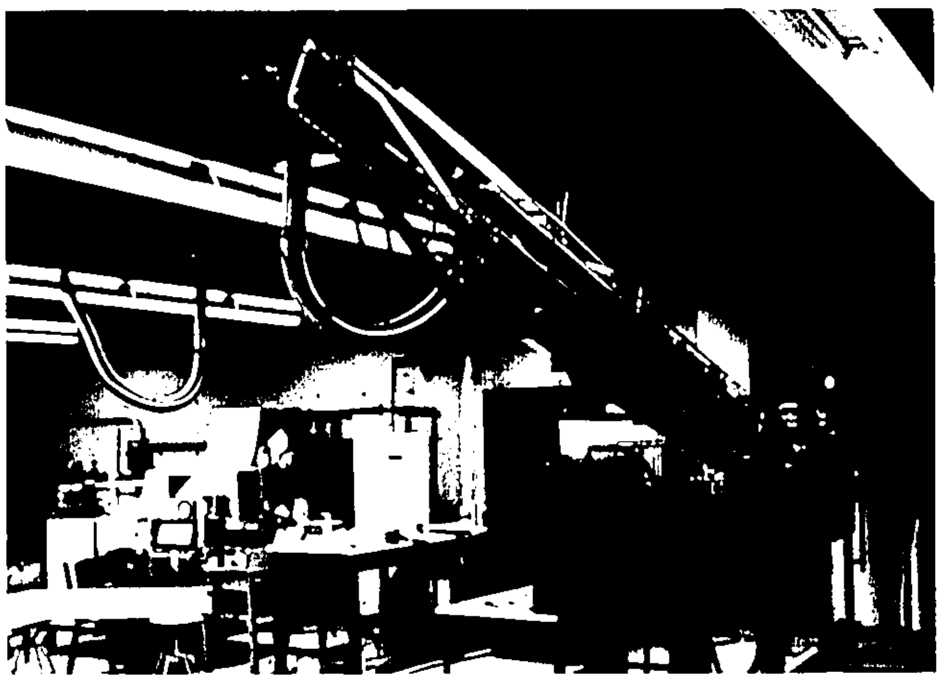

Fig. 3.1(b) Picture of Main Experimental Apparatus

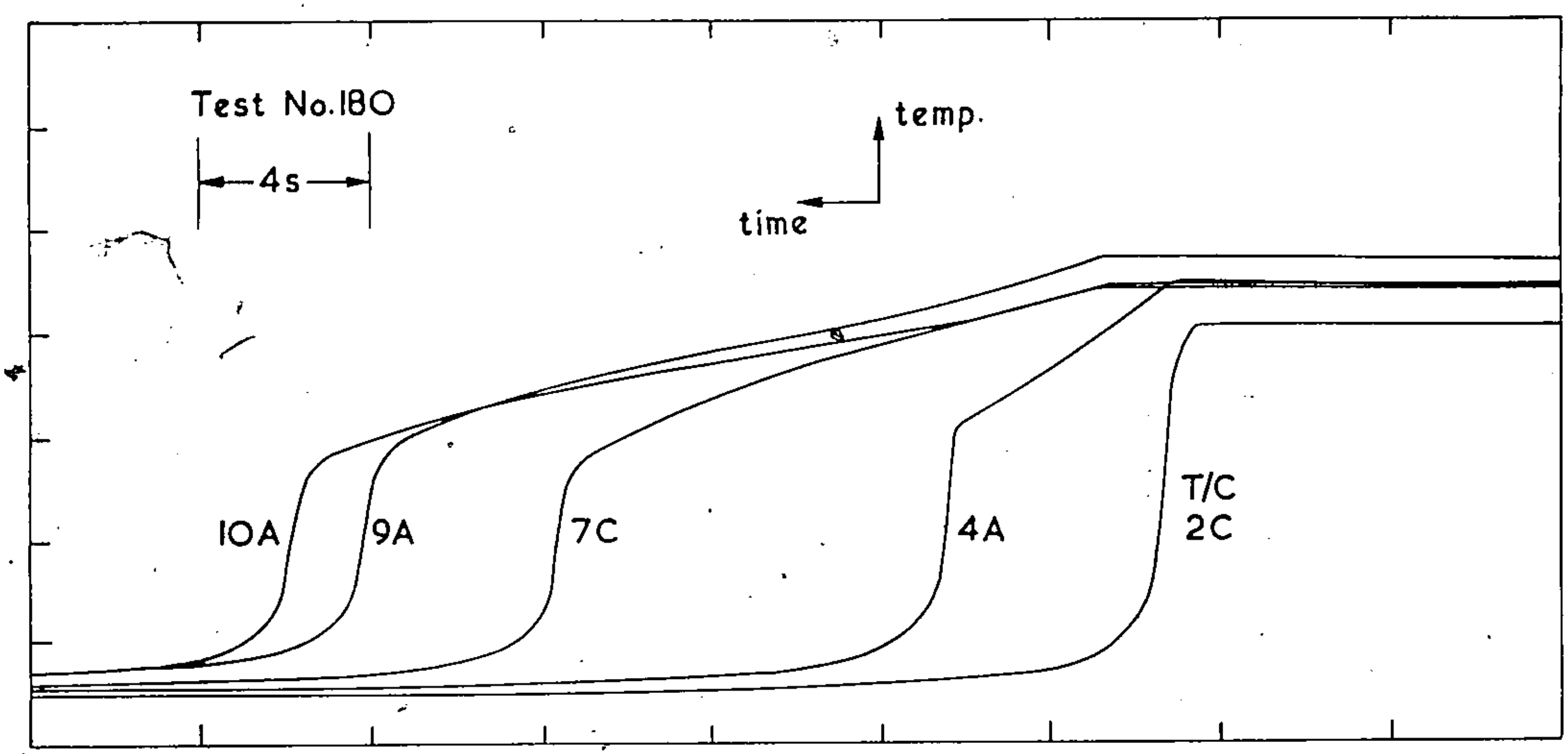

Fig. 3.2 Temperature vs. Time Traces

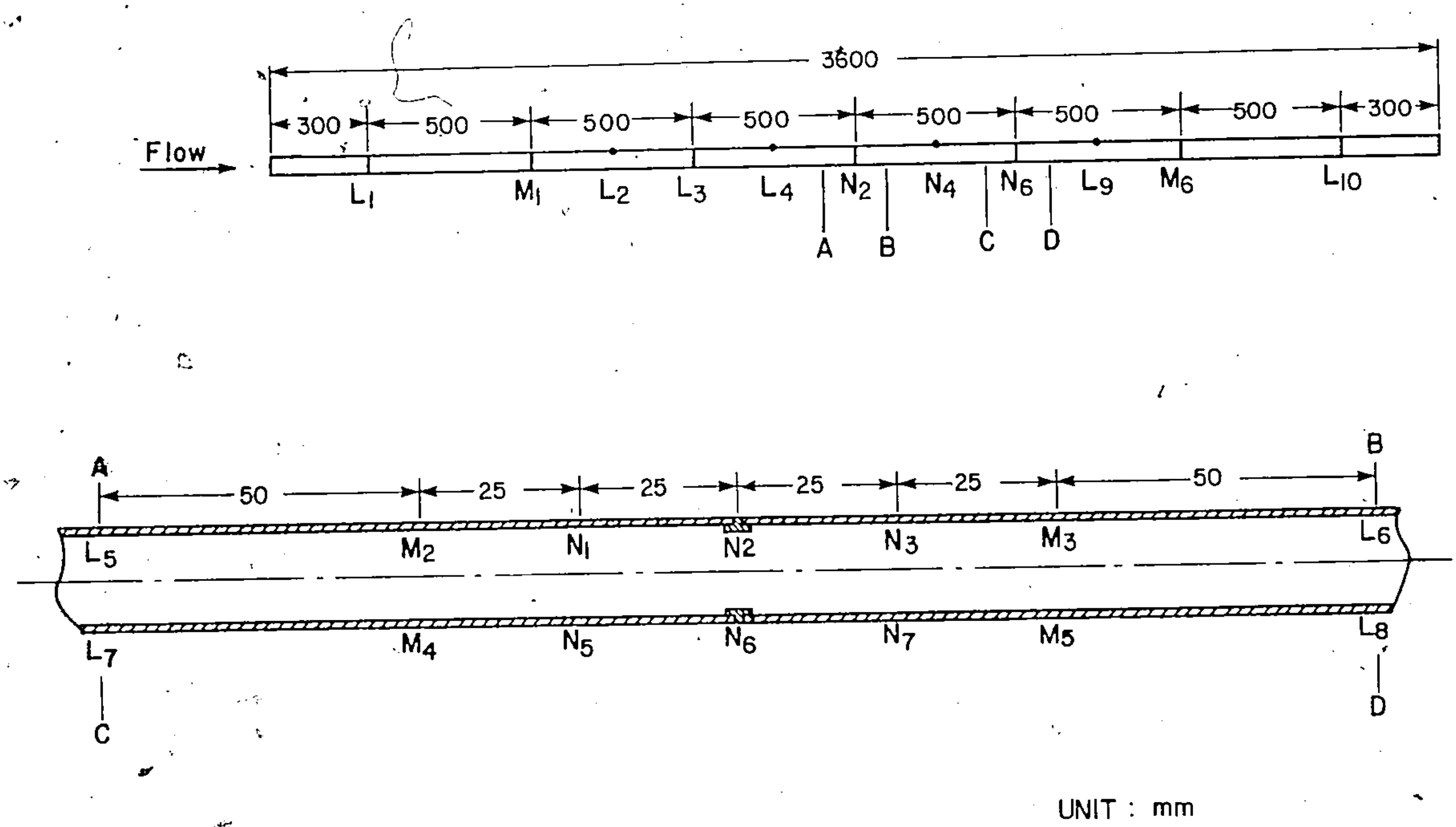

Fig. 3.3 Test Sections ; Location of Blockages and Thermocouples

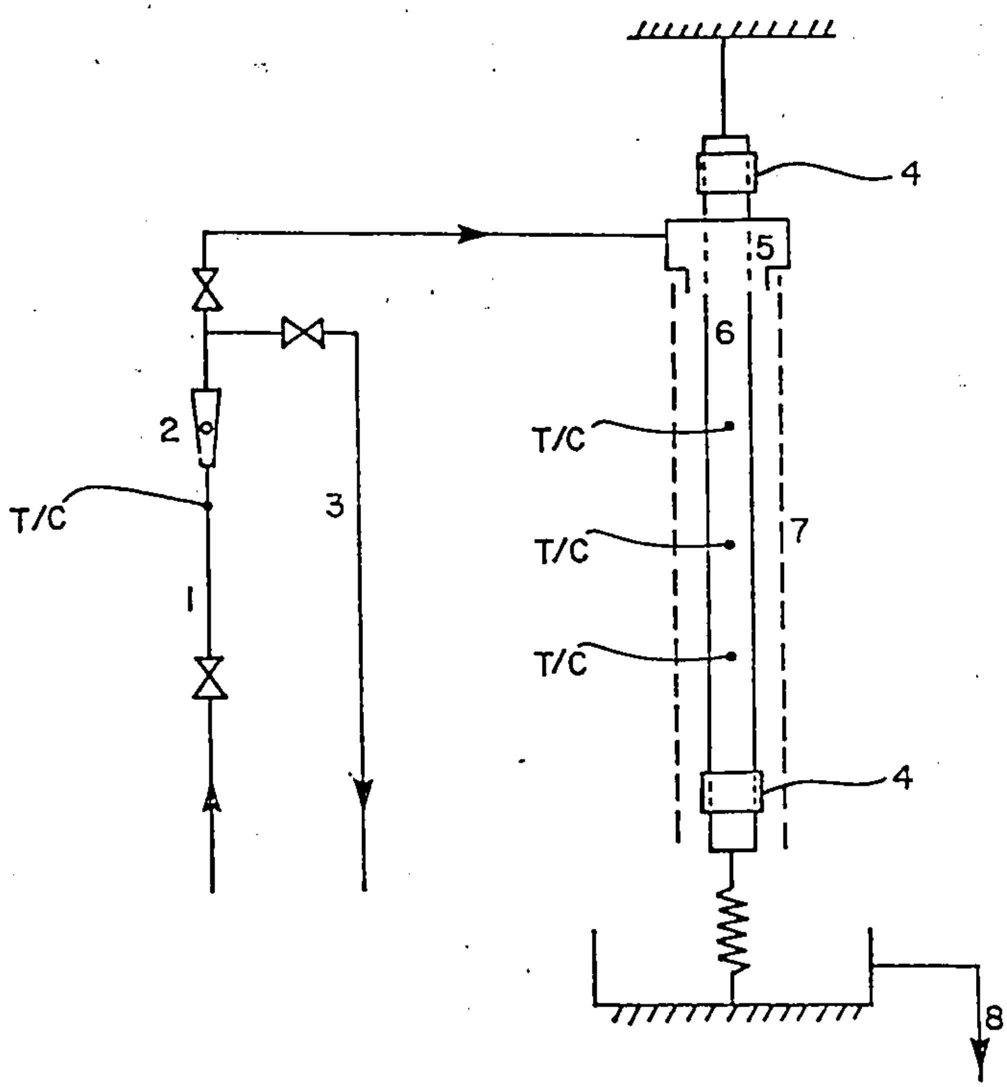

1 Water Supply
2 Rotameter
3 By-pass
4 Power Supply
5 Injection Nozzles
6 Test-Section
7 Removable Outer Jacket
8 Drain

Fig. 3.4 Schematic Diagram of Test Apparatus:
Unconfined top flooding

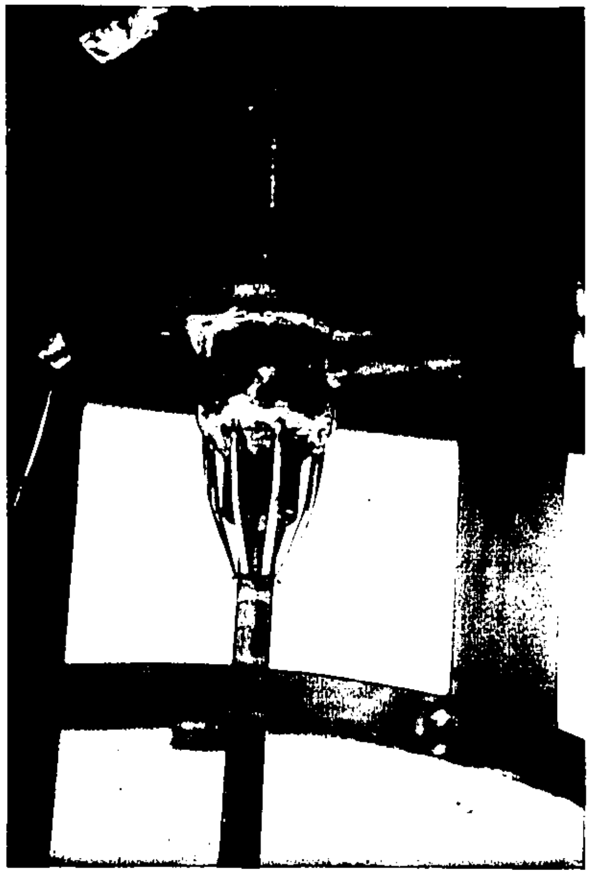

Fig. 3.5 Coolant Injection Nozzles, Unconfined Top-Flooding

Dimensions in mm

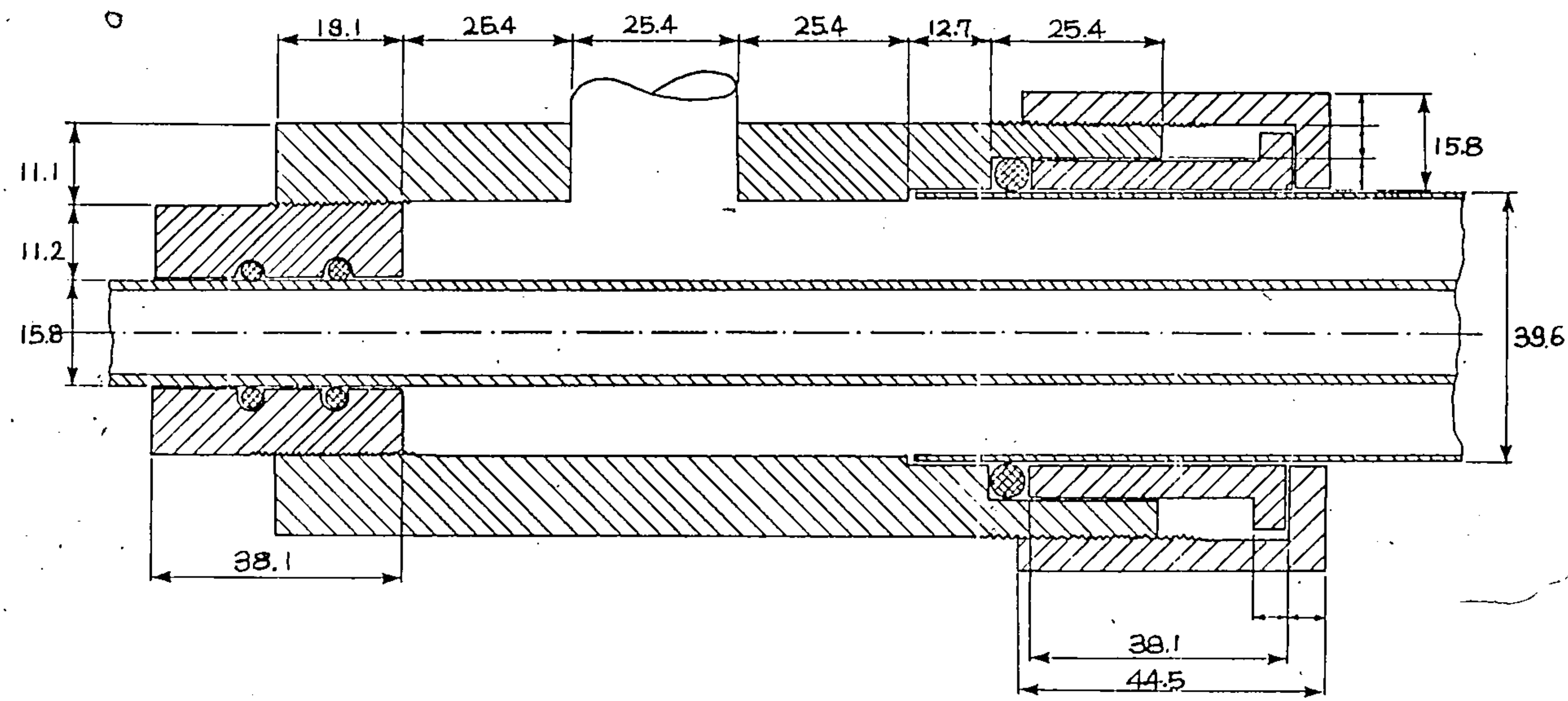

Fig. 3.6(a) End Connector Assembly, Concentric Annulus

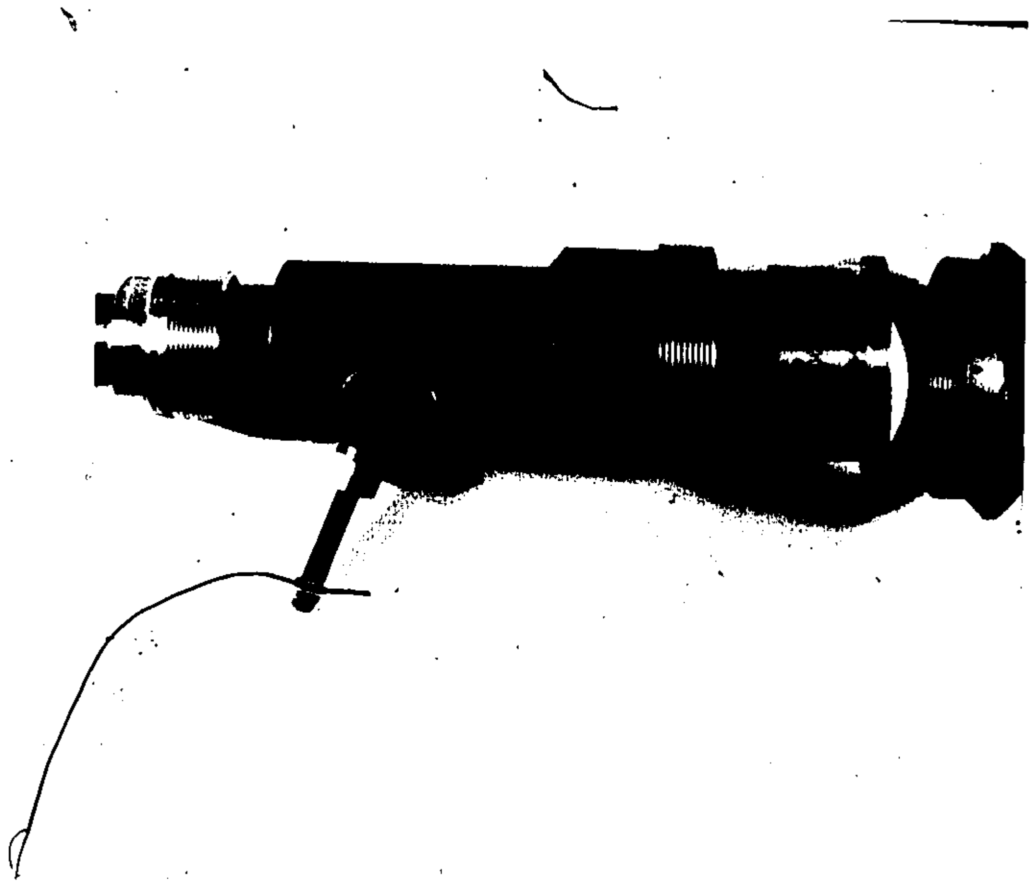

Fig 3.6(b) Picture of End Assembly for Annular Test-section

Dimensions in mm

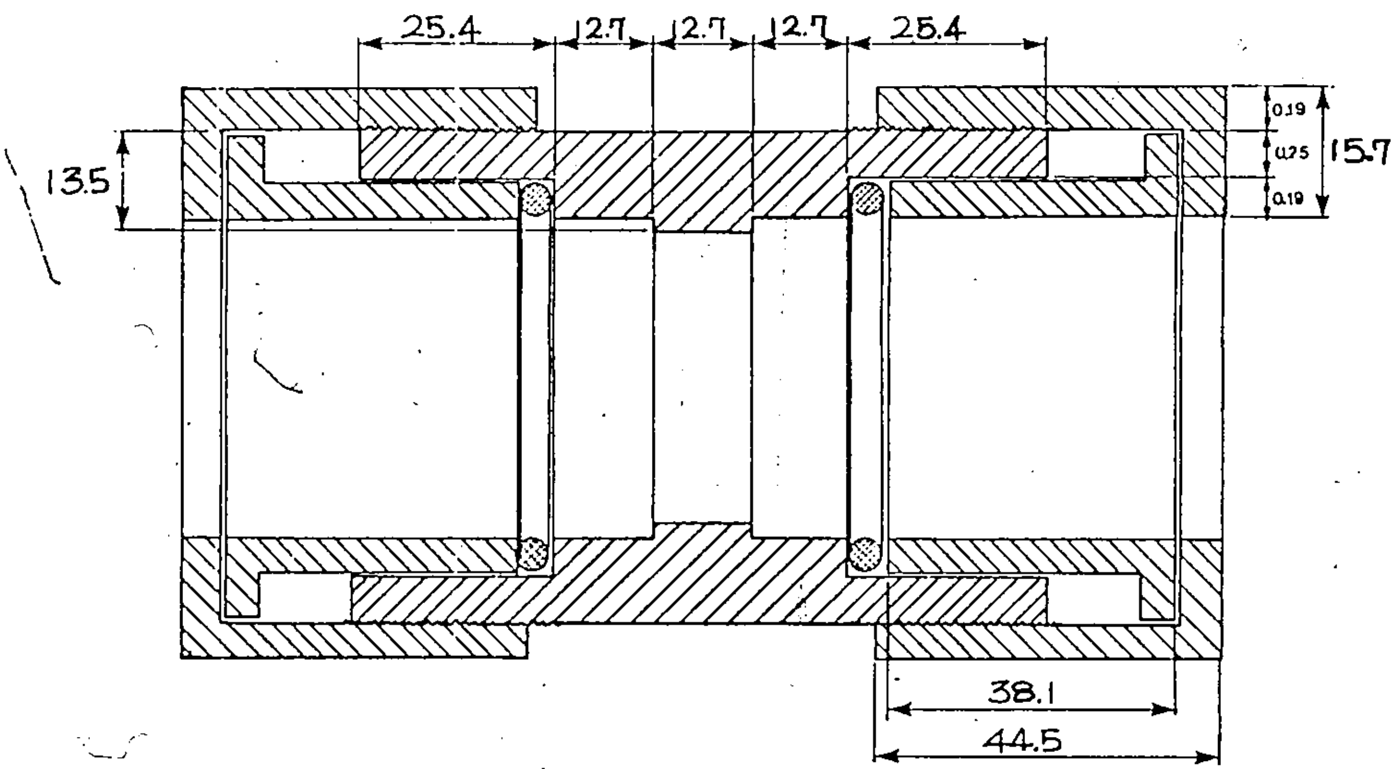

Fig 3.7 Connector Assembly, Middle Section, Concentric Annulus

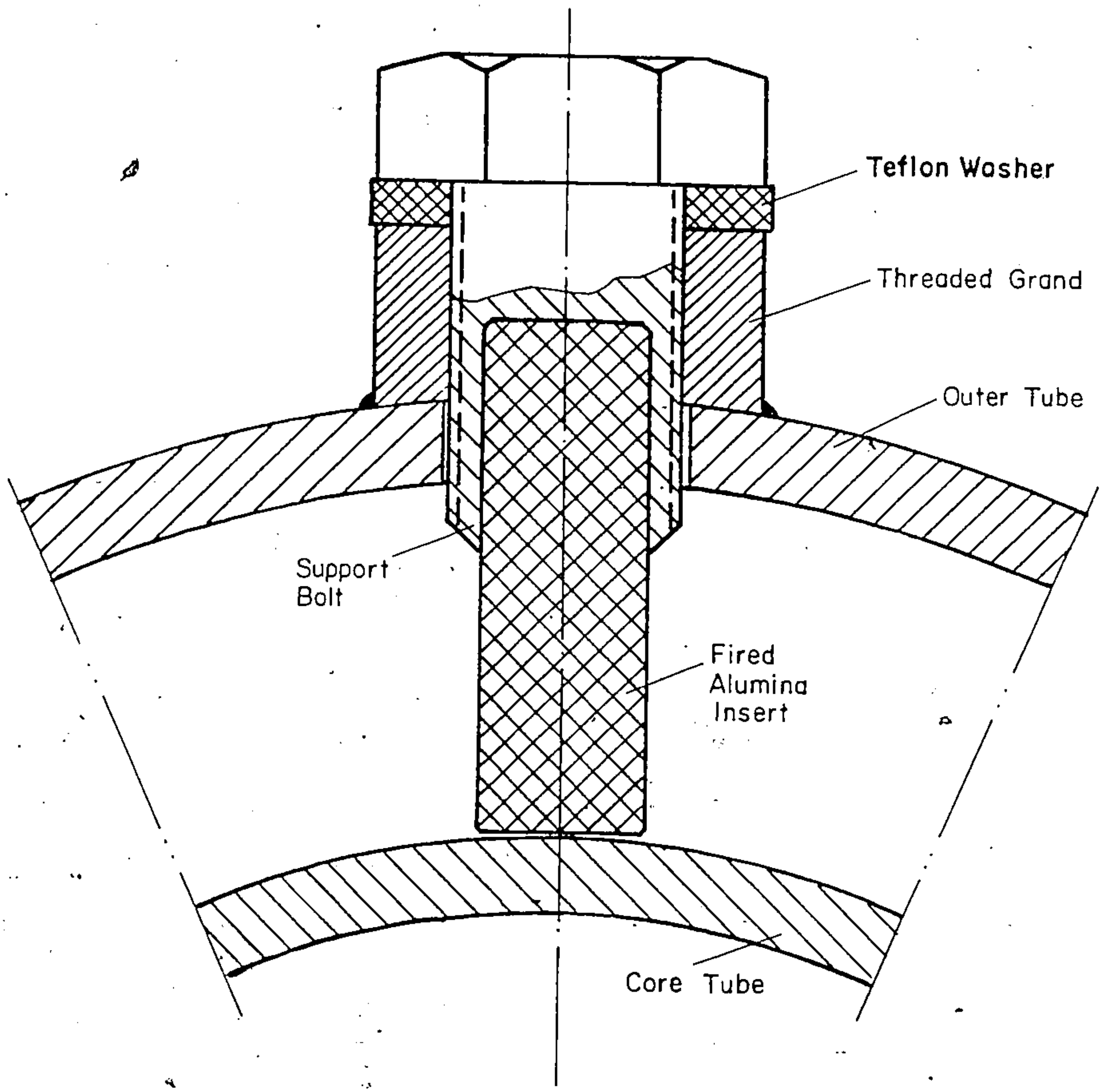

Fig. 3.8 Core Support ; Annular Test-section with Both Walls Heated

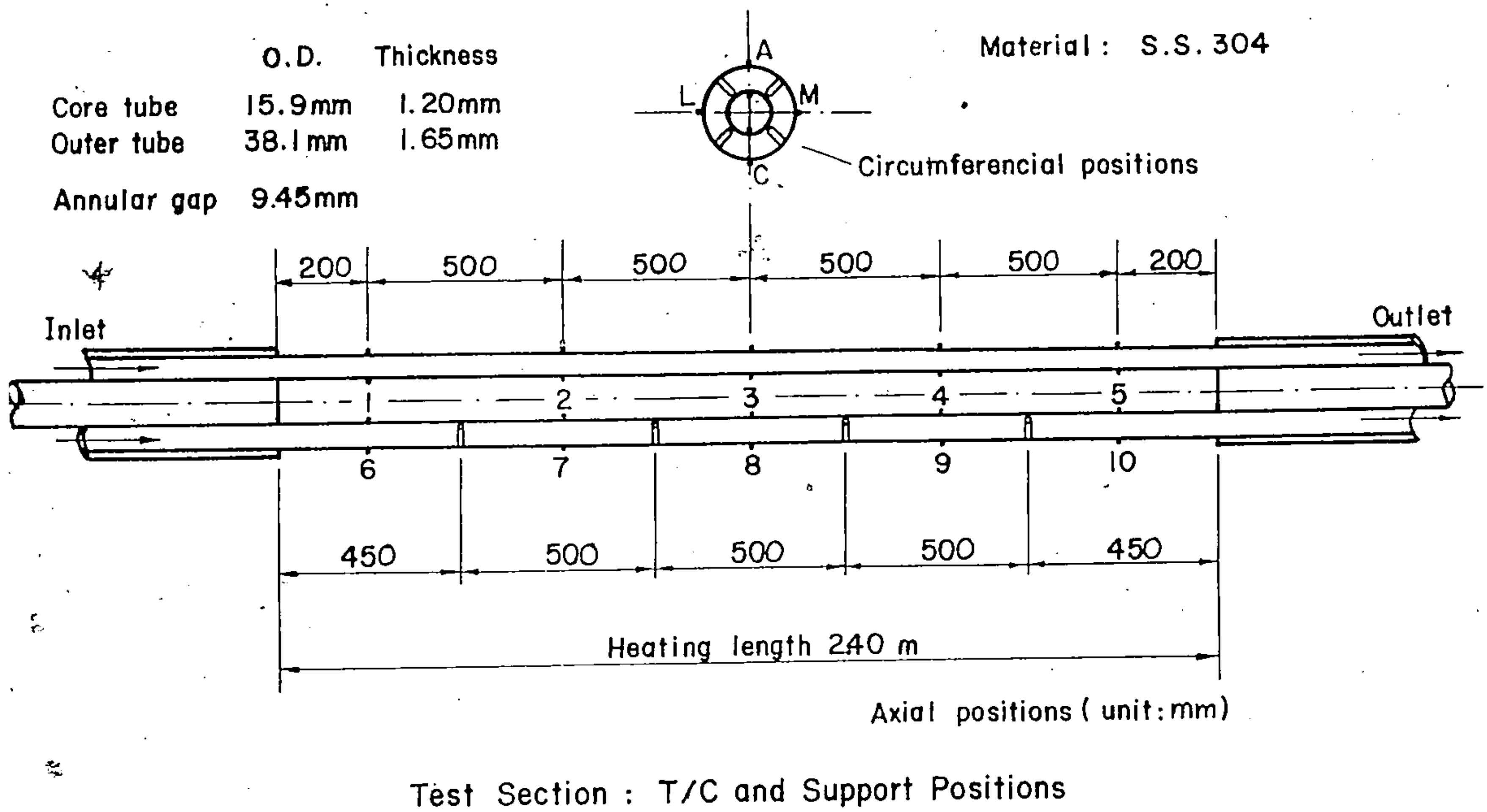

Fig. 3.9 Annular Test-section ; Location of Thermocouples and Core Supports

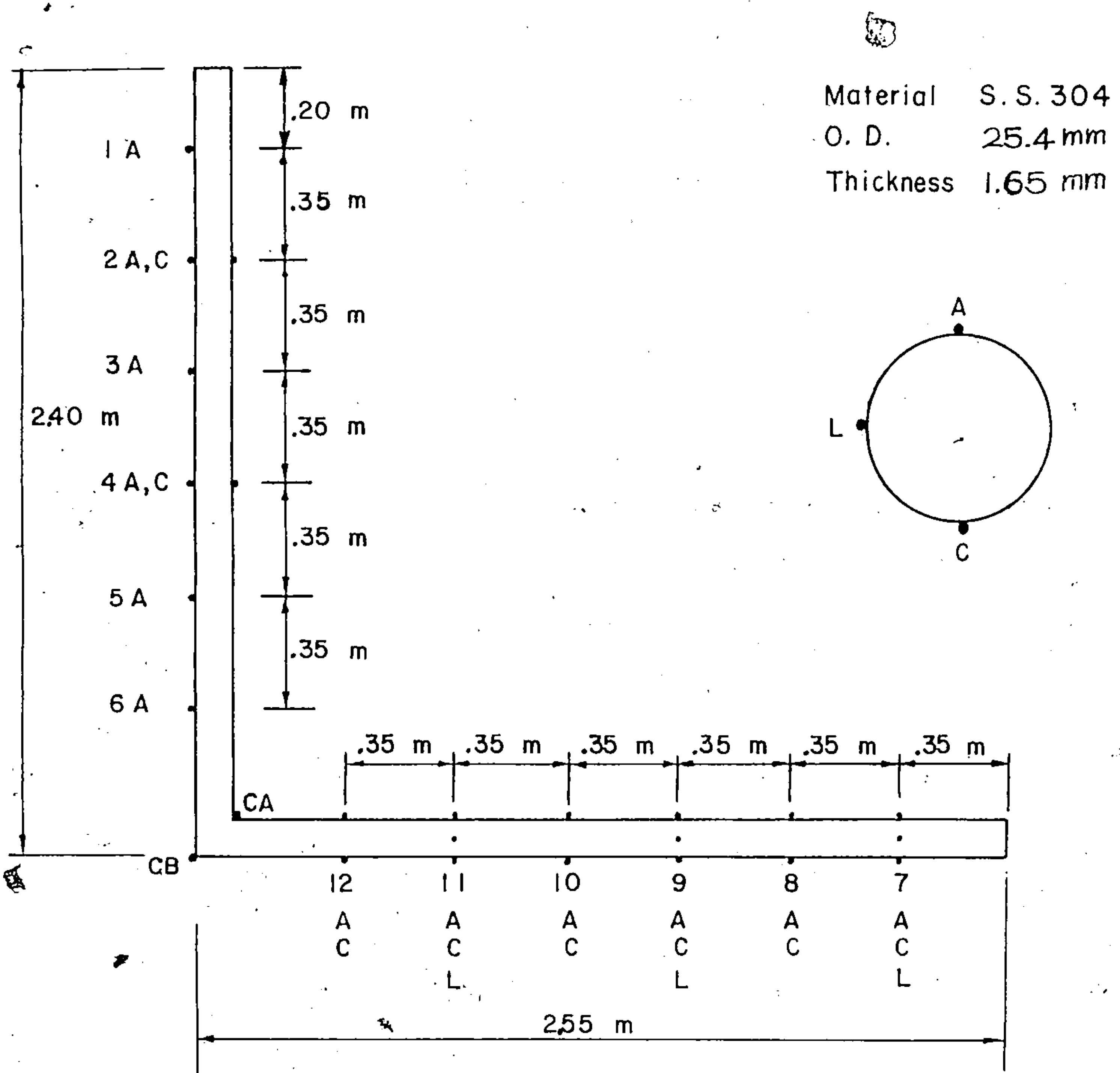

Fig. 3.10 "L"-shaped Test-section ; Location of Thermocouples

Figure 4.1 Unconfined Top Flooding

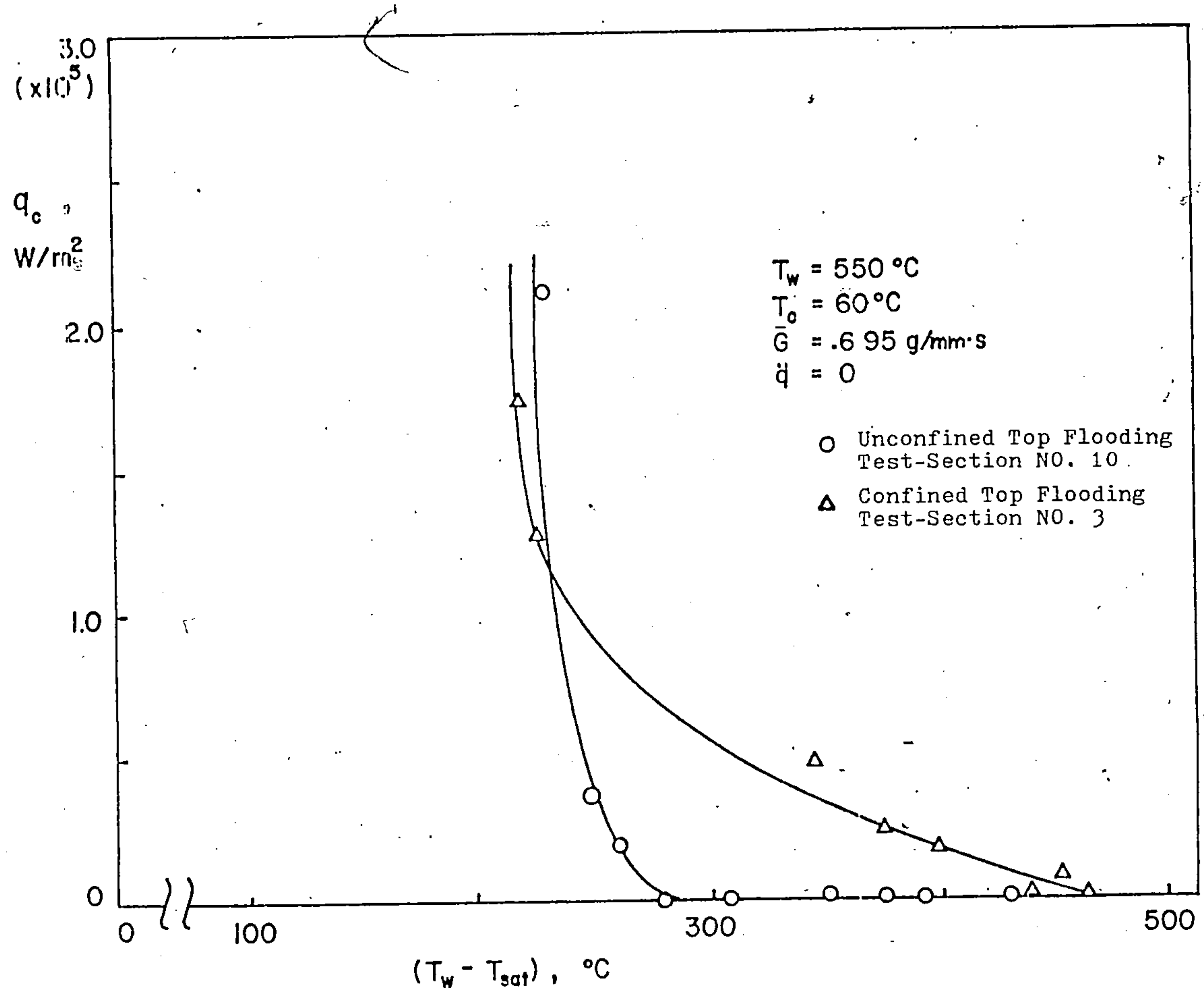

Figure 4.2 Surface Heat Flux Distribution in the Region ahead of the Rewetting Front

T_w = 450 C   G = 200 $Kg/m^2 \cdot s$ T_c = 60 C

Z = .25 m
(a)

Z = .45 m
(b)

Figure 4.3 Annular Bottom Flooding

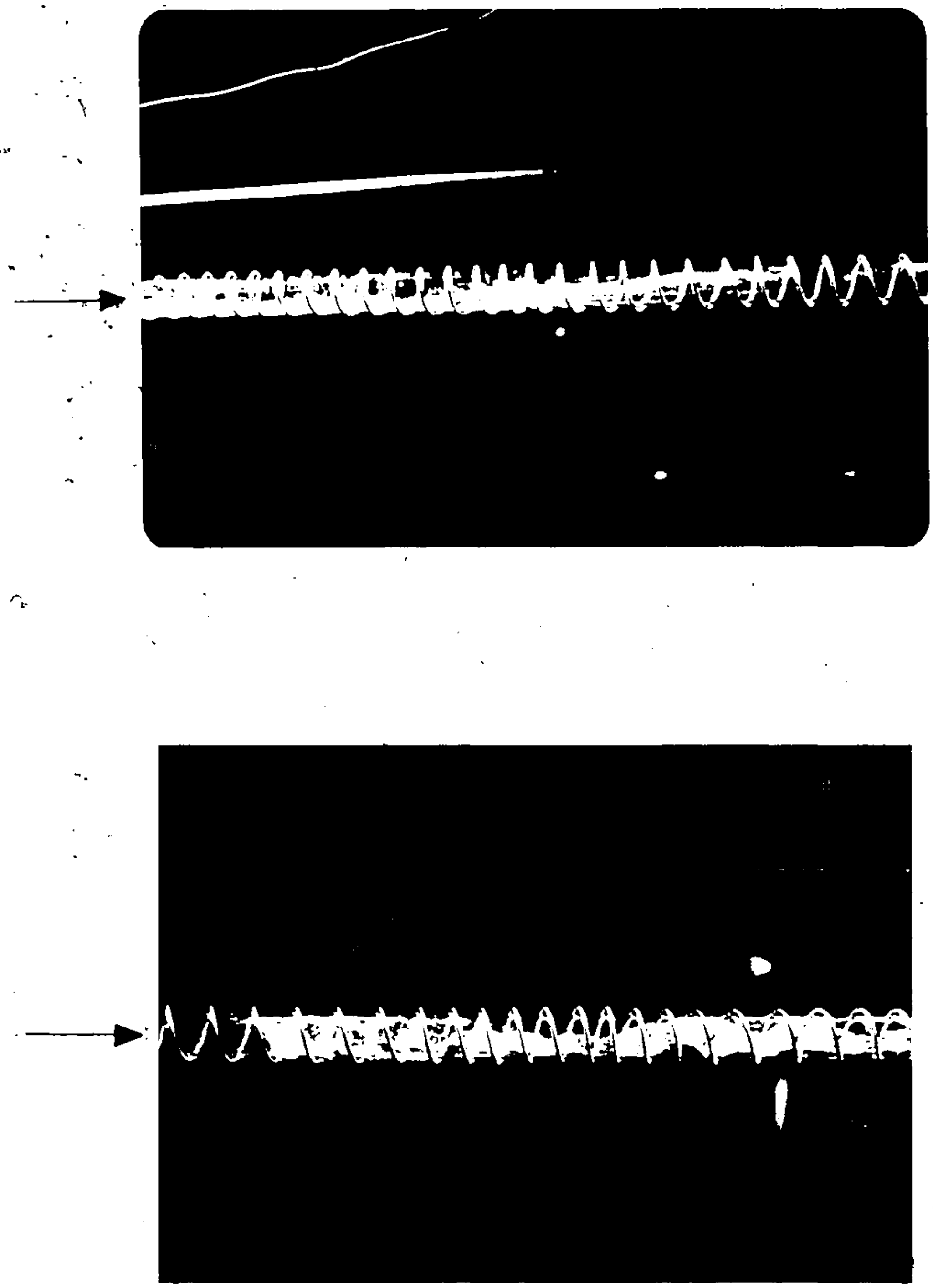

(b)

(a)

Figure 4.4 Confined Top Flooding, Vertical Single Tube

(c)

(d)

Figure 4.4 Confined Top Flooding, Vertical Single Tube (Cont'd)

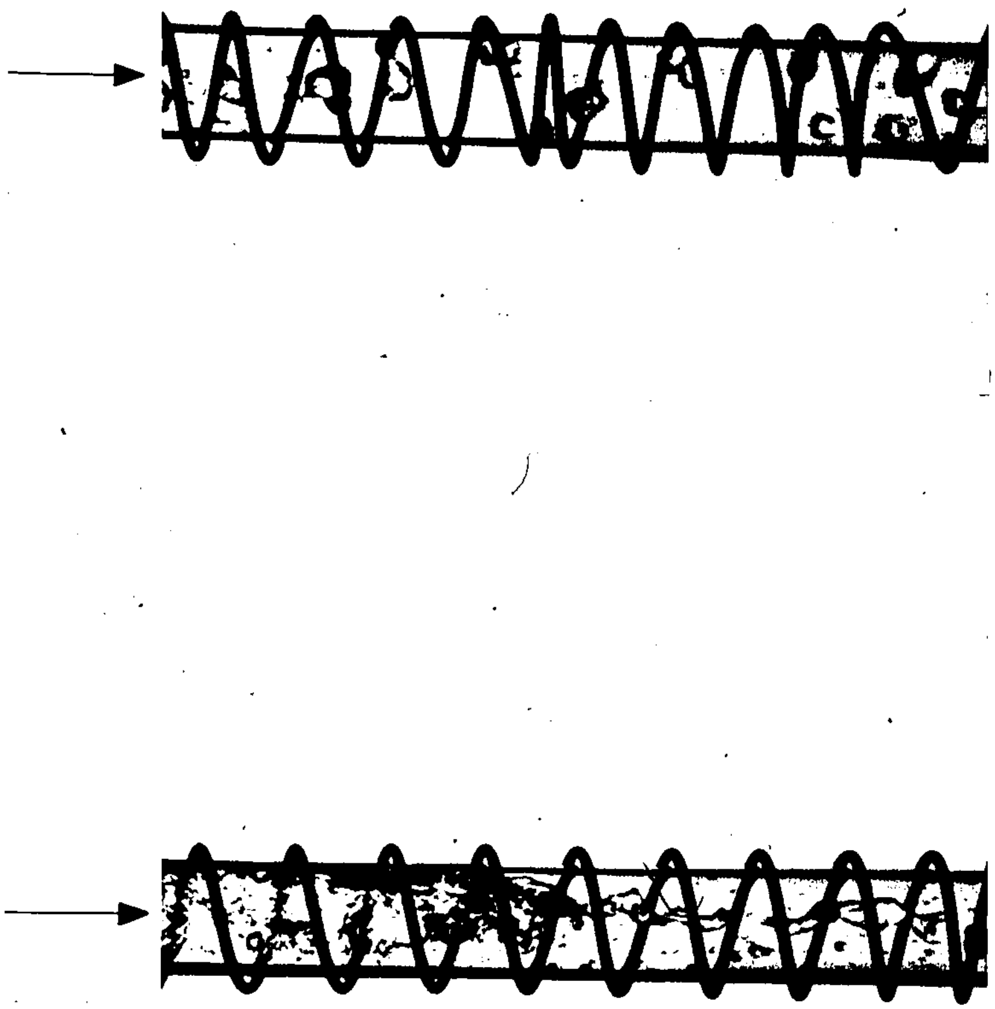

(f)

(e)

Figure 4.4 Confined Top Flooding, Vertical Single Tube (Cont'd)

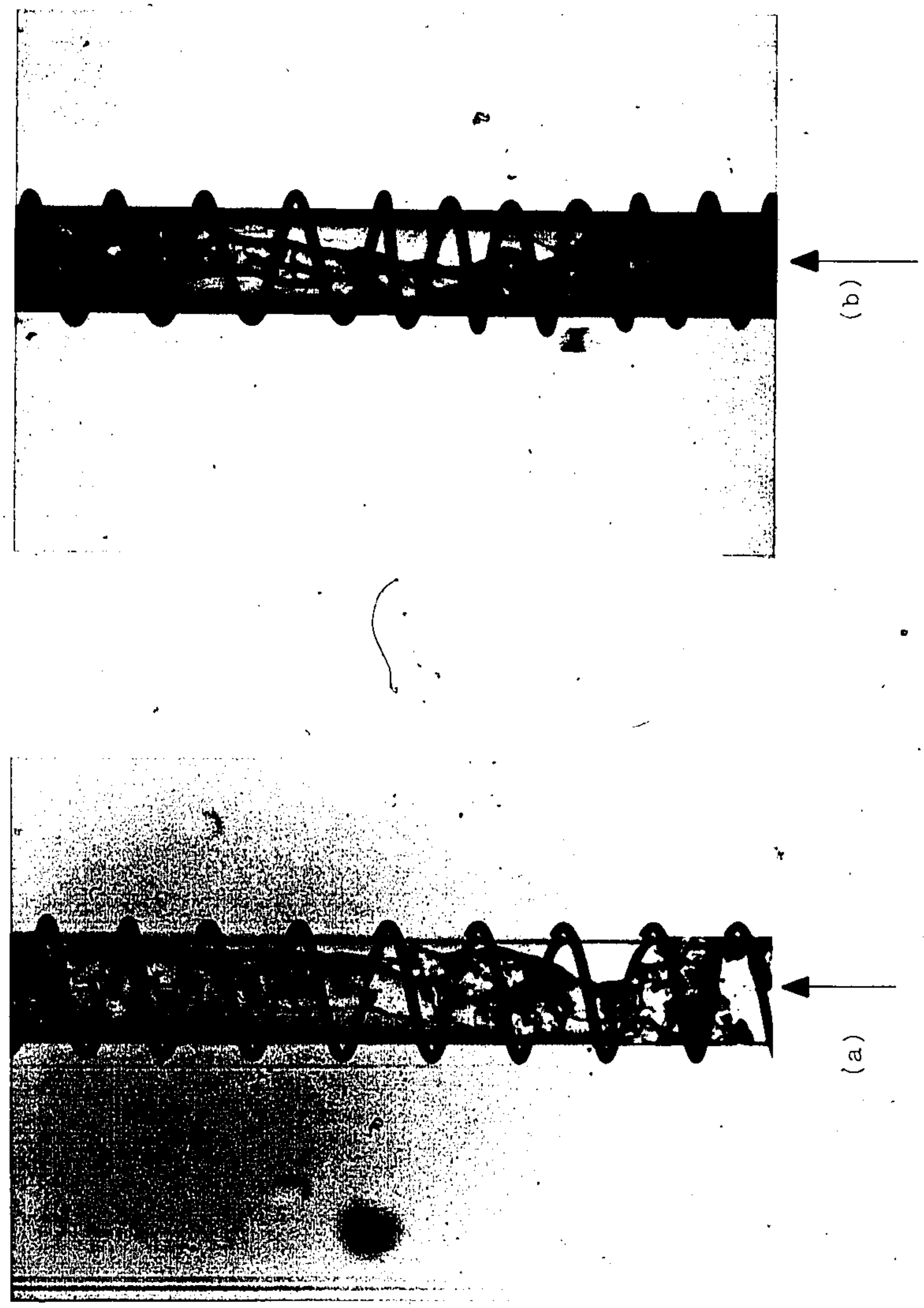

Figure 4.5 Bottom Flooding, Vertical Single Tube

(d)

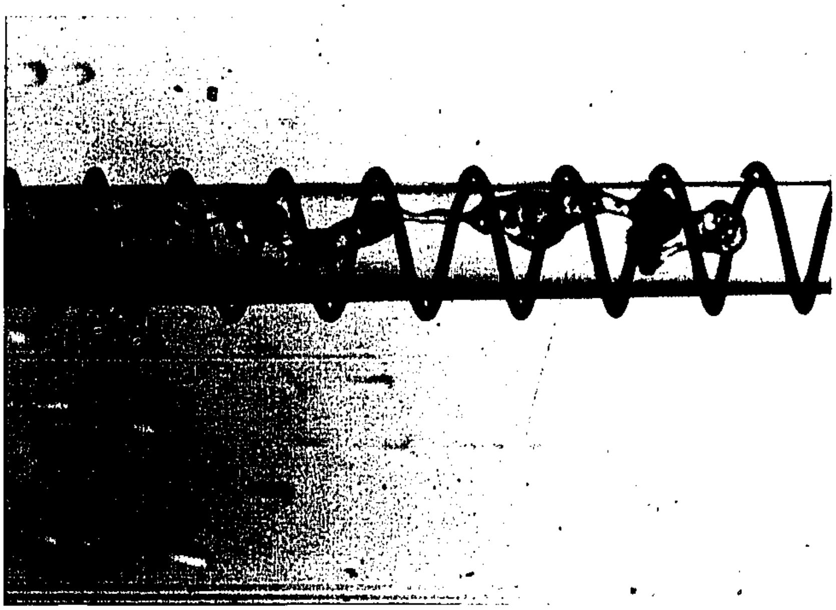

(c)

Figure 4.5 Bottom Flooding, Vertical Single Tube

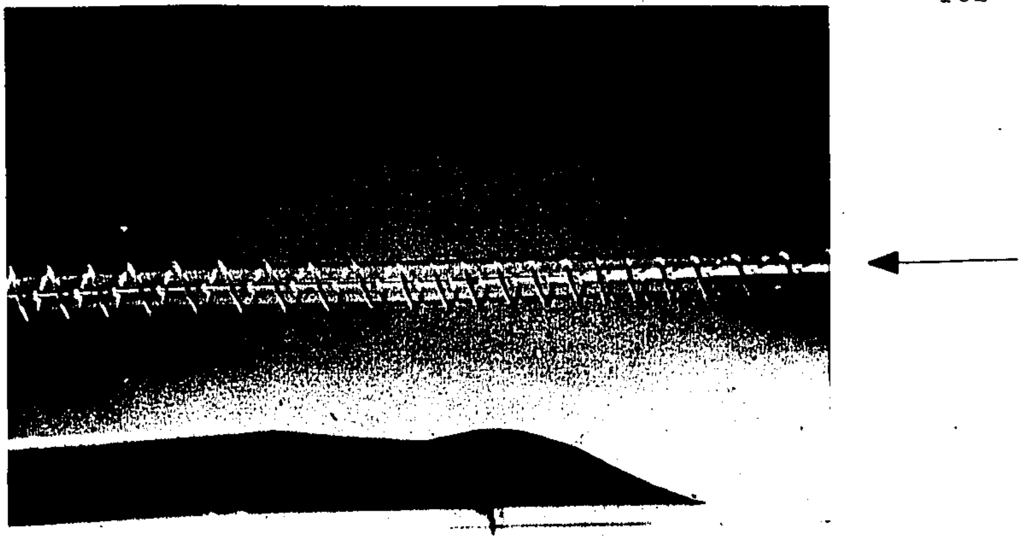

(a) Unheated, Flow Rate < 0.1 m/s

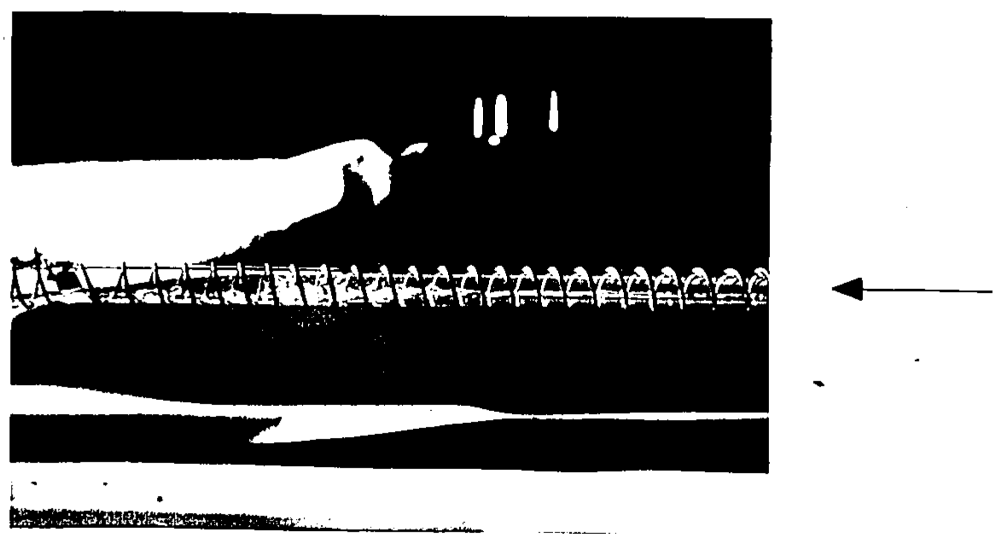

(b) Heated, Flow Rate < 0.1 m/s

Figure 4.6 Horizontal Flooding, Single Tube

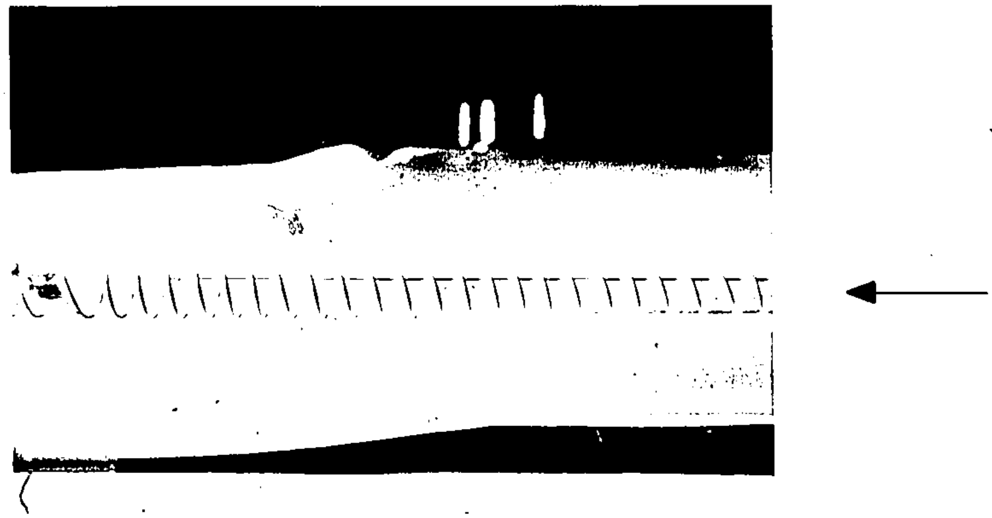

(c) Heated, Flow Rate < 0.1 m/s

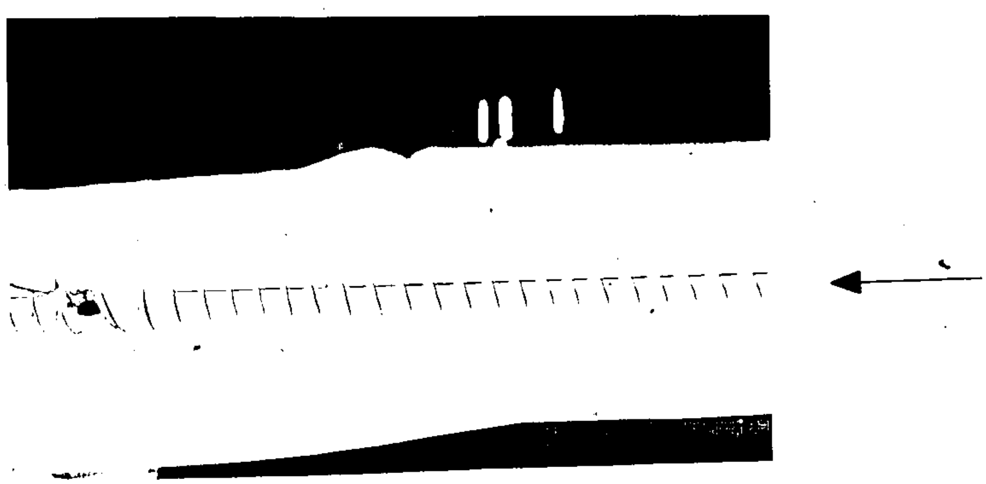

(d) Heated, Flow Rate < 0.1 m/s

Figure 4.6 Horizontal Flooding, Single Tube (Cont'd)

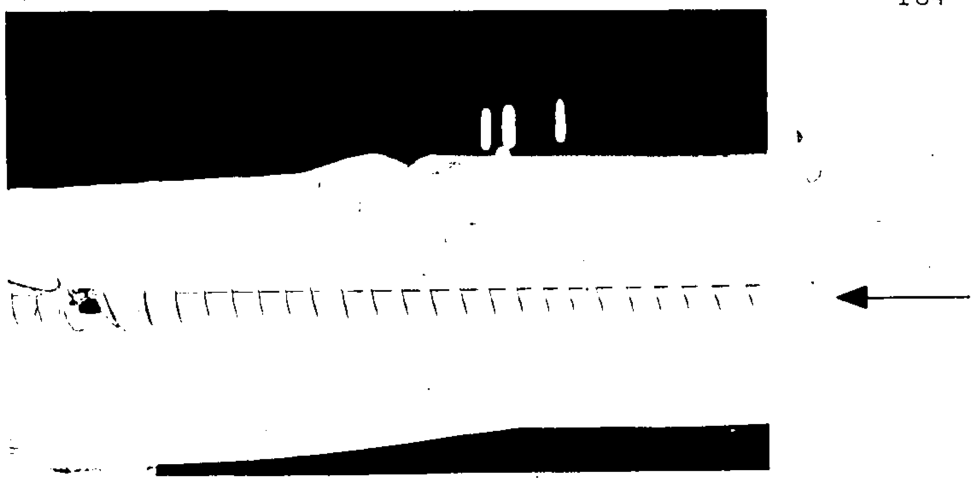

(e) Heated, Flow Rate < 0.1 m/s

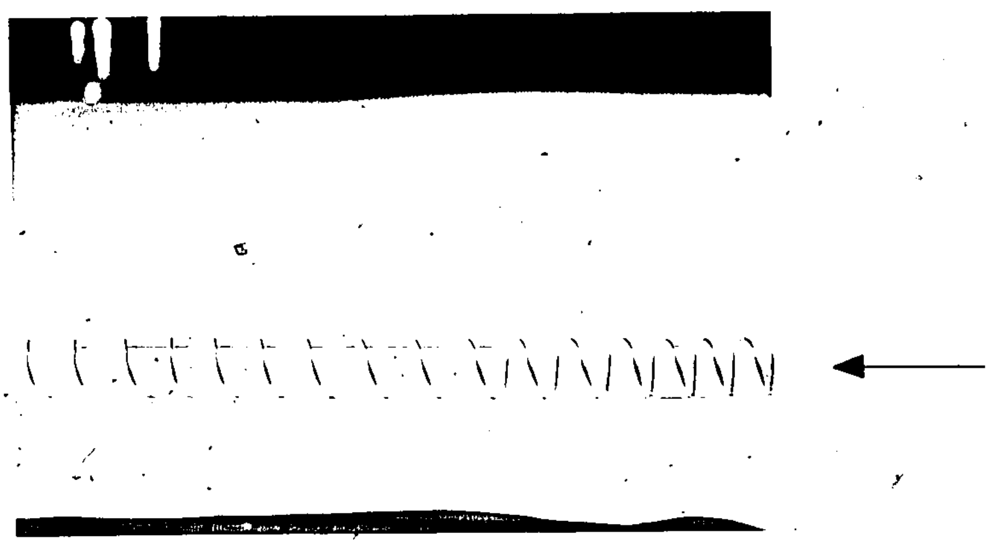

(f) Unheated, Flow Rate > 0.1 m/s

Figure 4.6 Horizontal Flooding, Single Tube (Cont'd)

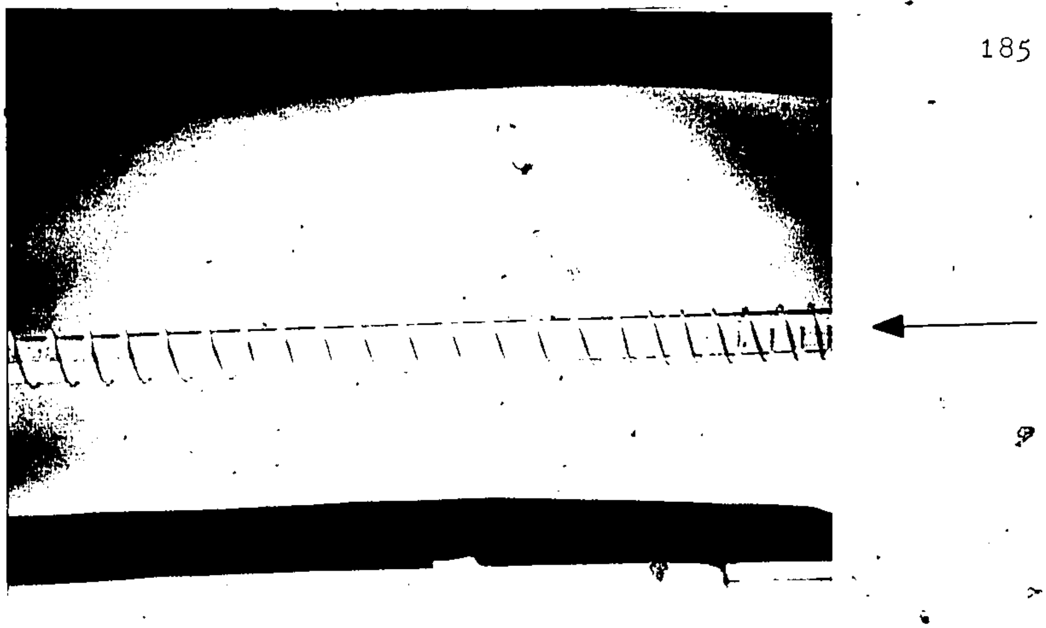

(g) Heated, Flow Rate > 0.1 m/s

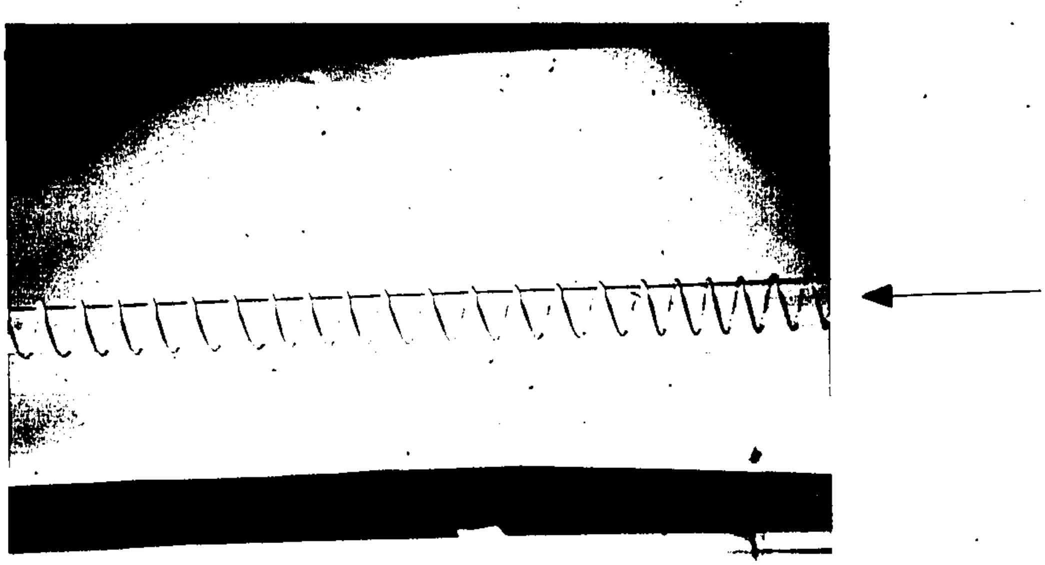

(h) Heated, Flow Rate > 0.1 m/s

Figure 4.6 Horizontal Flooding, Single Tube (Cont'd)

COLOURED PICTURES
Images en couleur

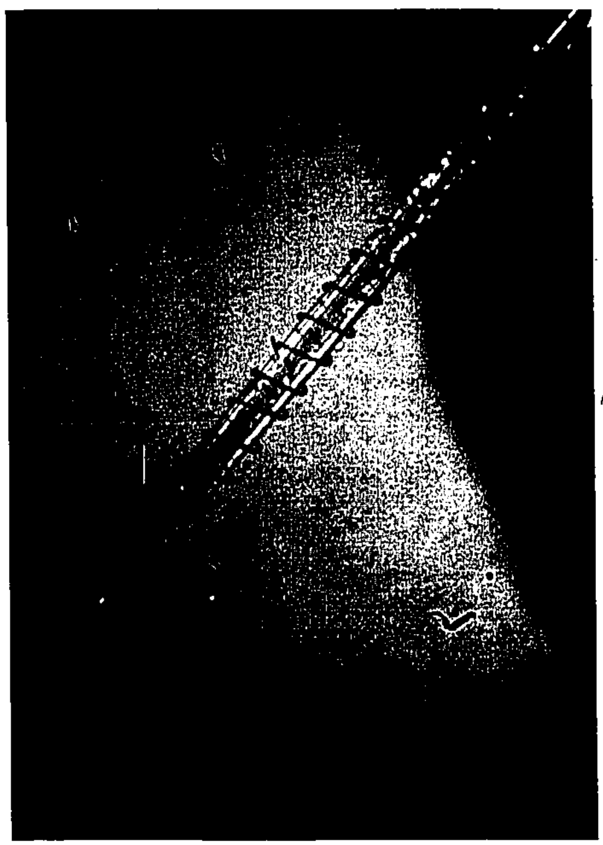

Figure 4.7 Bottom Flooding, Inclined Single Tube

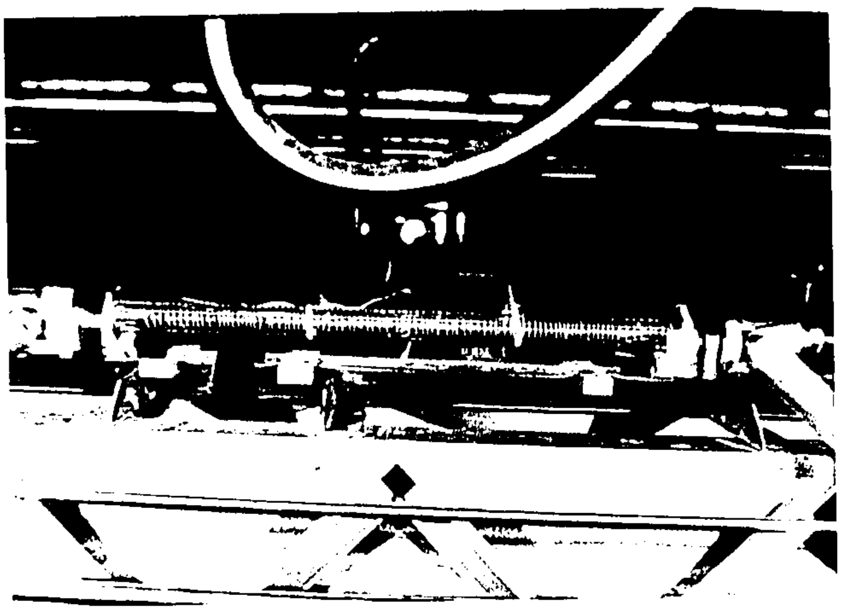

(a)

Figure 4.8 Annular Test-section, Both Walls Heated

COLOURED PICTURES
Images en couleur

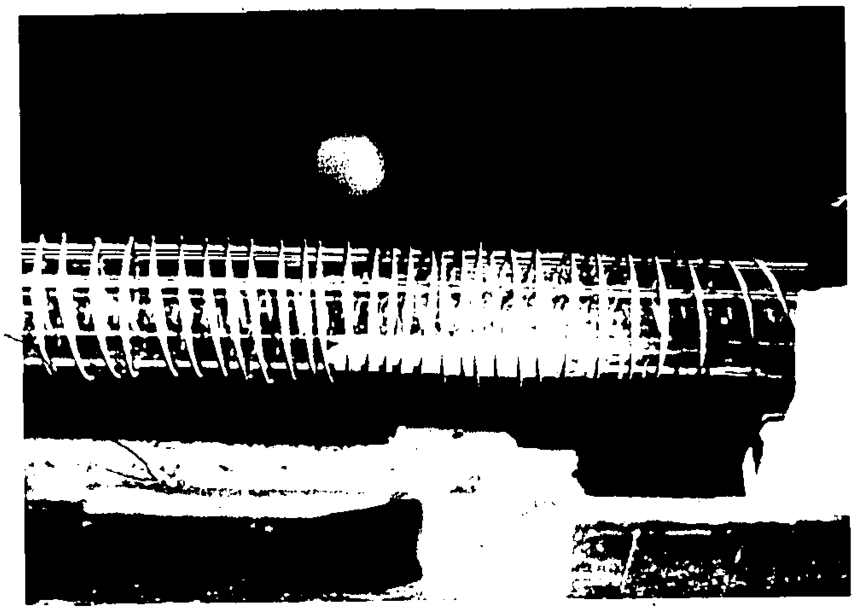

(b)

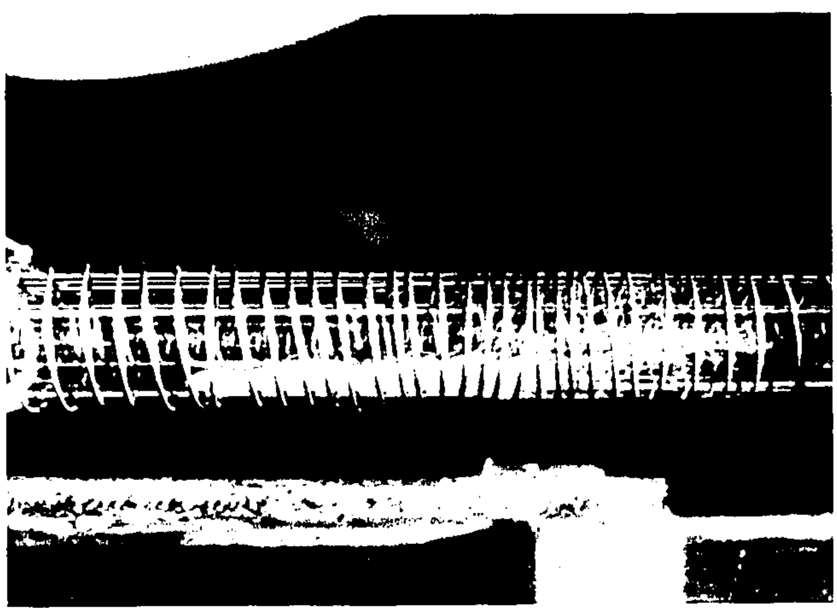

(c)

Figure 4.8 Horizontal Flooding, Annular Test-section (Cont'd)

COLOURED PICTURES
Images en couleur

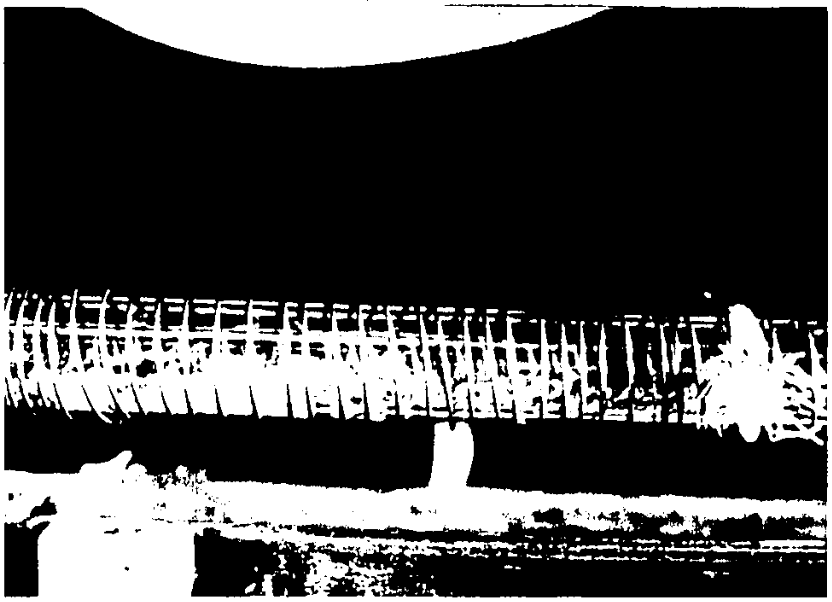

(d)

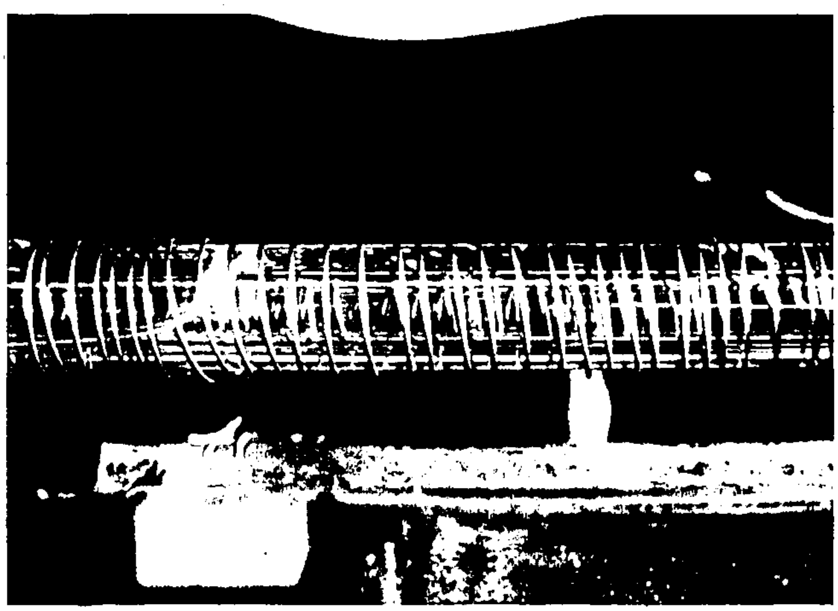

(e)

Figure 4.8 Horizontal Flooding, Annular Test-section (Cont'd)

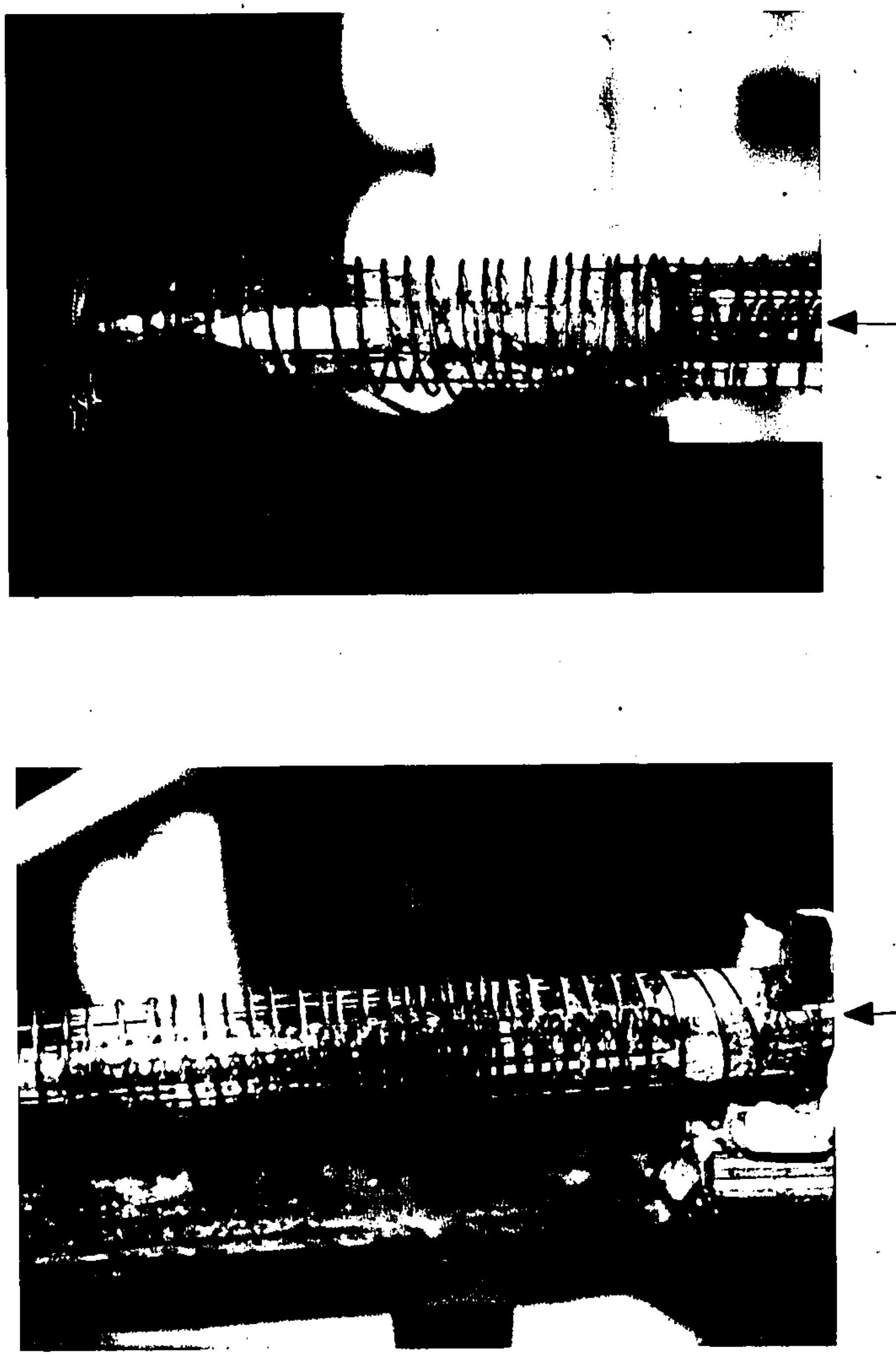

(a) Z = .15 m

(b) Z = .45 m

Fig. 4.9 Bottom Flooding, Annular Test-section, Both Walls Heated

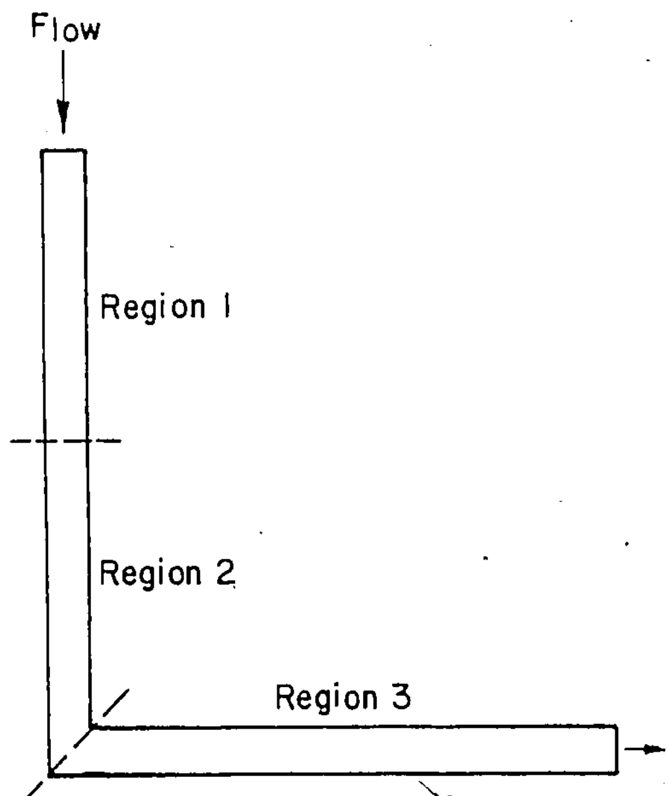

Top-followed-by-Horizontal Flooding Mode; THF Mode

Fig. 4.10 Rewetting Regions; "L"-shaped Test-section

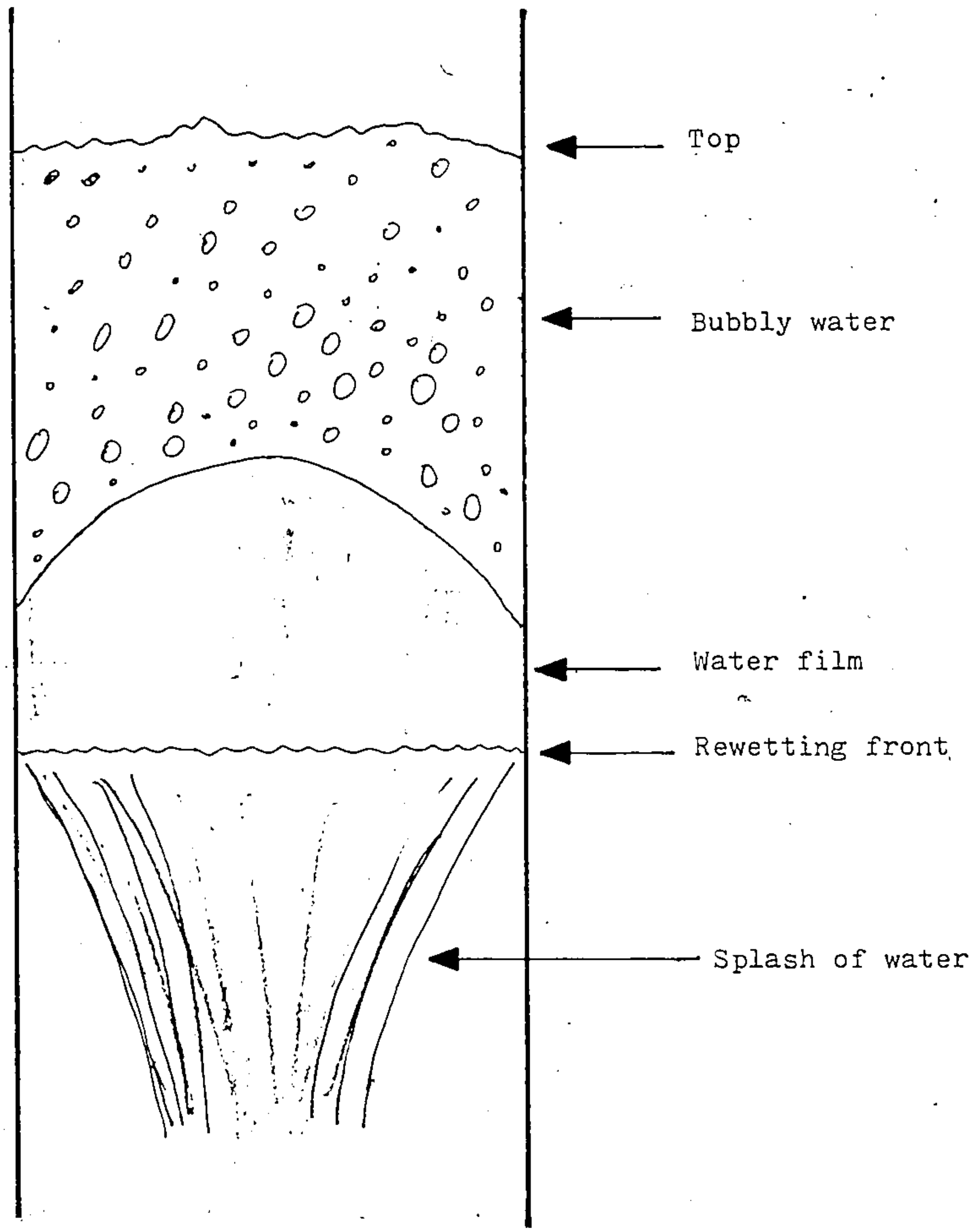

Fig. 4.11 Flow Characteristic in the Vertical Section of L-shaped Test Section

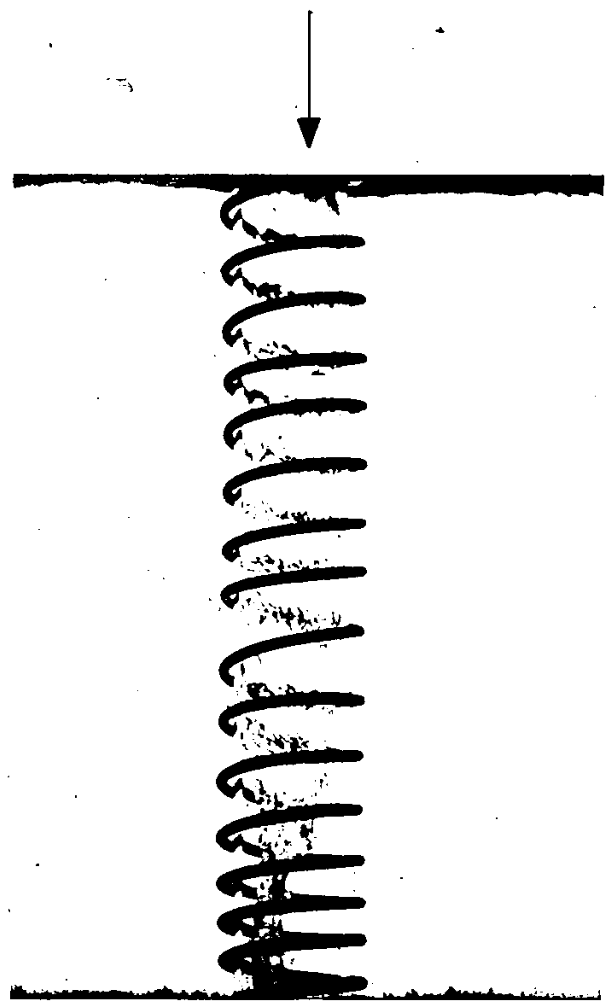

(a) Upper Section, Region 1, THF

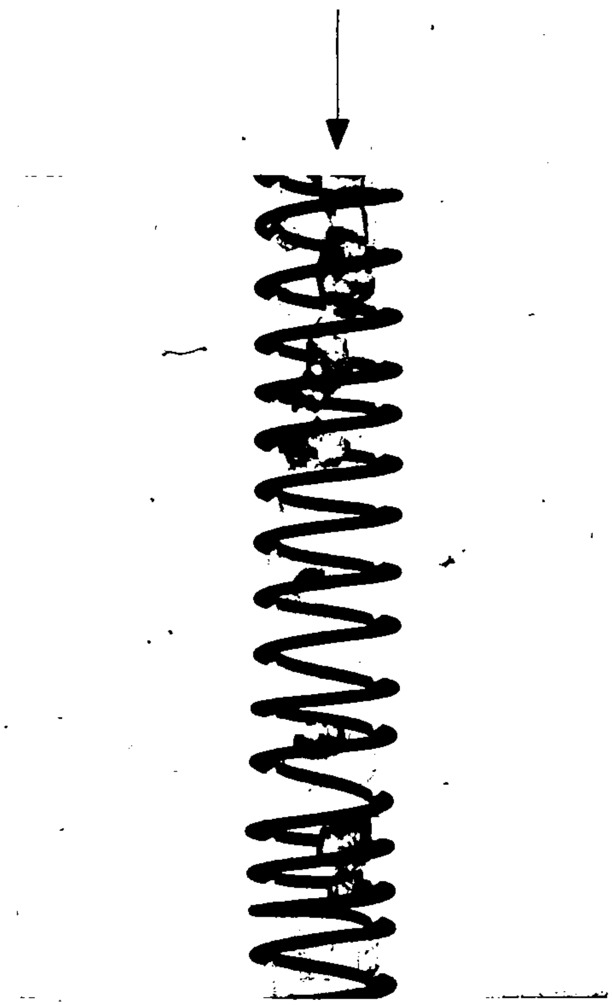

(b) Lower Section, Region 1, THF

Figure 4.12 Top Flooding, "L"-shaped Single Tube

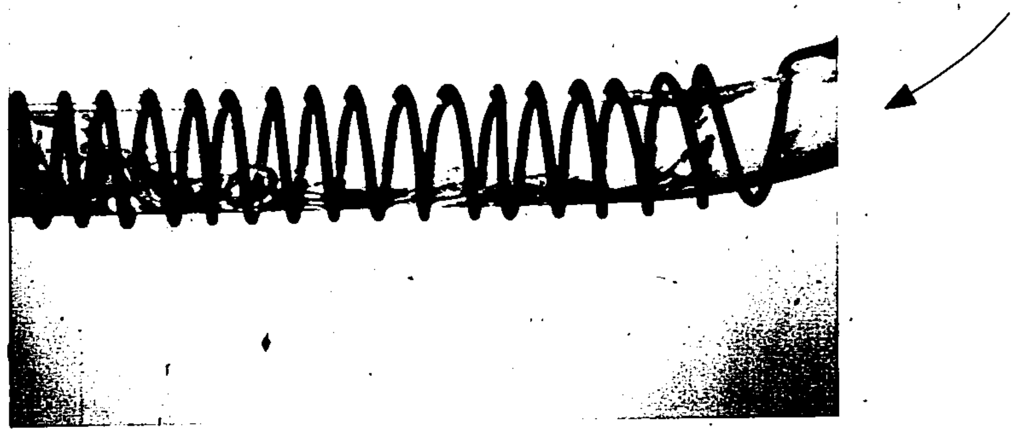

(c) Region 2, THF

Figure 4.12 Top Flooding, "L"-shaped Single Tube (Cont'd)

COLOURED PICTURES
Images en couleur

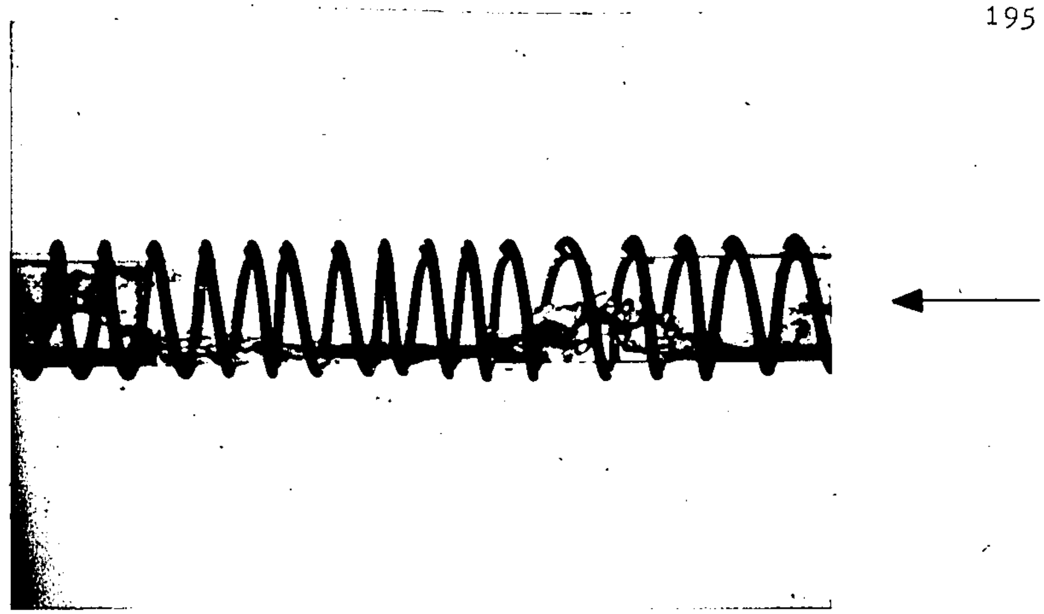

(d) Entrance to Region 3, THF

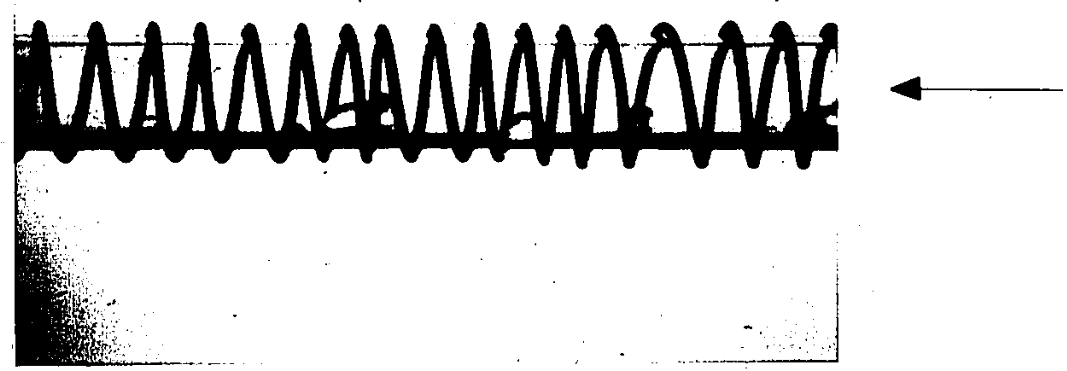

(e) Near the Exit of Region 3, THF

Figure 4.12 Top Flooding, "L"-shaped Single Tube (Cont'd)

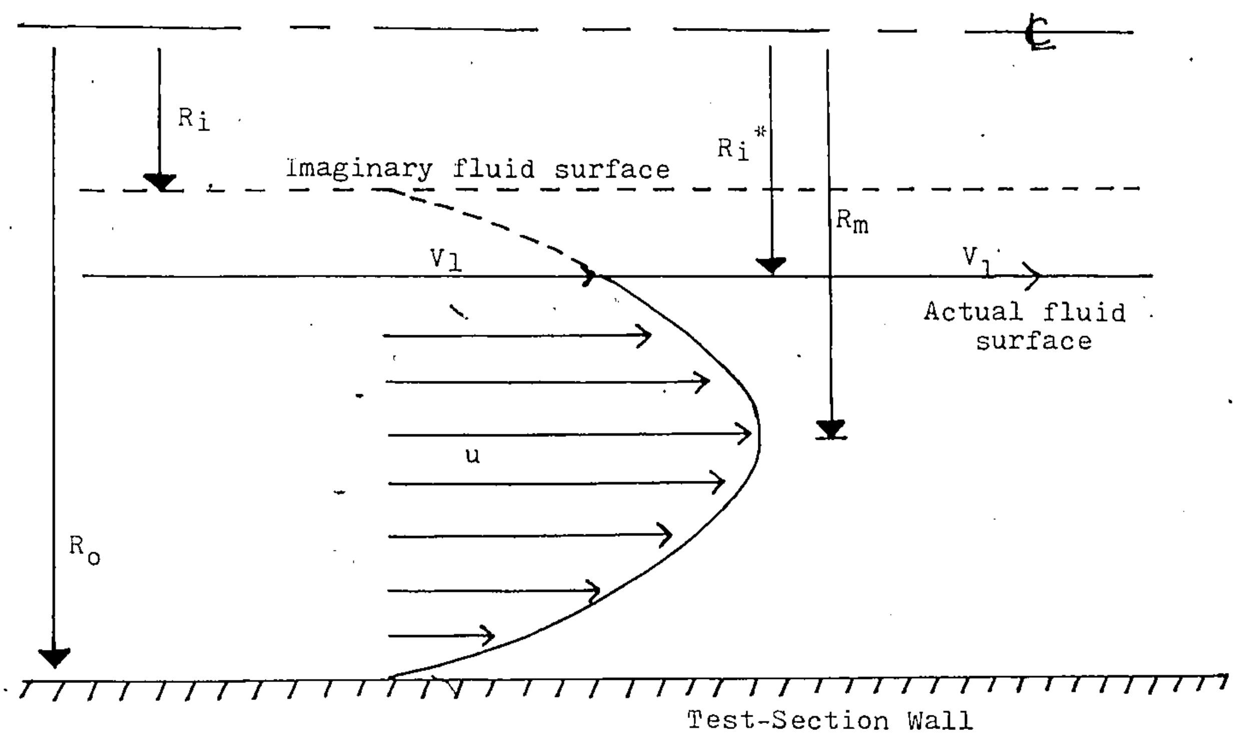

Fig 5.1 Vapour Velocity Profile in the Vapour Gap

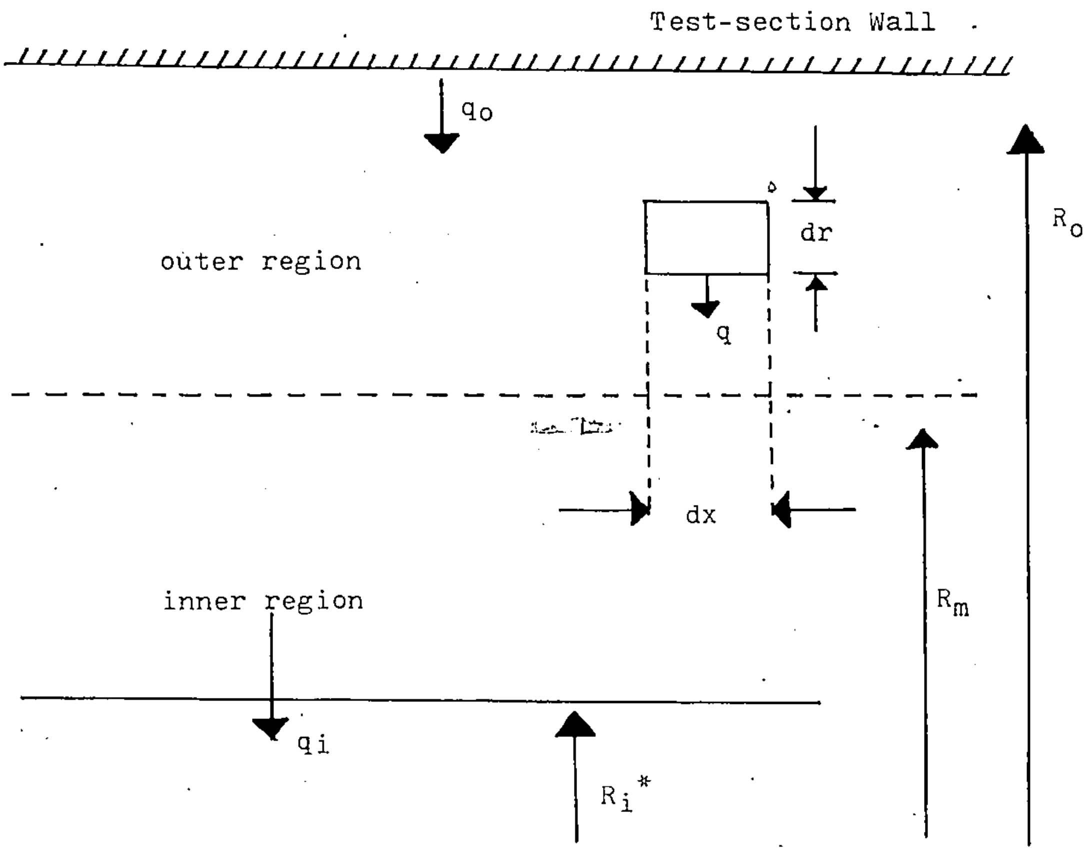

Fig. 5.2 Heat Flux Distribution in the Annulus Gap

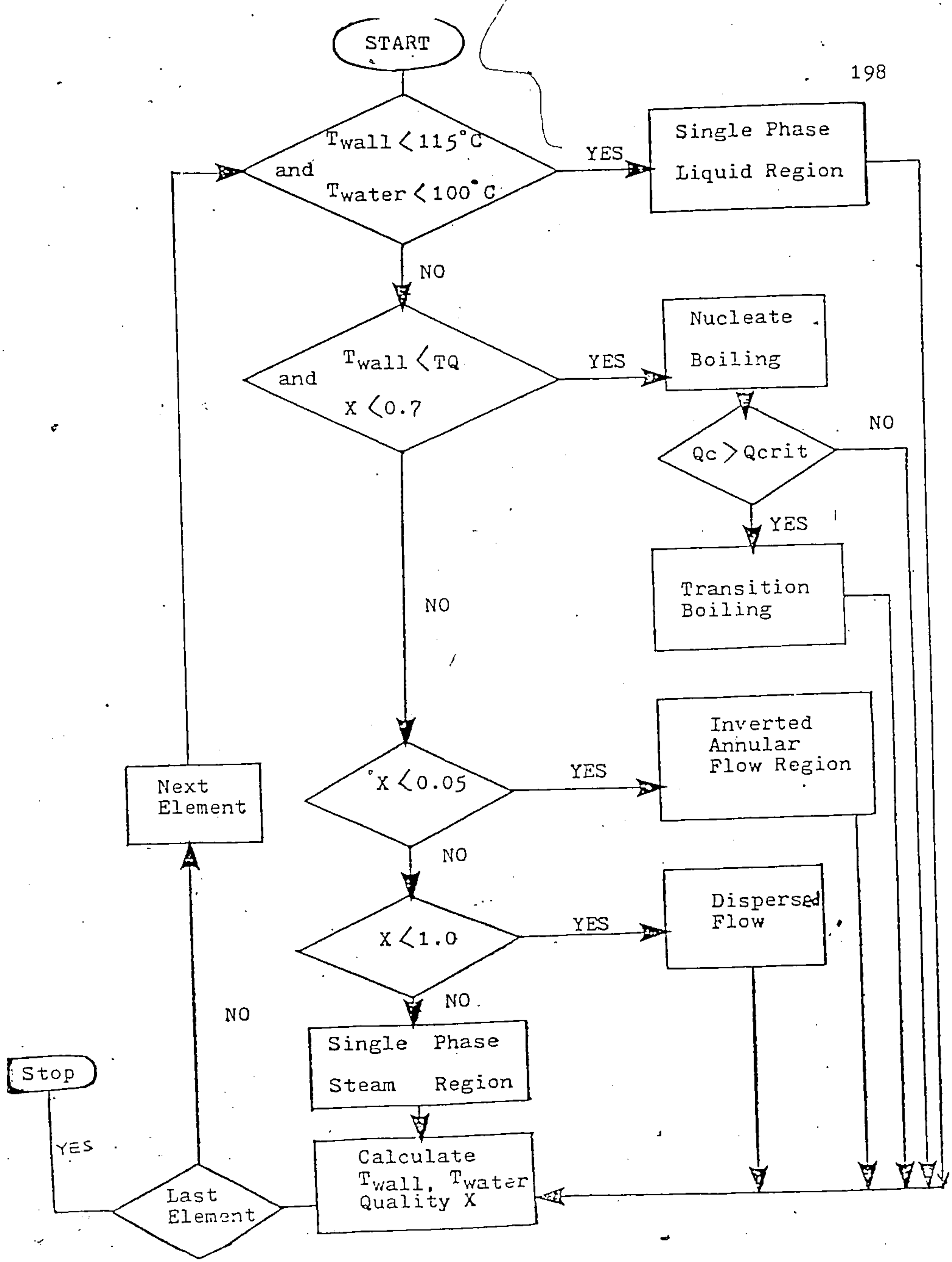

Fig. 5.3 Flow Chart

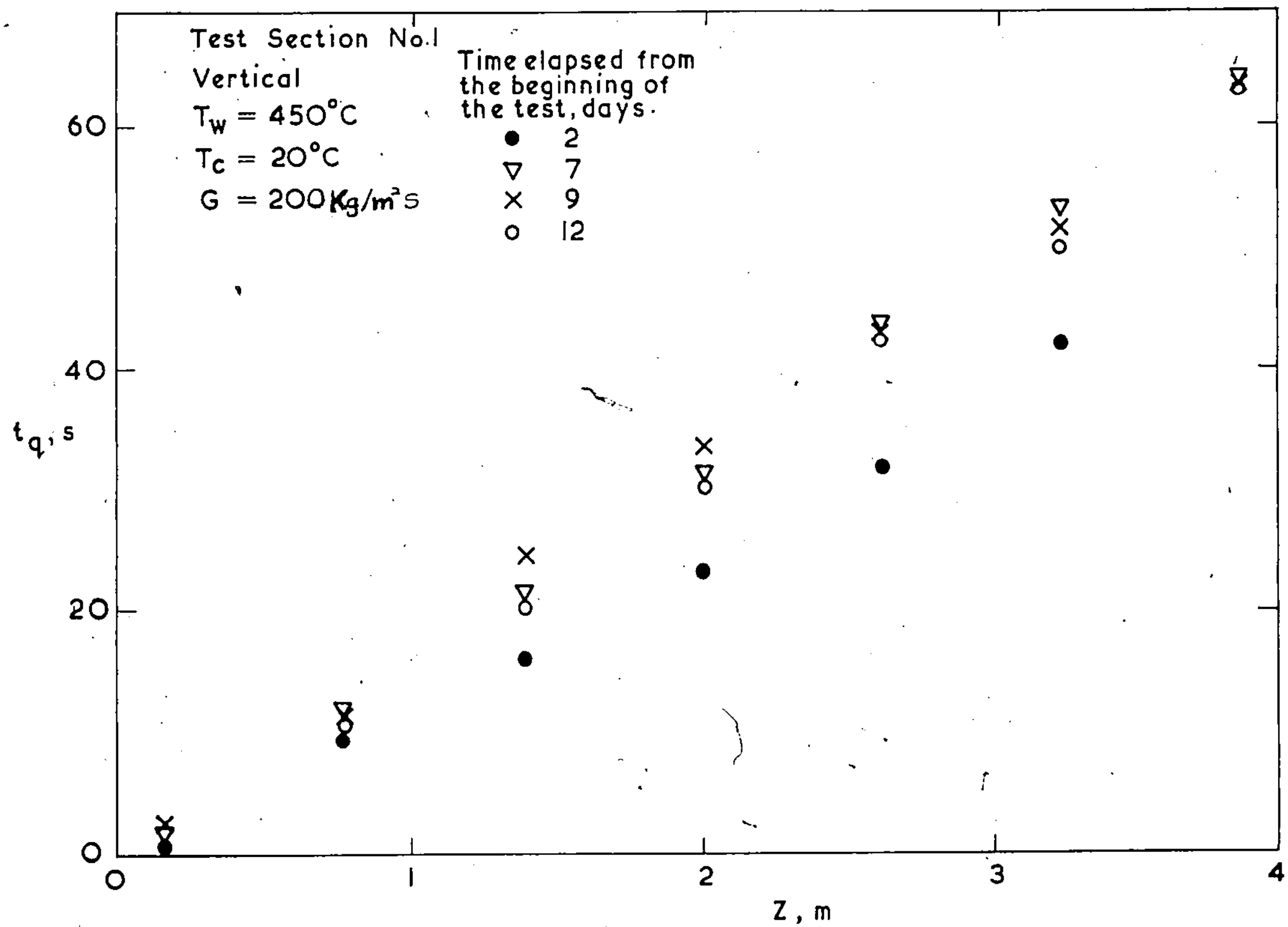

Fig. 6.1(a) Reproducibility of Test Results

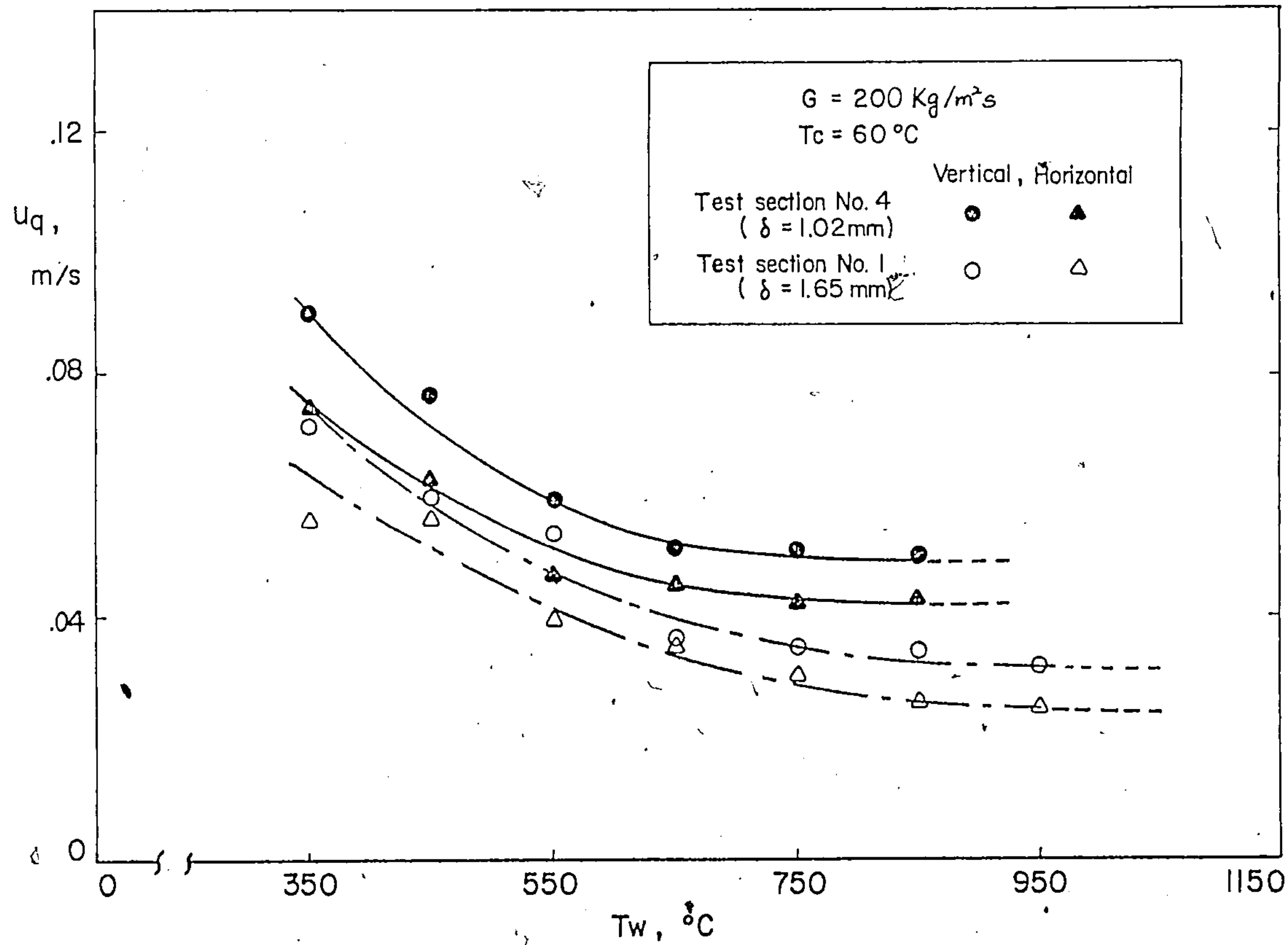

Fig. 6.1(b) Effects of Initial Wall Temperature and Wall Thickness

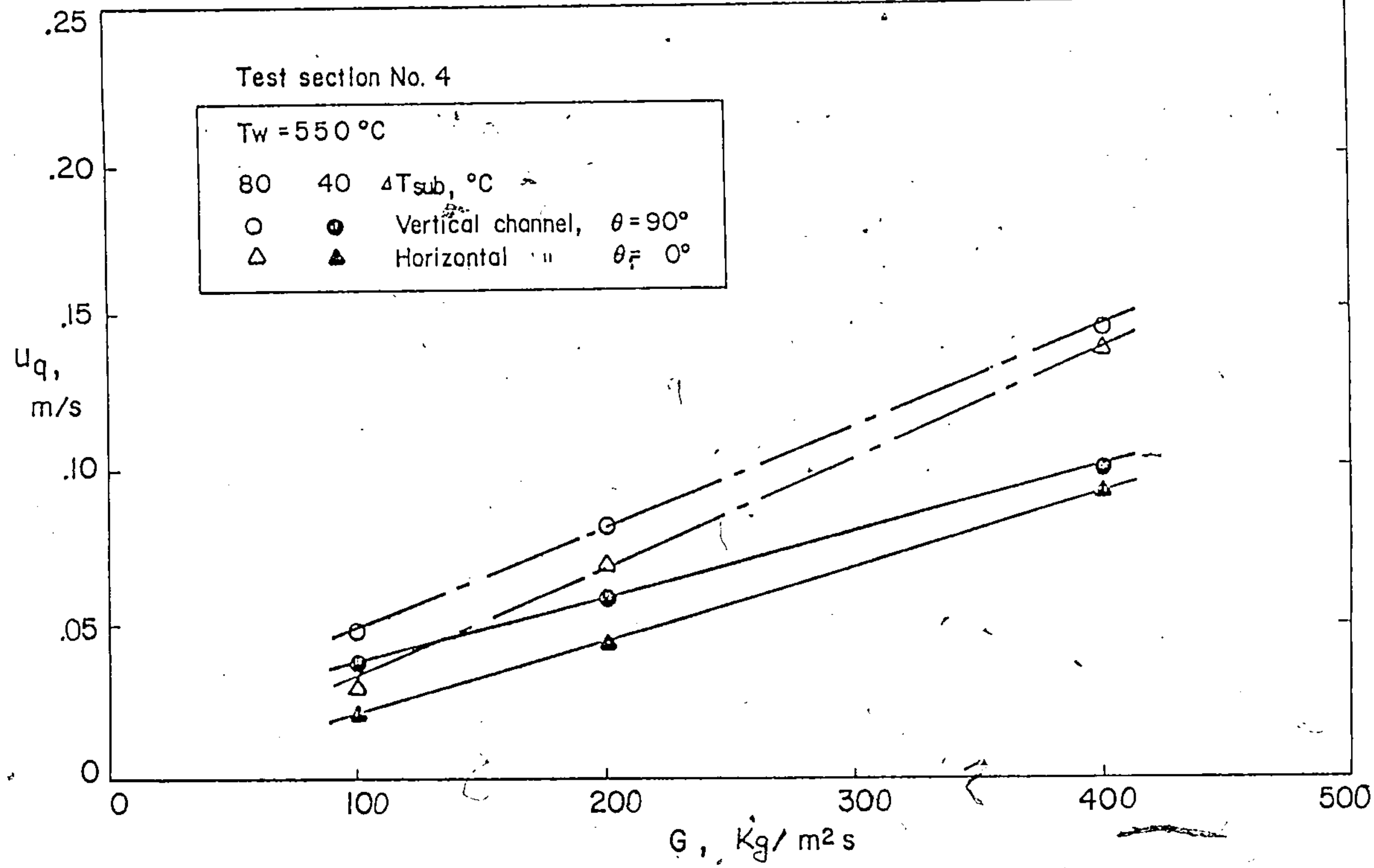

Fig. 6.1(c) Effects of Coolant Flow Rate and Inlet Subcooling

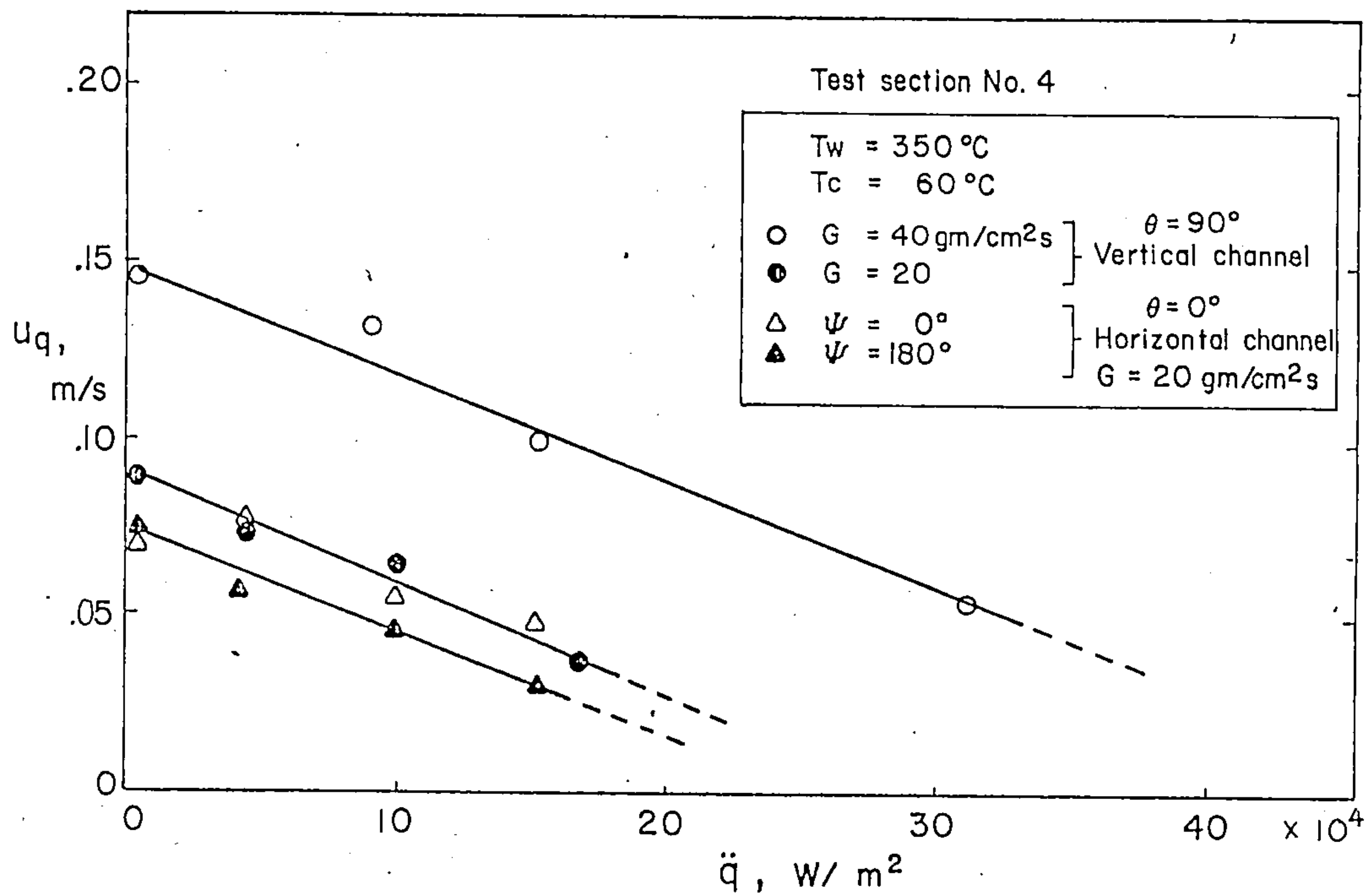

Fig. 6.1(d) Effect of Power Input During Rewetting Process

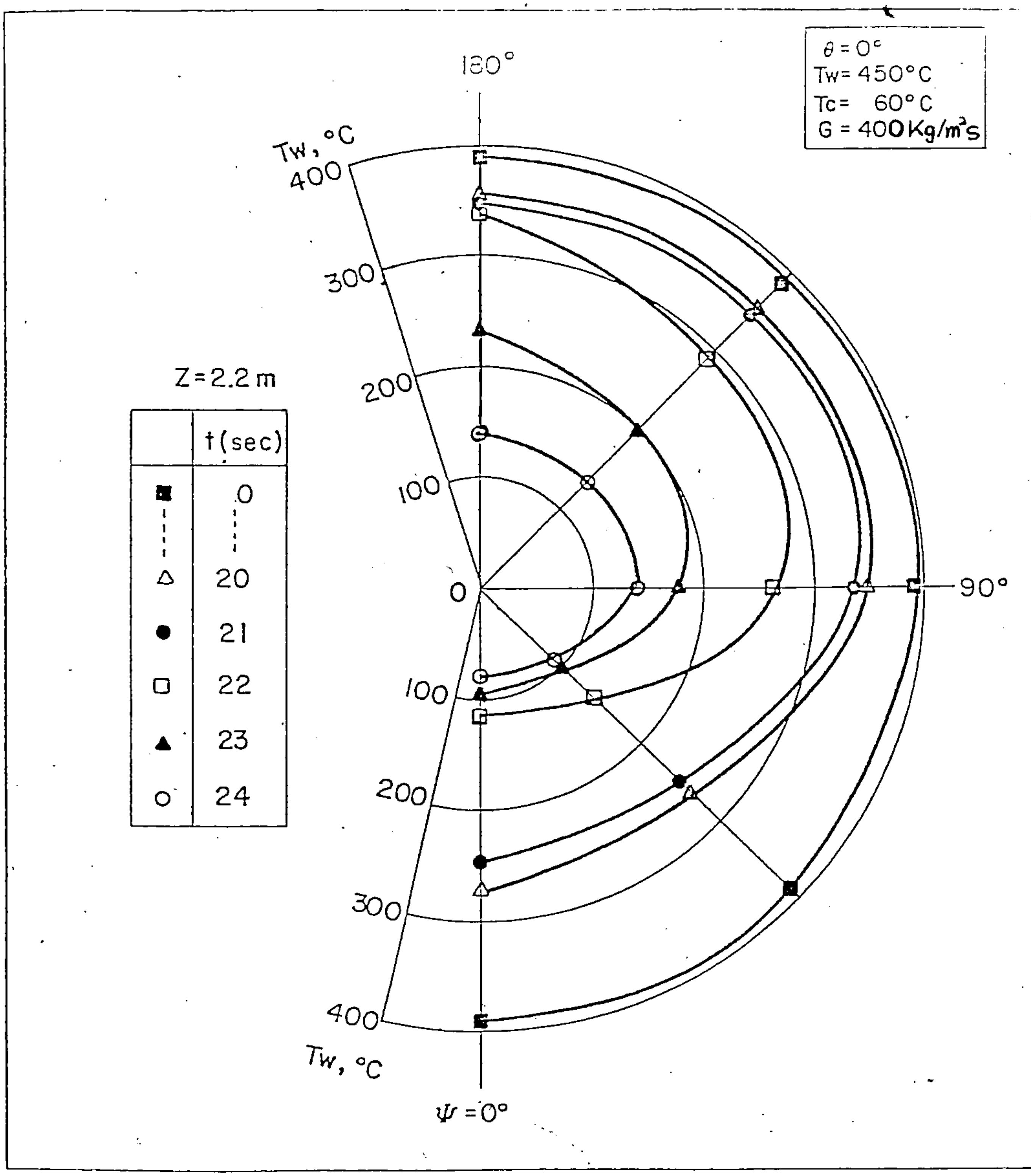

Fig. 6.2 Circumferential Temperature Distributions Horizontal Flooding, Test-section No.4

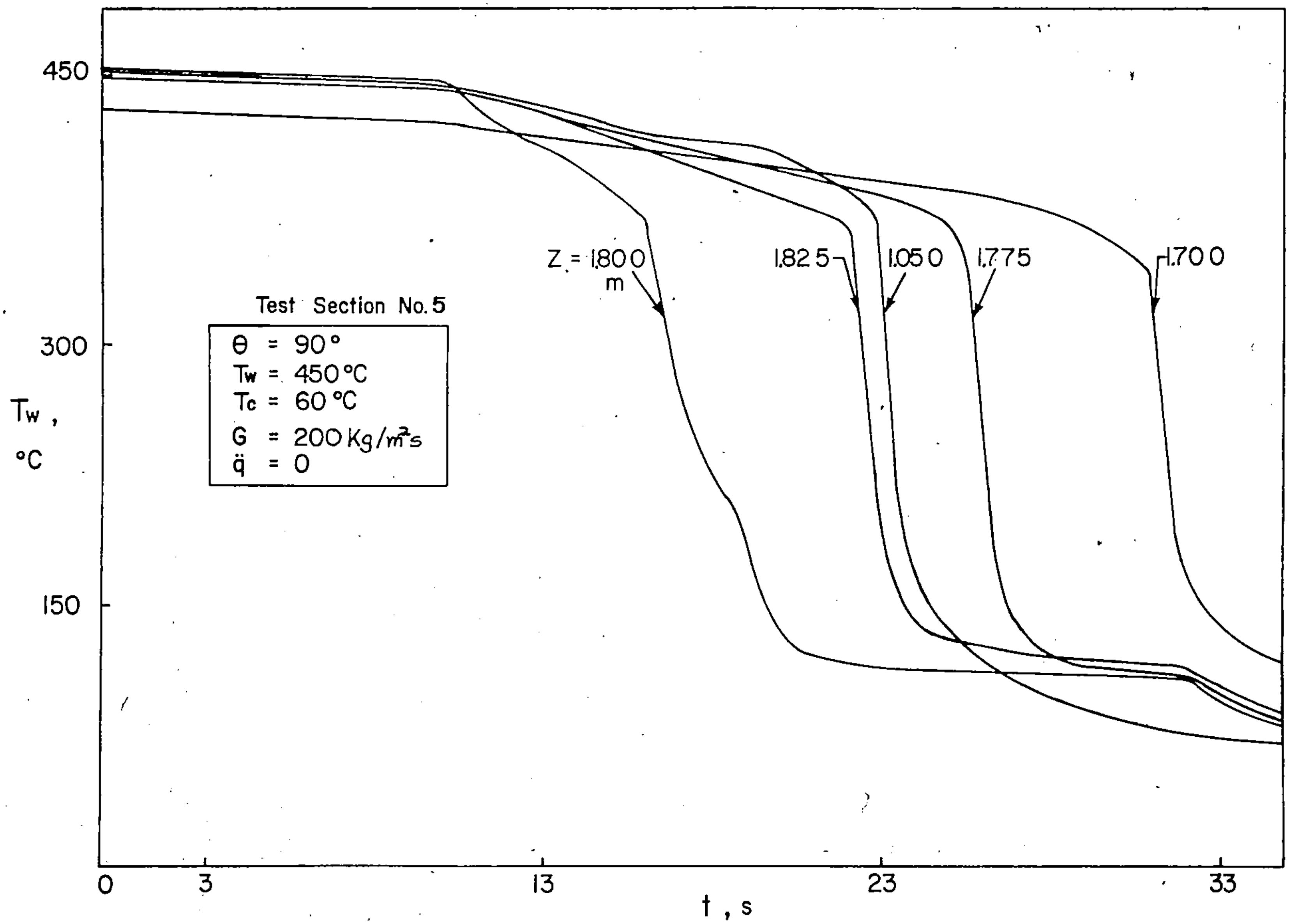

Fig. 6.3 Temperature-Time Traces ; 25% Blockage Bottom Flooding

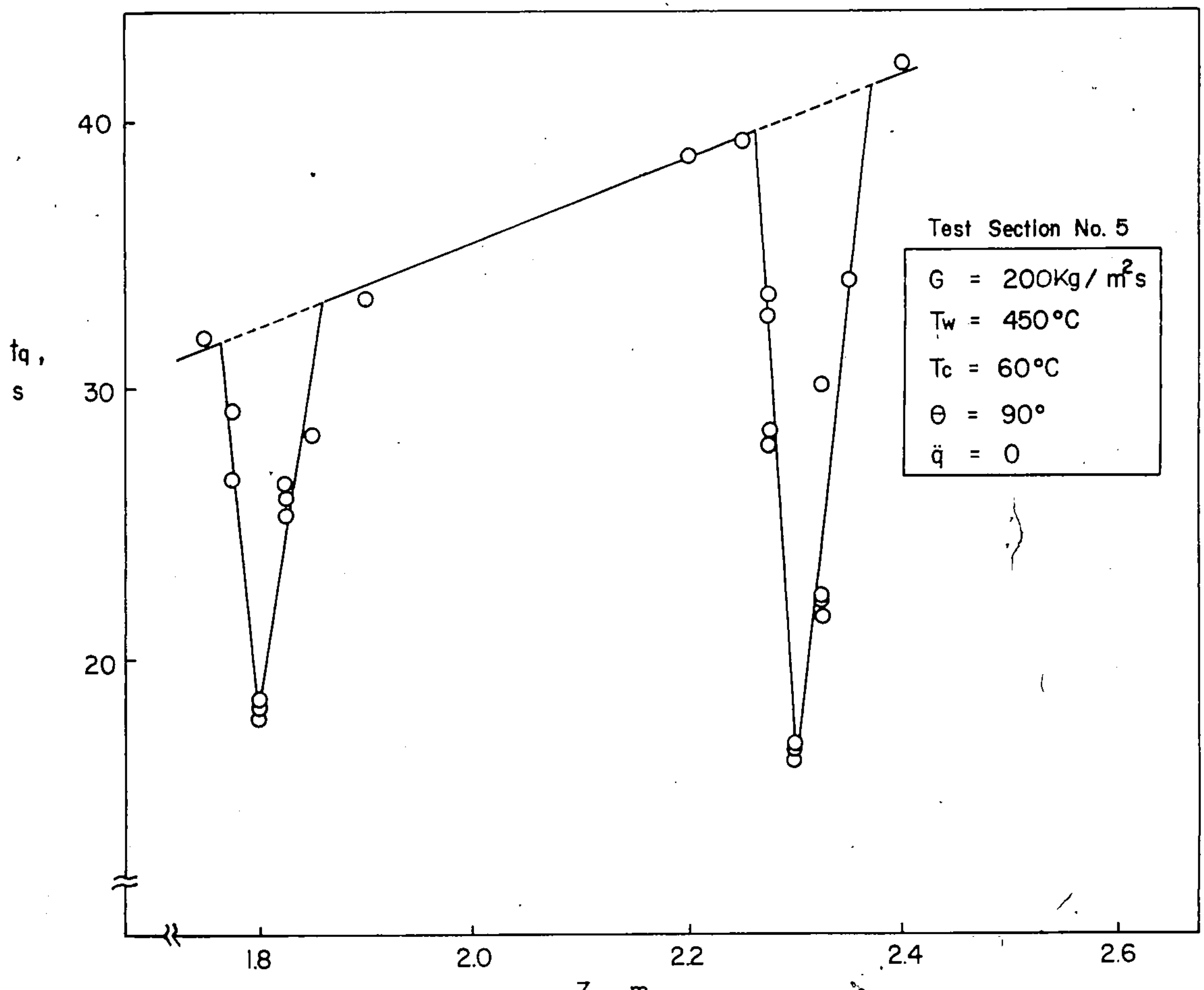

Fig. 6.4 Rewetting Time versus Axial Position 25% Blockage

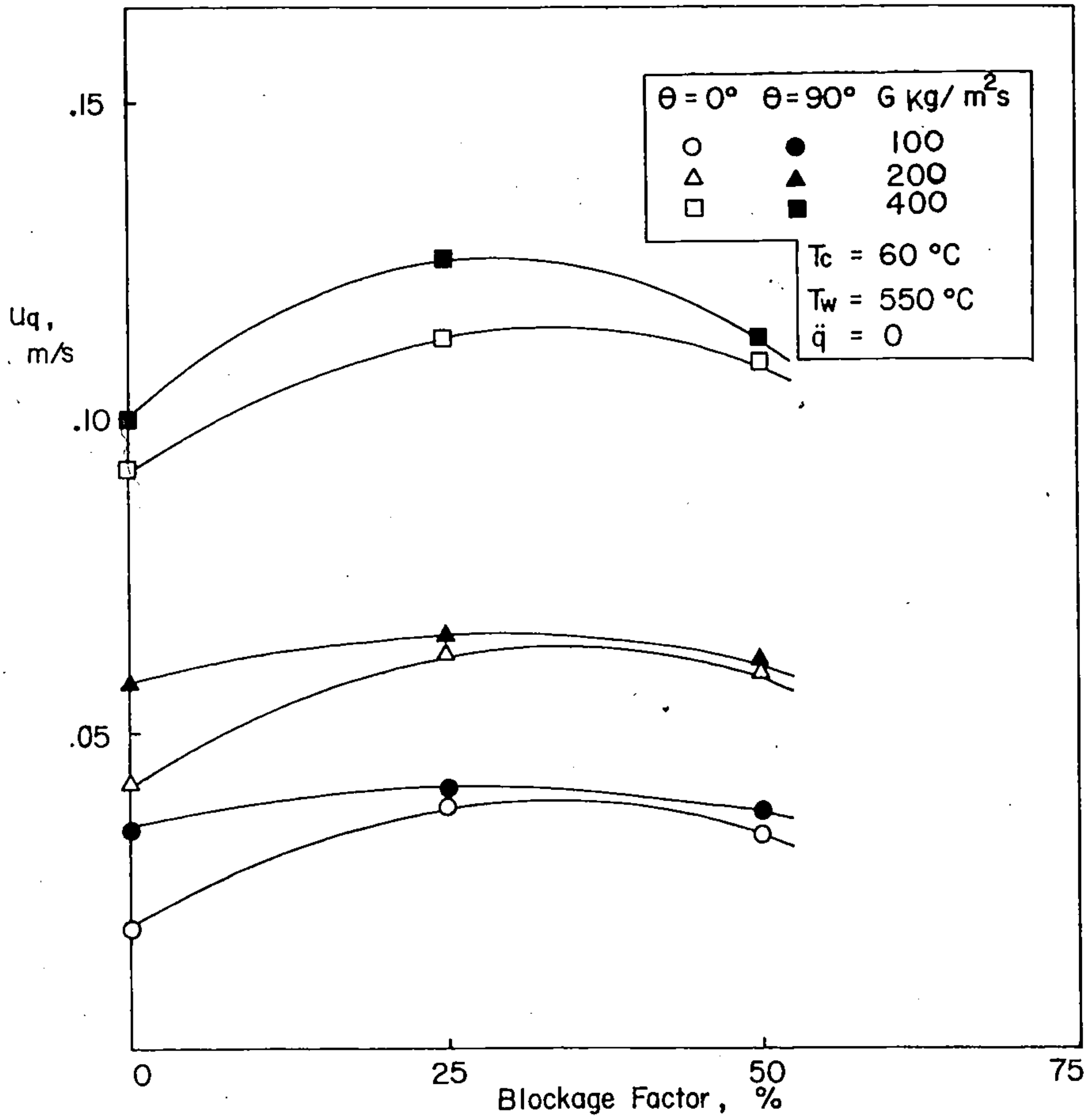

Fig. 6.5 Effect of Coolant Flow Rate in Partially Blocked Channels, Orifice Type

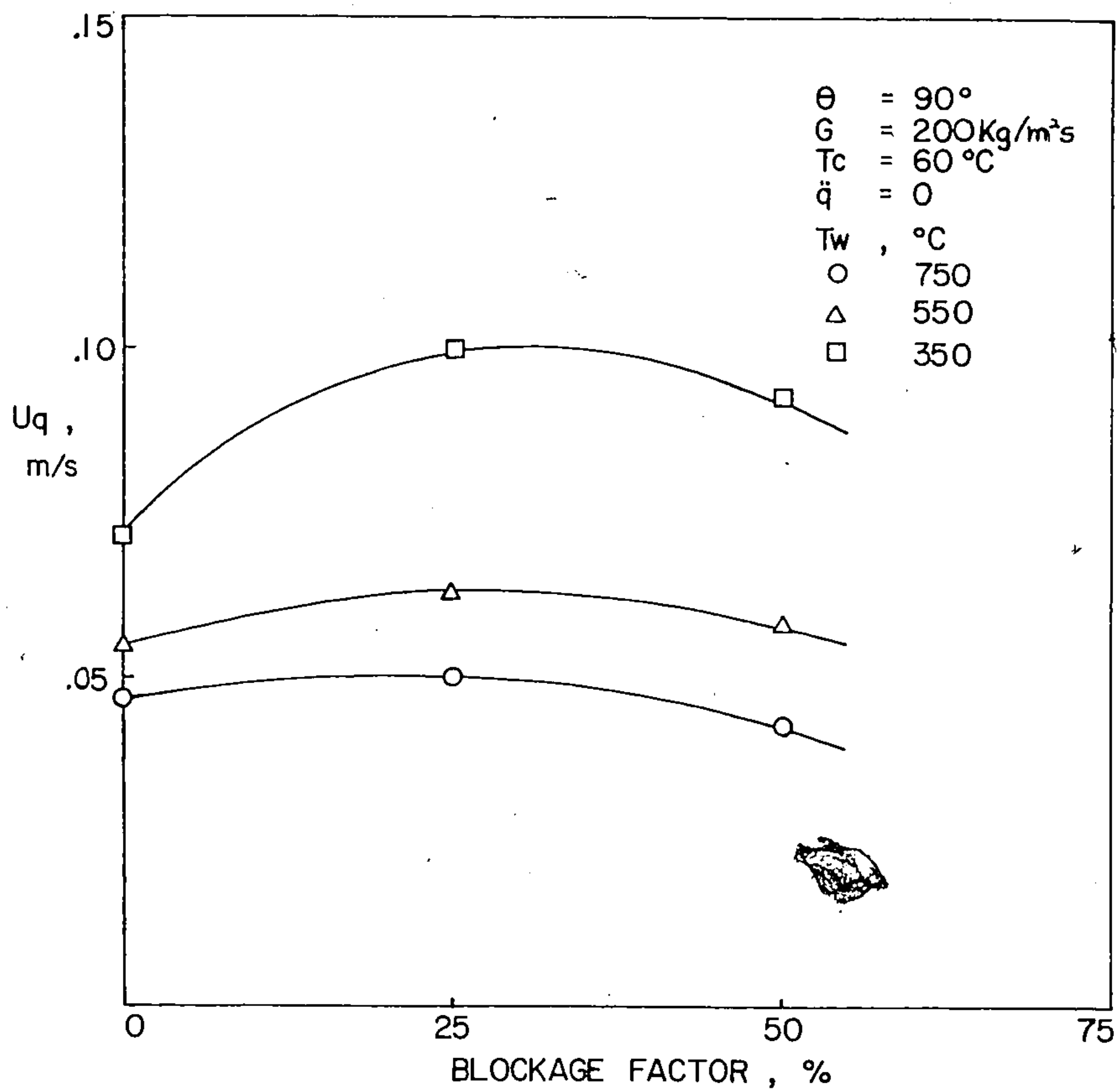

Fig. 6.6 Effect of Initial Wall Temperature in Partially Blocked Channels, Orifice Type

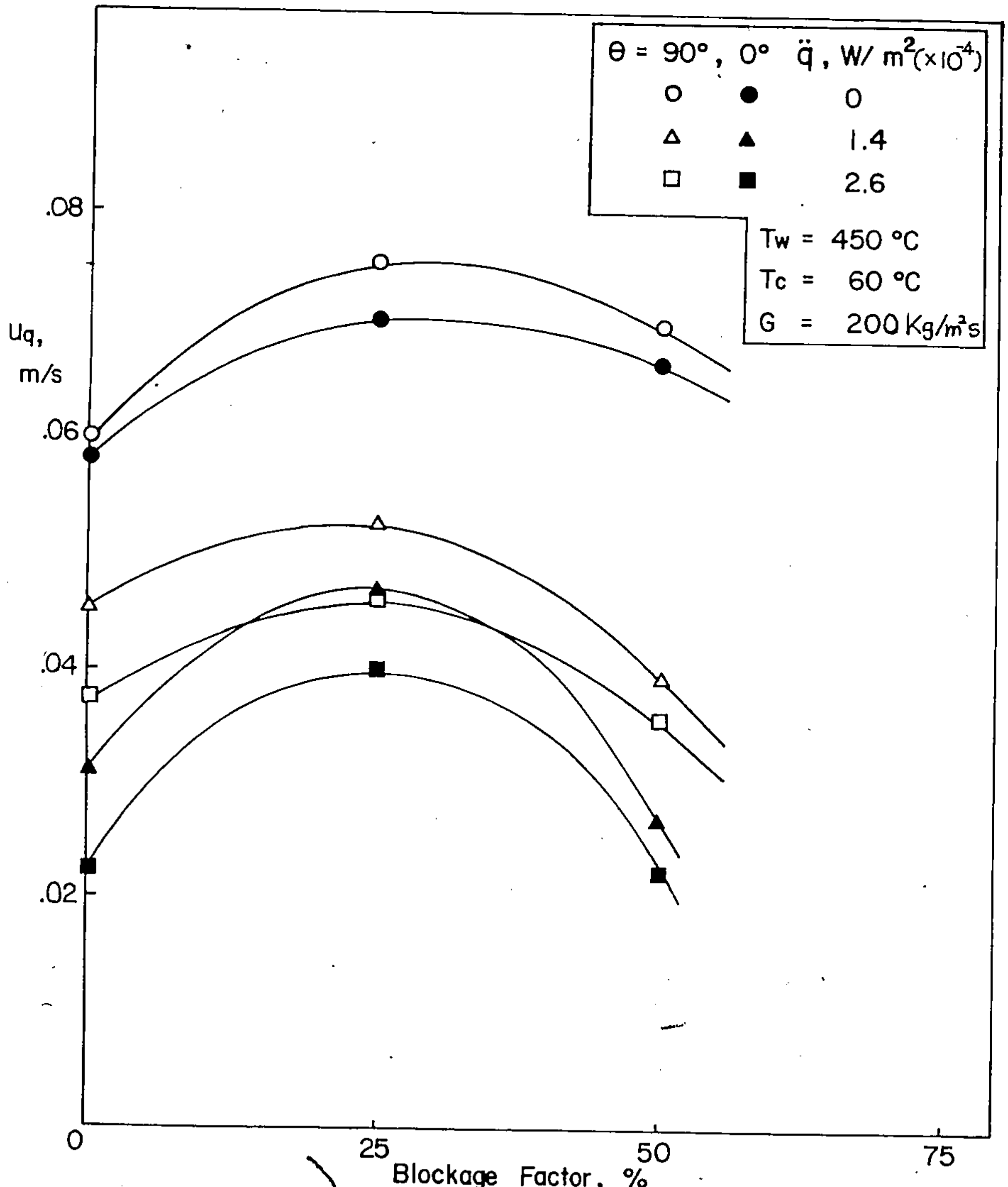

Fig. 6.7 Effect of Heat Generation in Partially Blocked Channels, Orifice Type

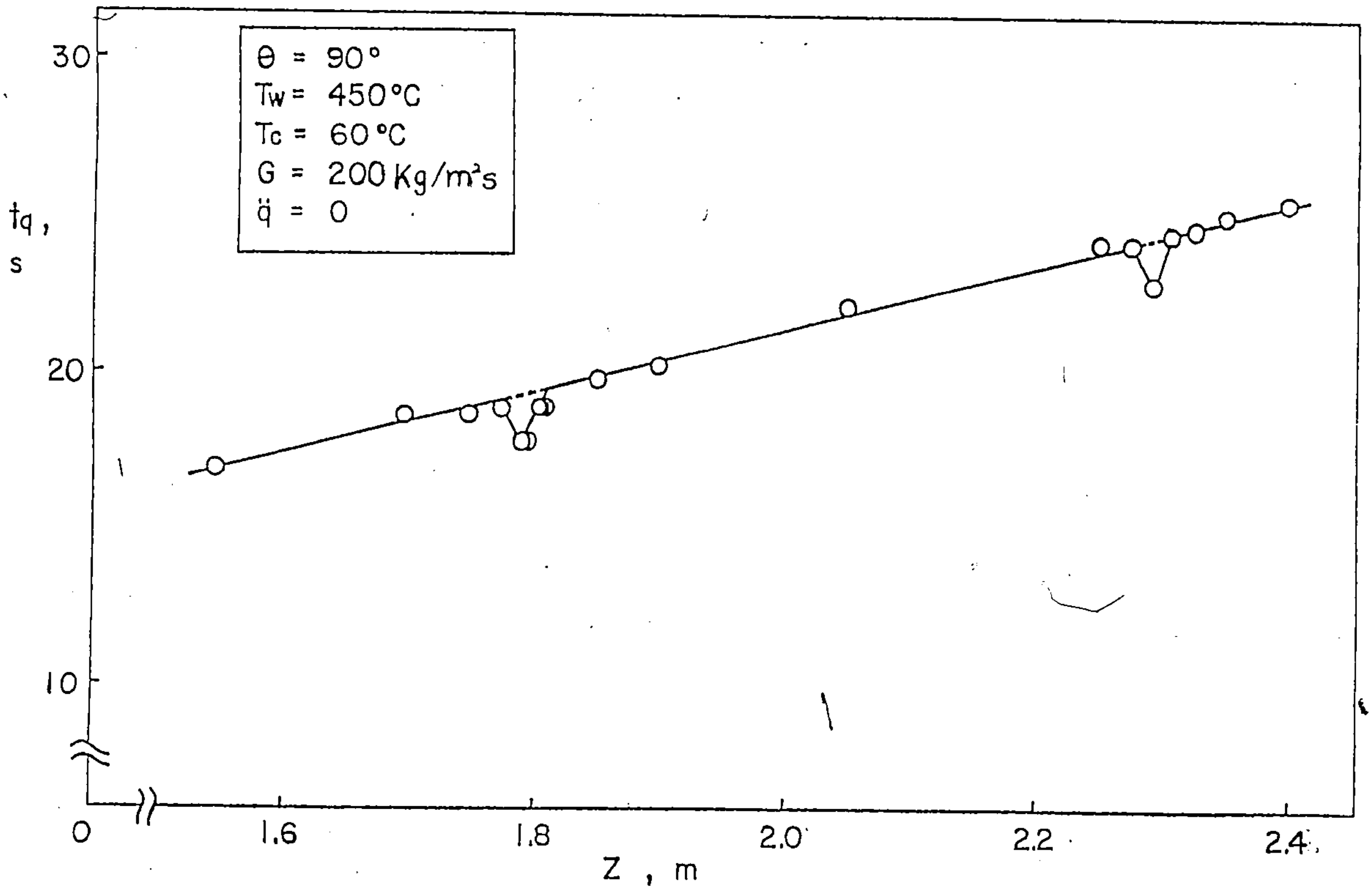

Fig. 6.8 Rewetting Time Versus Axial Location
Test-section NO. 7

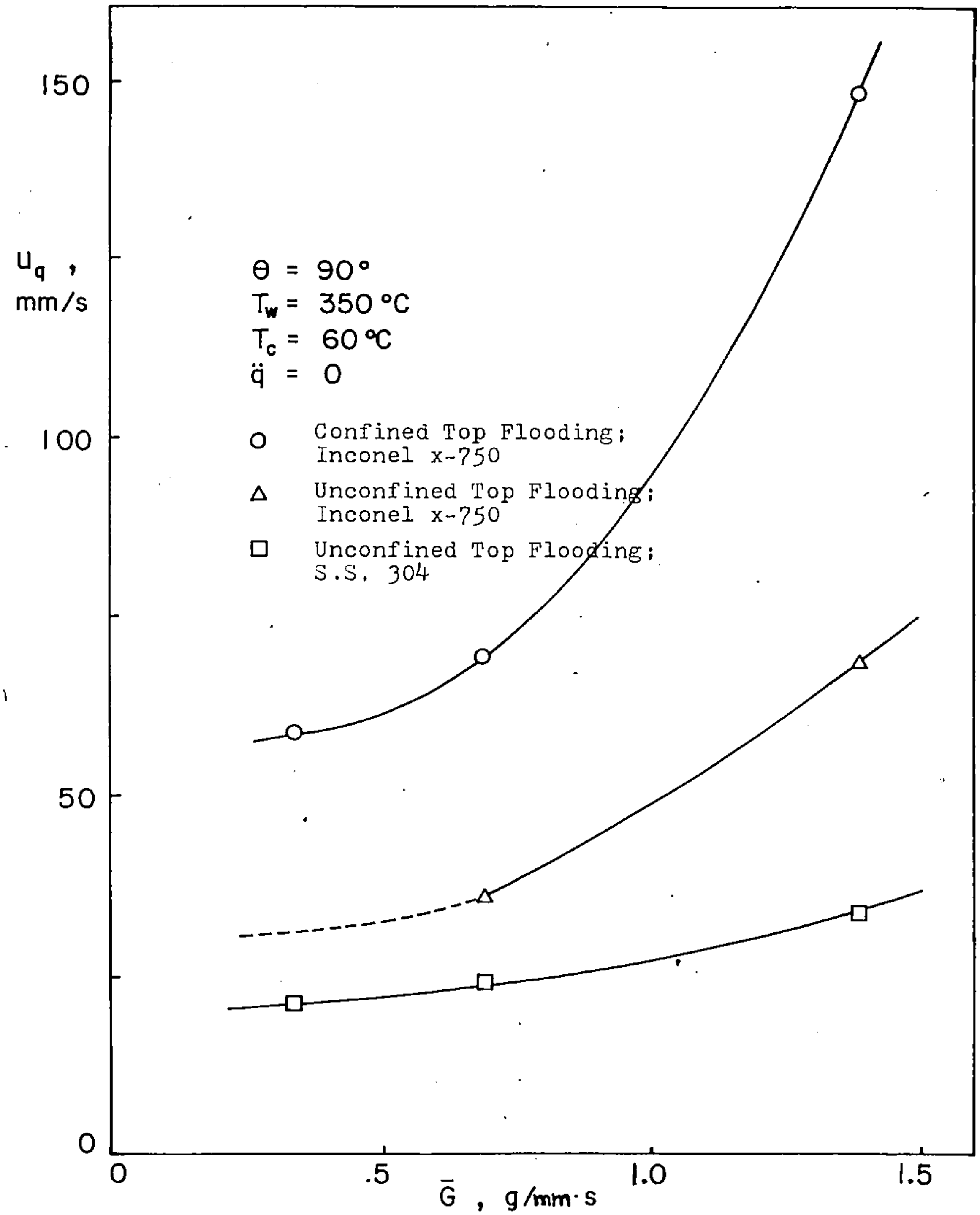

Figure 6.9 Effect of Coolant Flow Rate; Top Flooding

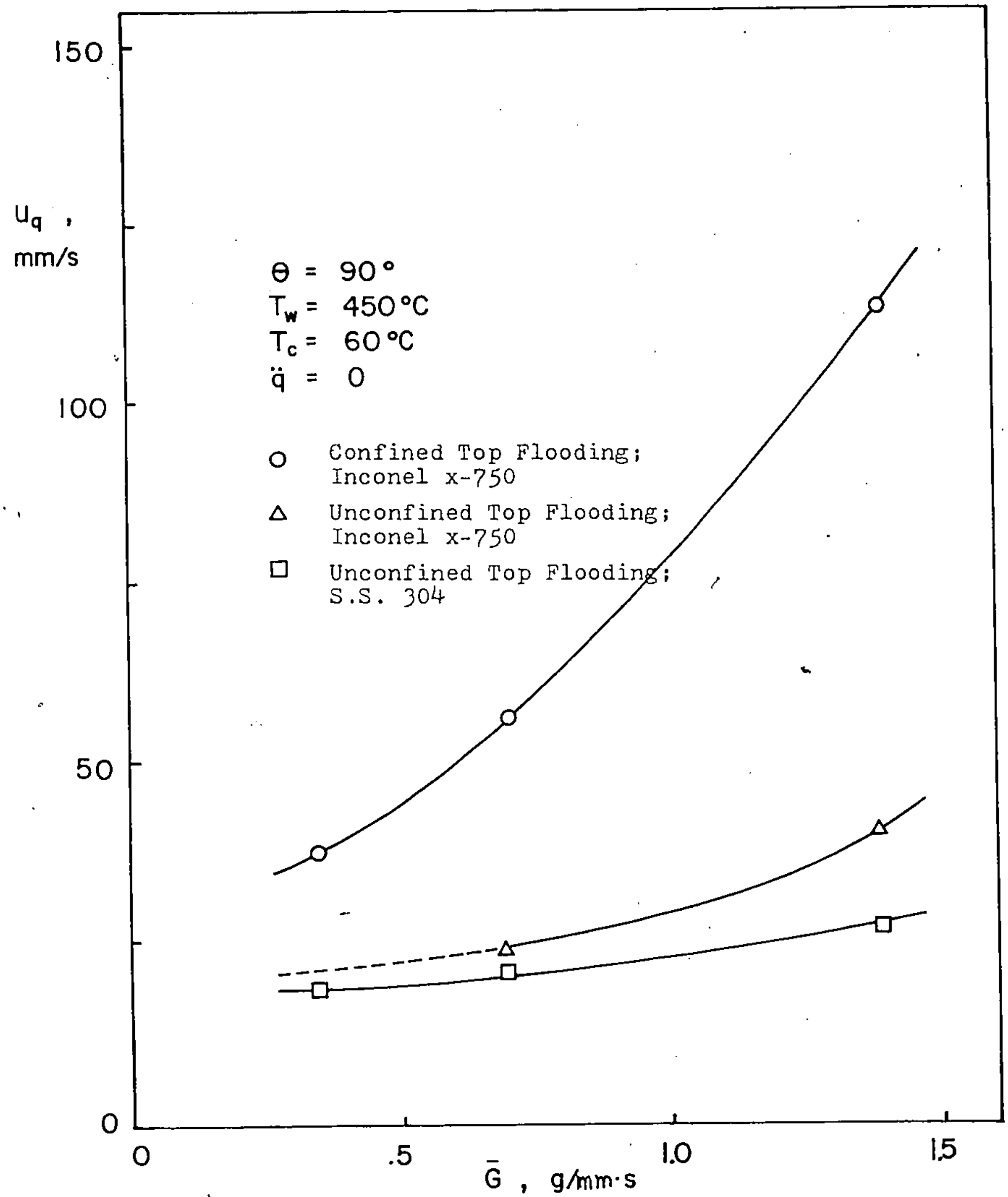

Figure 6.10 Effect of Coolant Flow Rate; Top Flooding

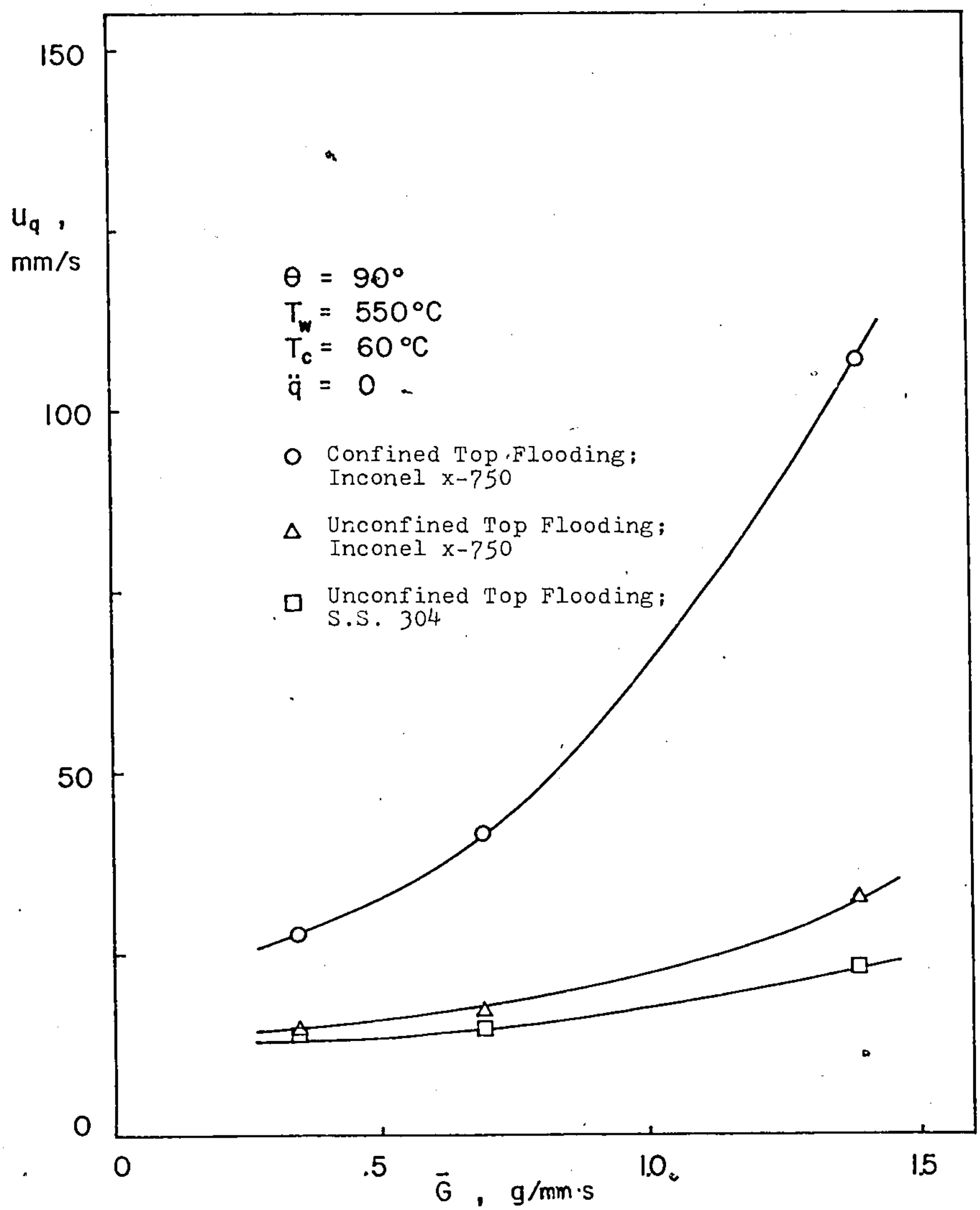

Figure 6.11 Effect of Coolant Flow Rate; Top Flooding

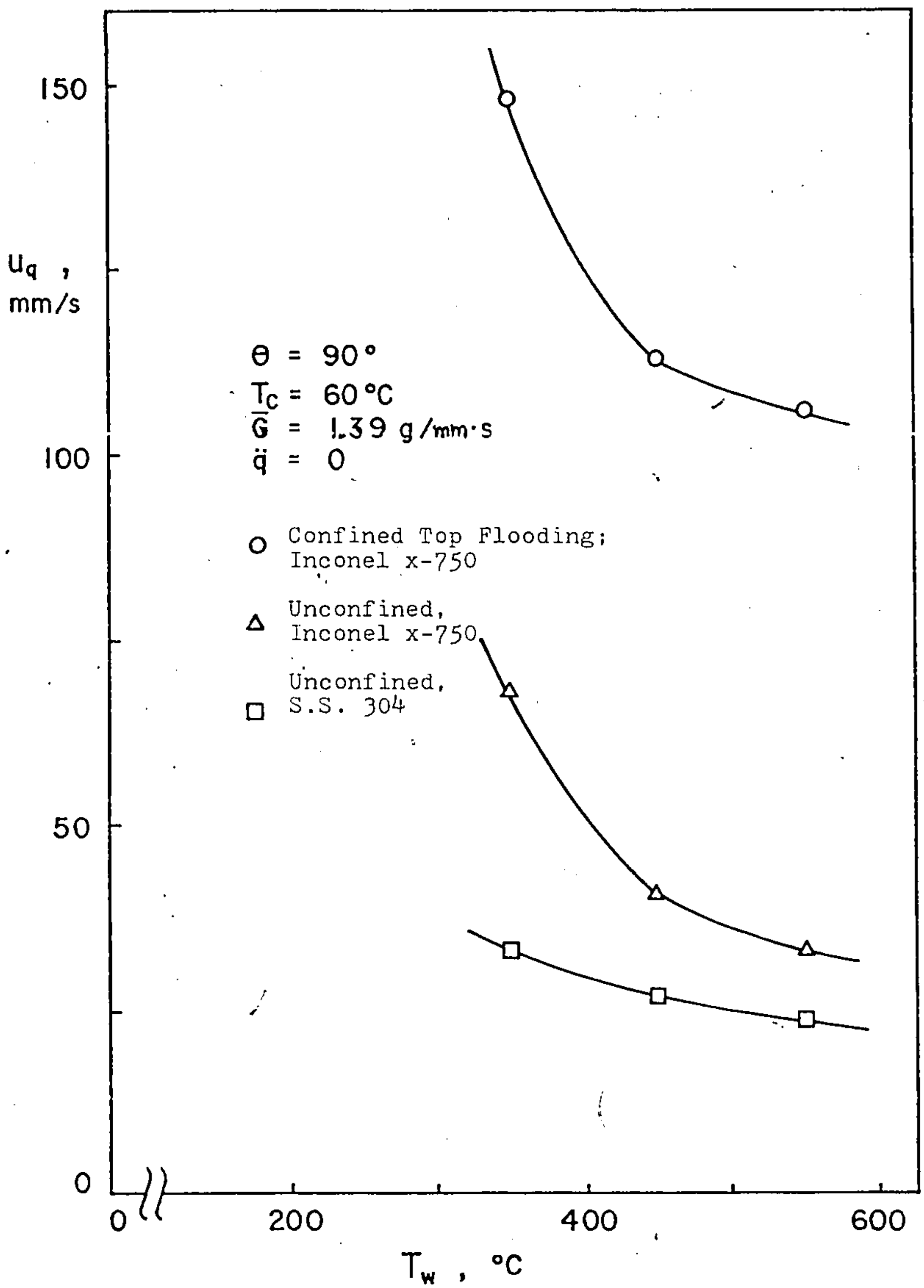

Fig. 6.12 Effect of Initial Wall Temperature; Top Flooding

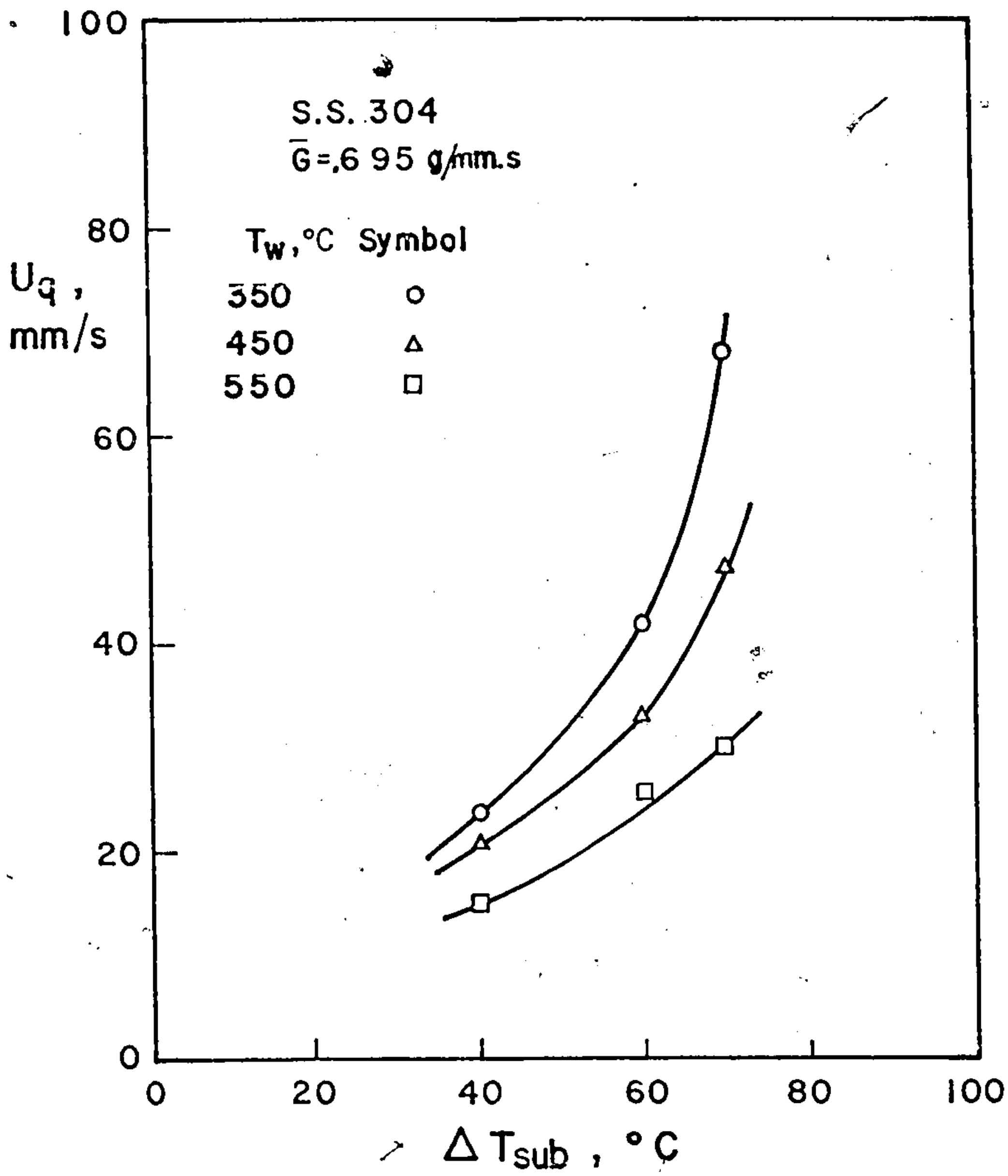

Fig. 6.13 Effect of Coolant Inlet Subcooling; Unconfined Top Flooding

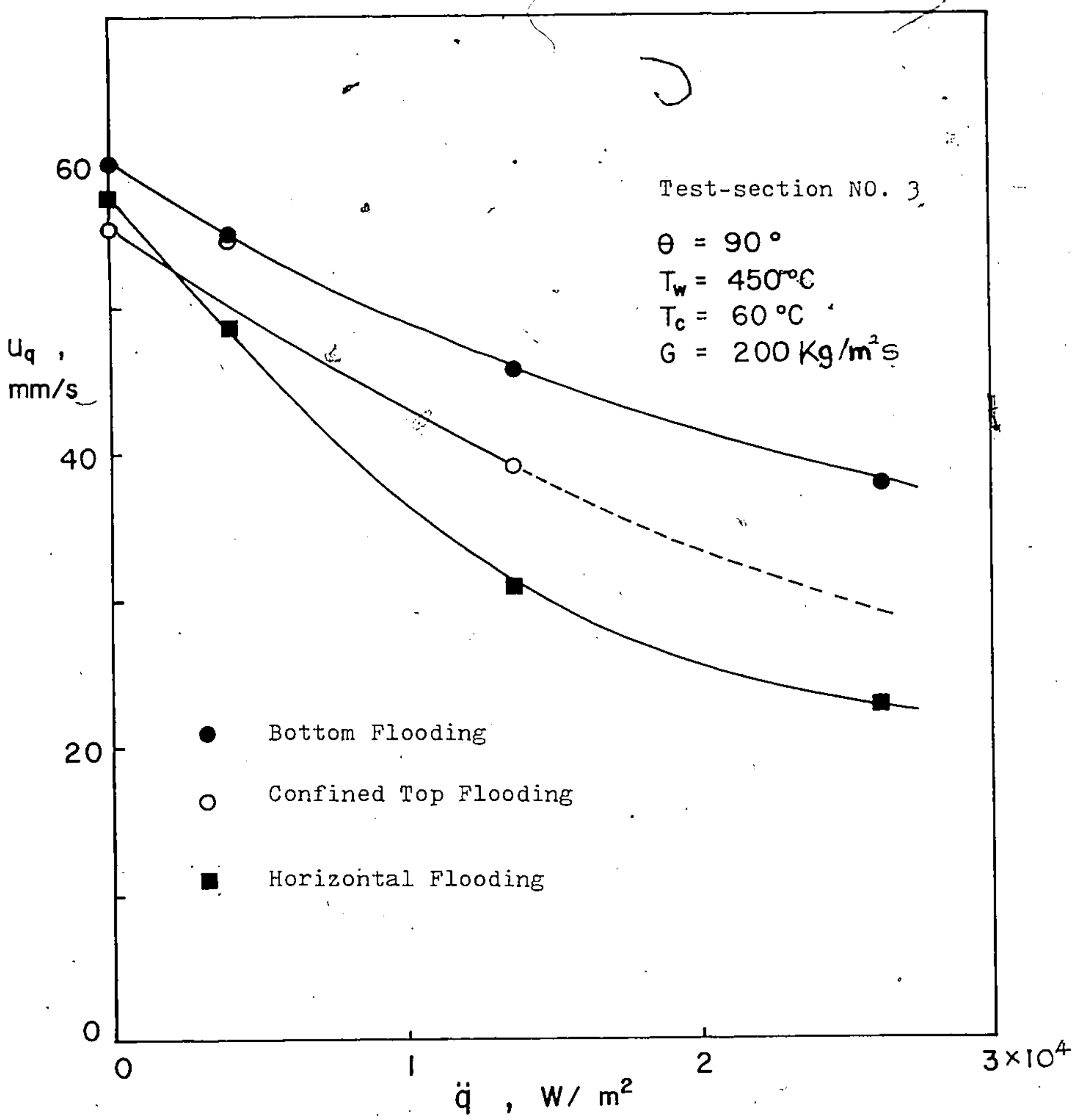

Fig. 6.14 Effect of Power Generation during Transient on Rewetting Velocity by Different Flooding Modes

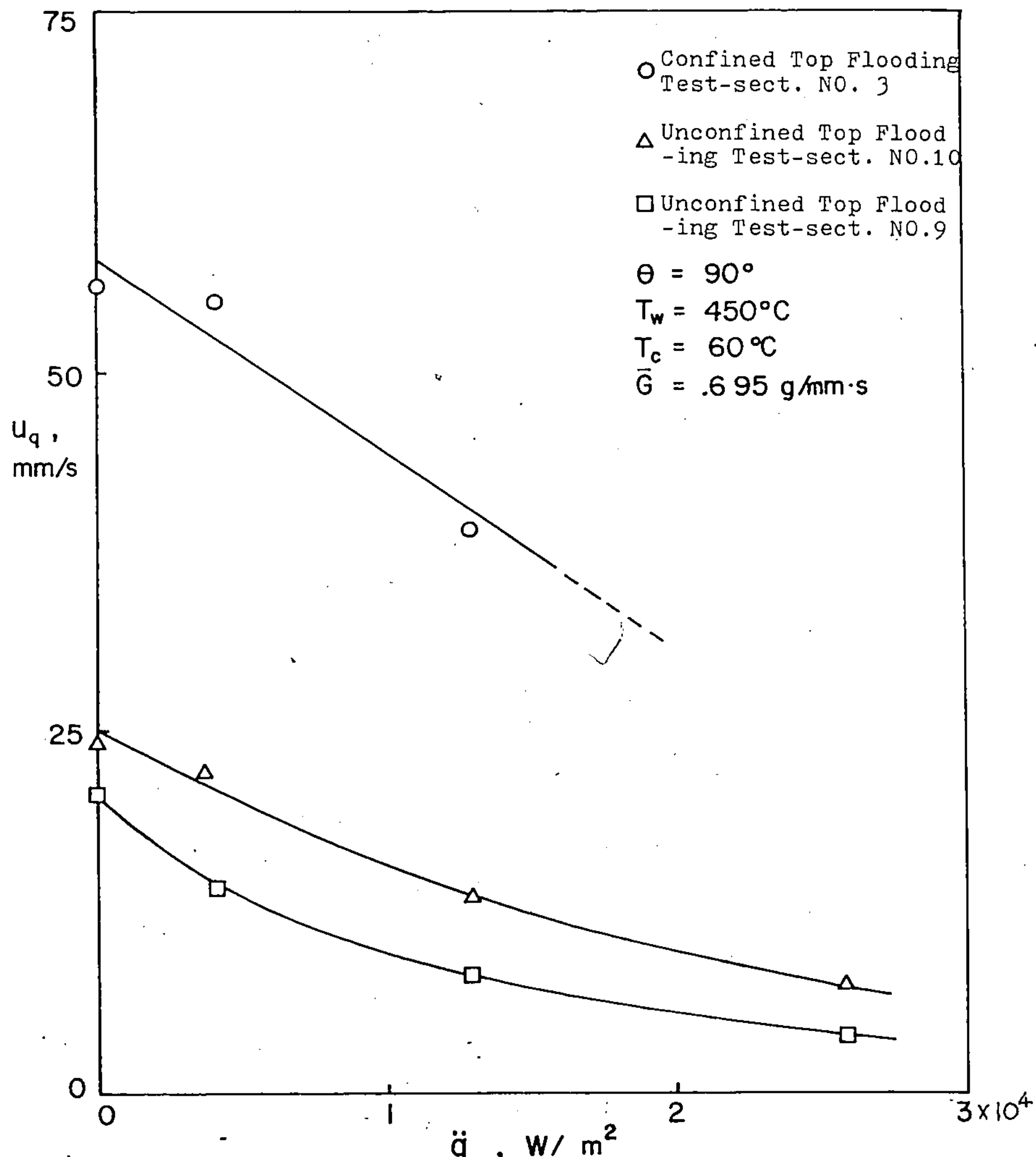

Fig. 6.15 Effect of Power Generation during Transient; Top Flooding

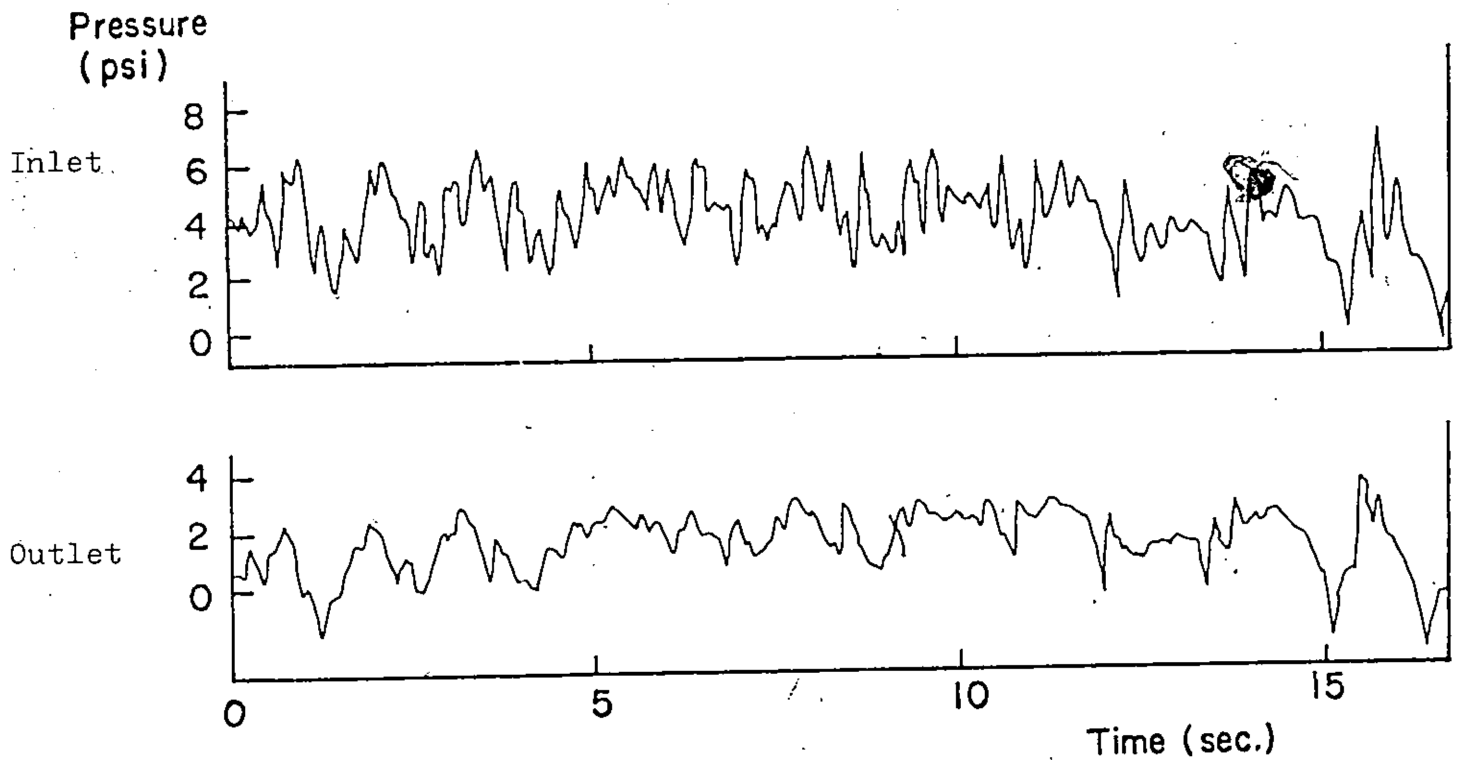

Figure 6.16 Pressure Transient; Confined Top-Flooding

T_w = 550 C, T_c = 40 C, G = 100 $Kg/m^2 \cdot s$

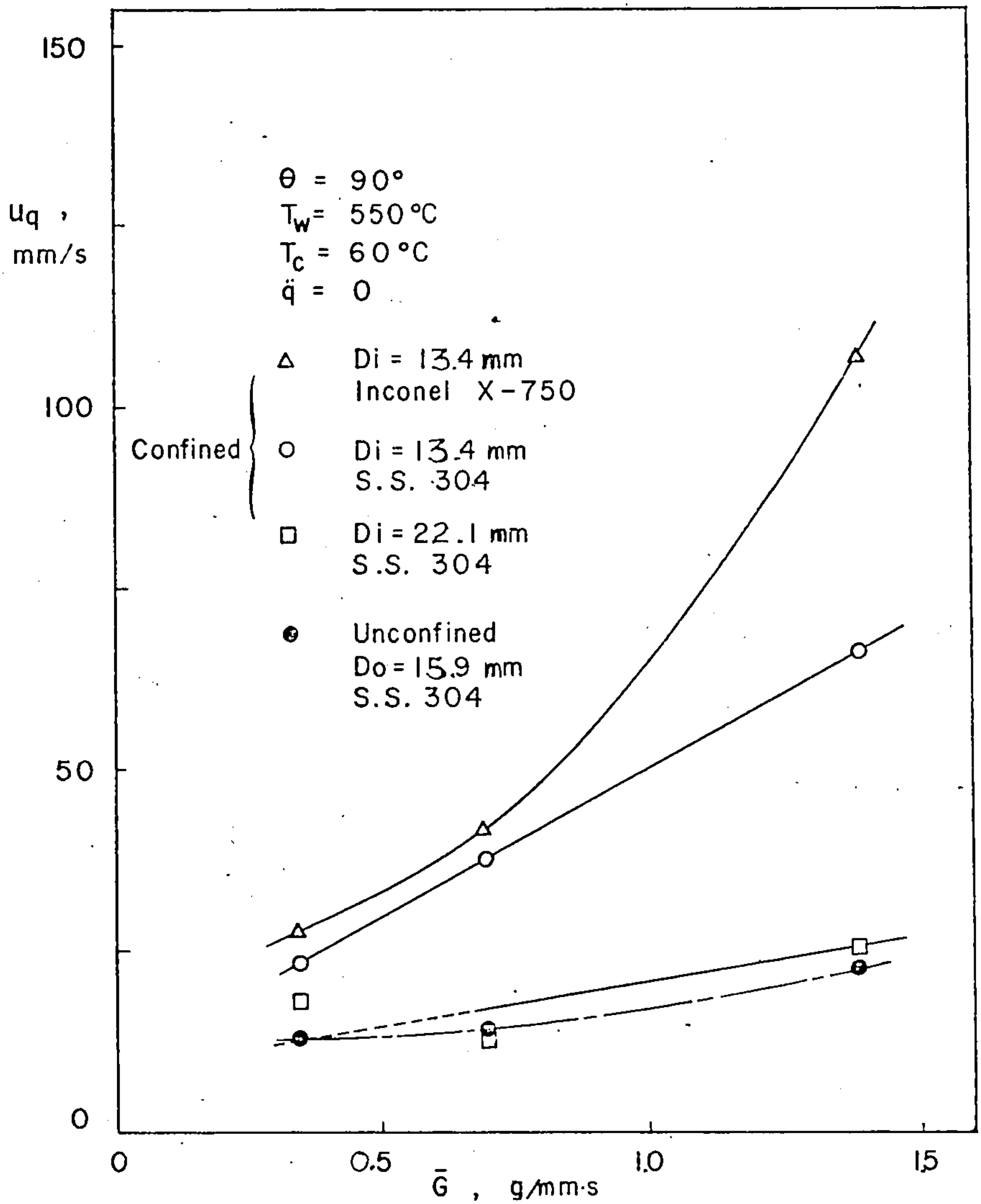

Fig. 6.17 Effect of Wall Material and Inside Diameter; Top-flooding

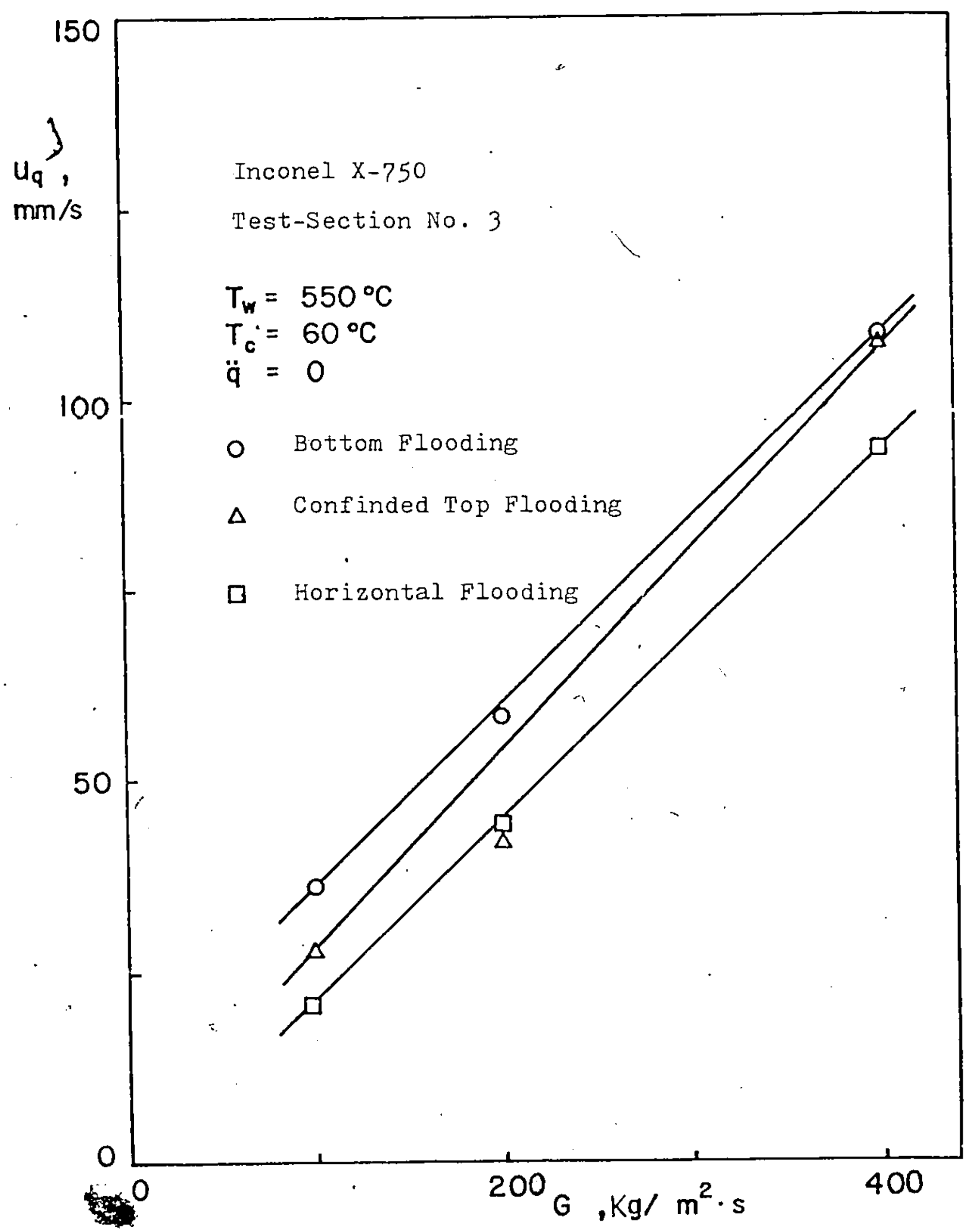

Figure 6.18 Effect of Coolant Flow Rate
Three Different Modes of Flooding

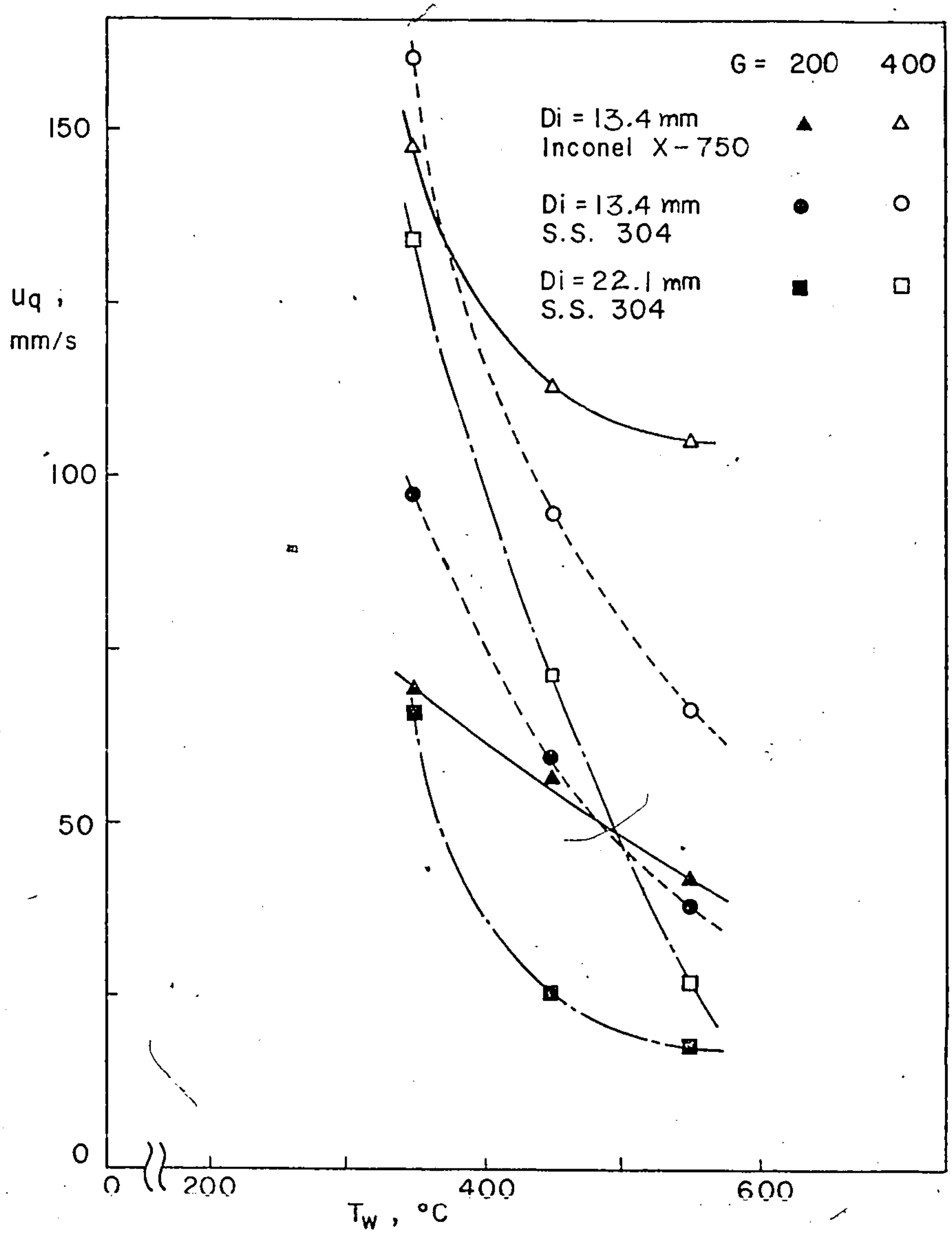

Fig. 6.19 Effect of Initial Wall Temperature

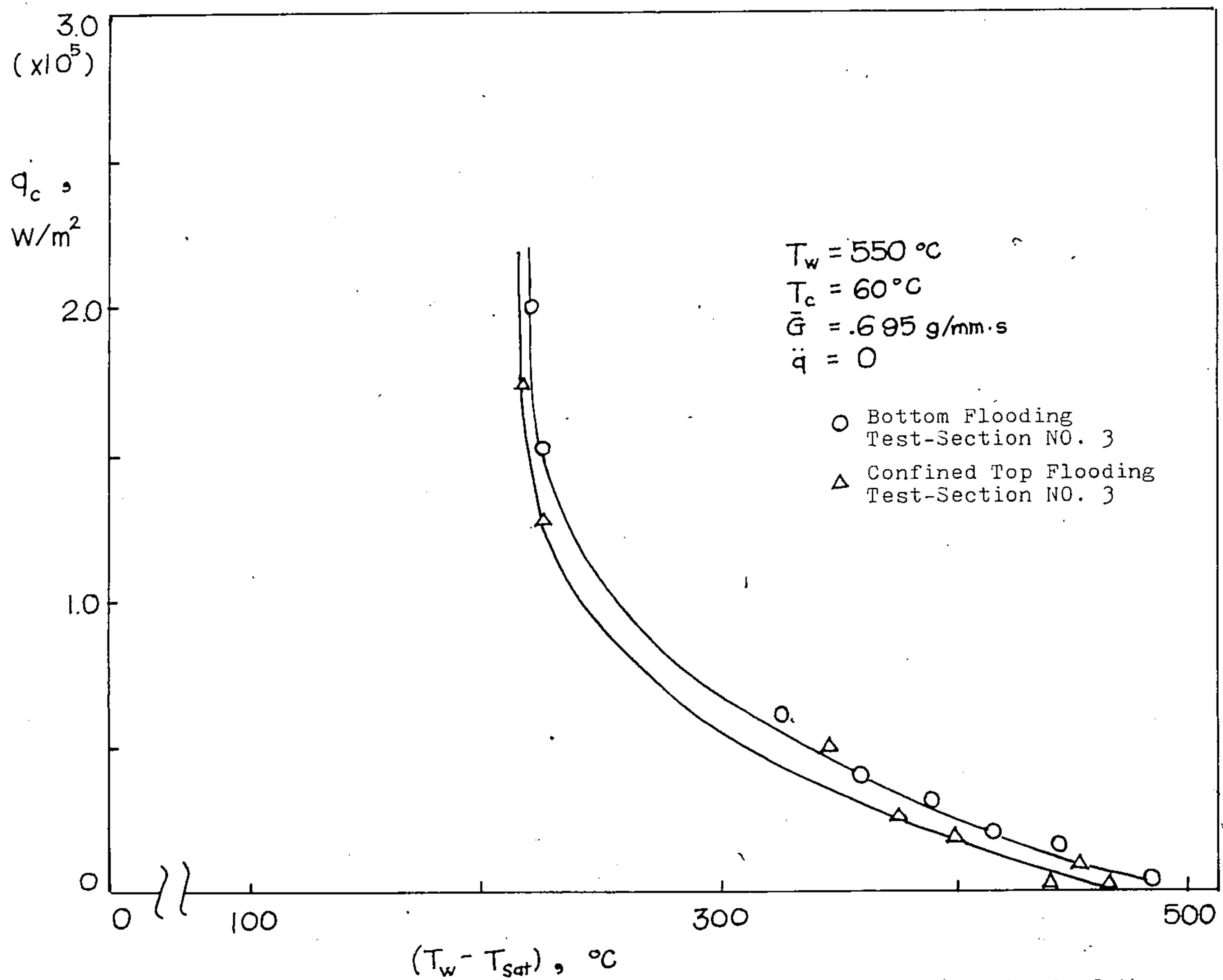

Figure 6.20 Surface Heat Flux Distribution in the Region ahead of the Rewetting Front

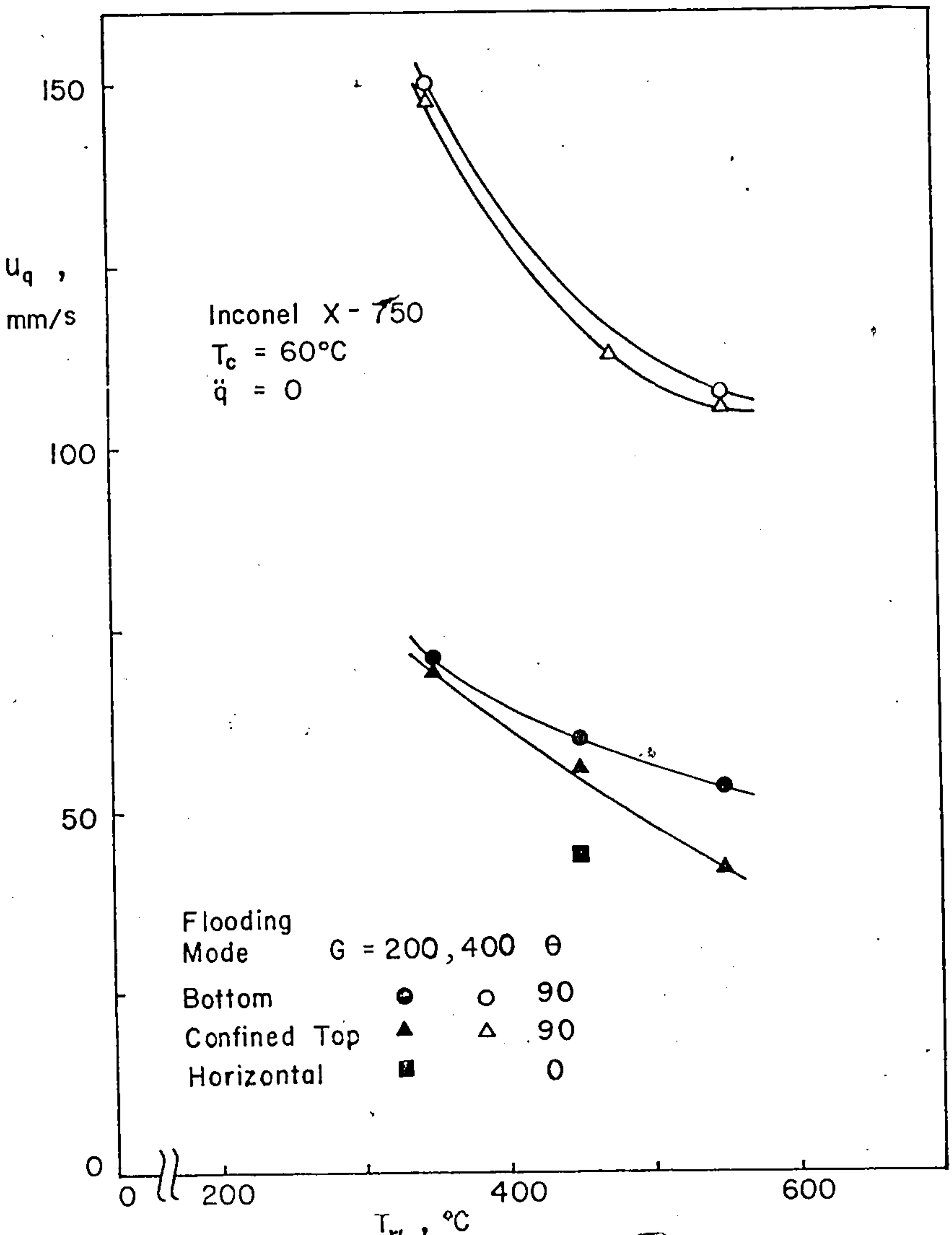

Figure 6.21 Effect of Initial Wall Temperature

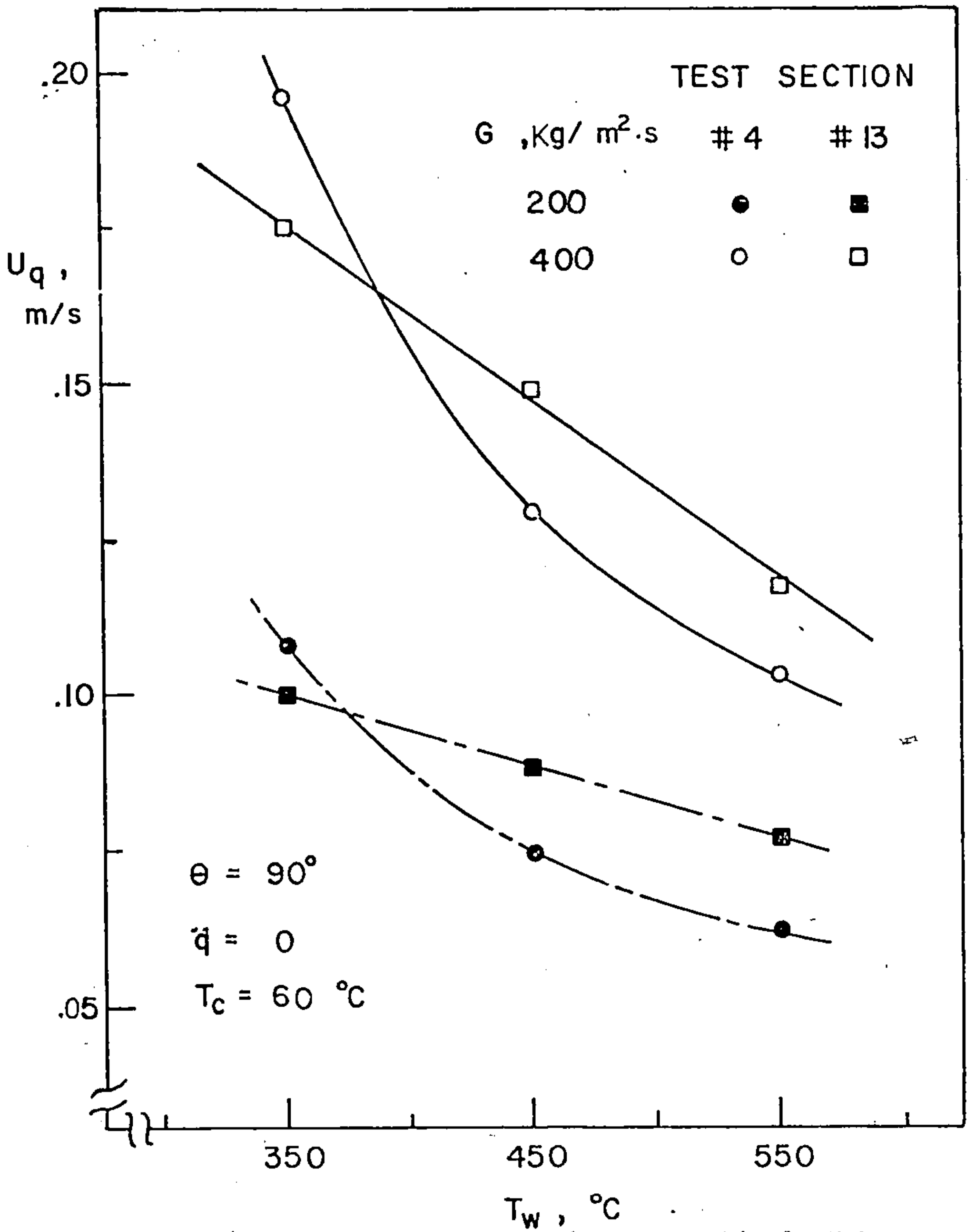

Fig. 6.22 Effect of Tube Diameters, Single Tubes; Vertical

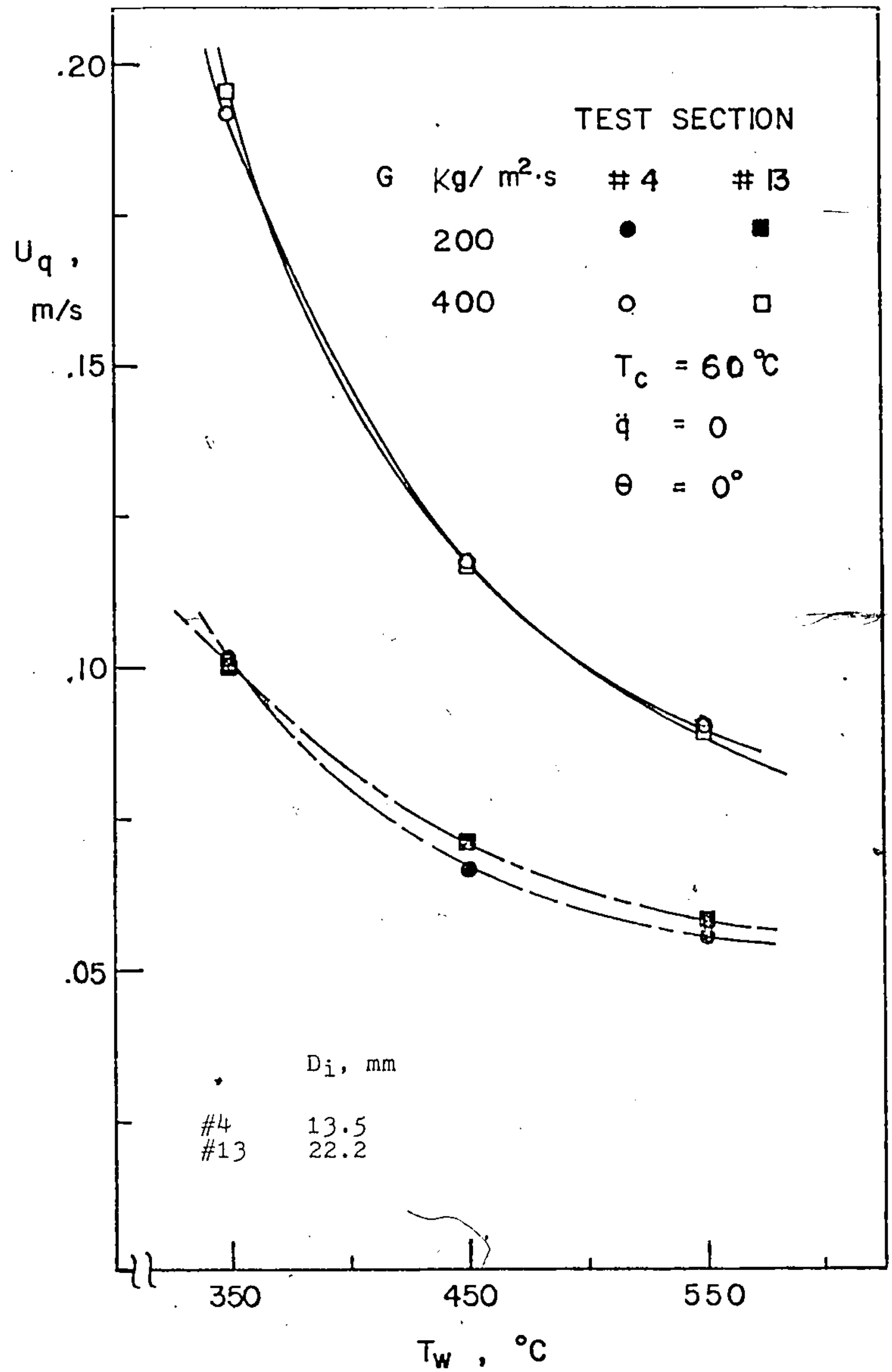

Fig. 6.23 Effect of Tube Diameters, Single Tubes;

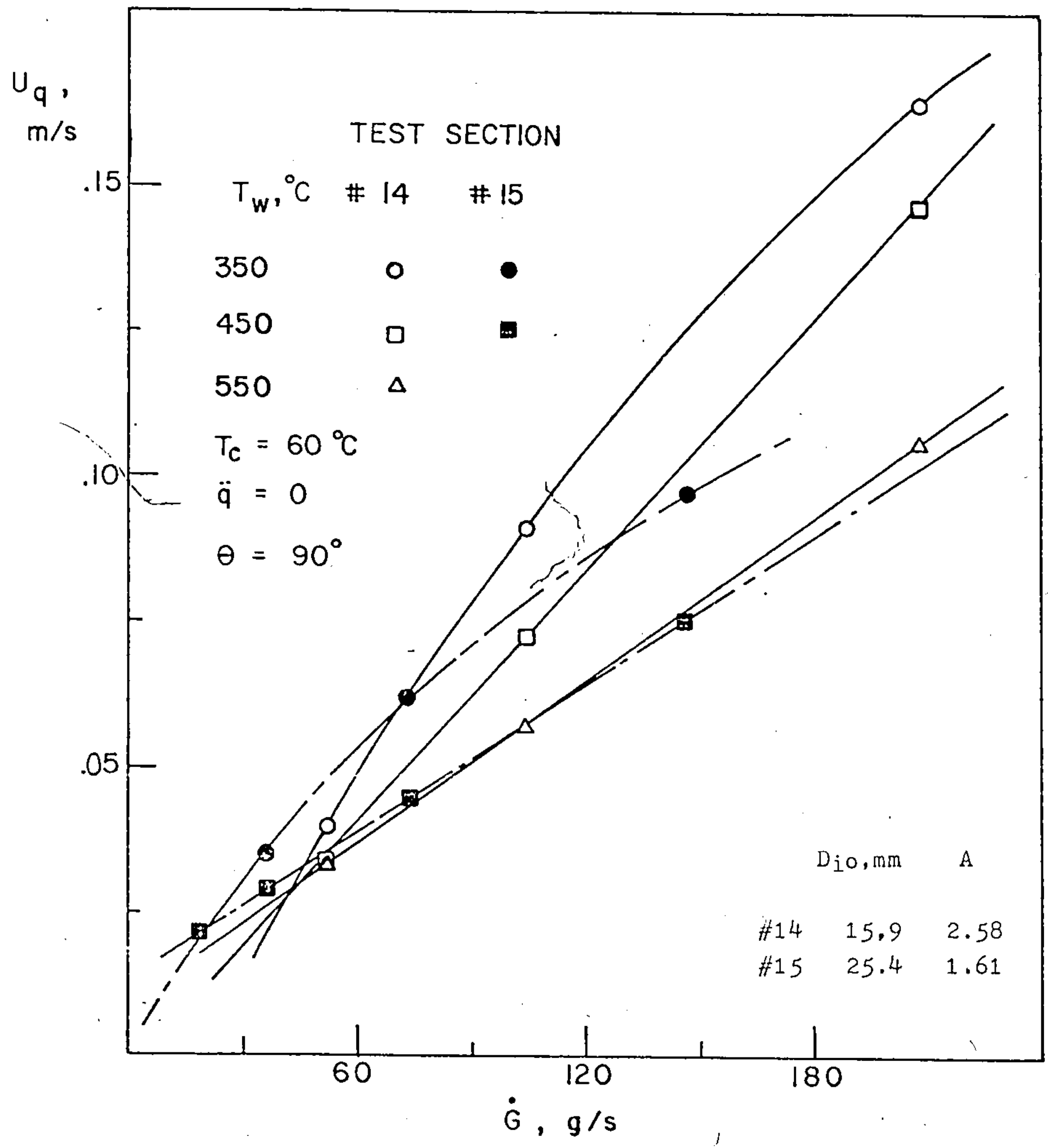

Fig. 6.24 Rewetting Velocity in Annular Test-Sections

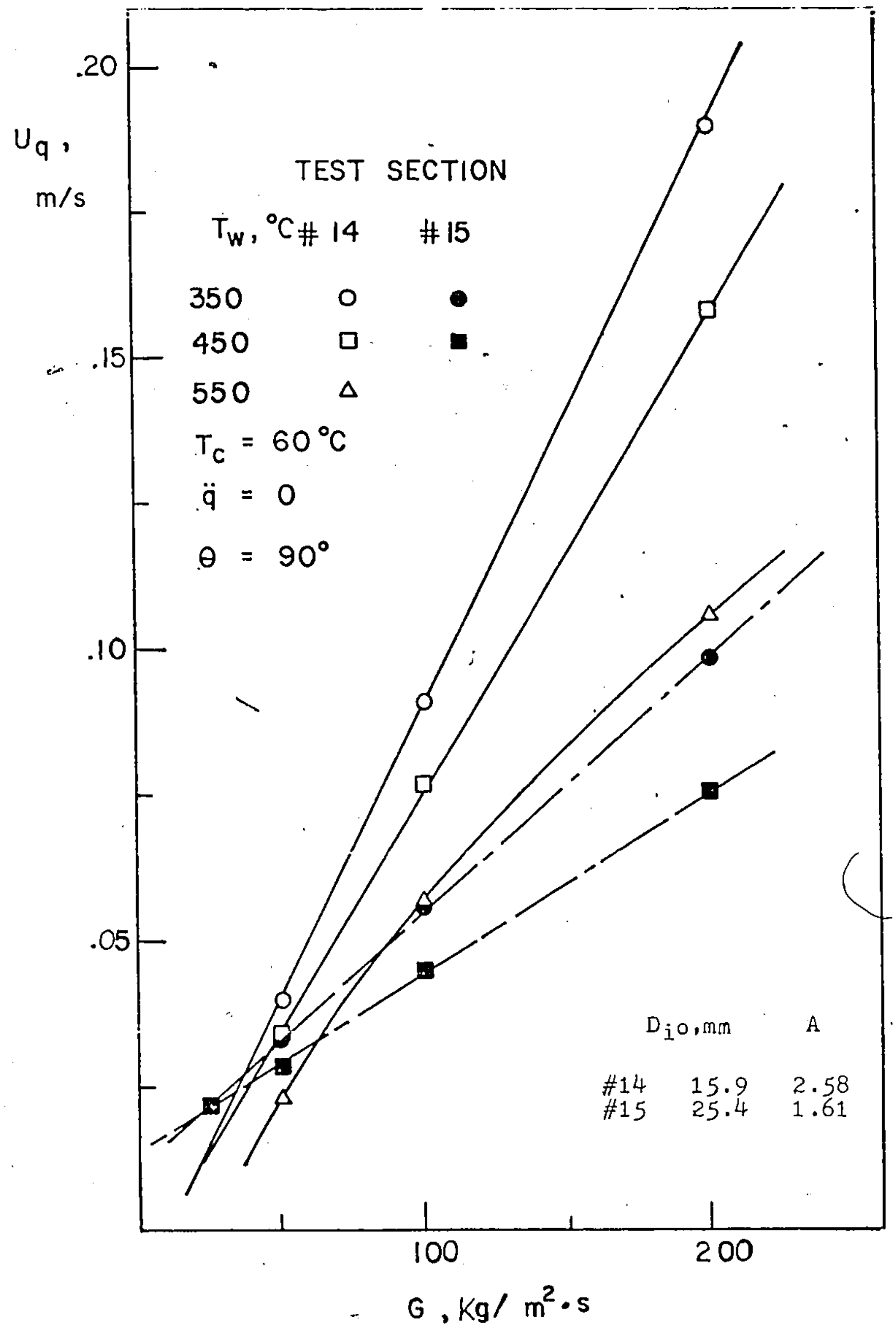

Fig. 6.25 Rewetting Velocity in Annular Test-Sections

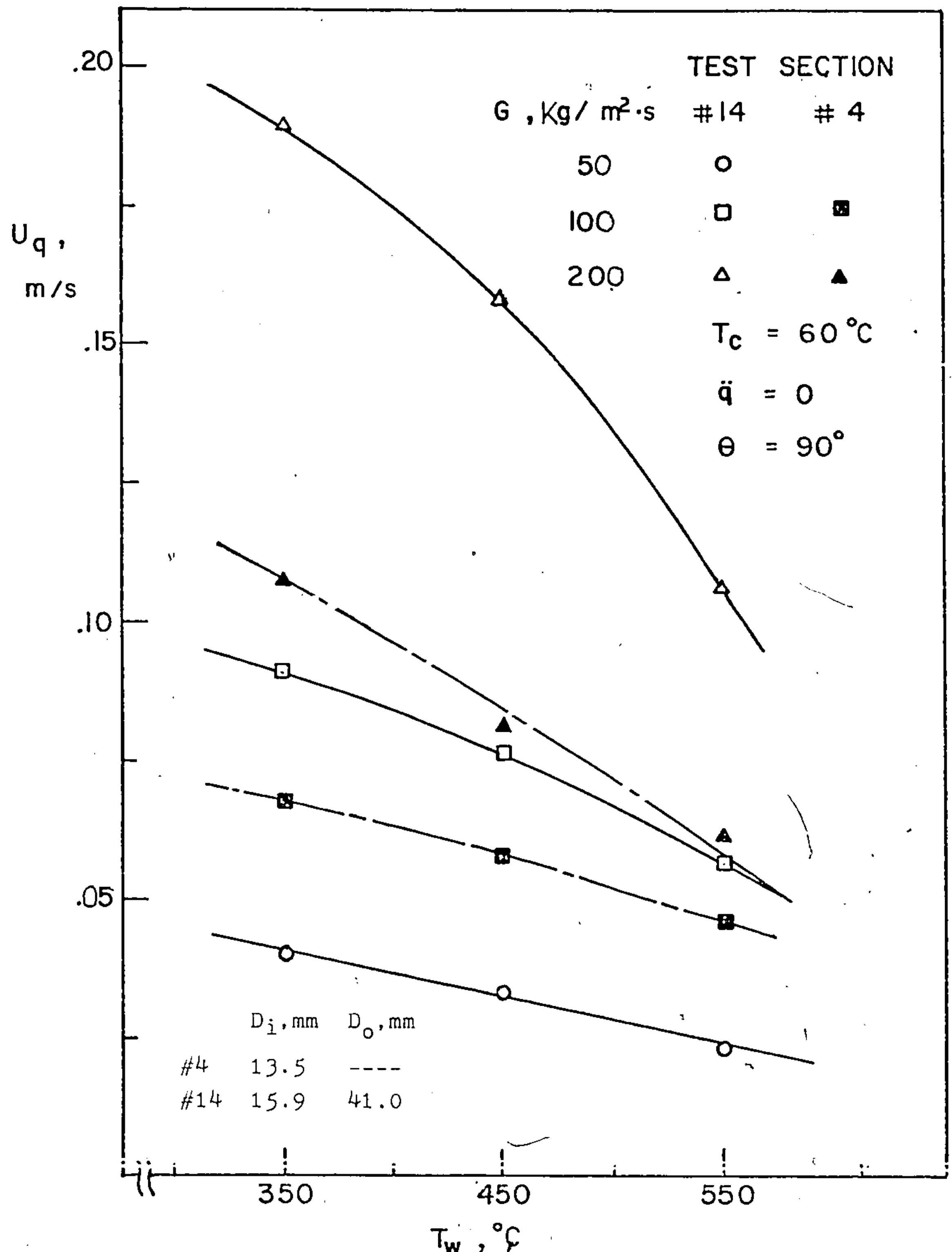

Fig. 6.26 Effect of Initial Wall Temperature;
A Single Tube and An Annulus

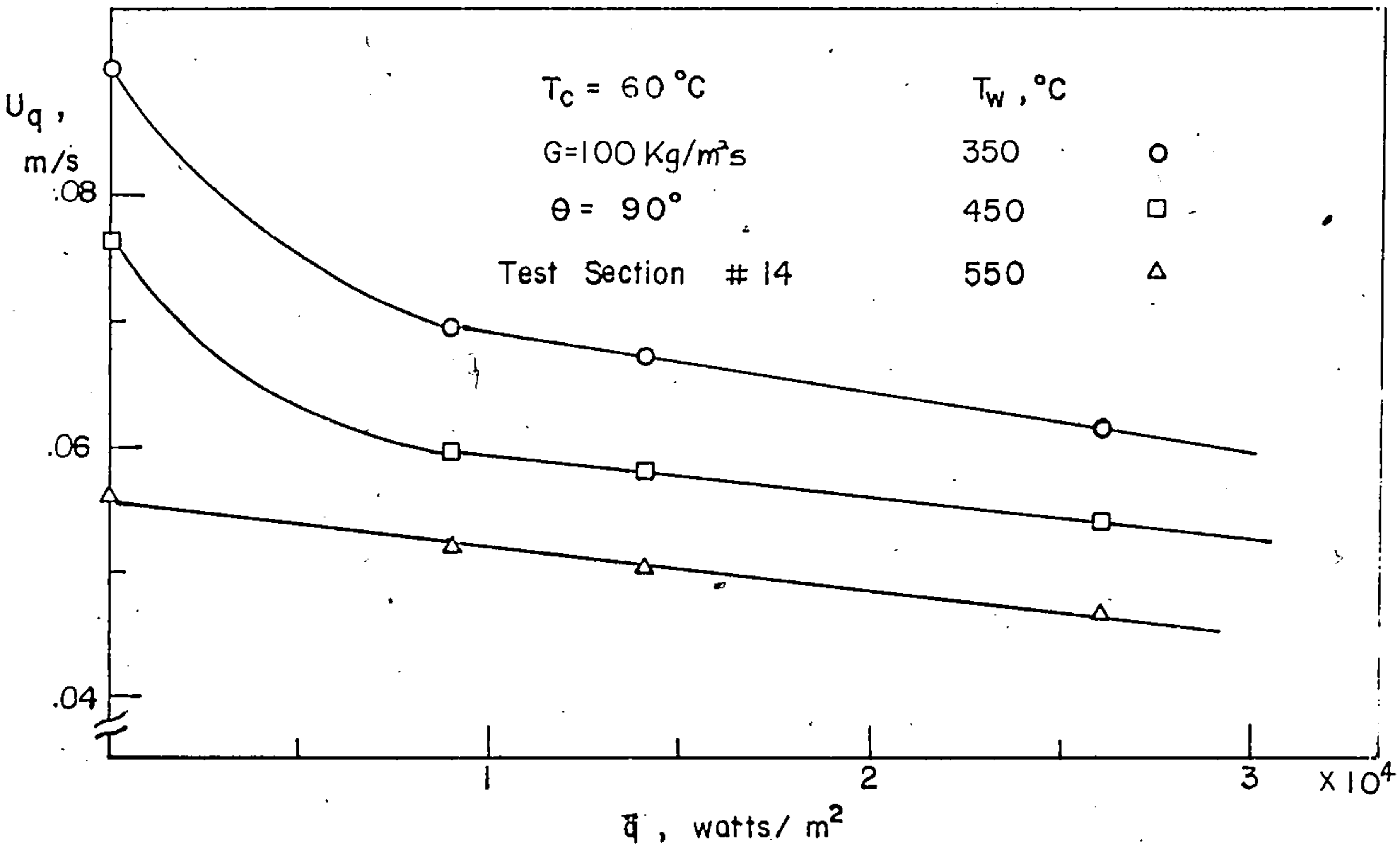

Fig. 6.27 Effect of Specific Heat Generation: An Annulus

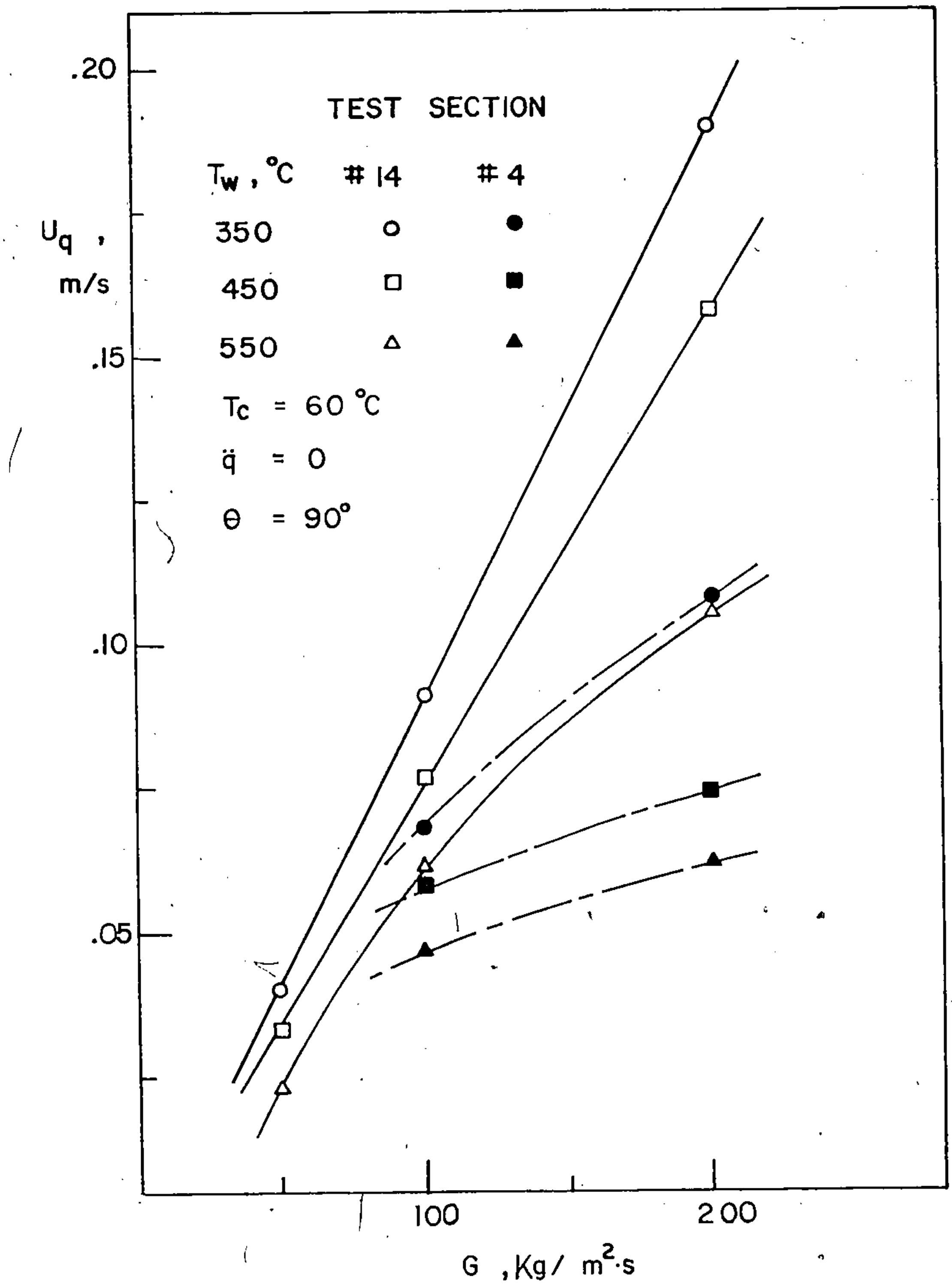

Fig. 6.28 Effect of Coolant Flow Rate; A Single Tube and An Annulus

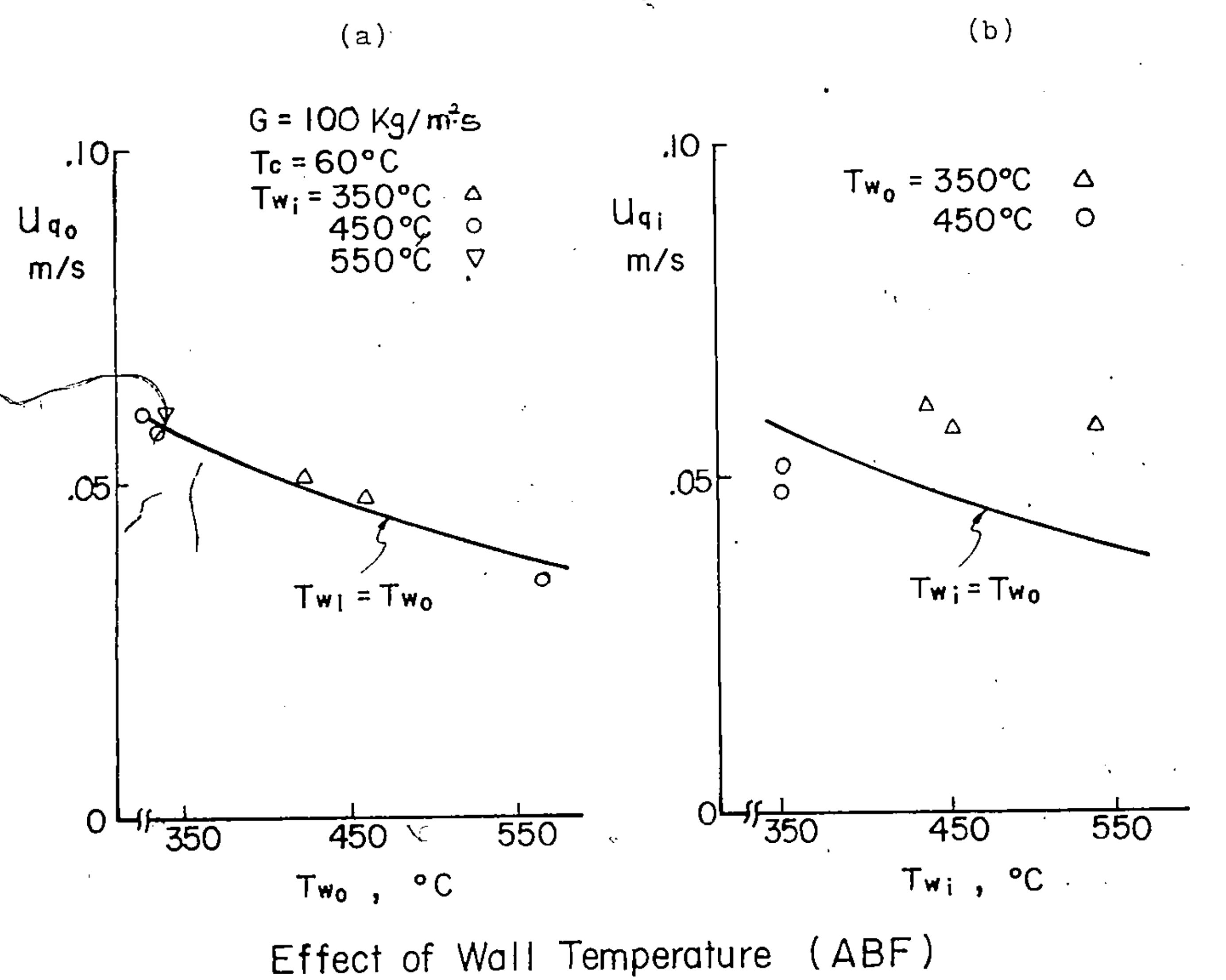

Fig. 6.29 Effect of Initial Wall Temperature : Bottom Flooding, Annular Test-section with Both Walls Heated (ABF Mode)

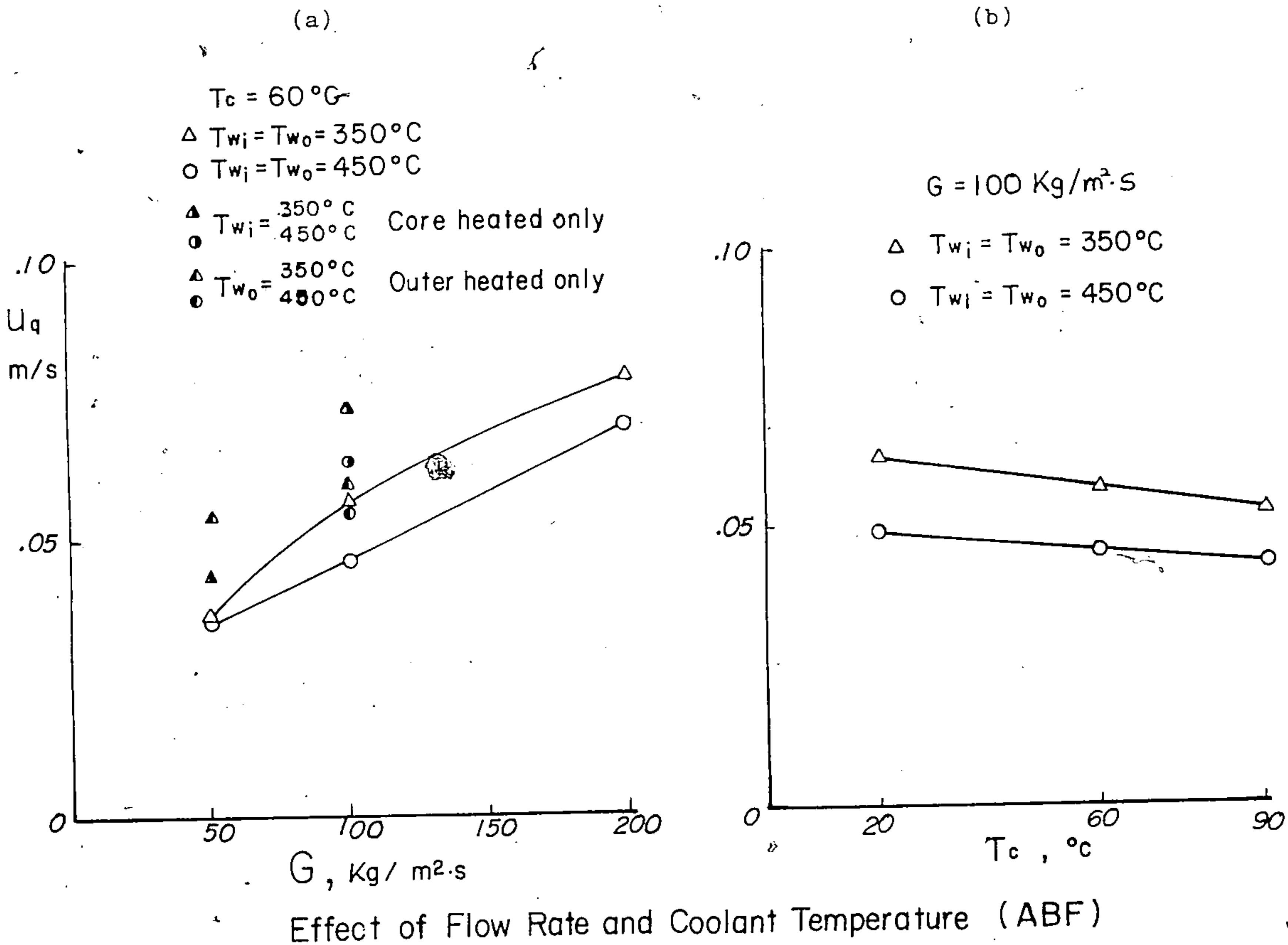

Fig. 6.30 Effects of Coolant Flow Rate and Coolant Inlet Temperature : ABF Mode

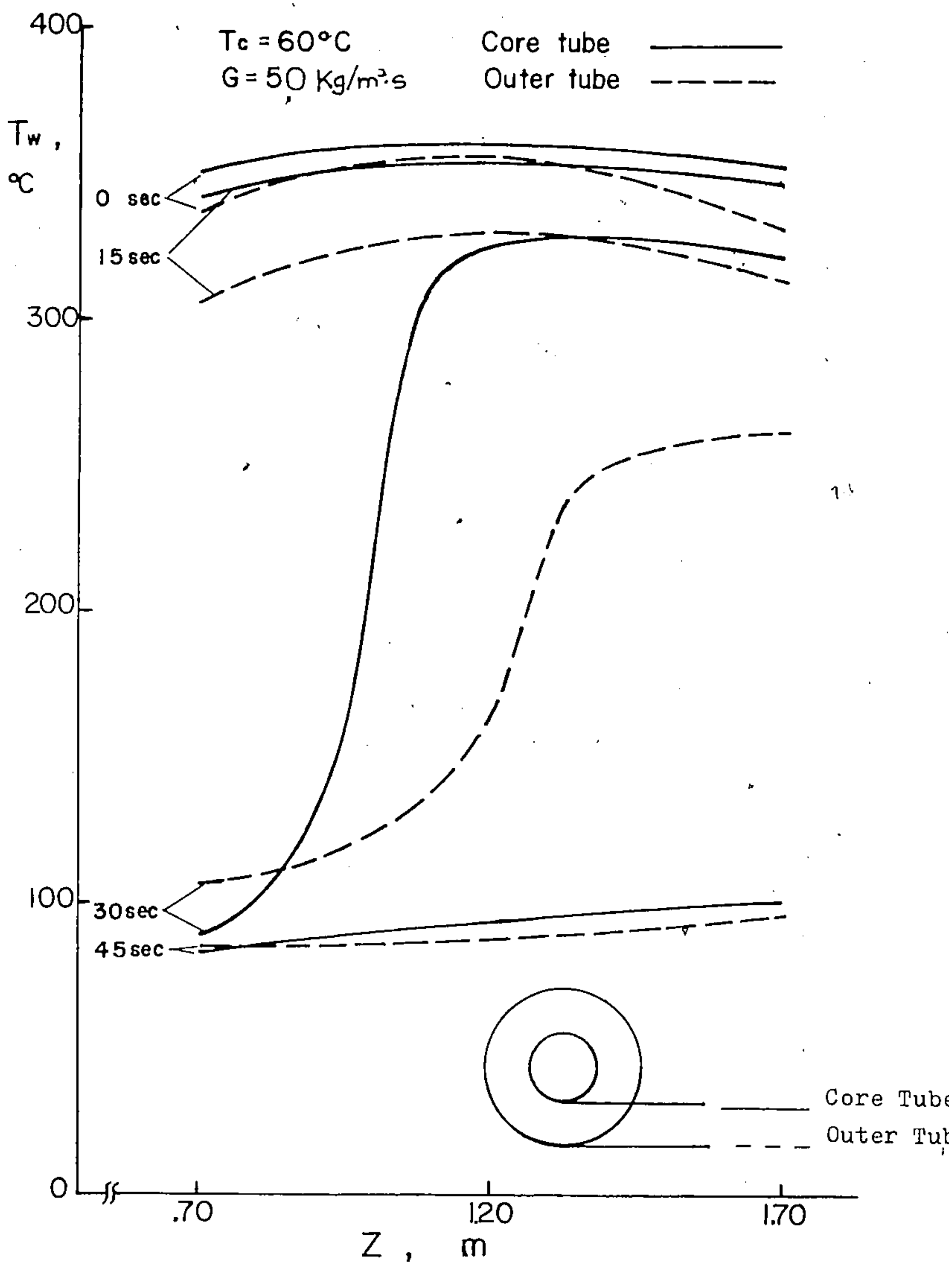

Axial Wall Temperature Distribution at Bottom (AHF)

Fig. 6.31 Axial Wall Temperature : Horizontal Flooding, Annular Test-section with Both Walls Heated (AHF Mode)

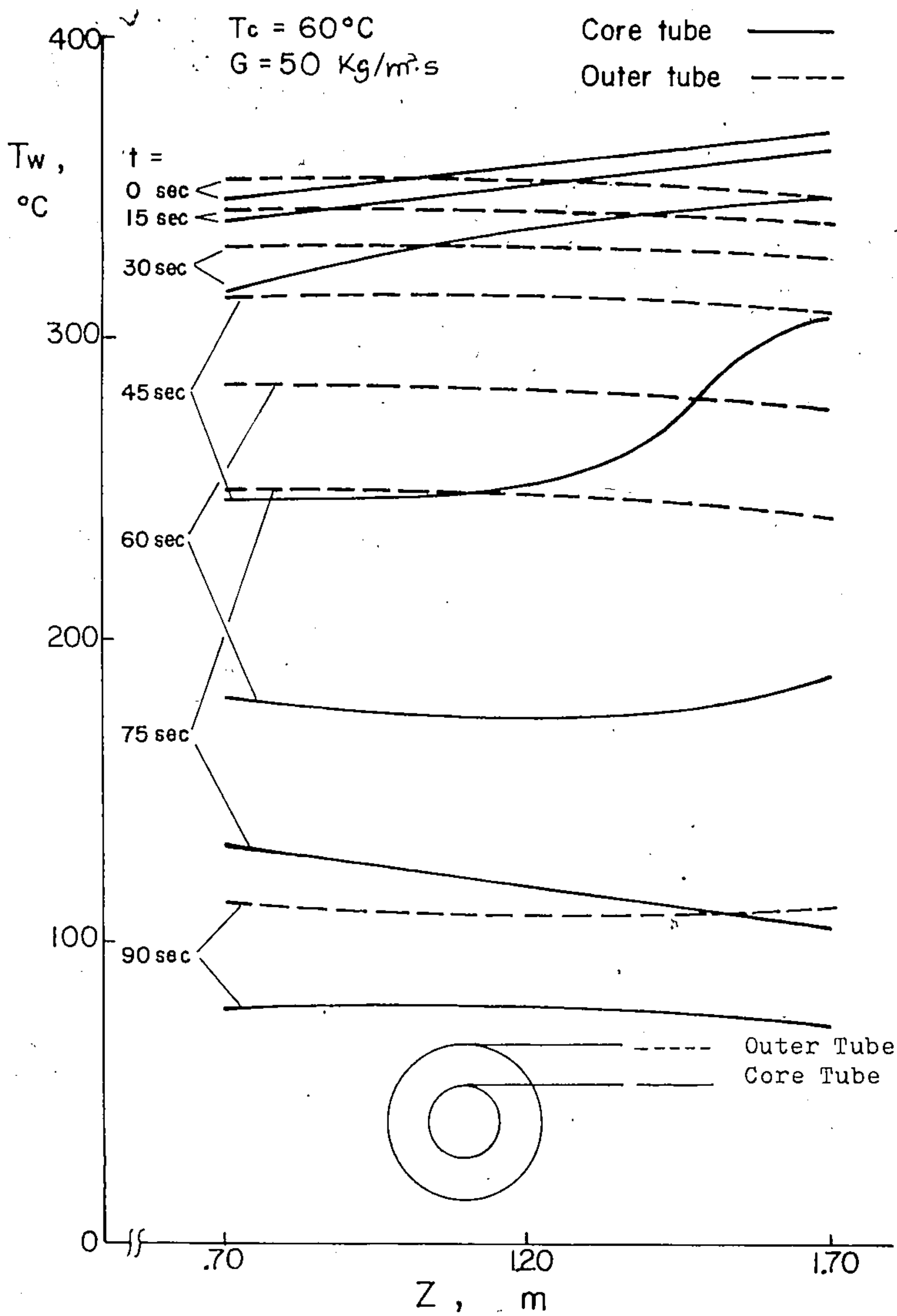

Axial Temperature Distribution (AHF) at Top

Fig. 6.32 Axial Wall Temperature : Horizontal Flooding Annular Test-section with Both Walls Heated (AHF Mode)

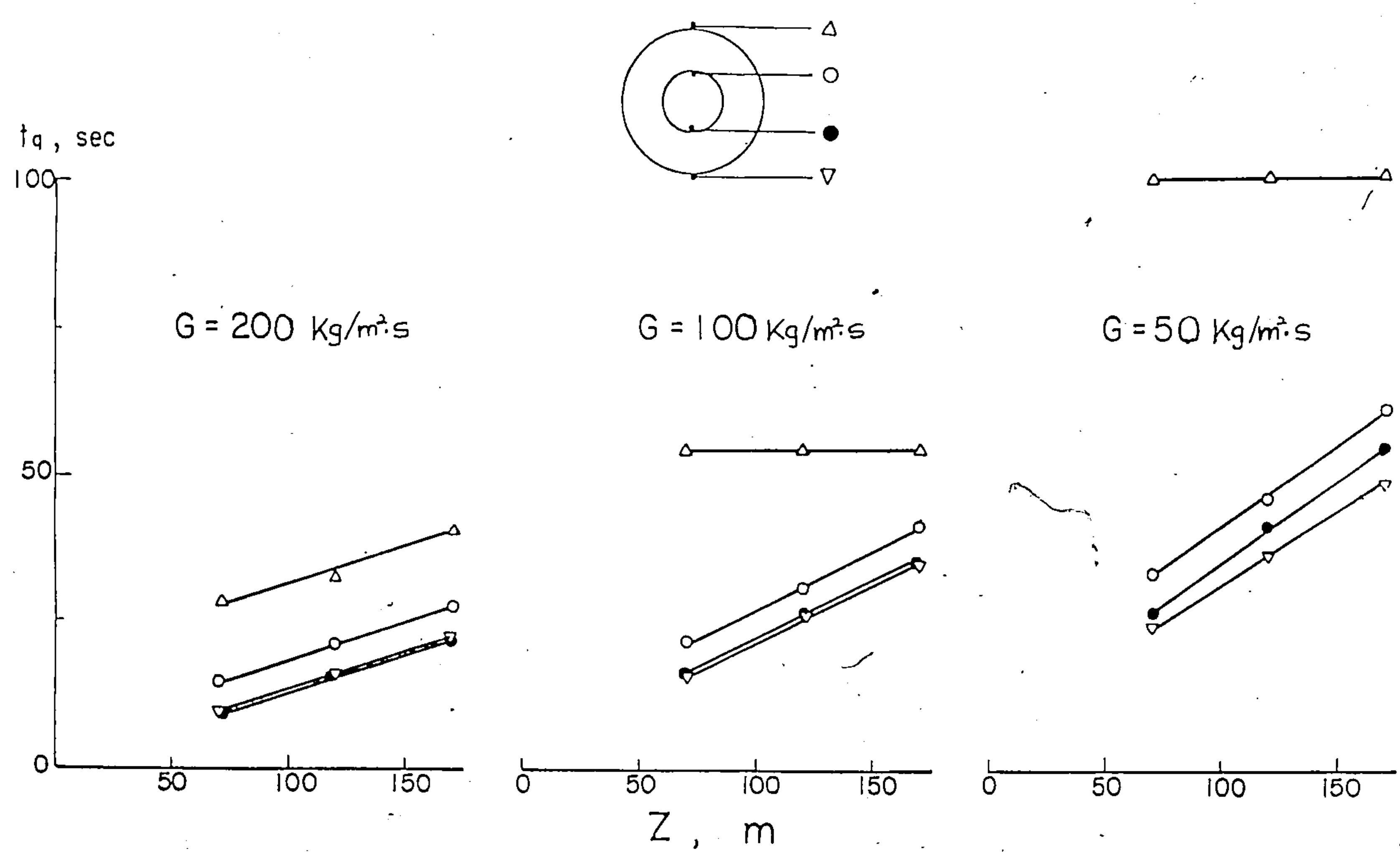

Fig. 6.33 Effect of Coolant Flow Rate on Quenching Time ; AHF Mode

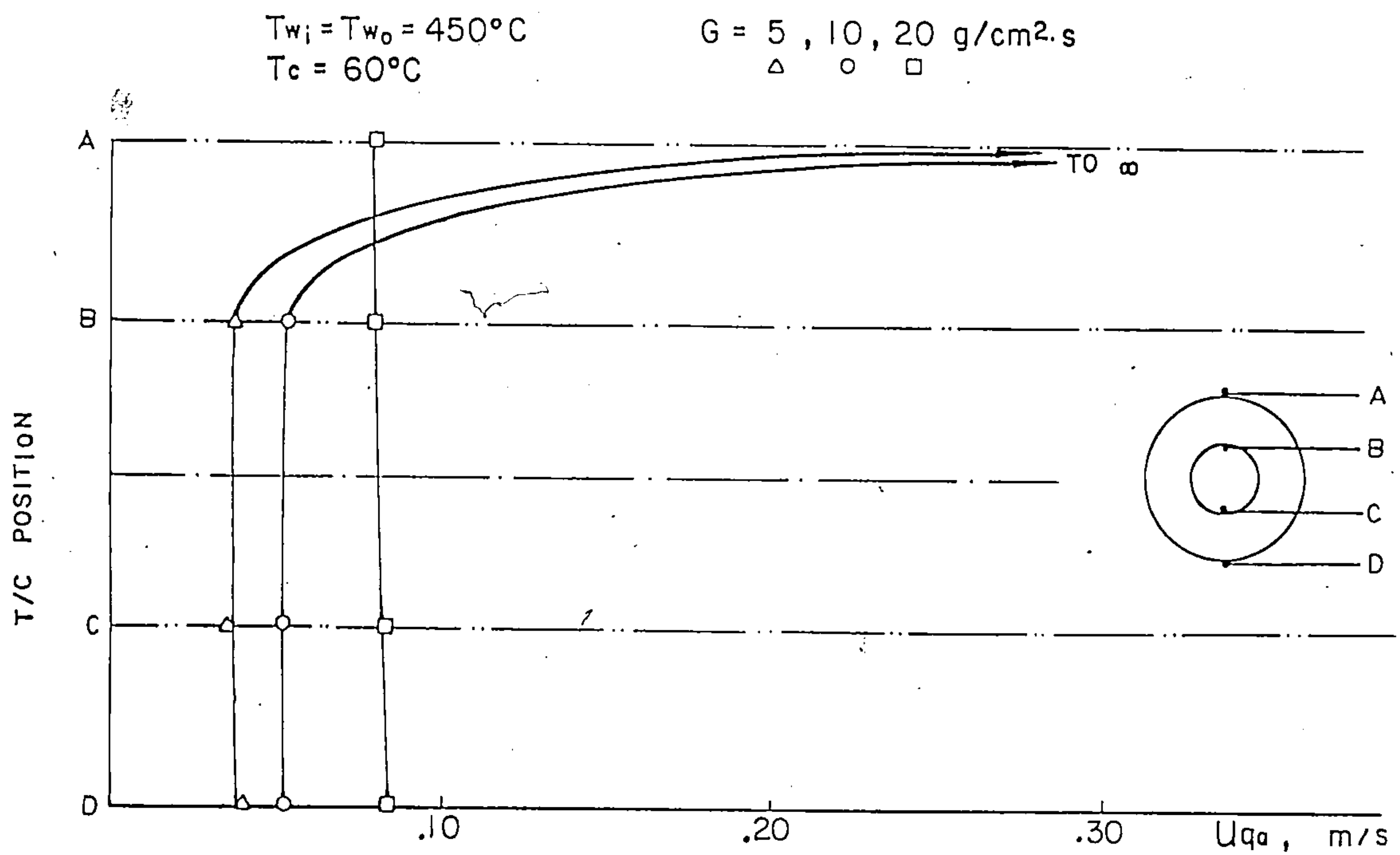

Fig. 6.34 Effect of Coolant Flow Rate on Apparent Quenching Velocity ; AHF Mode

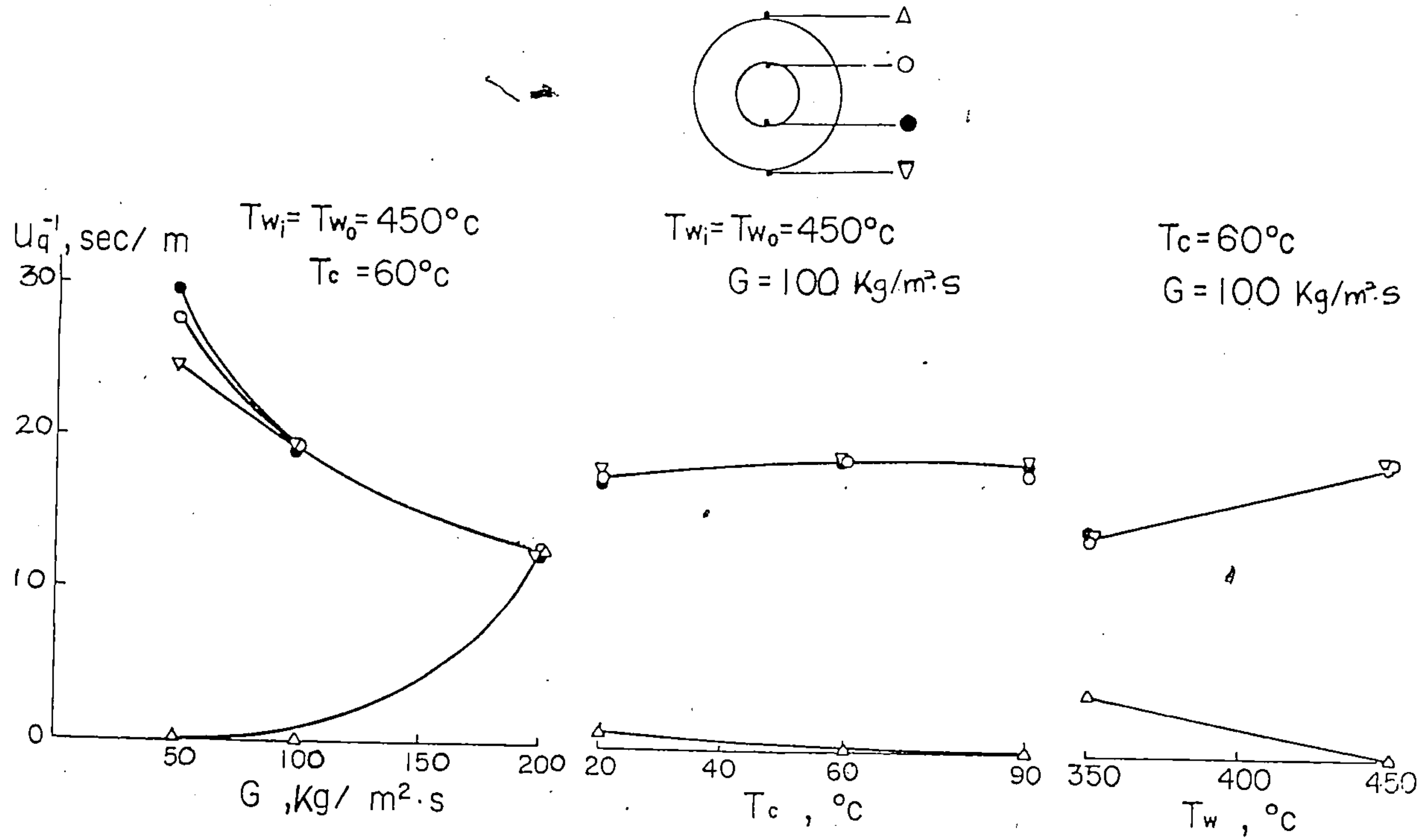

Fig. 6.35 Effects of Coolant Flow Rate, Coolant Inlet Temperature and Initial Wall Temperature on Apparent Quenching Velocity at Z = 1.2 m : AHF Mode

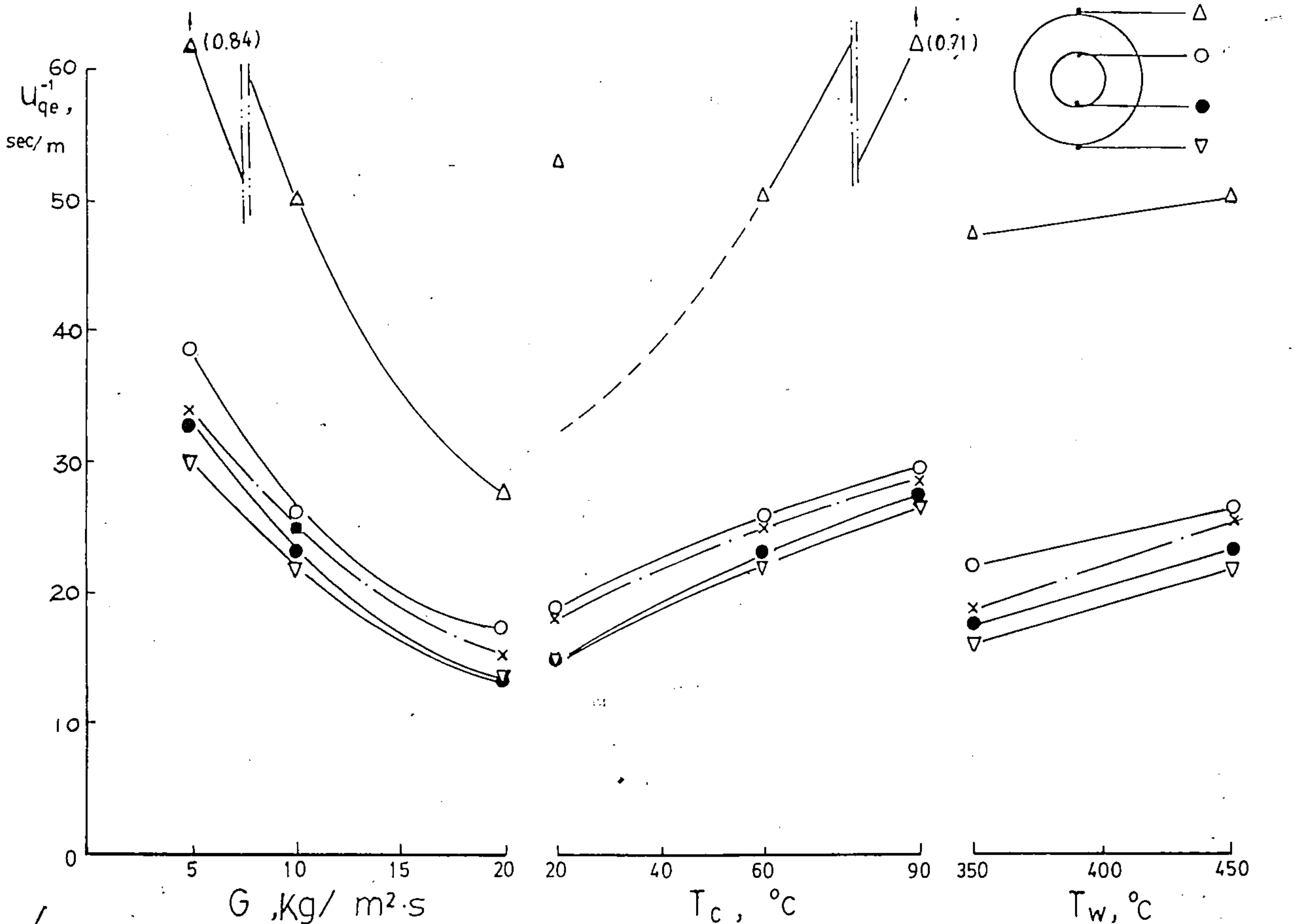

Fig. 6.36 Effects of Coolant Flow Rate, Coolant Inlet Temperature and Initial Wall Temperature on <u>Effective</u> Quenching Velocity at Z = 1.2 m ; AHF Mode

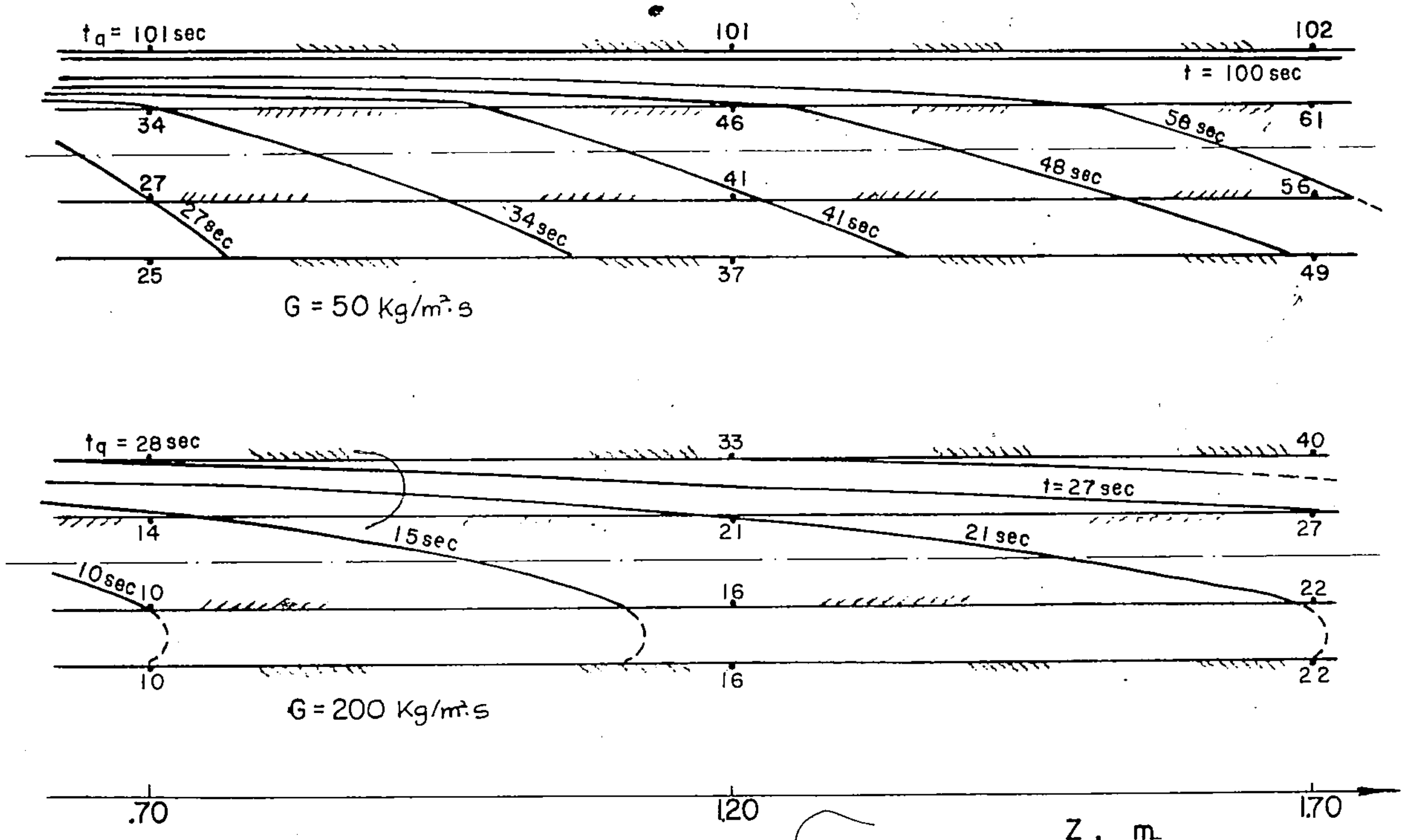

Progress of the quenching front (AHF)

Fig. 6.37 Propagation of Rewetting Front : AHF Mode

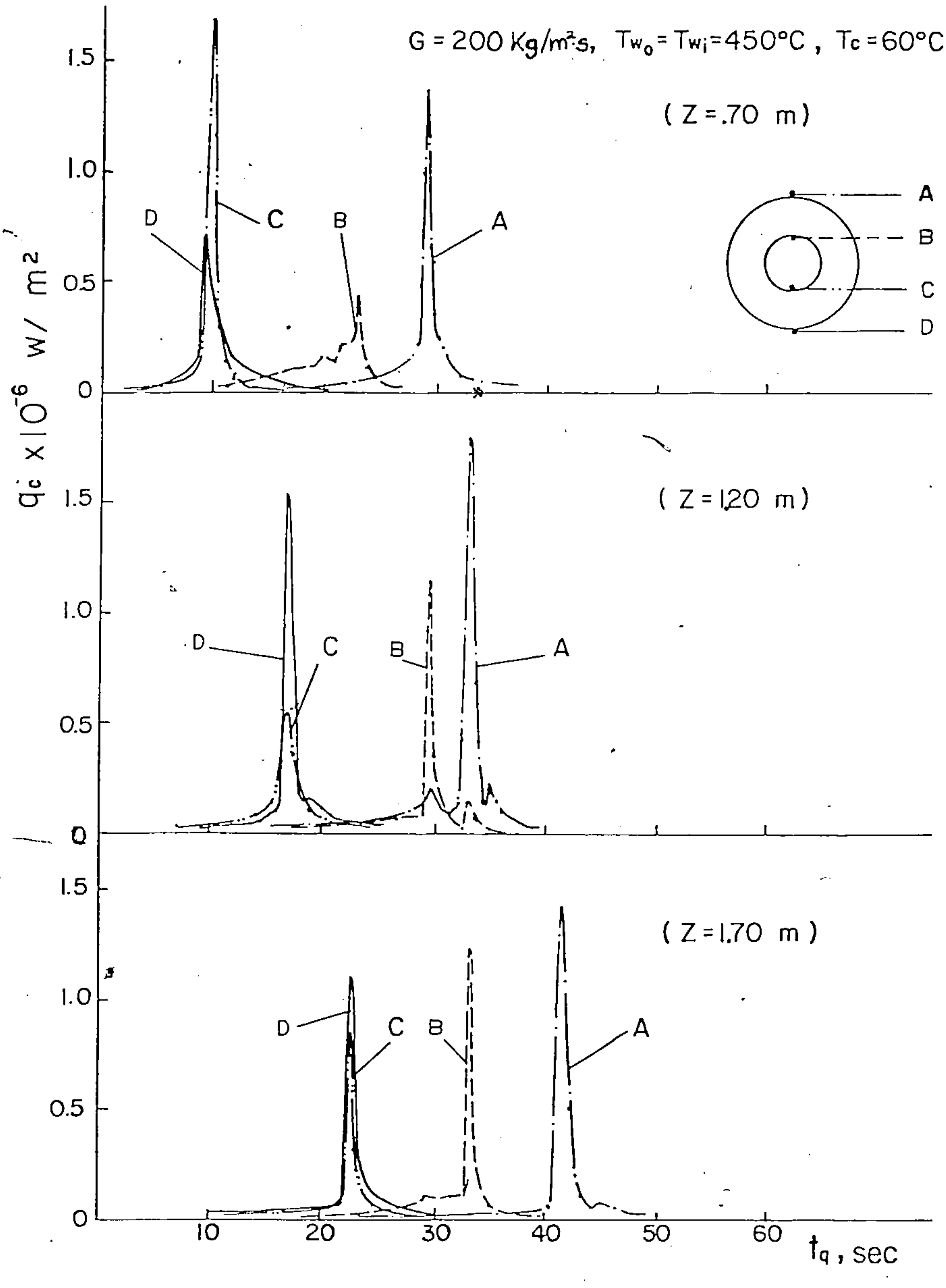

Fig. 6.38 Heat Flux Distribution : AHF Mode
(High Coolant Flow Rate)

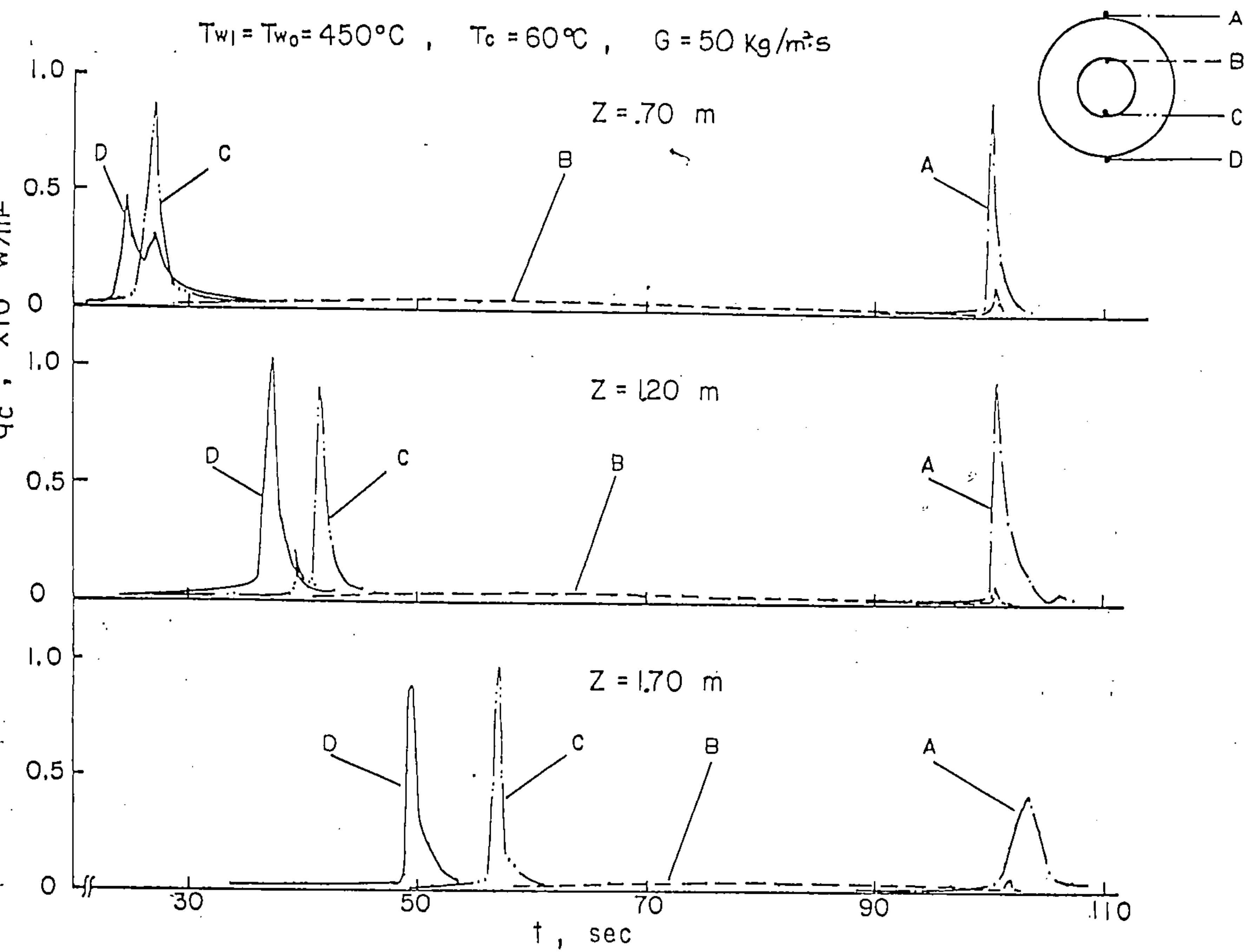

Fig. 6.39 Heat Flux Distribution : AHF Mode (Low Coolant Flow Rate)

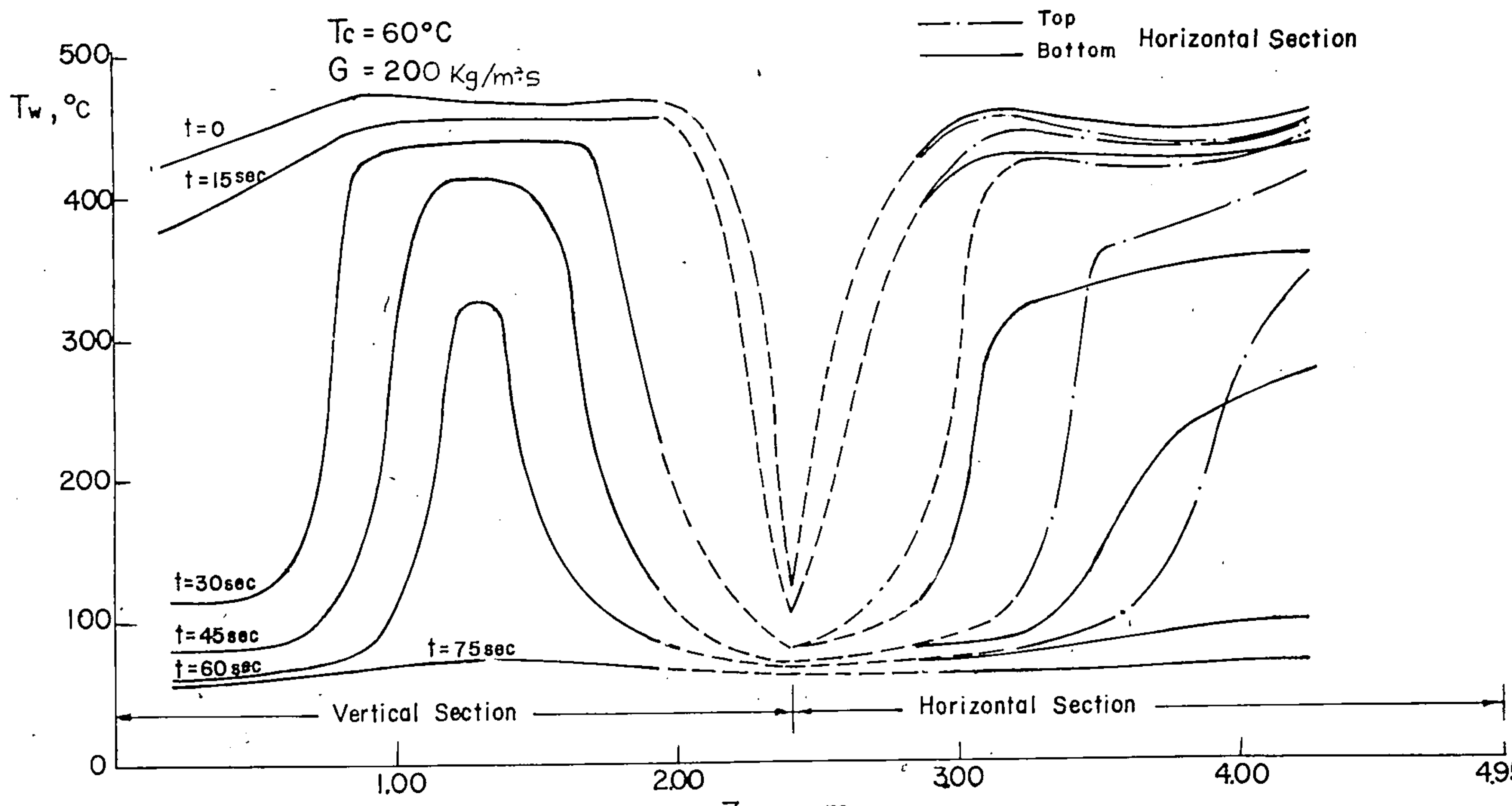

Fig. 6.40 Axial Temperature Distribution "L"-shaped Test-section ; THF Mode

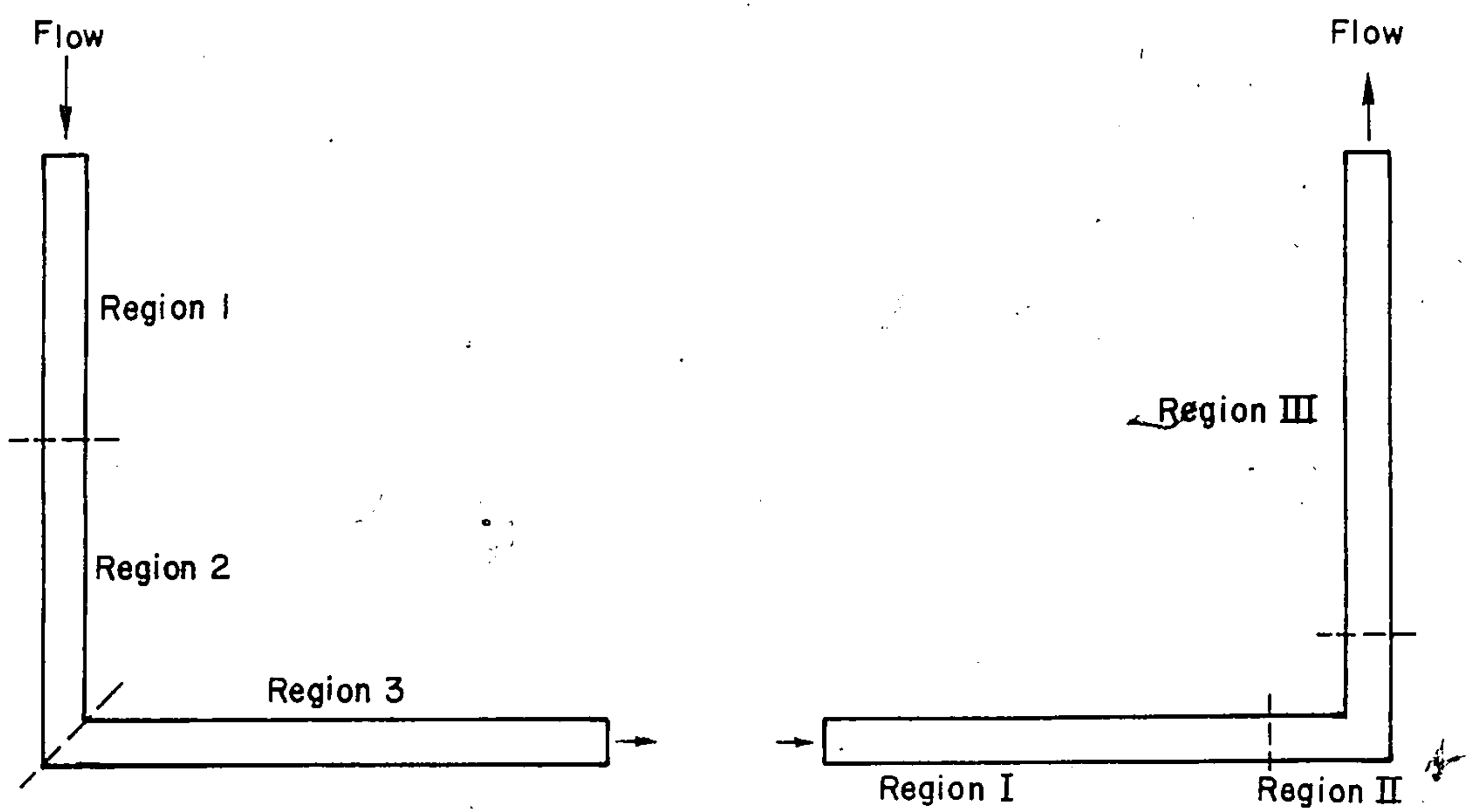

(a) Top-followed-by-Horizontal Flooding Mode; THF Mode

(b) Horizontal-followed-by-Bottom Flooding Mode; HBF Mode

Fig. 6.41 Two Modes of Flooding; "L"-shaped Test-section

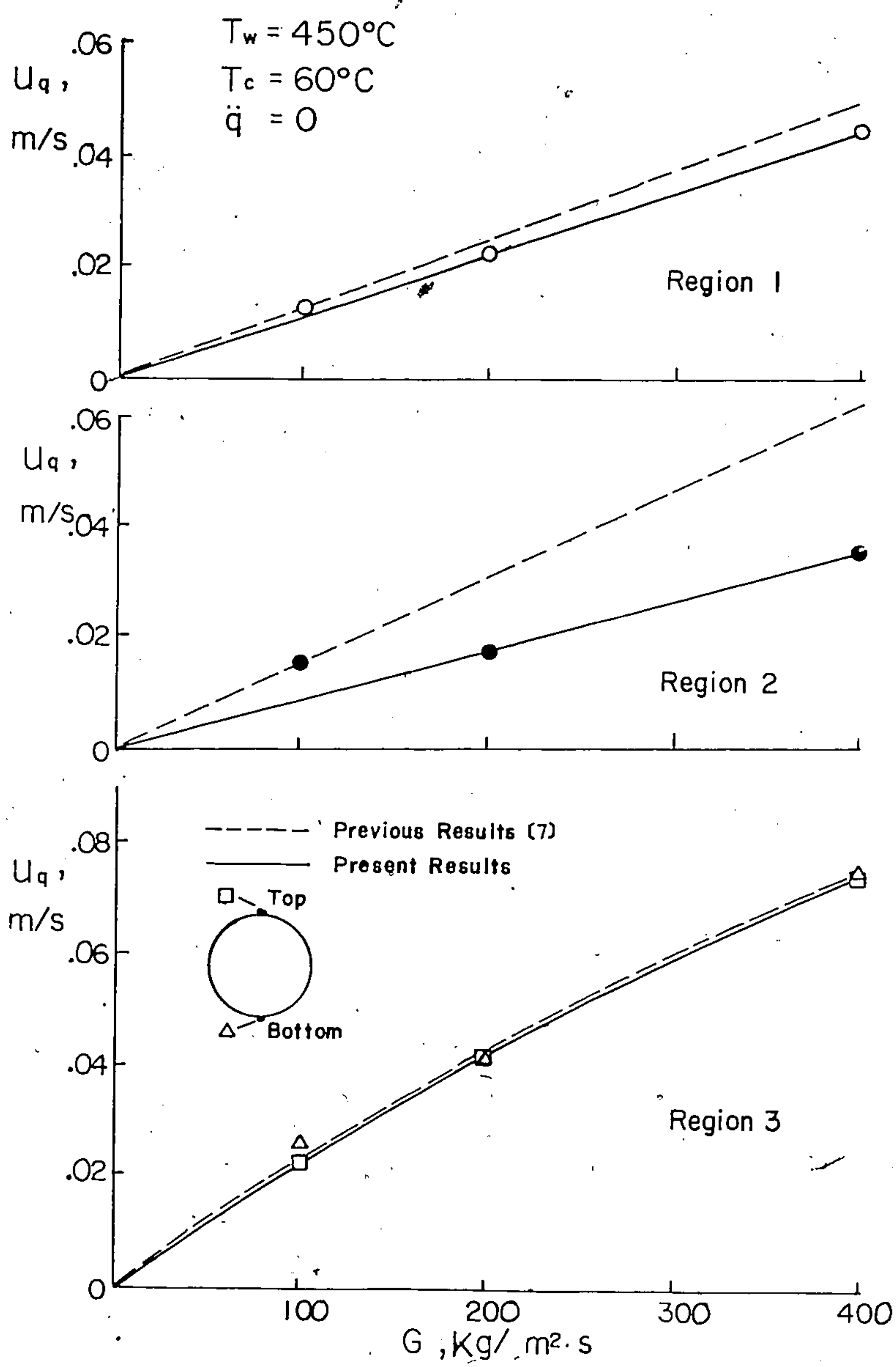

Fig. 6.42 Effect of Coolant Flow Rate: THF Mode

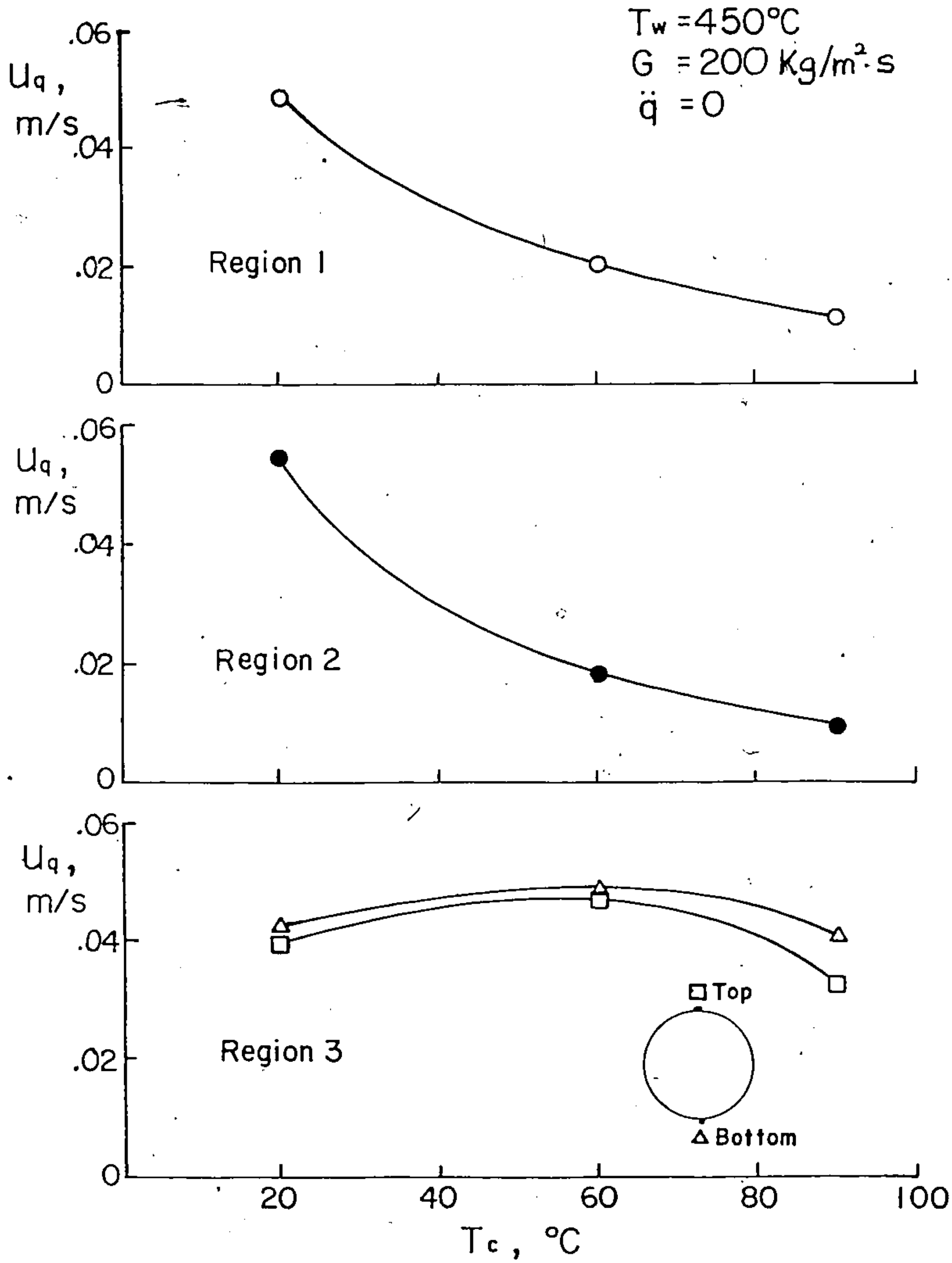

Fig. 6.43 Effect of Coolant Inlet Sub-cooling: THF Mode

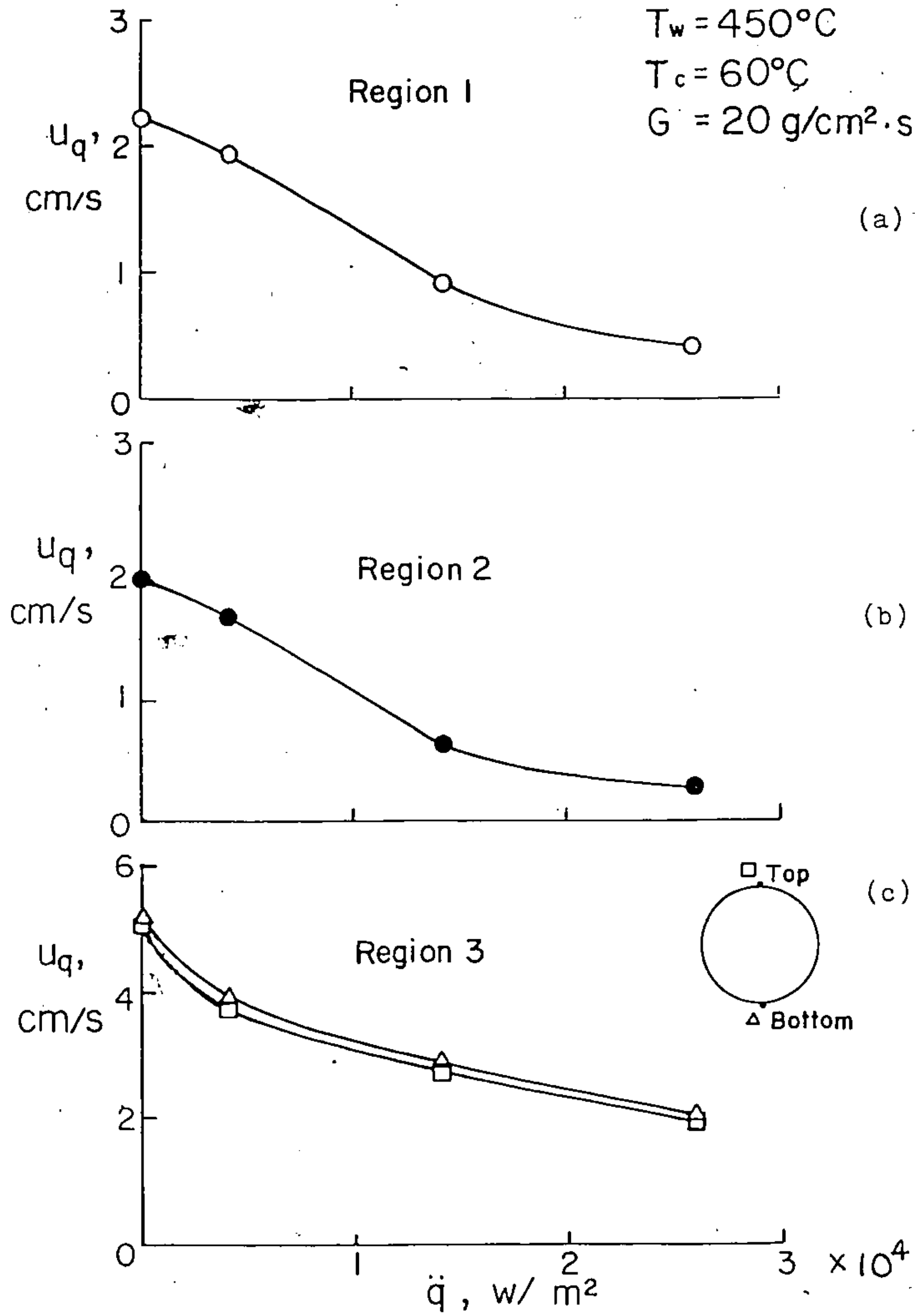

Fig. 6.44 Effect of Heat Generation: THF Mode

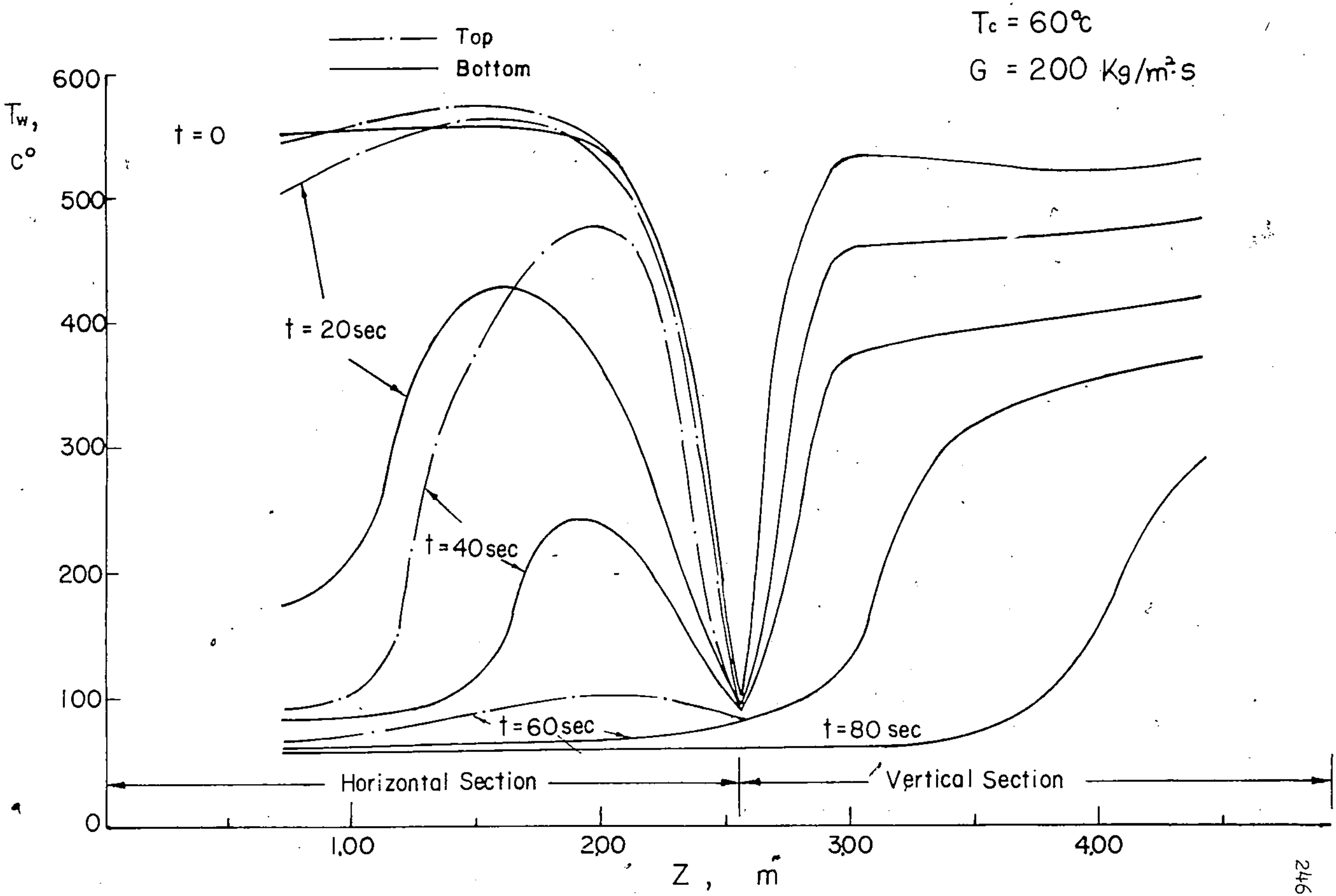

Fig. 6.45 Axial Temperature Distribution : "L"-shaped Test-section; HBF Mode

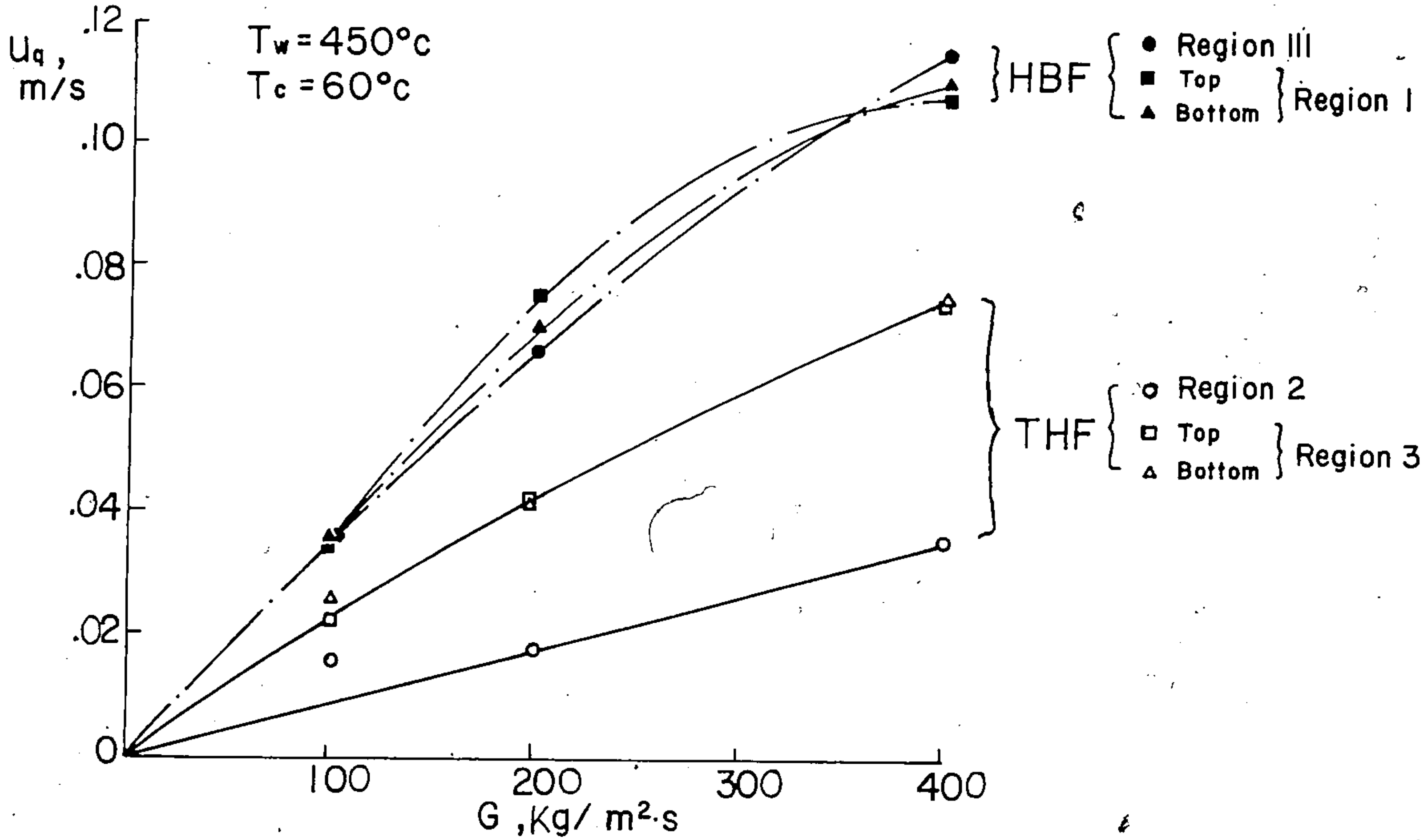

Fig. 6.46 Effect of Coolant Flow Rate : HBF Mode

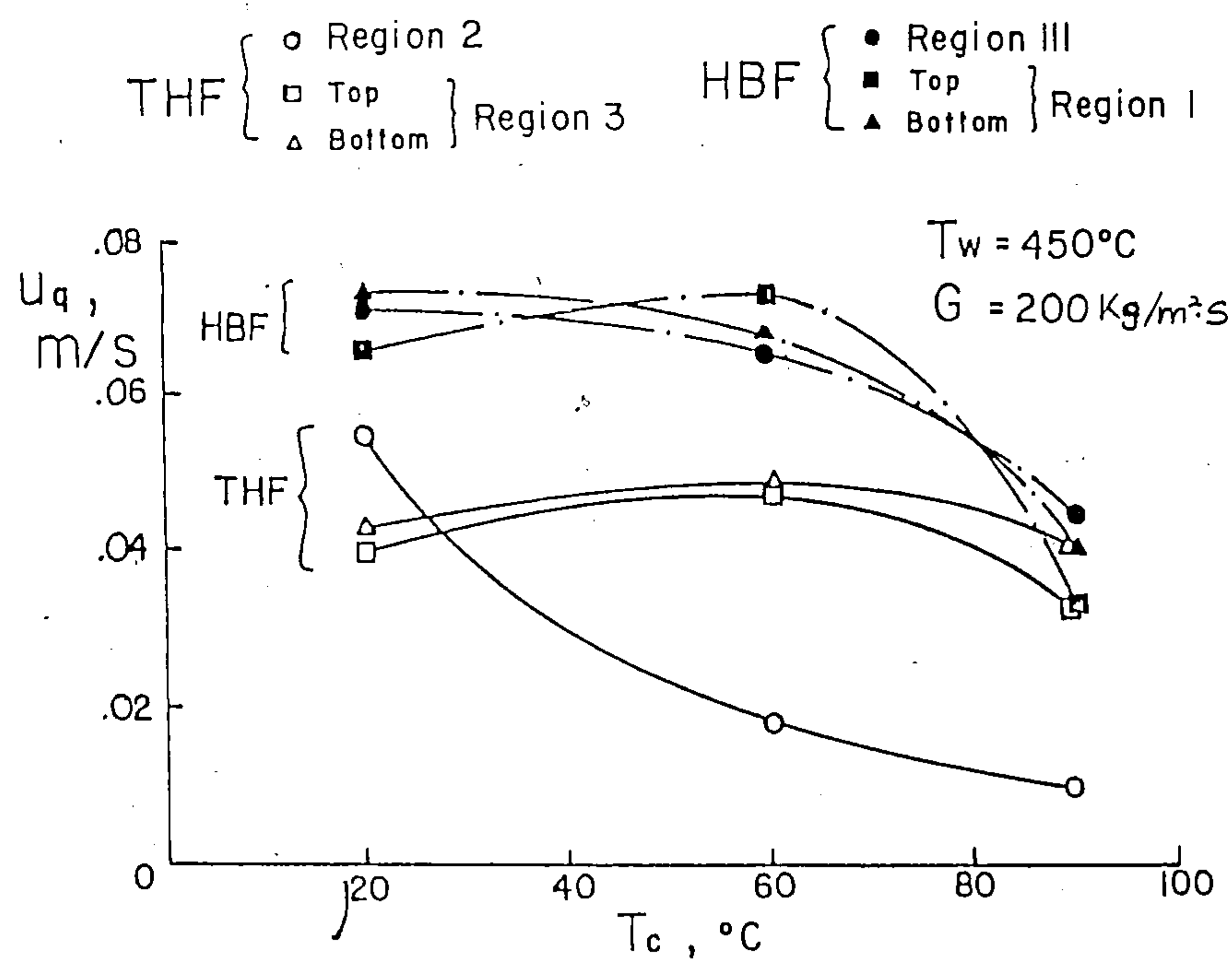

Fig. 6.47 Effect of Coolant Inlet Sub-cooling: HBF Mode

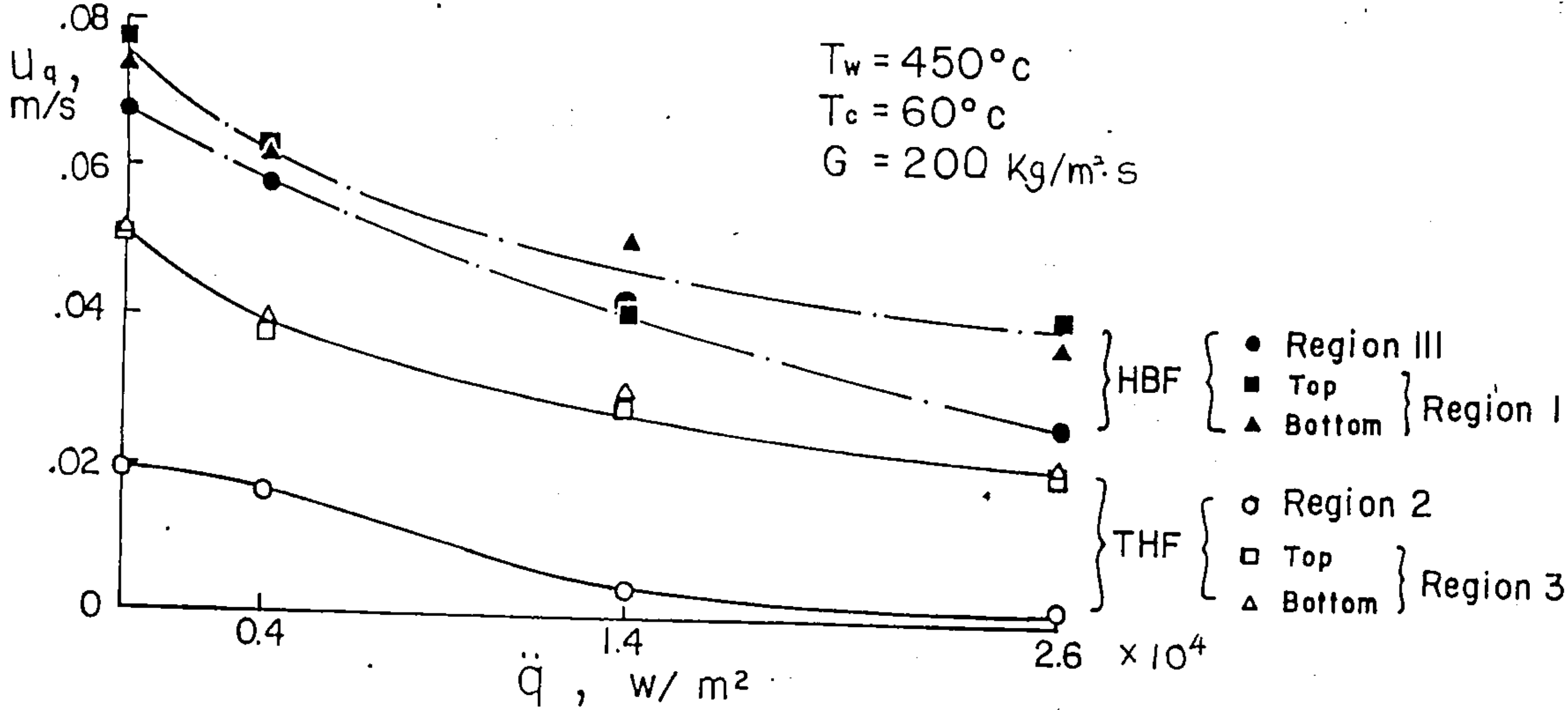

Fig. 6.48 Effect of Heat Generation: HBF Mode

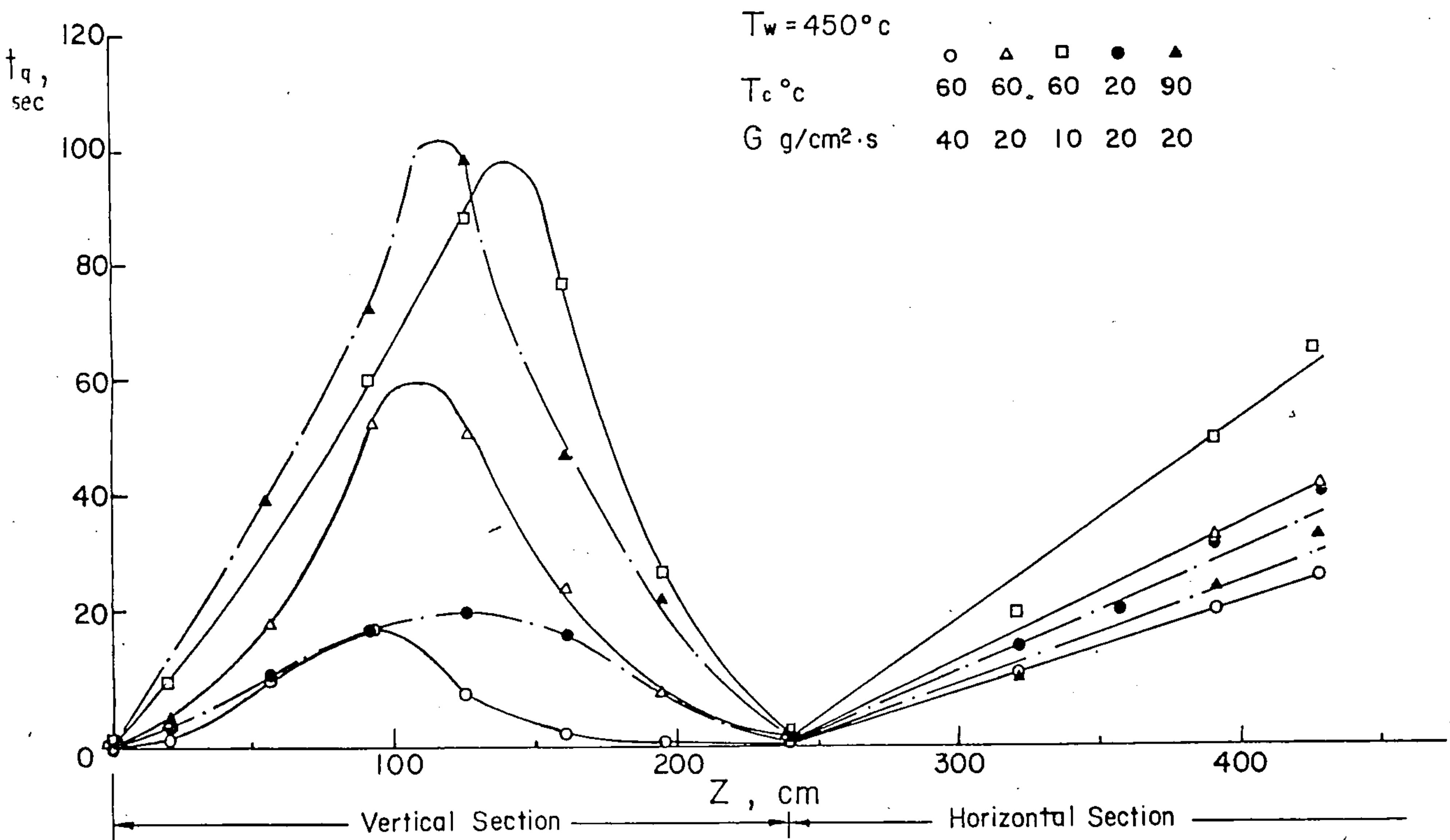

Fig. 6.49 Quenching Time: THF Mode in the "L"-shaped Test-section

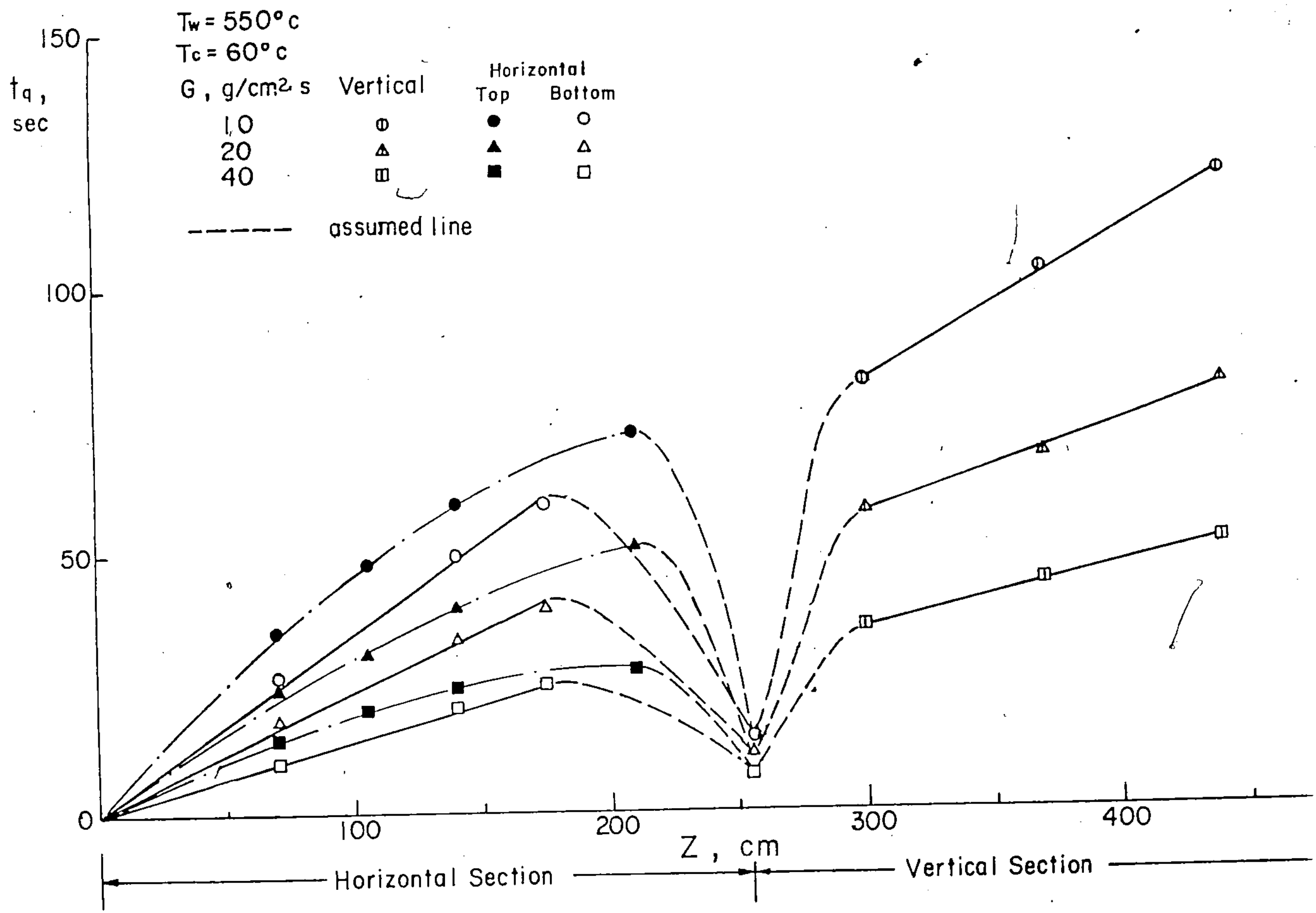

Fig. 6.50 . Quenching Time: HBF Mode in the "L"-shaped Test-section

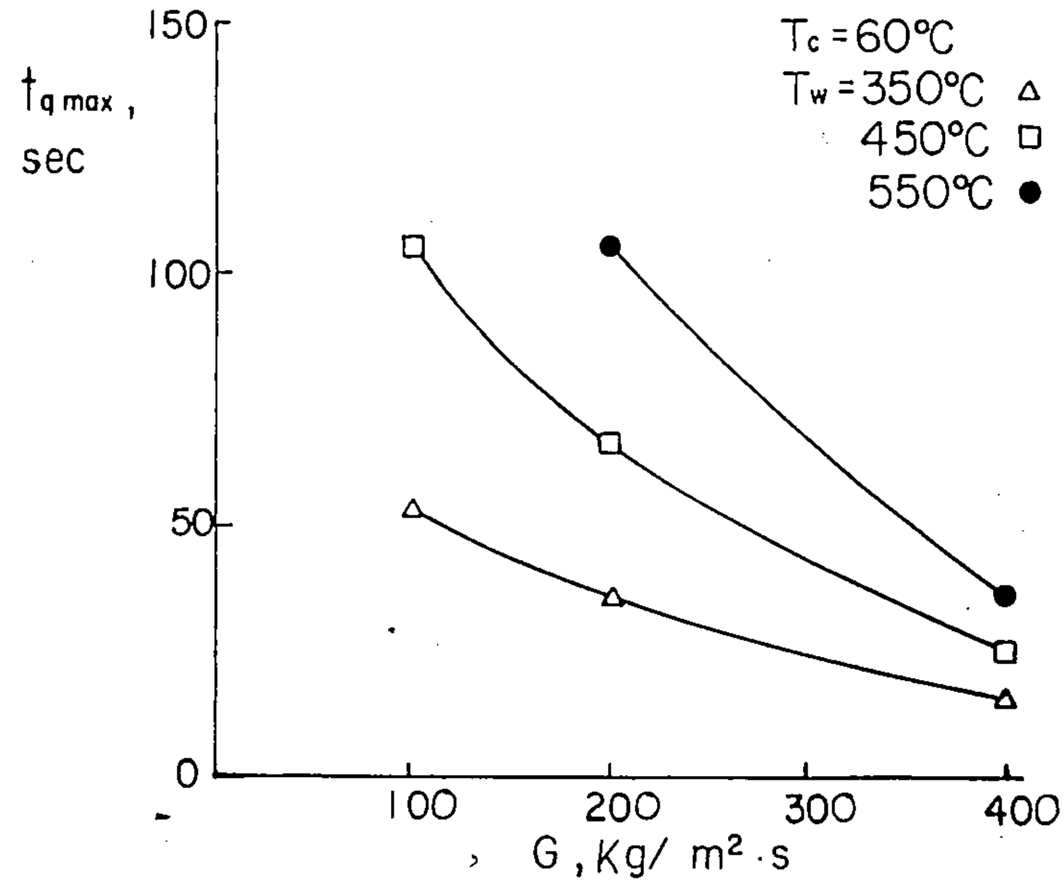

Fig. 6.51 Effects of Coolant Flow Rate and Initial Wall Temperature: THF Mode

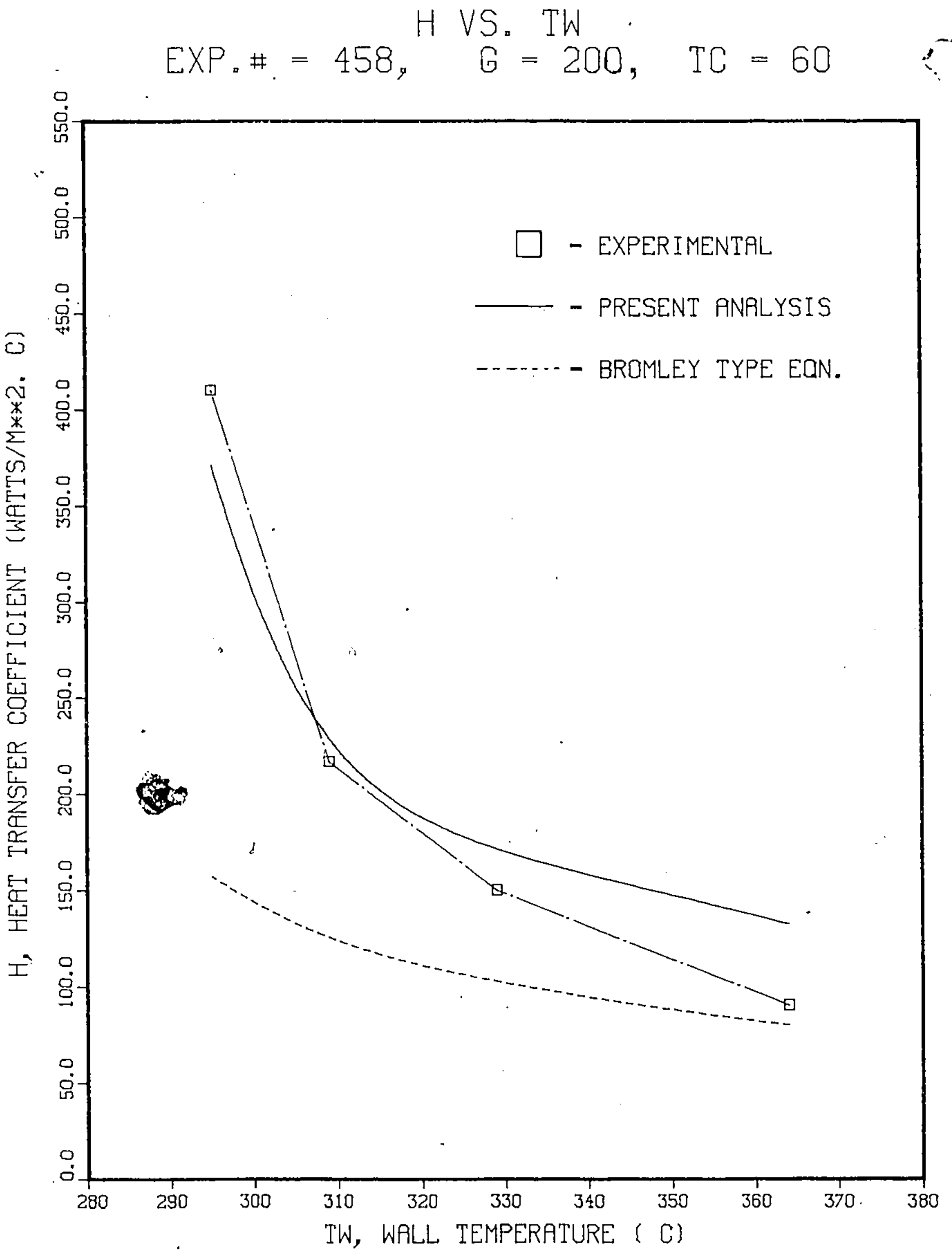

Fig 6.52 Heat Transfer Coefficient in Inverted Annular Region

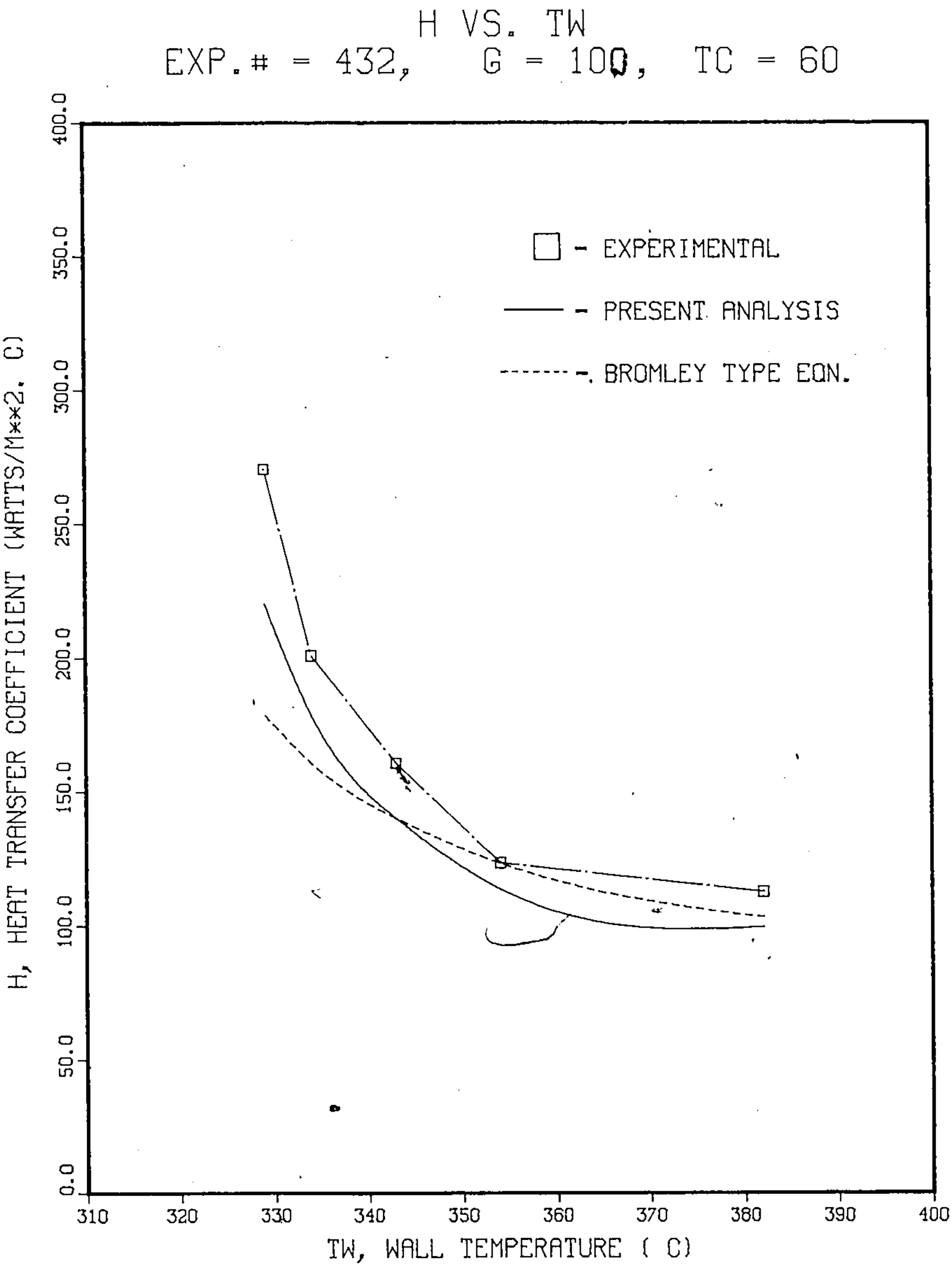

Fig. 6.53 Heat Transfer Coefficient in Inverted Annular Region

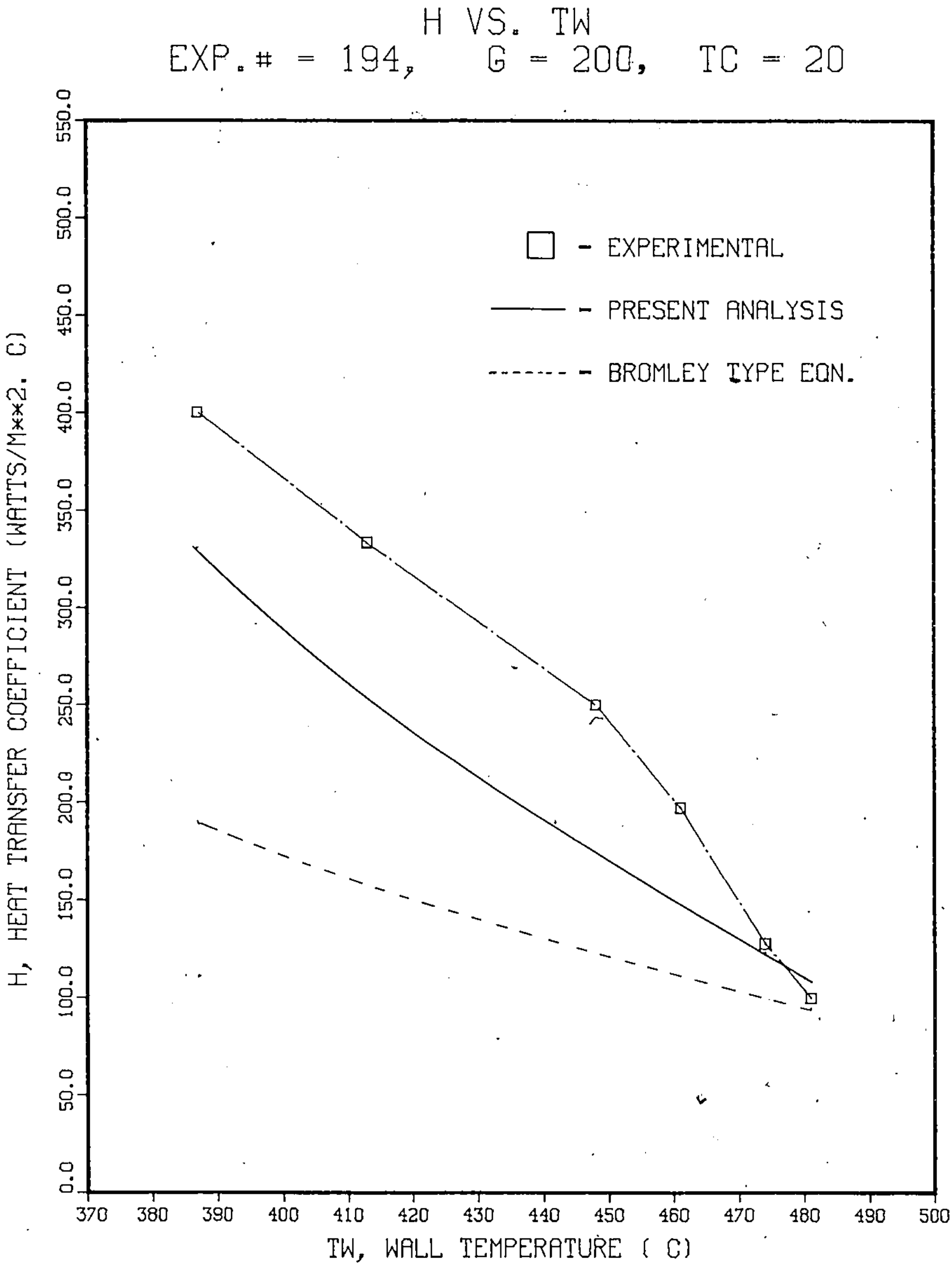

Fig. 6.54 Heat Transfer Coefficient in Inverted Annular Region

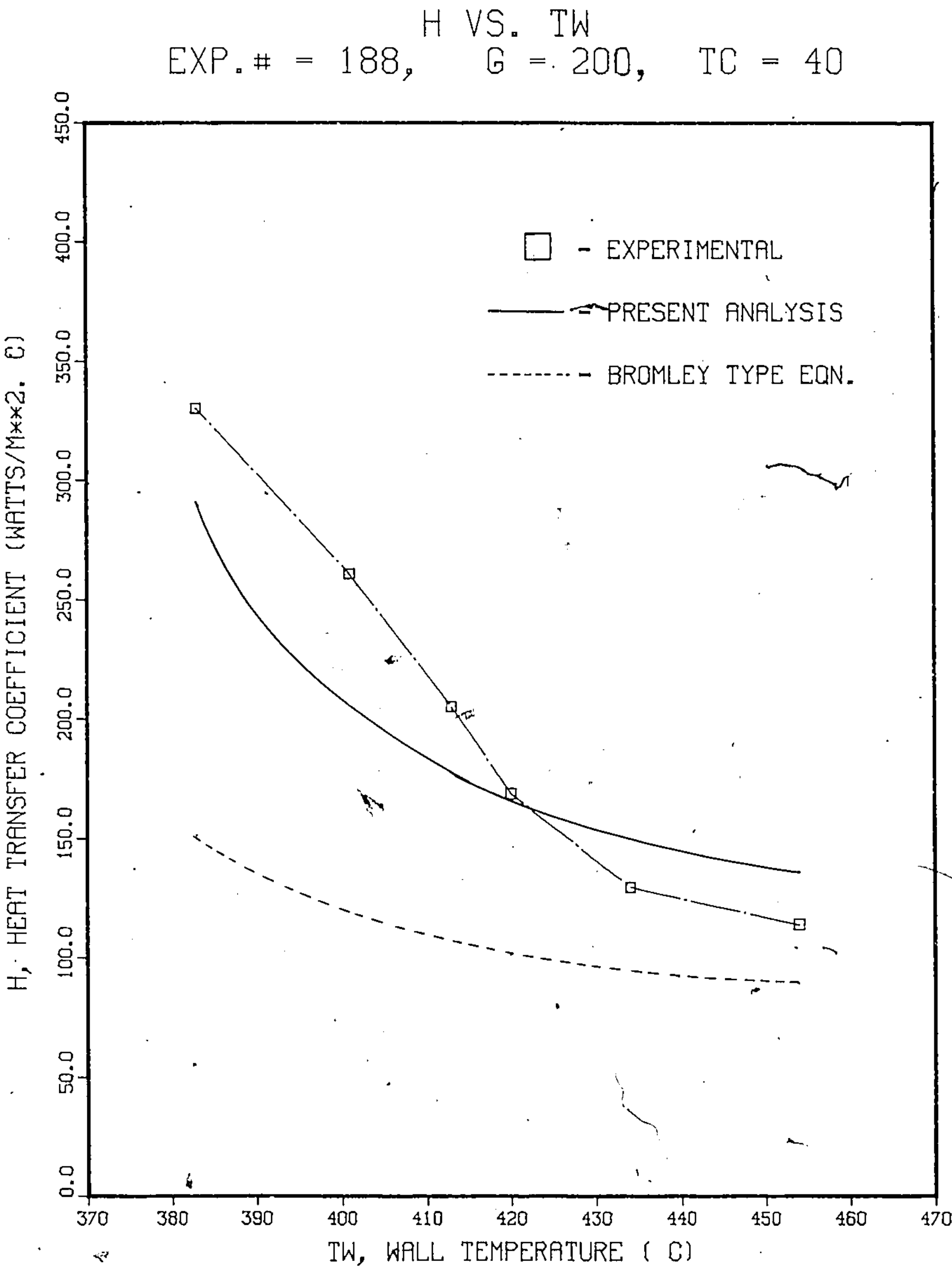

Fig. 6.55 Heat Transfer Coefficient in Inverted Annular Region

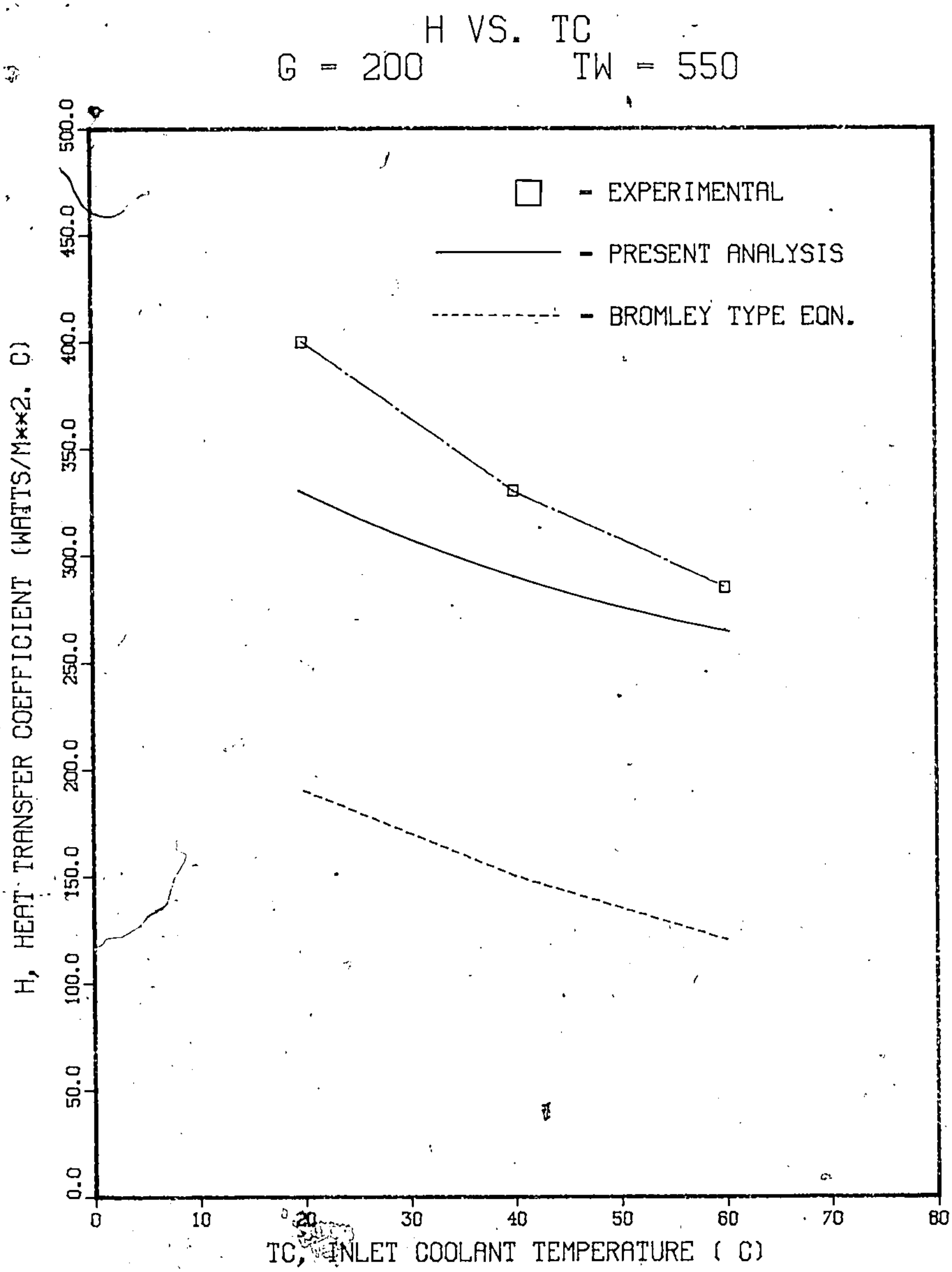

Fig. 6.56 Effect of Inlet Subcooling on Inverted Annular Flow Region Heat Transfer Coefficient

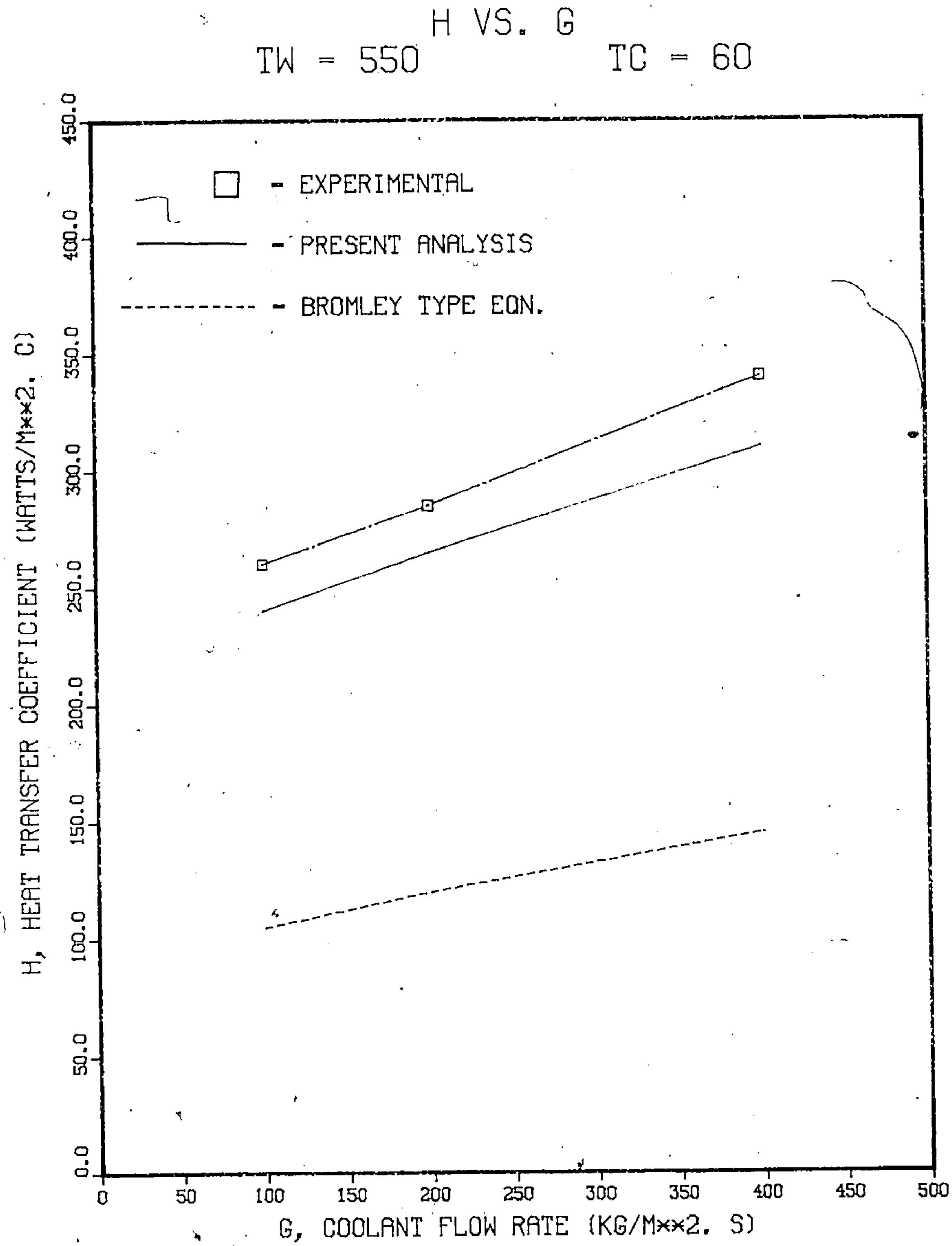

Fig. 6.57 Effect of Flow Rate on Heat Transfer Coefficient of Inverted Annular Flow Region

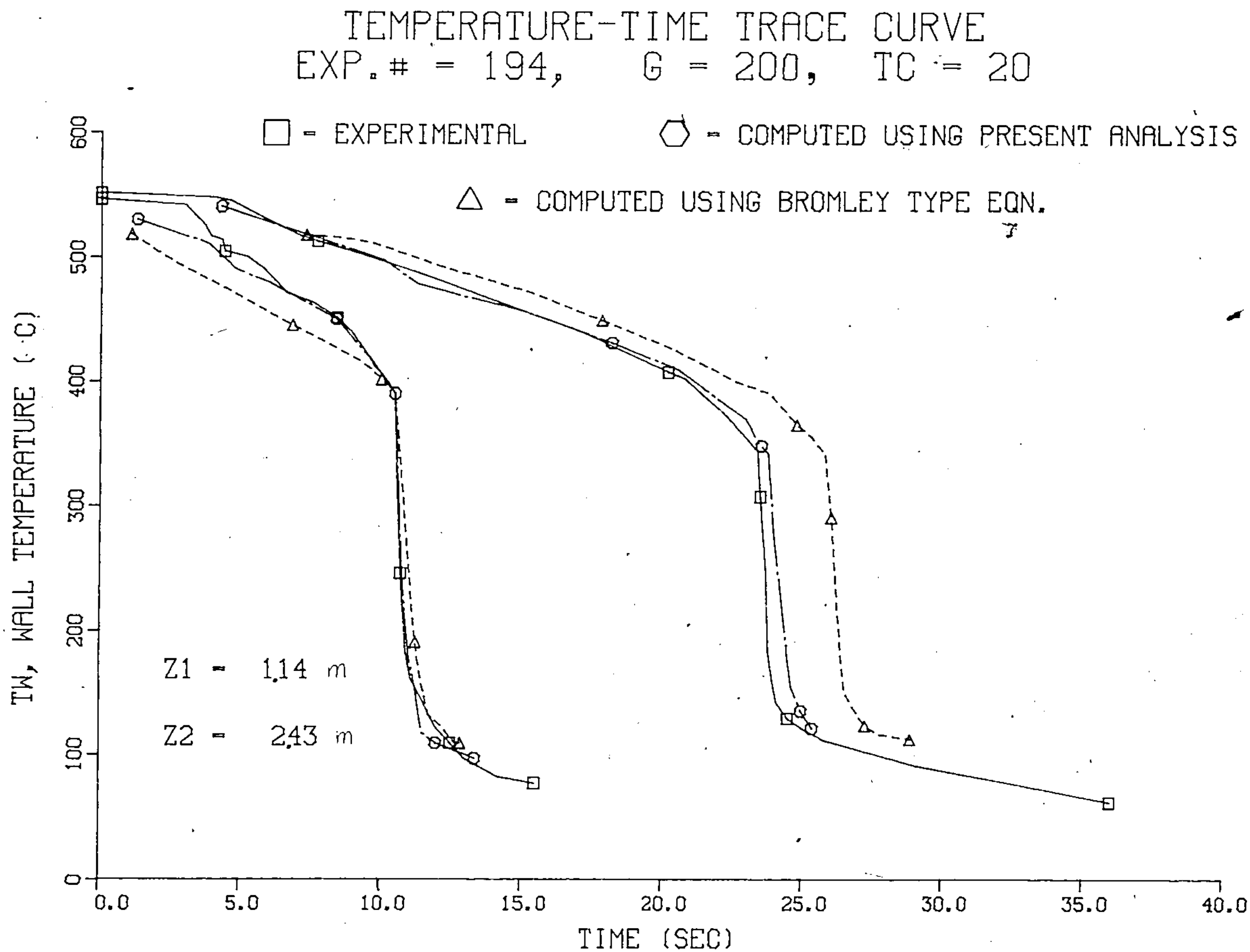

Fig. 6.58 Temperature-Time Trace Curve

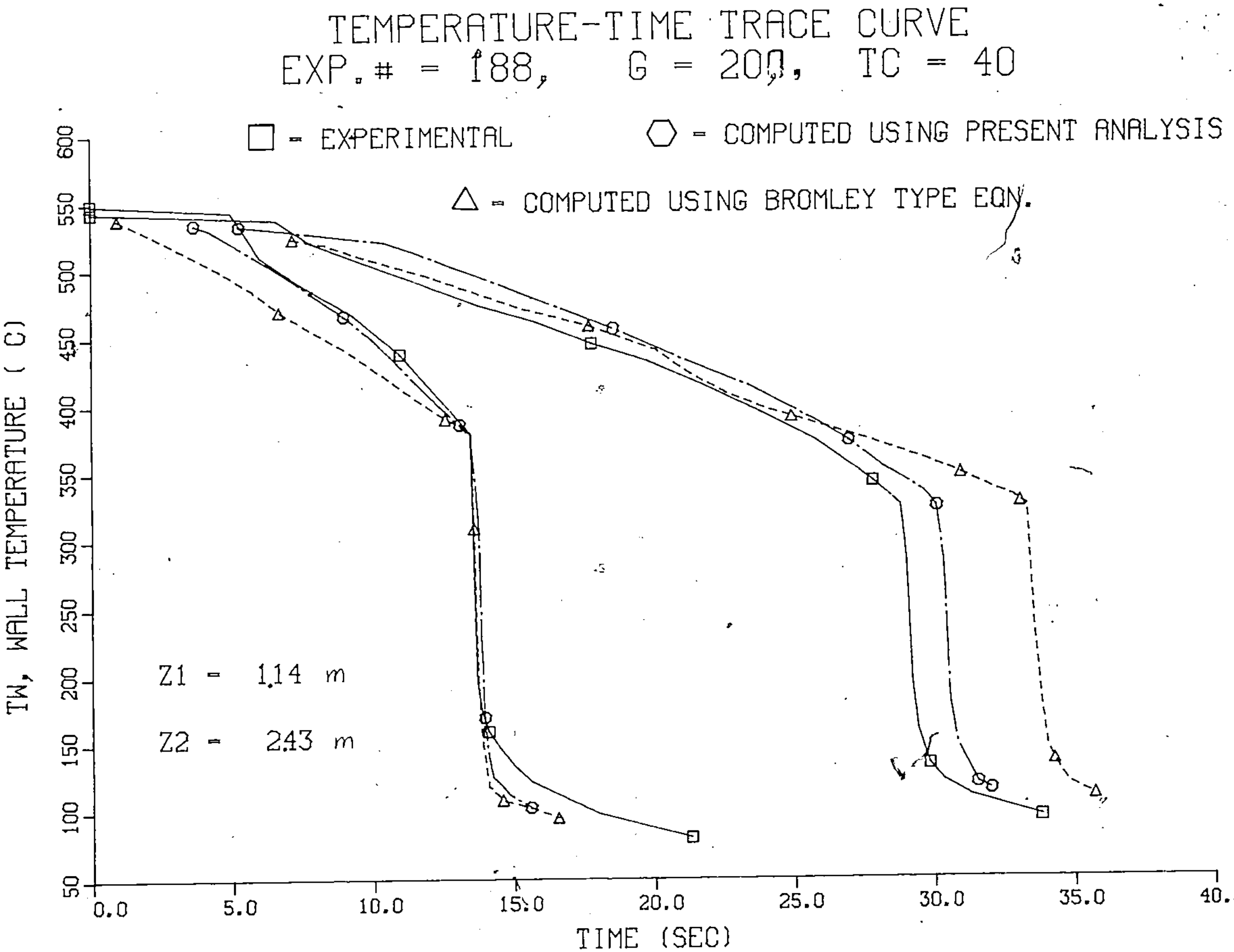

Fig. 6.59 Temperature-Time Trace Curve

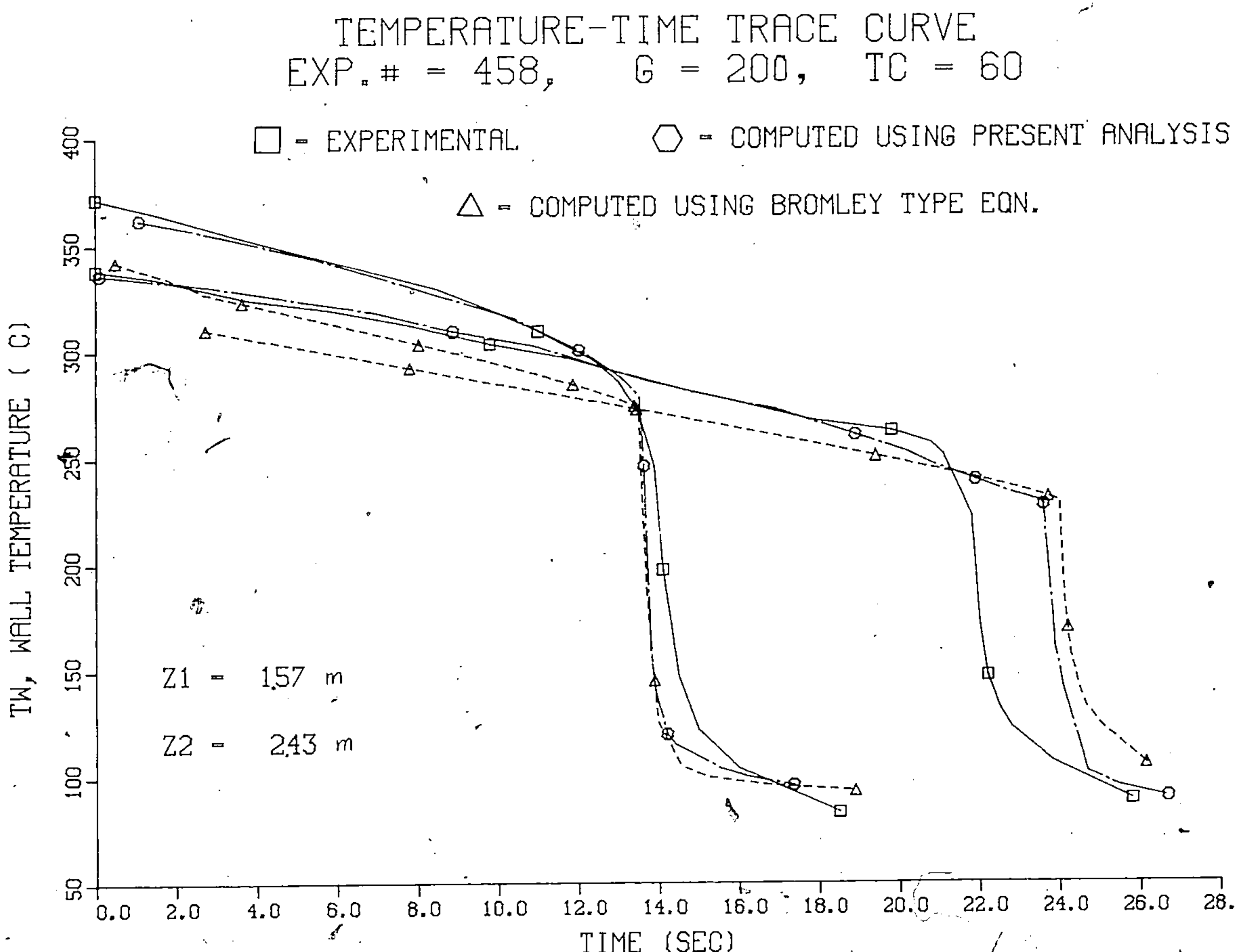

Fig. 6.60 Temperature-Time Trace Curve

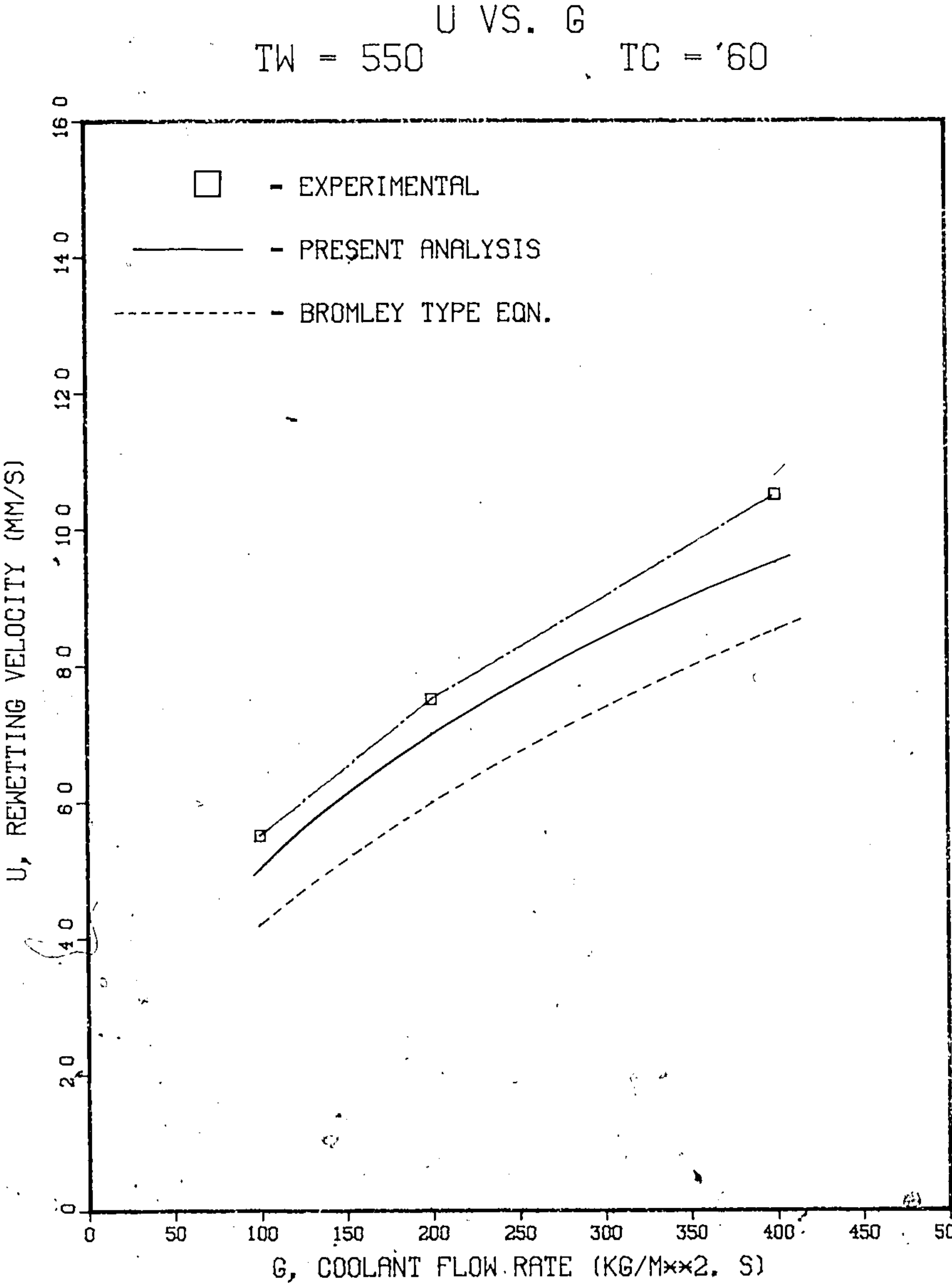

Fig. 6.61 Effect of Coolant Flow Rate on Rewetting Velocity

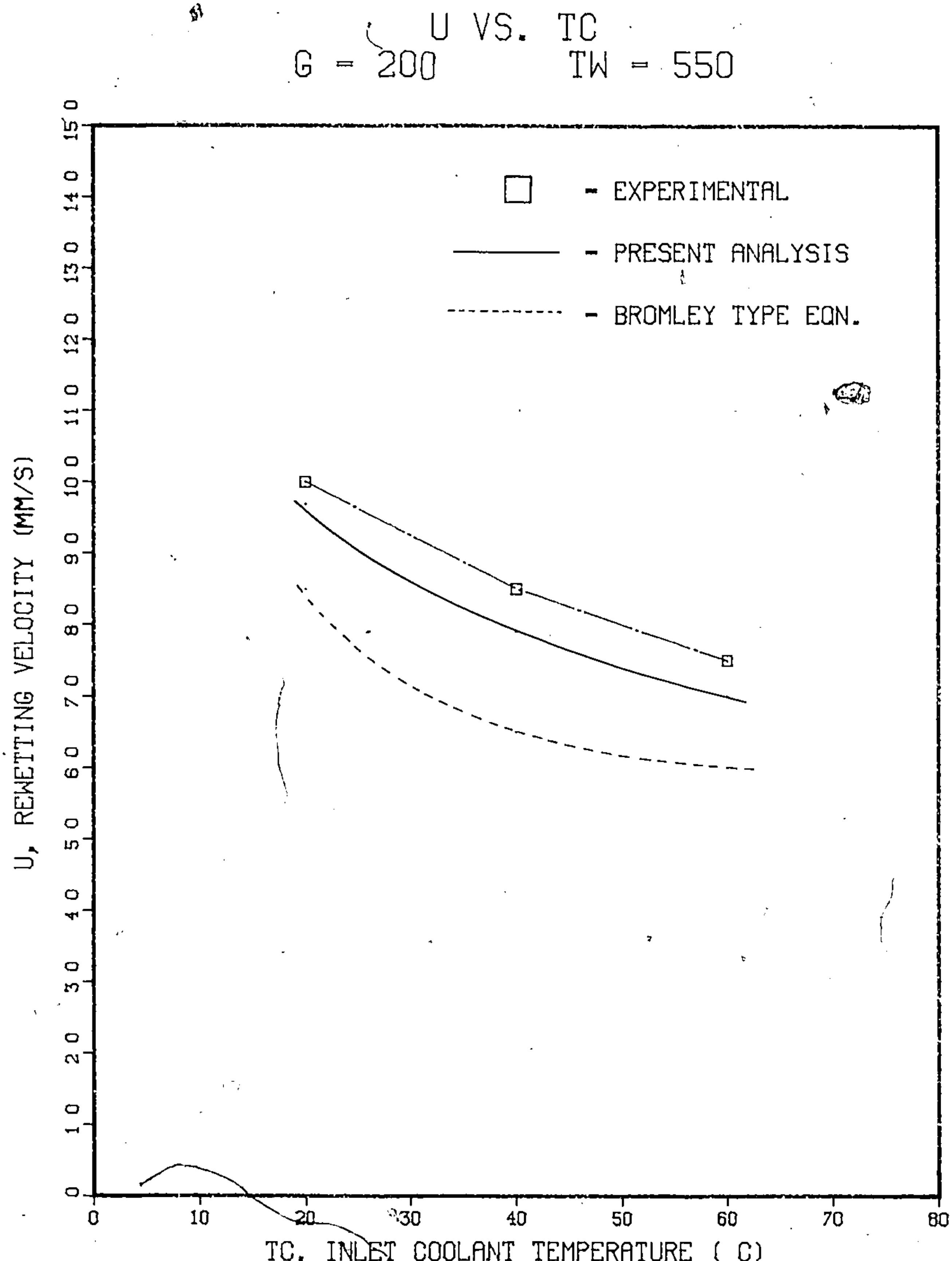

Fig. 6.62 Effect of Inlet Subcooling on Rewetting Velocity

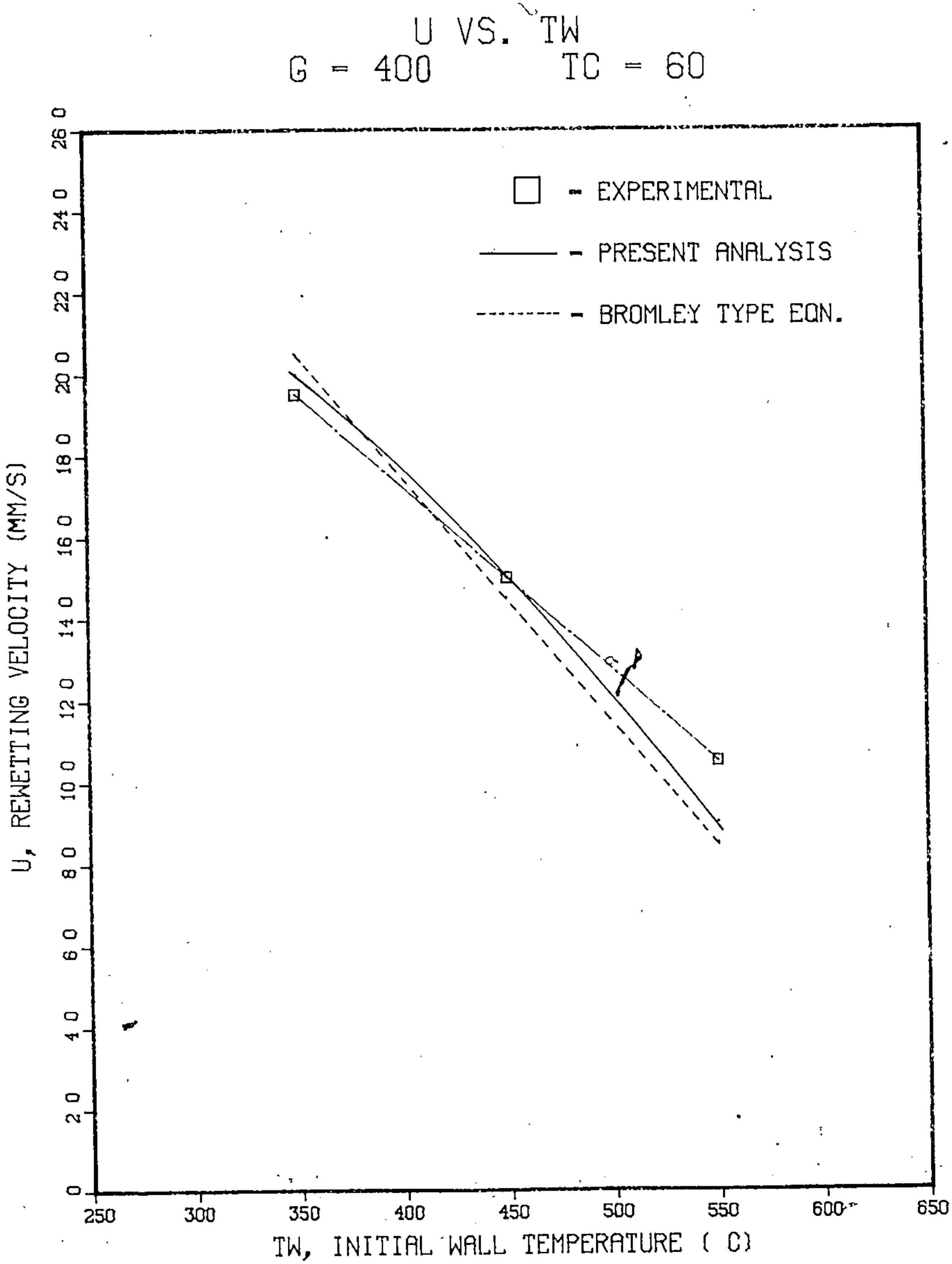

Fig. 6.63 Effect of Initial Wall Temperature on Rewetting Velocity

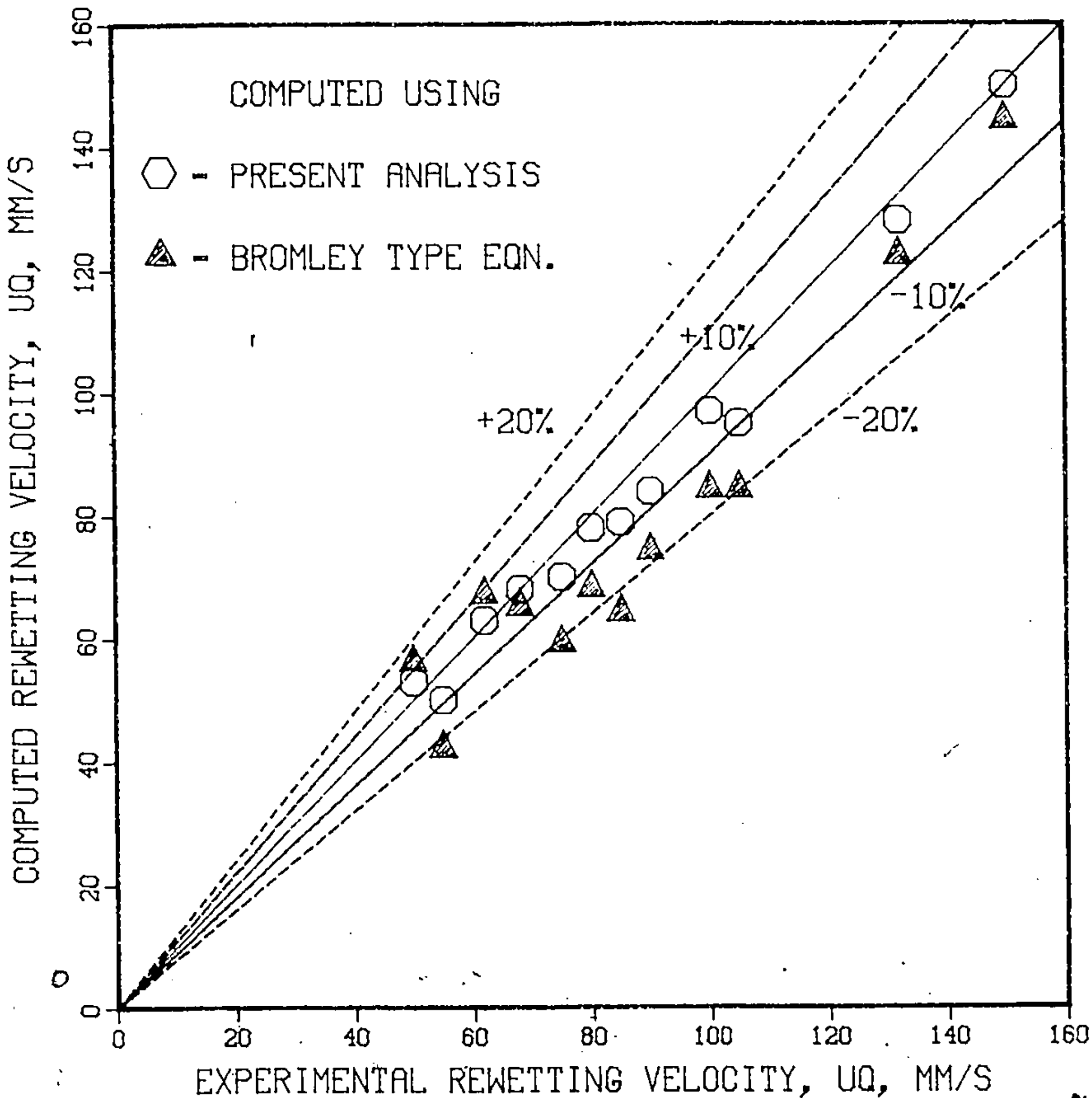

Fig. 6.64 Accuray of the Prediction of the Rewetting Velocity